1-1-2003

Structural elements influencing phase evolution in reactive polyurethanes.

Amy M. Heintz
University of Massachusetts Amherst

STRUCTURAL ELEMENTS INFLUENCING PHASE EVOLUTION IN REACTIVE POLYURETHANES

A Dissertation Presented

by

AMY M. HEINTZ

Submitted to the Graduate School of the
University of Massachusetts Amherst in partial fulfillment
of the requirements for the degree of

DOCTOR OF PHILOSOPHY

September 2003

Polymer Science and Engineering

STRUCTURAL ELEMENTS INFLUENCING PHASE EVOLUTION IN REACTIVE POLYURETHANES

A Dissertation Presented

by

AMY M. HEINTZ

Approved as to style and content by:

Shaw L. Hsu, Chair

Charles W. Paul, Member

Jacques Penelle, Member

Howard D. Stidham, Member

Thomas J. McCarthy, Department Head
Polymer Science and Engineering

DEDICATION

To my parents

ACKNOWLEDGEMENTS

I would like to thank my advisor, Shaw Ling Hsu, for his advice and encouragement over the past four years. His support has helped me to become a more aware and well-rounded scientist. I would also like to thank my committee members, Charles Paul, Jacques Penelle, and Howard Stidham, for providing motivation and guidance throughout all stages of my project.

I wish to express my appreciation to the Polymer Science and Engineering Department and the Materials Research Science and Engineering Center. I consider myself very lucky to work in a research environment with so many resources, and not just instruments, but friendly faculty, staff, and students willing to help.

The location of this department in the town of Amherst has also been critical to my development as a responsible scientist. Thanks must be extended to the 207 Speakeasy, the Young brothers, and Daniel Quinn for forever changing my outlook on this project, on science in general, and on the role I must play in society.

I need to thank Matt Morris whose actions are, and have always been, an inspiration to me. His constant objectivity has steadied me during the writing of this dissertation.

Finally, thank you to my parents and my brother. I have not the words to thank them for their unconditional love and support.

ABSTRACT

STRUCTURAL ELEMENTS INFLUENCING PHASE EVOLUTION IN REACTIVE POLYURETHANES

SEPTEMBER, 2003

AMY M. HEINTZ, B.S., UNIVERSITY OF MICHIGAN ANN ARBOR

Ph.D., UNIVERISITY OF MASSACHUSETTS AMHERST

Directed by: Professor Shaw Ling Hsu

The formation of specific phase-separated morphologies is central to achieving high performance polyurethanes. Polyurethanes are composed of various structural elements possessing a mixture of different functional groups, molecular weights, and sequence lengths. The chemistry, the phase behavior, and the kinetics of phase evolution will influence the type of phase-separated morphology formed. In fact, the phase behavior also depends upon the chemical structure and the molecular weight distribution of the components. Despite the importance of chemical structure, it is still not understood quantitatively. In addition, little is known about how the developing structure organizes into different phase-separated morphologies.

The work herein addresses these issues. The molecular weight distributions, end groups, and linkages of polyurethane structural elements were quantitatively determined. The structural elements included polyether and polyester macrodiols, polyurethane prepolymers, and polyurea hard segments. Under homogeneous conditions, the molecular weight distribution formed obeys a Schultz-Flory distribution; although when toluene diisocyanates are used as the diisocyanate the effect of change in reactivity narrows the

distribution. Under heterogeneous conditions, the phase separation of water causes a change in the local stoichiometry and narrows the distribution further. In the presence of typical polyurethane side reactions, the distribution is broadened. The formation of allophanate linkages was most prevalent in PPG prepolymers prepared at reaction temperatures of 145 °C .

Infrared spectroscopy was used to study the crystallization behavior of semi-crystalline polyurethanes and the reaction and morphological evolution of polyurethane foams. Hydrogen bonding between urethane groups was shown to influence all aspects of the crystallization behavior, including the initial state, nucleation and growth rates, and the final morphology. Hydrogen bonding proves to be less crucial in the onset of phase separation in polyurethane foams. The most crucial parameter was shown to be hard segment anisotropy. Foams prepared from diisocyanates yielding highly anisotropic hard segments phase separate at lower reaction conversion, with a faster rate, and to a higher degree of phase separation and perfection.

TABLE OF CONTENTS

LIST OF TABLES

LIST OF FIGURES

SYMBOLS AND ABBREVIATIONS

β_i	full width at half maximum of standard's diffraction peak
β_s	full width at half maximum of sample's diffraction peak
χ	Flory-Huggins parameter
χ_c	chi critical
ΔE_p	energy of primary crystallization
Δg_f	bulk free energy
ΔG_c	free energy of critical nucleus
ΔG_m	free energy of mixing
ΔH_f	enthalpy of fusion
ΔH_{HB}	enthalpy of hydrogen bonding
ΔS_f	entropy of fusion
ΔT	supercooling
ΔU^*	energy of transport
Δv	frequency shift in wavenumbers
γ	surface energy
λ	wavelength
ϕ_i	volume fraction of ith phase
Φ	cooling rate
ω	oscillator frequency
ω'	intermolecular coupling force constant
ω_o	unperturbed oscillator frequency

33-LV	1,4-diazobieyelo[2,2,2]oetane in dipropylene glyeol
A	area
aeet	aeetone
AFM	atomie foree mieroseopy
ATR	attenuated total refleetanee
BL-11	bis(dimethylaminoethyl) ether in dipropylene glyeol
bw	band width
eonst	eonstant
DBU	1,8-diazabieyelo[5.4.0]undee-7-ene
DEPT	distortionless enhaneement by polarization transfer
DMDEE	4,4-(oxydi-2,1-ethanediyl)bismorpholine
DMF	dimethylformamide
DMSO	dimethylsulfoxide
Eg	energy differenee between gauehe and trans
[free]	eoneentration of non-hydrogen bonded species
FT	Fourier transform
FWHM	full width at half maximum
G	linear growth rate
Go	erystallization eonstant
HDPE	high density polyethylene
HMQC	heteronuelear multiple-quantum eoherenee
HV	hydroxyl value
K	ratio of reaetivity

K	equilibrium constant
k_1	reactivity before reaction of one group
k_2	reactivity after reaction of one group
L_{hkl}	crystalline size along hkl
MALDI-TOF	matrix assisted laser desorption ionization time of flight
MCT	mercury cadmium telluride
MDI	methylene(bisphenyl isocyanate)
MeOH	methanol
MMA	methylmethacrylate
nBMA	n-butyl methacrylate
M	moles per liter
M_n	number average molecular weight
M_p	peak molecular weight
M_w	weight average molecular weight
n	degree of polymerization
NaTFAc	sodium trifluoroacetate
[NCO]	concentration of isocyanate
Nd:YAG	neodymium : yttrium aluminum garnet
n_i	degree of polymerization of ith phase
NMR	nuclear magnetic resonance
N_x	number fraction
[OH]	concentration of alcohol
oo	2,6-toluenediisocyanate

p	extent of reaction
PHMA	poly(hexamethylene adipate)
PHMS	poly(hexamethylene sebacate)
P(MMAnBMA)	poly(methylmethacrylate-co-butylmethacrylate)
PCL	poly(caprolactone)
PDI	polydispersity index
p_{NCO}	isocyanate conversion
p_{OH}	hydroxyl conversion
PPG	poly(propylene glycol)
ppm	parts per million
PU	polyurethane
pyr	pyridine
r	stoichiometric imbalance
r_c	critical nucleus radius
SAXS	small angle X-ray scattering
SEC	size exclusion chromatography
T°	solid-liquid equilibrium
T-9	stannous octanoate
T-80	80% 2,4-toluenediisocyanate, 20% 2,6 toluenediisocyanate
T_c	peak crystallization temperature
TDI	toluenediisocyanate
TEM	transmission electron microscopy
T_g	glass transition temperature

THF	tetrahydrofuran
T_m	crystalline melting temperature
t_{rxn}	reaction time
T_{rxn}	reaction temperature
UV	ultra-violet
V3137	Voranol 3137
vh	van't Hoff method
v/v	volume to volume ratio
w_{12}	interaction energy between segment 1 and segment 2
w_{11}	interaction energy between segment 1 and segment 1
WAXS	wide angle X-ray scattering
X_n	number average degree of polymerization
X_w	weight average degree of polymerization
z	lattice constant

CHAPTER 1

INTRODUCTION

1.1 Thesis Overview

This thesis is divided into seven chapters. Chapter 1 presents an introduction to the relevant topics about polyurethanes. The connection between chemistry, phase evolution, morphology, and mechanical properties is discussed. In Chapter 2, the polyurethane systems used in this study are described. This chapter includes characterization of the starting materials and the synthetic methods used. In Chapter 3, the molecular weight distribution of polyurethane prepolymers and polyurea hard segments is quantitatively determined and compared with step polymerization theory. In Chapter 4, the influence of processing conditions, such as reaction temperature and time, on the formation of secondary linkages is determined quantitatively for polyurethane prepolymers. In Chapter 5, the influence of hydrogen bonding on the crystallization behavior of polyurethanes is examined. The molten state, the kinetics and the final morphology are studied in a set of semi-crystalline polyurethanes. In Chapter 6, the kinetics of structural evolution in foams is observed. Foams based on two different diisocyanates are considered in order to understand the importance of excluded volume in morphology development. Finally Chapter 7 presents a summary of the dissertation.

1.2 Polyurethane Background

Polyurethanes are one of the most versatile classes of polymers that exist. They are used in a range of applications such as foams, coatings, elastomers, and adhesives. It

is estimated that the average family probably owns somewhere between 25 and 100 pounds of polyurethane.[1] Flexible polyurethane foams are used to make bedding, cushions, and car seats. Rigid foams are used for insulation. Form-fitting clothing contains the polyurethane elastomer, Spandex. The soles of many running shoes are made from tough elastomeric polyurethanes. The auto industry makes dashboards, bumper covers, moldings and fenders out of polyurethane. Polyurethane coatings are used to seal boat decks and line tanks. Polyurethanes are also used for a variety of medical applications such as catheter tubing, wound dressings and short term implants. A new application is polyurethane glass, which may be used in safety glasses or as bulletproof glass.[2]

Polyurethanes were first developed in the early 1940's by I. G. Farbenindustrie to compete with DuPont's nylon products.[3] While Carothers had recently pioneered polycondensation chemisty, Bayer was studying the polyaddition chemistry of diisocyanates with diols and diamines. Early work by Bayer led to the rather unsuccessful commercialization of polyurethane fibers, the first patent in this area involving semi-crystalline polyurethane based on 1,6-hexane diisocyanate.[4,5] The Germans later developed polyurethane adhesives during World War II. However, worldwide success of polyurethanes was not known until the development of flexible foams. Since then annual world production has increased to about 9 million tons.

1.2.1 Polyurethane Chemistry

The reason for polyurethane's versatile nature is partially related to the richness of isocyanate chemistry, shown in Figure 1.1 for an aromatic isocyanate. The basic reaction

takes place between an alcohol and an isocyanate, yielding a carbamate, or urethane. Isocyanates can react with other nucleophiles as well, such as water and amines. Reaction between isocyanate and water yields an unstable carbamic acid linkage, which loses carbon dioxide to give an amine. Amines react with isocyanates to give urea. The high reactivity of isocyanates and the nucleophilicity of the typical products, such as urethane and urea groups, make side reactions in polyurethane synthesis common. Reaction with urethane and urea groups yields allophanate and biuret groups, respectively. In addition, isocyanates can dimerize and trimerize to give uretidinedione and isocyanurate, respectively. These reactions can be favored using specific catalysts to obtain different properties.[6-15] For example, some rigid foams contain a high concentration of isocyanurate in order to increase the crosslink density.[16] In other cases, the formation of these "secondary" linkages may be undesirable, as they may increase the functionality of a polymer from 2 to 3 or increase the molecular weight.

In practice, the carbamate linkage and its secondary linkages are only a small part of polyurethane structure. The name "polyurethane" is given to any one of a family of polymers containing a carbamate group and encompasses an array of structures. Three examples are shown in Figure 1.2. An adhesive may be prepared by reacting a diisocyanate in stoichiometric excess with a blend of two macrodiols, one crystalline (such as polycaprolactone, PCL) and one amorphous (such as polypropylene glycol, PPG), producing a polyurethane prepolymer, whose terminal NCO groups can later react with water and cure the adhesive. An elastomer may be prepared by reacting a diisocyanate with a high molecular weight diol (PPG) and a low molecular weight diol, producing a segmented polyurethane. Finally, a foam may be prepared by reacting a

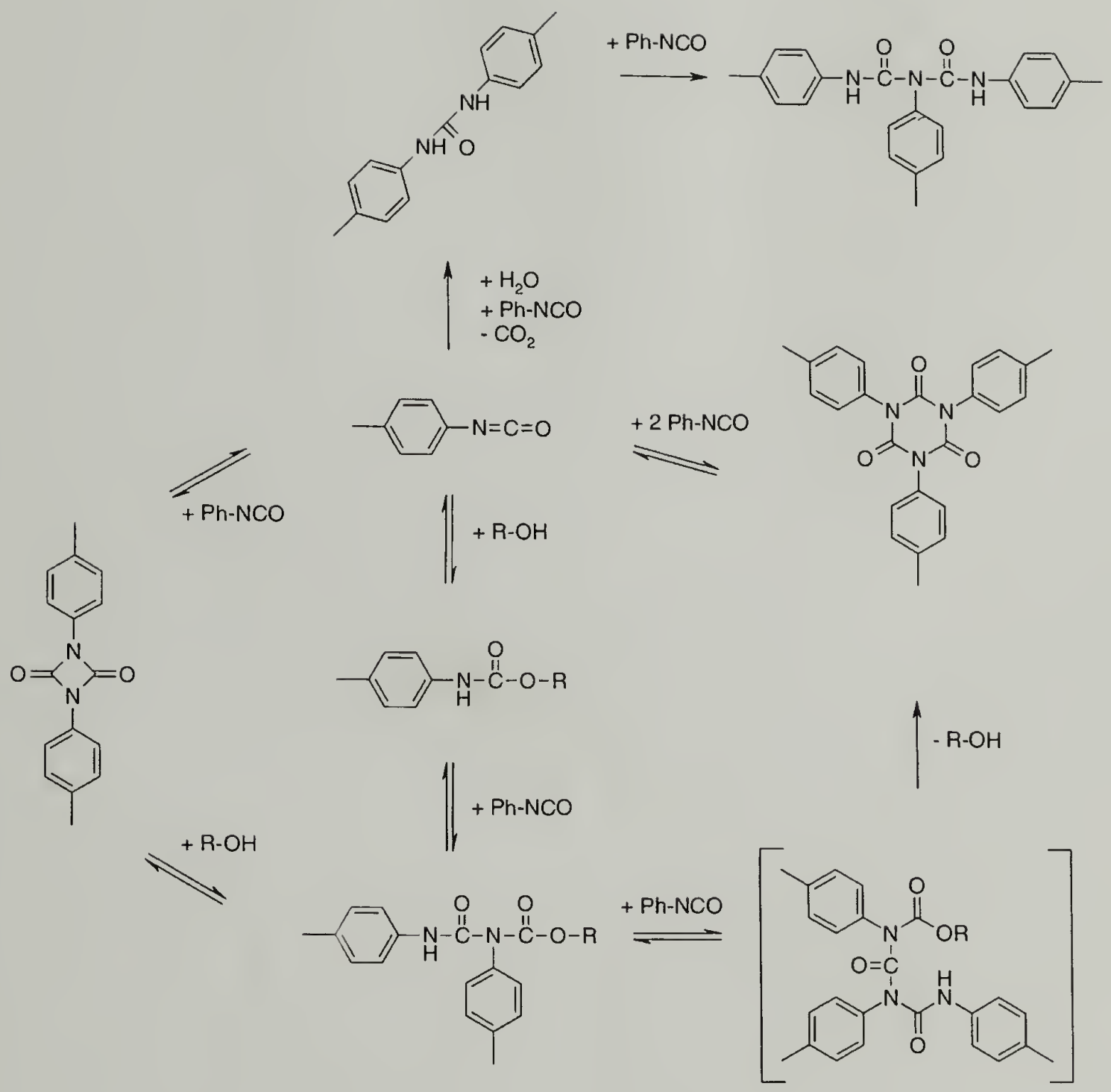

Figure 1.1 Possible reactions that may occur in polyurethane systems.

1. Polyurethane Adhesive Prepolymer

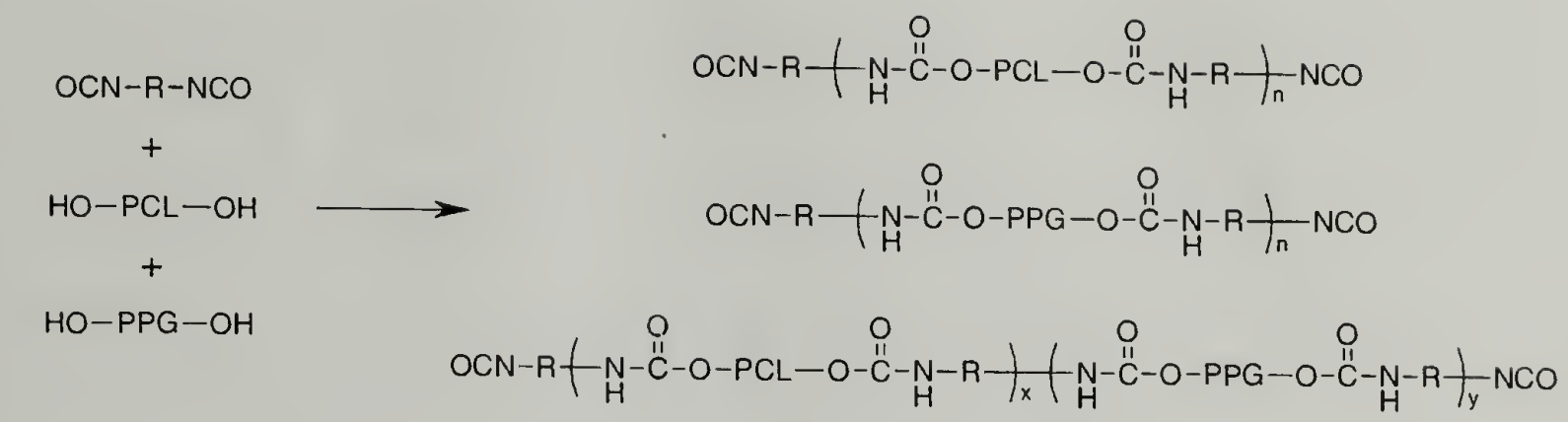

2. Segmented Polyurethane Elastomer

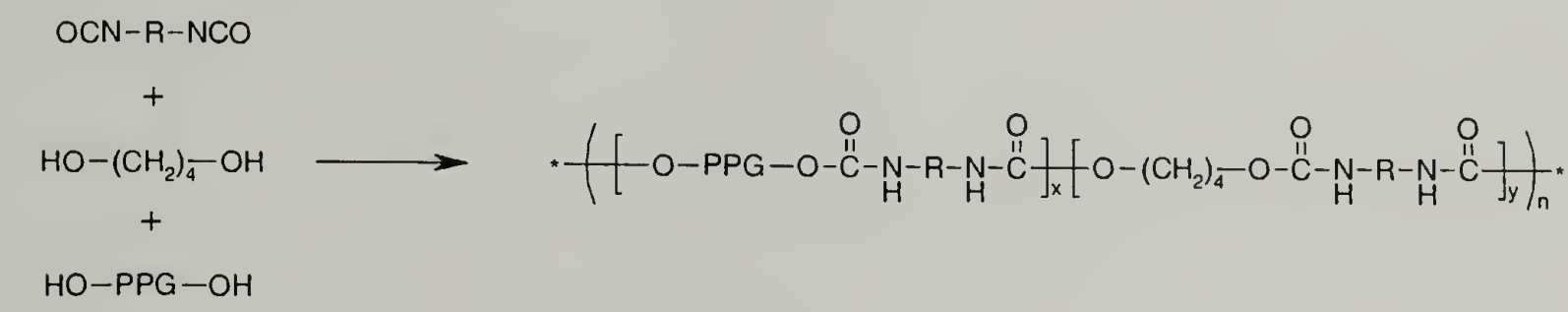

3. Crosslinked Polyurethane Foam

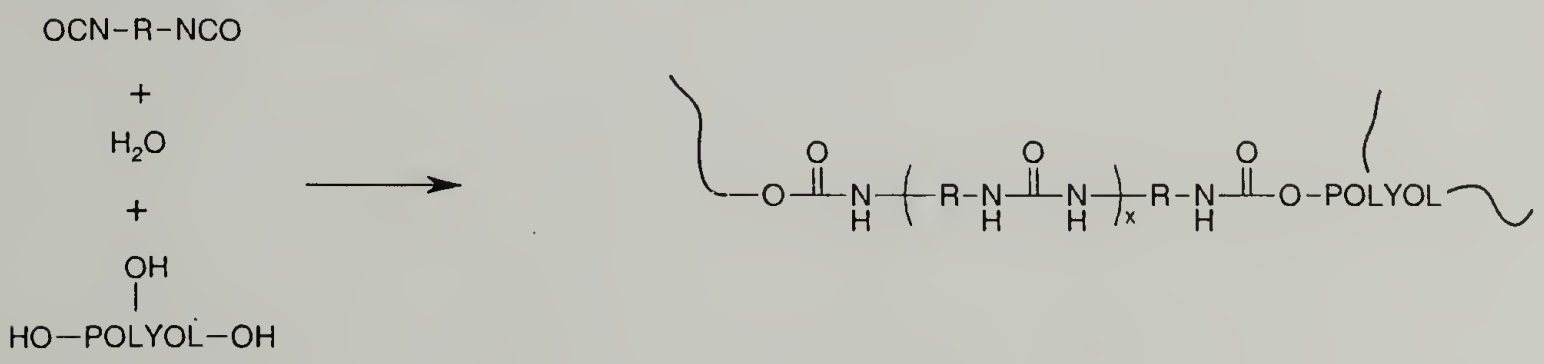

Figure 1.2 Examples of different types of polyurethanes.

diisocyanate with water and a high molecular weight triol (POLYOL), producing CO_2 and a chemically crosslinked segmented polyurethane.

In these examples, the entire polyurethane can be broken into structural elements. In Example 1, reaction between diisocyanate and the two macrodiols can lead to essentially 3 structural elements: the two homo-prepolymers and a co-prepolymer. The macrodiols had a molecular weight distribution before reaction, and after reaction different end groups, linkages (urethane) and molecular weight distribution. The co-prepolymer is further characterized by sequence distribution. In addition, monomeric diisocyanate will remain. In Example 2, successive reaction between diisocyanate and 1,4-butanediol results in a "hard segment." This structural element is characterized by its linkages, molecular weight distribution, rigidity, and perfection. The macrodiol forms a copolymer with these hard segments. The entire copolymer is characterized by its sequence distribution. Finally, Example 3 is similar to Example 2, being composed of a hard segment distribution, except with urea linkages instead of urea.

1.2.2 Morphology/Property Relationships

It is really the phase behavior of these structural elements, and the resulting morphology, that is crucial for manipulating the properties. For example, the hard segments in elastomers and foams tend to phase separate from the polyol (soft) matrix into domains. The phase-separated morphology, characterized by the degree of phase separation and hard domain volume, size, perfection, and interconnectivity, is crucial to obtaining the desirable properties, such as high modulus[17-19] and low hysteresis.[20] The hard domains are likened to filler particles in rubber, and as such they increase the

modulus when their volume fraction is increased.[21-23] In foams, the initial modulus build-up is attributed to the formation of these domains. At later stages, there is evidence that the domains may aggregate further to form larger precipitates.[24,25] The domains may have significant anisotropy and interconnectivity. Materials with interconnected hard domains exhibit higher modulus than those with isolated hard domains.[26-29] On the other hand, the hysteresis tends to increase when the domains are interconnected.[26,30,31]

Besides phase separation of hard segments from the soft matrix, other types of phase separation may occur in polyurethane systems. In the adhesive prepolymer system shown above, a blend of two polymers is used. A ternary blend, containing a third, non-reactive, glassy component (e.g. an acrylic), is usually used to achieve the desirable properties for a hot melt adhesive, such as good thermal stability, high green strength, fast cure, controllable set speed, and good adhesion.[32-36] The adhesive prepolymer is melted and applied to a joint where it will begin reacting with adventitious moisture. As it cools, the contributions from the different components (vitrification, crystallization, and moisture curing) give a bond. In either the binary or the ternary system, liquid/liquid phase separation can occur. The compatibility of the acrylic has a direct relationship with the performance properties of the adhesive.[37,38] Phase separation of the crystallizable component to the surface may decrease the peel strength.[39]

Phase separation can also occur due to crystallization. In adhesive prepolymers, the crystallization behavior determines the set speed.[38,40,41] Other studies have shown that adhesion is decreased when slower cooling rates are used, which demonstrates that the crystal size or perfection influences adhesion.[42,43] The curing kinetics are also influenced by the crystalline morphology.[44] The morphology changes due to polymer liquid/liquid

phase separation or crystallization are also important in the elastomer and foam systems shown above. For example, strain induced crystallization of the soft segment causes the material to become brittle and increases hysteresis.

1.3 Polymer Phase Separation

Regardless of the specific polyurethane system, the thermodynamics and kinetics of phase evolution determine the type of morphology achieved. Likewise, the chemistry determines the thermodynamics and kinetics of phase evolution. The miscibility behavior of a binary blend of flexible chains depends upon the free energy of mixing (ΔG_m). The free energy of mixing can be calculated using a simple lattice model as shown in Equation 1.1.

$$\frac{\Delta G_m}{N_A RT} = \left(\frac{\phi_1 \ln(\phi_1)}{n_1} + \frac{\phi_2 \ln(\phi_2)}{n_2} \right) + \chi \phi_1 \phi_2 \qquad (1.1)$$

In this equation, ϕ_i is the volume fraction of the ith component, n_i is the degree of polymerization of the ith component, and χ is the Flory-Huggins parameter. The first two parameters describe the change in translational entropy upon mixing, while the last term describes the change in local interactions and motions of the monomers. This latter term is mostly due to enthalpic contributions and χ may be described by equation 1.2.

$$\chi = \frac{z\phi_1 \cdot [w_{12} - 0.5 \cdot (w_{11} + w_{22})]}{N_A RT} \qquad (1.2)$$

The χ-parameter depends upon the interaction energies for segments of different kind (w_{12}) versus the same kind (w_{11} and w_{22}), where z is the lattice coordination number. Generally, interaction energies between segments of the same type are stronger than those between different types, and χ is positive. In the limit of infinite molecular weight,

the entropic terms are negligible, and therefore ΔG_m is also positive. In other words, most polymer blends tend to phase separate.

If there are special interactions between polymer pairs, such as dipole-dipole or hydrogen bonding interactions, then χ may be negative. The chemical structure of the polymer repeat units,[45,46] copolymer composition and sequence distribution,[47,48] chain branching,[49] and end groups[50] can all influence segmental interaction energies. In addition, shrinkage or expansion of the total volume results in a change in the entropic part of χ.[51] Finally, the entropic contribution to ΔG_m becomes more significant at lower molecular weight. For example, many of the macrodiols used to prepare prepolymers have a degree of polymerization between 20 and 50. For symmetric blends, with equal degrees of polymerization miscibility is expected as described by Equation 1.3.

$$\chi < \chi_c = \frac{2}{n} \tag{1.3}$$

At infinite n, χ must be less than 0 for the blend to be miscible. For lower n, χ can have somewhat larger values.

In solutions containing asymmetric particles, such as long rods, phase separation may occur, even if χ is negative, due to excluded volume effects of a pair of rods.[52] Such a system undergoes an orientational order-disorder transition from the isotropic state. Flory has treated this problem extensively for monodisperse and polydisperse mixtures of rods in solvent and in flexible polymer blends.[53-56] Polydispersity widens the coexistence region and a fractionation effect occurs, where the longer rods preferentially go into the anisotropic phase. Even for an undiluted polydisperse mixture of rods, biphasic behavior is predicted for X_n between 2.3 and 17.5.

A molecular simulations technique was used to determine the miscibility behavior of rod/polymer blends accounting for both the excluded volume and segmental interaction effects.[57] Similar to the calculations by Flory, two phases may form: an anisotropic phase consisting only of rods and an isotropic phase consisting of rods dissolved in polymer. Increasing the length of the rod decreased the concentration of rods found in the isotropic phase. On the other hand, increasing the molecular weight of the polymer had a small effect; increasing the molecular weight from 1000 to 3000 $g \cdot mol^{-1}$ increased the concentration of rod found in the isotropic phase.

The mechanism of phase evolution is different depending on whether the sample is quenched into the binodal or spinodal region. Within the binodal, the system must overcome an energy barrier and phase separation occurs via nucleation and growth. Within the spinodal, phase separation occurs via continuous growth of concentration fluctuations, leading to two interpenetrating phases. The concentration of the rich component in each phase changes over time until a constant value is achieved. Then coalescence may occur. At equilibrium, the resulting compositions should be the same regardless of mechanism. However, polymer systems may not reach equilibrium. In polyurethanes, phase separation is considered to be incomplete.[58] In high viscosity systems, or where chemical crosslinking or vitrification occurs during phase separation, spinodally decomposed systems can become "pinned" as interconnected structures.[59,60]

1.3.1 Polyurethane Foams

Studies on the phase behavior of polyurethane foams are relatively rare. However, because both elastomers and foams are based on segmented polyurethanes, many of the

results from elastomer phase behavior can be extrapolated to foams. The behavior generally agrees with what is expected based on the theories outlined above. Increasing the average hard segment length increases the degree of phase separation and the anisotropy of the domains.[26,28,58,61-63] In most studies, the volume fraction of hard segment repeat units increases with the hard segment length (due to synthetic procedures). For example, elastomers with different hard segment lengths were prepared as shown in Equation 1.4.

$$HO\text{-}(P)_m\text{-}OH + OCN\text{-}(R)_x\text{-}NCO \qquad (1.4)$$

The length of the hard segment (x) was varied for each elastomer, but since the length of the polyol (m) and the stoichiometric balance OH/NCO are kept constant, the volume fraction of R increased.[63] Thus the importance of chain rigidity versus segment interaction energy cannot be distinguished. By preparing elastomers using either a one-step or a two-step procedure, yielding different average molecular weight, [64] Cooper confirmed that increasing the hard segment length increases the degree of phase separation.[22]

In fact, the importance of excluded volume is often neglected when the phase behavior of polyurethanes is discussed; although most data tends to agree with the theory outlined above for the phase separation of rods. Besides length, increasing hard segment "rigidity" increases the degree of phase separation.[65,66] Constraining polyurethanes by decreasing film thickness decreases the degree of phase separation.[67] Finally, in systems where the interaction between segments of different type is stronger (i.e. χ is negative), phase separation still occurs.[68]

By applying thermodynamics principles, the influence of chemical structure on polyurethane phase behavior can be predicted and generally confirmed. However, the final morphology achieved represents the consequences of both thermodynamics and kinetics. In foams, the phase separation occurs during reaction, and the morphology that develops in a given system depends upon the competitive reactions that occur, one yielding the hard segments necessary for phase separation and the other yielding a crosslinked network at high conversion. Because the reactions are exothermic, the temperature inside the foam may rise as high as 140 °C.[69,70] The rate of crosslinking relative to phase separation influences the phase evolution. In one study, molded foams were prepared under isothermal conditions at temperatures between 50 and 150 °C.[70] Samples prepared at higher temperatures exhibited higher degrees of phase mixing. This was attributed to an increase in the rate of chemical crosslinking relative to hard domain formation. A similar conclusion was reached in work on flexible molded foams prepared with different crosslinking density. The sample with higher chemical crosslink density exhibited more phase mixing.[71] Chemical crosslinking is also shown to delay the onset of phase separation.[24]

Several *in situ* studies have followed the reaction and morphology development of foaming under adiabatic conditions.[24,72-77] Initially, reaction produces short urea hard segments, mostly only one unit in length. These short hard segments are soluble in the polyol. As reaction proceeds, the hard segments become longer and less soluble in polyol.[75] Hydrogen bonding occurs between these longer hard segments, corresponding to the appearance of a "monodentate" urea peak in the infrared spectrum. Simultaneously, the reaction between isocyanate and polyol occurs, yielding urethane linkages. The hard

segment length increases still further, and a "bidentate" urea peak is observed in the infrared spectrum. The formation of bidentate urea has been correlated to the onset of phase separation. Synchrotron small angle X-ray scattering (SAXS) suggests that the phase separation occurs by a spinodal decomposition mechanism.[74] Finally, a plateau in the association of hard segment is observed. This is thought to occur due to vitrification of the hard segment rich phase, which stops further phase separation.

In these studies, the reaction and phase separation was complete after about 3 min, and the onset of phase separation occurred in less than 1 min. Such conditions are meant to replicate the conditions found during "real" foaming. However, they are not necessarily ideal for studying fundamental issues of phase separation kinetics. The temperature and chemical crosslinking are not controlled and the rapid kinetics limit the amount of information that can be obtained from most techniques.

1.4 Research Objectives

It is clear that in order to fully understand how to control the properties of polyurethane systems, the effect of various processing conditions on the chemistry and the build-up structural elements (molecular weight, linkage, branching, chain rigidity) must be fully understood. Despite the tremendous amount of research on polyurethanes, little is understood about the structure of this family of polymers. The analysis of polyurethane structures has in large part relied on techniques, such as titrations, that give averages of end-group concentrations and molecular weights. Others have developed structure-property relationships based on changes in the starting materials, assuming ideal chemistry or random statistics. In fact, there are virtually no studies that have

quantitatively analyzed prepolymer and hard segment molecular weight distributions, particularly under "real" conditions. Similarly, few studies have quantitatively analyzed the functional groups that form during reaction to determine the extent of secondary reactions. The goals of the first part of this dissertation are to quantitatively characterize the various structural elements formed during prepolymer and foam synthesis. This includes the molecular weight distribution and end groups and linkages of all the macrodiol, polyol, prepolymer and polyurea components.

It is also clear that in order to fully understand how to control the properties of polyurethane systems, the effect of structure on the kinetics of phase evolution must be fully understood. Studies following the kinetics of phase evolution have been limited to those mentioned above that were carried out under adiabatic conditions. The goals of the second part of this dissertation are to characterize the phase evolution of polyurethane systems. The kinetics of structure development in foams prepared under isothermal conditions from different diisocyanates is studied. While the order within the hard domains has often been directly related to the degree of phase separation, the phase separation and the development of spatial order should be studied separately, since they may or may not be related. Finally, the role of hard segment anisotropy in phase separation will be considered by studying foaming kinetics for different types of hard segments.

1.5 References

(1) Buist, J. M. *Developments in Polyurethanes*; Applied Science Publishers: London, 1978.

(2) McGrath, J. "Promoting The Benefits of Polyurethanes," *Alliance for the PolyurethaneIndustry,*accessedJune2003http://www.polyurethane.org/news_pubs/news_releases/products_applications/composite_liners.html

(3) Saunders, J. H.; Frisch, K. C. *Polyurethanes: chemistry and technology*; Interscience Publishers: New York, 1962; Vol. 1.

(4) Bayer, O.; Siefken, W.; Rinke, H.; Orthner, L.; Schlid, H., "A process for the production of polyurethanes and polyureas." German Patent 728,981, 1937.

(5) Bayer, O. *Angew. Chem.* **1947**, *A59*, 275.

(6) Satchell, D. P. N. S., R.S. *Chem. Soc. Rev.* **1971**, 231.

(7) Stovbun, E. V.; Kuzaev, A. I.; Baturin, S. M. *Polym. Sci., Ser. A.* **1996**, *38*, 691.

(8) Querat, E.; Tighzert, L.; Pascault, J. P.; Dusek, K. *Angew. Makromol. Chem.* **1996**, *242*, 1.

(9) Raspoet, G.; Nguyen, M. T.; McGarraghy, M.; Hegarty, A. F. *J. Org. Chem.* **1998**, *63*, 6878.

(10) Robertson, W. G. P.; Stutchbury, J. E. *J. Chem. Soc.* **1964**, *19*, 4000.

(11) Entelis, S. G.; Nesterov, O. V. *Russ. Chem. Rev.* **1966**, *35*, 917.

(12) Caraculacu, A. A.; Coseri, S. *Prog. Polym. Sci.* **2001**, *26*, 799.

(13) Schwetlick, K.; Noack, R.; Stebner, F. *J. Chem. Soc.-Perkin Trans. 2* **1994**, 599.

(14) Schwetlick, K.; Noack, R. *J. Chem. Soc.-Perkin Trans. 2* **1995**, *2*, 395.

(15) Pisareva, I. V.; Bakalo, L. A.; Gritsenko, V. P. *Kinet. Kat.* **1988**, *29*, 547.

(16) Saunders, J. H.; Frisch, K. C. *Polyurethanes Chemistry and Technology. Part I. Chemistry*; John Wiley & Sons: New York, 1962; Vol. XVI.

(17) Lin, S. B.; Hwang, K. S.; Tsay, S. Y.; Cooper, S. L. *Colloid Polym. Sci.* **1985**, *263*, 128.

(18) Neff, R.; Adedeji, A.; Macosko, C. W.; Ryan, A. J. *J. Polym. Sci., B Polym. Phys.* **1998**, *36*, 573.

(19) Abouzahr, S.; Wilkes, G. L. *J. Appl. Polym. Sci.* **1984**, *29*, 2695.

(20) Moreland, J. C.; Wilkes, G. L. *J. Appl. Polym. Sci.* **1991**, *43*, 801.

(21) Cooper, S. L.; Tobolsky, A. V. *J. Appl. Polym. Sci.* **1966**, *10*, 1837.

(22) Miller, J. A.; Lin, S. B.; Hwang, K. K. S.; Wu, K. S.; Gibson, P. E.; Cooper, S. L. *Macromolecules* **1985**, *18*, 32.

(23) Li, C.; Cooper, S. L. *Polymer* **1990**, *31*, 3.

(24) Elwell, M. J.; Ryan, A. J.; Grunbauer, H. J. M.; Van Lieshout, H. C. *Macromolecules* **1996**, *29*, 2960.

(25) Li, W.; Ryan, A. J.; Meier, I. K. *Macromolecules* **2002**, *35*, 6306.

(26) Seymour, R. W.; Allegrezza, A. E.; Cooper, S. L. *Macromolecules* **1973**, *6*, 896.

(27) Seymour, R. W.; Cooper, S. L. *J. Polym. Sci. Polym. Symp.* **1974**, *46*, 69.

(28) Wang, C. B.; Cooper, S. L. *Macromolecules* **1983**, *16*, 775.

(29) Kaushiva, B. D.; Wilkes, G. L. *Polymer* **2000**, *41*, 6981.

(30) Paik Sung, C. S.; Smith, T. W.; Hu, C. B.; Sung, N.-H. *Macromolecules* **1979**, *12*, 538.

(31) Paik Sung, C. S.; Smith, T. W.; Sung, N. H. *Macromolecules* **1980**, *13*, 117.

(32) Chambers, J.; Moore, T.; Huber, L.; Frank, D. *Adhesives Age* **1998**, *8*, 24.

(33) De Genova, R.; Grier, L.; Murray, D. P.; Clay, W. *TAPPI J.* **1998**, *81*, 196.

(34) De Genova, R. D.; Harper, M. D.; Clay, W. A.; Cranley, P. E.; Hunter, M. K. *TAPPI J.* **1996**, *79*, 196.

(35) Forschner, T. C.; Gwyn, D. E.; Xiao, H. X.; Suthar, B.; Sun, L.; Frish, K. C. *Adhesives Age* **1999**, 20.

(36) Vick, C. B.; Okkonen, E. A. *For. Prod. J.* **1998**, *48*, 71.

(37) Turreda, L. D.; Sekiguchi, Y.; Takemoto, M.; Kajiyama, M.; Hatano, Y.; Mizumachi, H. *J. Appl. Polym. Sci* **1998**, *70*, 409.

(38) Takemoto, M.; Kajiyama, M.; Mizumachi, H.; Takemura, A.; Ono, H. *J. Appl. Polym. Sci.* **2002**, *83*, 726.

(39) Shih, H. H.; Hamed, G. R. *J. Appl. Polym. Sci.* **1997**, *63*, 333.

(40) Shih, H. H.; Hamed, G. R. *J. Appl. Polym. Sci.* **1997**, *63*, 323.

(41) Fernandes, E. G.; Lombardi, A.; Solaro, R.; Chiellini, E. *J. Appl. Polym. Sci.* **2001**, *80*, 2889.

(42) Longhenry, J. L.; Love, B. J.; Murthy, N. S. *J. Mater. Sci.* **1997**, *32*, 2283.

(43) Nakao, K. *J. Adhesion* **1972**, *4*, 95.

(44) Cui, Y. J.; Chen, D. H.; Wang, X. L.; Tang, X. Z. *Int. J. Adh. Adh.* **2002**, *22*, 317.

(45) Ellis, T. S. *Macromolecules* **1995**, *28*, 1882.

(46) Ahn, T. O.; Lee, M.; Jeong, H. M.; Cho, K. *J. Polym. Sci., B Polym. Phys.* **1998**, *36*, 201-212.

(47) Roe, R. J.; Rigby, D. *Adv. Polym. Sci.* **1987**, *82*, 103.

(48) Winey, K. I.; Berba, M. L.; Galvin, M. E. *Macromolecules* **1996**, *29*, 2868.

(49) Chai, Z.; Sun, R.; Li, S.; Karasz, F. E. *Macromolecules* **1995**, *28*, 2297.

(50) Lee, M. H.; Fleisher, C. A.; Morales, A. R.; Koberstein, J. T.; Koningsveld, R. *Polymer* **2001**, *42*, 9163.

(51) Strobl, G. *The Physics of Polymers*; 2nd ed.; Springer-Verlag: Berlin, 1997.

(52) Flory, P. J. *Proc. R. Soc., London A* **1956**, *234*, 73.

(53) Flory, P. J. *Statistical Mechanics of Chain Molecules*; Interscience Publishers: New York, 1969.

(54) Flory, P. J. *Macromolecules* **1978**, *11*, 1138.

(55) Flory, P. J. *Macromolecules* **1978**, *11*, 1119.

(56) Flory, P. J.; Frost, R. S. *Macromolecules* **1978**, *11*, 1126.

(57) Tao, H.-J.; Fan, C. F.; MacKnight, W. J.; Hsu, S. L. *Macromolecules* **1994**, *27*, 1720.

(58) Leung, L. M.; Koberstein, J. T. *Macromolecules* **1986**, *19*, 706.

(59) Ryan, A. J. *Polymer* **1990**, *31*, 707.

(60) Glotzer, S. C.; Gyure, M. F.; Sciortino, F.; Antonio, C.; Stanley, H. E. *Phys. Rev. E* **1994**, *49*, 247.

(61) Clough, S. B.; Schneider, N. S.; King, A. O. *J. Macromol. Sci.-Phys.* **1968**, *B2*, 641.

(62) Harrell, L. L., Jr. *Macromolecules* **1969**, *2*, 607.

(63) Christenson, C. P.; Harthcock, M. A.; Meadows, M. D.; Spell, H. L.; Howard, W. L.; Creswick, M. W.; Guerra, R. E.; Turner, R. B. *J. Polym. Sci., Part B: Polym. Phys.* **1986**, *24*, 1401-1439.

(64) Peebles, L. H., Jr. *Macromolecules* **1976**, *9*, 58.

(65) Schneider, N. S.; Paik Sung, C. S.; Matton, R. W.; Illinger, J. L. *Macromolecules* **1975**, *8*, 62.

(66) Nitzsche, S. A.; Hsu, S. L.; Hammond, P. T.; Rubner, M. F. *Macromolecules* **1992**, *25*, 2391.

(67) Tao, H.-J.; Meuse, C. W.; Yang, X.; MacKnight, W. J.; Hsu, S. L. *Macromolecules* **1994**, *27*, 7146.

(68) Lee, H. S.; Wang, Y. K.; Hsu, S. L. *Macromolecules* **1987**, *20*, 2089.

(69) Van Gheluwe, P.; Leroux, J. *Journal of Applied Polymer Science* **1983**, *28*, 2053.

(70) Yontz, D. J.; Hsu, S. L.; Lidy, W. A.; Gier, D. R.; Mazor, M. H. *J. Polym. Sci., B Polym. Phys.* **1998**, *36*, 3065.

(71) Thomas, O.; Priester, R. D., Jr.; Hinze, K. J.; Latham, D., D. *J. Polym. Sci,. B Polym. Phys.* **1994**, *32*, 2155.

(72) Artavia, L. D.; Macosko, C. W. *J. Cell. Plast.* **1990**, *26*, 490.

(73) Priester, R. D.; McClusky, J. V.; O'Neill, R. E.; Turner, R. B.; Harthcock, M. A.; Davis, B. L. *J. Cell. Plast.* **1990**, *26*, 346.

(74) Elwell, M. J.; Mortimer, S.; Ryan, A. J. *Macromolecules* **1994**, *27*, 5428.

(75) McClusky, J. V.; Priester, R. D., Jr.; O'Neill, R. E.; Willkomm, W. R.; Heaney, M. D.; Capel, M. A. *J. Cell. Plast.* **1994**, *30*, 338-360.

(76) Neff, R.; Macosko, C. W. In *Proc. Polyurethanes, Society of the Plastics Industry*: Chicago, IL, 1995; p 344.

(77) Elwell, M. J.; Ryan, A. J.; Grunbauer, H. J. M.; Van Lieshout, H. C. *Polymer* **1996**, *37*, 1353.

CHAPTER 2

MATERIALS AND SYNTHETIC METHODS

2.1 Chapter Overview

In the previous chapter, the importance of different structural features on the phase evolution, morphology, and properties of polyurethanes was emphasized. The physical and mechanical properties are largely determined by the phase-separated morphology. The phase-separated morphology depends on a combination of thermodynamic and kinetic parameters, which are dictated by the structure. For prepolymer blends, the main structural features that may affect the phase behavior are the molecular weight distribution, repeat unit structure, end groups, and molecular architecture. For polyurethane foams, an additional feature is the excluded volume of the hard segment.

In this chapter, the three systems used to explore the structure and phase evolution of polyurethanes are presented. The first system is an example of a polyurethane hot melt adhesive. A ternary blend of a polyether prepolymer, polyester prepolymer, and an acrylic comprises the adhesive. Its synthesis by melt polyaddition is presented here. The second system is an example of a semi-crystalline polyurethane, similar to the one first prepared by Bayer. These polymers are also prepared by melt polyaddition. Finally, the last system is an example of a flexible foam. The main goal of this chapter is to present the experimental details necessary for subsequent chapters. In addition to the synthetic methods used, detailed characterization of the starting materials is described in this Chapter.

2.2 Polyurethane Hot Melt Adhesives

The influence of reaction temperature and time on the build-up of molecular weight distribution and secondary linkages will be examined for polyurethane prepolymers. These polyurethane prepolymers, based on methylenebis(phenyl isocyanate) (MDI) reacted with poly(propylene glycol) (PPG) and a polyester such as poly(hexamethylene adipate) (PHMA) or poly(hexamethylene sebacate) (PHMS) are two of the components of a hot melt adhesive. The third component is a copolymer of methyl methacrylate and *n*-butyl methacrylate (P(MMAnBMA)). Their structures are shown in Figure 2.1. While this particular blend is used in hot melt adhesive application, prepolymers are used to prepare elastomers and coatings, as well. Thus, prepolymer synthesis and characterization is of fundamental importance to many applications.

In this blend, the polyether and polyester prepolymers provide reactive functional groups (see Chapter 1 Figure 1.2) for curing with water. Crystallization of the polyester increases the set speed.[1] The elastic polyether toughens the joints. The acrylic copolymer, due to its high molecular weight, increases the green strength (viscosity in the melt) and, due to its high T_g, increases the toughness.[2] The acrylic has also been found to be critical to providing compatibility in some of the blends.[3]

The prepolymers are prepared by melt polyaddition. Because the main purpose of studying these prepolymers is to quantitatively determine the structures that are formed, their starting materials must also be fully characterized. Prior to synthesis, the end groups and molecular weight distribution of the starting materials were determined using a combination of matrix assisted laser desorption ionization time of flight mass spectrometry (MALDI-TOF), size exclusion chromatography (SEC), and ^{13}C and ^{1}H nuclear magnetic

PPG

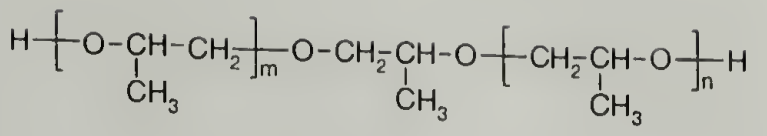

PHMA

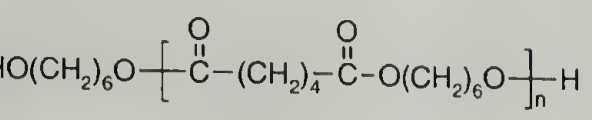

PHMS

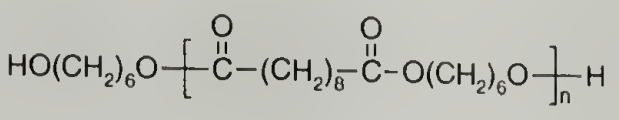

MDI

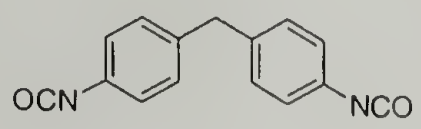

P(MMAnBMA)

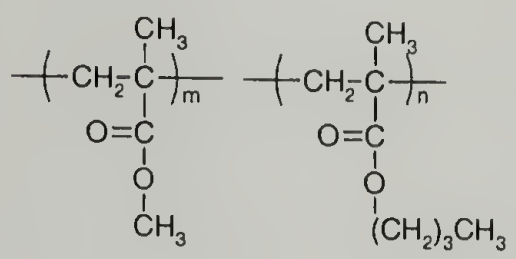

Figure 2.1 Chemical structures of raw materials used to prepared polyurethane prepolymers.

resonance spectroscopy (NMR). These details of the starting materials will be presented first, followed by the synthetic methods to prepare the prepolymers.

2.2.1 PPG

PPG was obtained from Arch Chemical (PPG 2056). It is a liquid at room temperature. The hydroxyl value is reported as 56 mg KOH/g. M_n can be calculated from

the hydroxyl value (HV), assuming all species are terminated with two hydroxyl groups using Equation 2.1.

$$\frac{1}{M_n} = \frac{HV mg_{KOH}}{g_{polymer}} \cdot \frac{mmol_{KOH}}{58 mg_{KOH}} \cdot \frac{mmol_{OH}}{mmol_{KOH}} \cdot \frac{mmol_{polymer}}{2 mmol_{OH}} \cdot \frac{1}{1000} \qquad (2.1)$$

Equation 2.1 gives M_n = 2000 g·mol^{-1}. PPG is prepared by anionic ring opening polymerization of propylene oxide.[4] Depending upon the specific initiator and terminating agent, the chain ends can be either primary or secondary hydroxyls. This PPG, specifically for polyurethane prepolymers, is reportedly terminated with secondary hydroxyls. The chemical structure shown in Figure 2.1 was determined by MALDI-TOF, as will be described below. Because primary hydroxyls are more reactive than secondary hydroxyls, the end groups need to be confirmed.

NMR spectroscopy was used for end group analysis. All spectra were recorded on a Bruker DPX300. Distortionless enhancement by polarization transfer (DEPT)[5] can be used to distinguish ^{13}C resonances associated with methynes and methyl groups from those associated with methylene groups. The DEPT spectrum obtained with a 135° pulse is shown in Figure 2.2 for PPG in $CDCl_3$ and compared to the ^{13}C spectrum. A 135° pulse results in positive CH and CH_3 groups and negative CH_2 groups. The resonances corresponding to the methylene and methyne within the repeat are found between 72 and 76 ppm (positions are calibrated to $CHCl_3$ triplet at 77.2 ppm). Carbons alpha to an OH should be found further upfield than those adjacent to an ether oxygen.[6] The small doublet of doublets at 66.63 ppm (J=2.8 and 121.5 Hz) corresponds to these terminal carbons. DEPT 135 shows that they are indeed methyne.

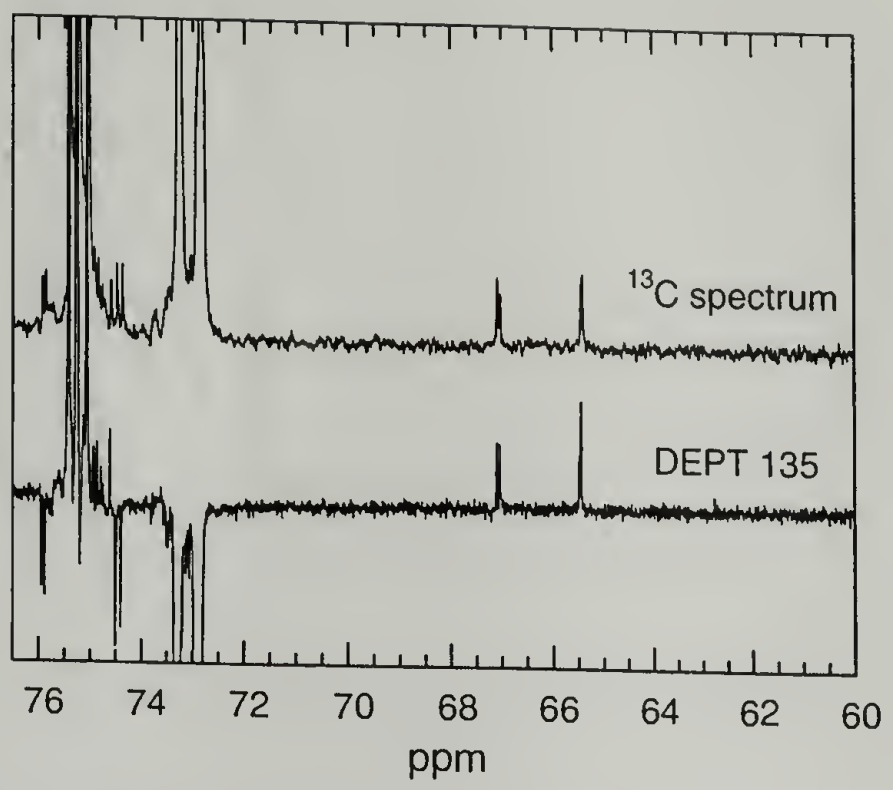

Figure 2.2 ^{13}C and DEPT 135 NMR spectra of PPG.

While all the hydroxyl end groups are secondary, not all the end groups are necessarily hydroxyl groups. Chain transfer to monomer occurs readily during synthesis.[4] Chain transfer involves proton abstraction from the methyl groups attached to the monomer, followed by ring cleavage to give allyl alkoxide. This species can isomerize to the enolate anion. Both species are shown in Figure 2.3. Allyl alkoxide and its enolate anion can initiate further polymerization, resulting in monofunctional chains. Protons attached to alkenes exhibit distinct resonances in the region between 5 and 6.5 ppm. ^{1}H NMR spectroscopy of PPG in acetone-d_6 reveals a doublet of doublets (J=105 and 8.5 Hz) and a multiplet at 5.19 and 5.90 ppm, respectively. Based on the expected splitting for each isomer, these resonances correspond to allyl and 1-propenoxy groups, respectively.

The amount of each type of end group can be determined if resonances from all three species were observed (hydroxyl, allyl, and propenoxy). Unfortunately, in acetone-d_6, the methyne alpha to the hydroxyl cannot be resolved from the protons associated

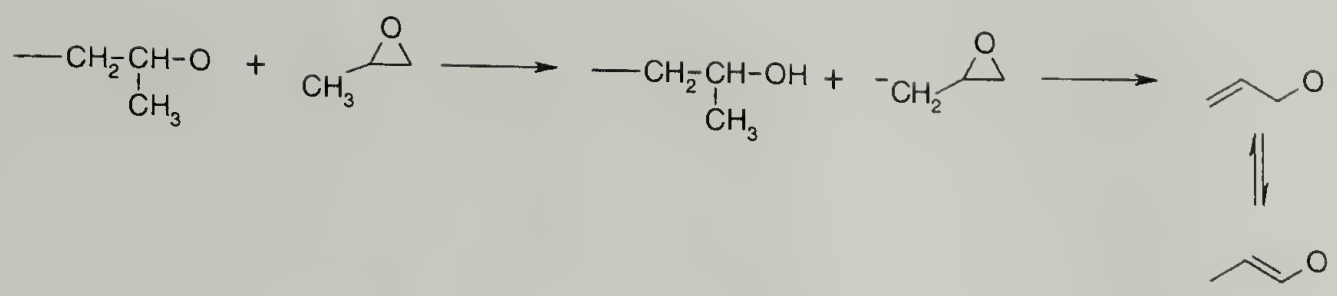

Figure 2.3 Chain transfer to monomer during anionic polymerization of propylene oxide.

with the backbone. However, if pyridine-d_5 is used as a solvent instead, the resonance from the terminal methyne is shifted significantly downfield.[7] In this case, the contribution from each end group can be determined by integration (after accounting for the number of protons associated with each peak). The amount of hydroxyl, allyl, and 2-propenoxy is 95.10, 2.62, and 2.28 mole %, respectively.

MALDI-TOF mass spectrometry was also used to analyze PPG. MALDI-TOF mass spectra were recorded using a Bruker Daltonics Reflex III operating in linear mode using 24 kV acceleration voltage and 337 nm laser excitation. Solutions of 10 $mg \cdot ml^{-1}$ PPG in $CHCl_3$ and 30 $mg \cdot ml^{-1}$ dithranol in $CHCl_3$ were prepared and mixed together by volume in the ratio 1:10. 1 μL of this solution was spotted onto a stainless steal target where sodium trifluoroacetate had been predeposited from MeOH. The results are shown in Figure 2.4 in the range from 250 to 3000 m/z. Two different distributions are evident, one with low molecular weight and one with high molecular weight. The peaks in each distribution are separated by 58 m/z, the mass of a repeat unit. If the mass of Na is subtracted from each peak, assuming the species are Na adducts, and the results are divided by 58x, where x is integer, the remainder for each species is 18 and 0. These values correspond to what is expected for the structure of PPG diol and monofunctional

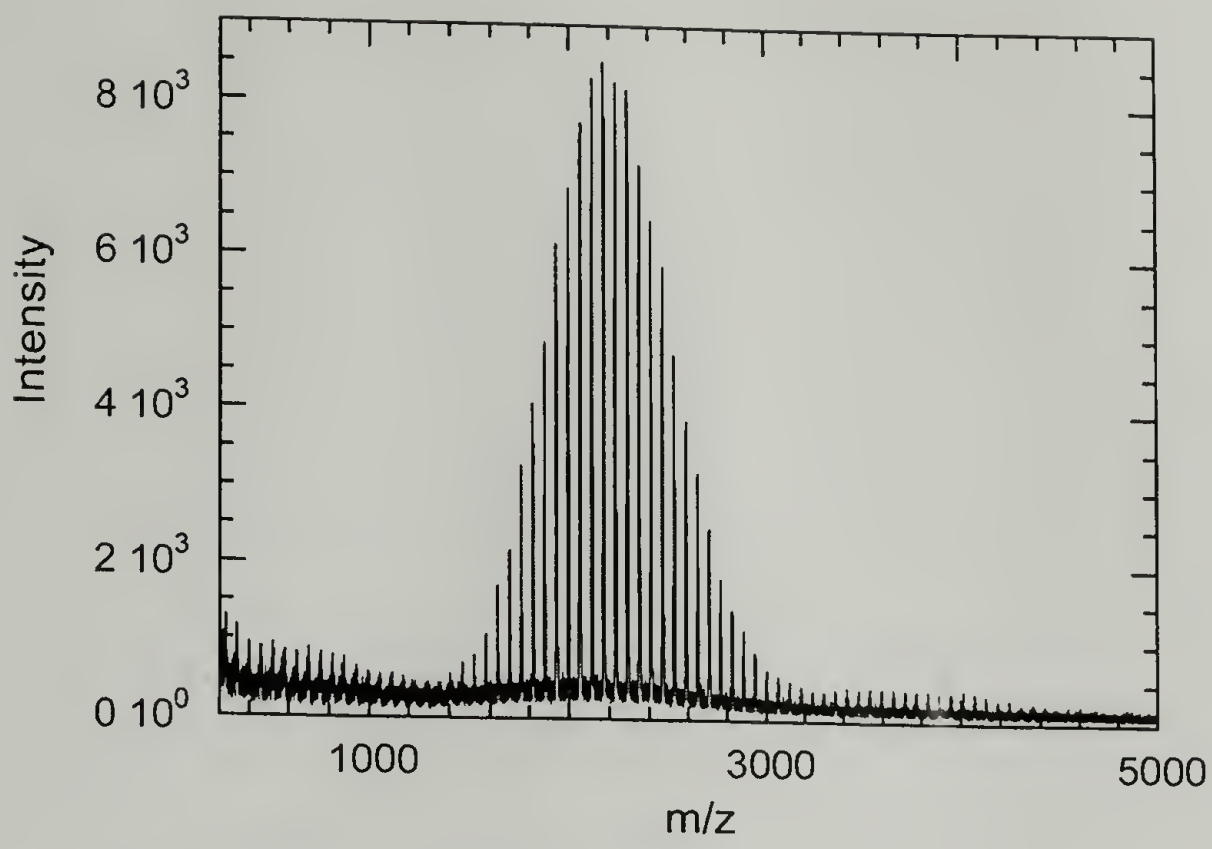

Figure 2.4 MALDI-TOF mass spectrum of PPG.

PPG. The lower molecular weight distribution arises from the monofunctional species. The main distribution shows a high molecular weight tail.

The intensity observed in MALDI-TOF is related to the number of each species present. Using the integrated intensity of each peak, M_n and M_w can be calculated for both distributions and for the entire sample. Including both components M_n=1905 $g \cdot mol^{-1}$ and PDI = 1.05. The amount of monofunctional species is in the range from 2.5 to 5 mole %, which agrees well with the results from ^1H NMR.

2.2.2 Polyesters

PHMA is sold under the trade name Dynacoll 7360 from DeGussa. The melting point is 55 ˚C, and the hydroxyl value is between 27-34 mg KOH/g. This range of hydroxyl values gives M_n = 4300-3400 $g \cdot mol^{-1}$, assuming all species contain two

hydroxyl chain ends. In contrast to PPG, PHMA is prepared by step polymerization. In principle, adipic acid is reacted with an excess of 1,6-hexanediol to obtain the alcohol-terminated product. In practice, polyesters are rarely synthesized by direct reaction of diacid with diol. Nonetheless, one of the major end group impurities is an acid end group. The presence of acid end groups is detectable by titration procedure.[8] The acid number of PHMA is less than 0.034 mmol CO_2H per g polymer (less than 2 mg KOH/g).

The MALDI-TOF mass spectrum of PHMA is shown in Figure 2.5. The conditions were the same as for PPG. The distribution has a different shape than that observed for PPG, typical of step versus chain polymerization. The mass of a repeat unit is 228 $g \cdot mol^{-1}$, and each peak in the mass spectrum is separated by 228 m/z. At least three different distributions are observed. The mass, intensity, number fraction, and weight fraction of these three distributions is shown in Table 2.1.

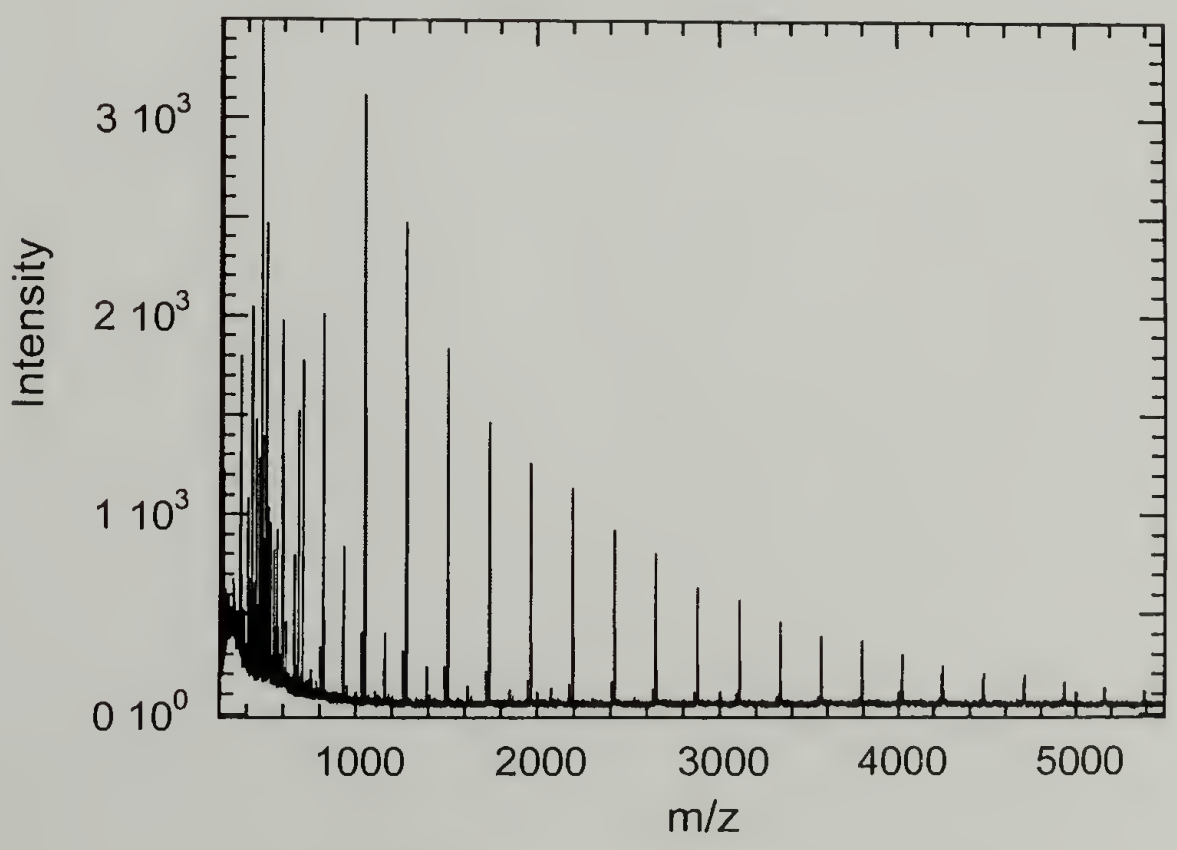

Figure 2.5 MALDI-TOF mass spectrum of PHMA.

Table 2.1 Data obtained from MALDI-TOF of PHMA

Distribution 1		Distribution 2		Distribution 3	
M_i (m/z)	Intensity	M_i (m/z)	Intensity	M_i (m/z)	Intensity
369	1504	351	153.86	251	1395.6
597	1835	579	279.95	479	3724.8
826	1930	807	254.19	707	1678
1054	3067	1036	359.01	936	720.46
1282	2431	1264	273.3	1164	352.47
1510	1793	1492	201.62	1392	195.17
1739	1416	1721	172.43	1621	98.93
1967	1215	1949	126.49	1849	78.12
2195	1087	2177	103.39	2077	88.58
2423	876	2407	116.68	2306	38.5
2652	758	2634	82.62	2535	43.99
2880	588	2862	67.28		
3109	524	3092	57.78		
3337	425	3319	51.53		
3565	340	3548	40.24		
3793	321	3775	39.31		
4021	257	4004	43.5		
4250	196	4235	36.39		
4479	164	4458	34.75		
4706	153				
4935	115				
5162	90				
5391	78				
5620	73				
5847	57				
6074	47				
6302	40				
M_n	1735		1613		638
M_w	2505		2252		869
%	66		8		26

The overall M_n = 1440 g·mol^{-1} and PDI = 1.6, which is less than the predicted value of 2. The higher molecular weight species may not be completely accounted. The three distributions have M_n = 1735, 1615, and 638 g·mol^{-1}. The main component is obviously from the polyester diol. Accounting for the end groups and Na, these species would obey the relation 141 + 228x, which is true. Several other structures are candidates for the other two distributions. One possibility is the structure with one acid end group, 41 + 228x. However, the masses of neither distribution correspond to this structure.

Another possibility is a cyclic product. Cyclization always competes with linear polymerization in step polymerization.[9,10] A cyclic structure is composed only of repeat units, so only the mass of Na needs to be added: 23 + 228x. This equation indeed describes the lower molecular weight distribution ("Distribution 3"). Finally, the last distribution may correspond to a monofunctional species, where one of the chain ends has been dehydrated, leaving a double bond: 123 + 228x.

The data is shown more clearly in Figure 2.6 where the intensity for each distribution is plotted versus the degree of polymerization (Xn), determined based on the expected mass. As defined here, a species with a repeat unit composed of an adipate and a hexane diol has X_n = 1, whether it is terminated by another hexanediol or by connecting to itself. The amount of difunctional, monofunctional, and cyclic species is 66, 8, and 26 mole %, respectively. This is a significant amount of cyclic material. Cyclic dimers are the most abundant of these species.

^{1}H NMR also confirmed that the amount of cyclic species in this sample was very high. The integrals from (1) resonances from the internal adipate methylene at 1.25 ppm (2x protons found in all species, where x is the number of repeat units), (2) terminal

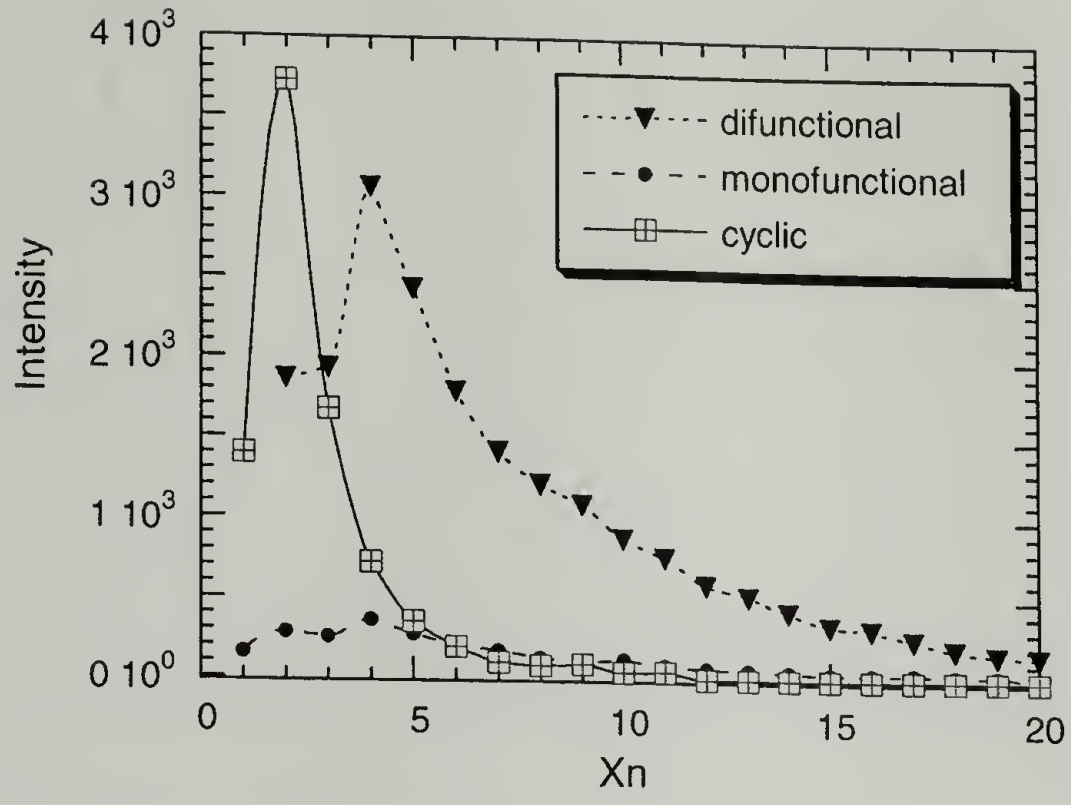

Figure 2.6 Distributions of different species found in PHMA by MALDI-TOF.

methylene alpha to alcohol at 3.71 ppm (4 found in difunctional species, 2 found in monofunctional species), and (3) terminal alkene CH_2 at 4.8 ppm (2 found in monofunctional species) can be used to determine the amount of each species. The average number of repeat units was determined from MALDI-TOF. ^{1}H NMR gives 56, 12, and 32 mole % of each species. These values are in qualitative agreement with MALDI-TOF data. The sample contains a significant amount of cyclic structures.

The large amount of cyclic material may be one of the reasons the molecular weight determined by the hydroxyl value, where all species are assumed to have two hydroxyl chain ends, was so much higher. If for every g of polymer, 1.4 mmol of OH is assumed instead of 2, the hydroxyl values from 27-34 give M_n = 2900-2300 g·mol^{-1}, in much better agreement with the observed M_n. An additional reason the MALDI-TOF gives a lower M_n may be due to a mass bias towards lower oligomers, due to both

instrumental and ionization effects. This has been previously observed for polyesters in this molecular weight range using similar conditions. [11,12]

The other polyester, PHMS, is sold under the trade name Dynacoll 7381 from DeGussa. The melting point is 65 °C, and the hydroxyl value is also between 27-34 mg KOH/g. PHMA was analyzed using MALDI-TOF in the same way as PHMA. Similarly, difuntional, monofunctional, and cyclic structures were observed. M_n = 14o0 and PDI = 1.5. As discussed for PHMA, these measured values may be lower than actually exists due to MALDI-TOF conditions. The amount of difunctional, monofunctional, and cyclics is 63, 4, and 32 mole %, respectively.

2.2.3 P(MMAnBMA)

The acrylic copolymer is sold under the trade name Elvacite 2013 from Ineos. Its Tg = 80 °C. P(MMAnBMA) is prepared by emulsion polymerization of methyl methacrylate (MMA) and n-butyl methacrylate (BMA). For this reason, it can be quite wet. Its composition was determined by ^{1}H NMR and is 0.75 and 0.25 mole fraction of MMA and nBMA, respectively.

The molecular weight of this material is quite high, which made MALDI-TOF difficult. Instead, the molecular weight distribution was determined using SEC relative to PMMA standards. SEC was carried out with a Waters 510 HPLC pump equipped with three columns from Polymer Labs, Inc., having 5 μm bead size (two with MIXED-D and one with 50 Å pore sizes). THF was used as the eluent. A Waters R401 differential refractometer was used as the detector. SEC showed M_w = 30,900 g·mol^{-1}.

2.2.4 MDI

MDI was used as received from Aldrich (98%). The molecular weight of MDI is 250.3 $g \cdot mol^{-1}$. Its purity was checked prior to use using the ASTM standard procedure. [13] A solution of butyl amine in toluene was prepared with a concentration of approximately 2 M. The solution was dried and stored over 4 Å molecular sieves. Prior to determining the NCO content of MDI, a known volume of dibutyl amine solution (e.g. 2.0 mL) was diluted with isopropanol, and the actual concentration determined by titration with 0.1 M HCl to its bromophenol blue endpoint. A known volume of this dibutyl amine solution was added in molar excess to a solution of MDI in dry toluene. The solution was stirred at room temperature for 10 min. The resulting urea typically precipitated from the solution. Isopropanol was added until the solution was clear, and the remaining dibutylamine was titrated with 0.1 M HCl to its bromophenol blue endpoint. Based on the amount of dibutyl amine remaining, the NCO content can be determined. The NCO content of MDI was determined as 7.84 mmol NCO per g MDI (98% pure). Infrared spectroscopy shows a peak at 1776 cm^{-1}, which comes from MDI dimer, uretidinedione. This was the only impurity evident.

MDI was stored in the refrigerator. The melting point of pure MDI is 37 °C. When the concentration of uretidinedione is low, it can be removed by melting the sample. The dimer either decomposes to MDI, or material remains unmelted and can be removed by a syringe filter prior to injection. As the concentration of uretidinedione increases, the molecular weight of MDI can increase. Particularly old samples were observed to yellow, and these samples remained solids at temperatures as high as 120 °C. Presumably this is due to the formation of dimer or trimer polymers.

2.2.5 Prepolymer Synthesis

Prepolymers were prepared under a variety of conditions. Reaction temperatures from 75 to 145 °C and reaction times from 0.2 to 20 h were used. For some of the prepolymers, the cure catalyst 4,4-(Oxydi-2,1-ethanediyl)bismorpholine (DMDEE) was added. DMDEE was used as received from Aldrich. Its structure is shown in Figure 2.7. The molecular weight is 244.3 $g \cdot mol^{-1}$. Polymers were prepared from a single macrodiol or from the blend. A defoaming agent, either Modaflow or Resiflow, was used for ternary blends. Two main procedures were used, depending on the melt viscosity of the components. These are described below.

Prepolymers prepared from PPG maintain a fairly low viscosity for reaction times under 10 h, and thus a magnetic stir bar can be used for synthesis. A typical procedure is as follows. A three-neck round bottom flask equipped with a stir bar, a nitrogen/vacuum adapter, and a rubber septum was charged with 20.0 g (19.99 mmol OH) of PPG. The system was evacuated to 100 mTorr and degassed by successive cycles of nitrogen fill/vacuum evacuation for at least 2 h at 100°C. The water content at this point was found to be below the Karl Fisher limit (<0.02 wt%).[14] Sometimes a liquid was observed

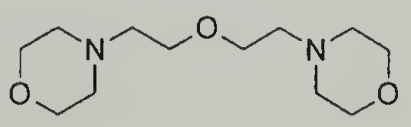

Figure 2.7 Structure of the cure catalyst 4,4-(Oxydi-2,1-ethanediyl)bismorpholine (DMDEE).

to condense on the surface of the flask. Infrared spectroscopy showed that this was PPG, most likely of low molecular weight. After 2 h, the system was either evacuated and closed at 100 mTorr or filled and maintained under constant N_2 pressure, and then it was equilibrated at the reaction temperature. Next, 4.18 g MDI (32.74 mmol) was added in one of two ways: melted in a syringe and then added to the evacuated system or simply added as a solid to the system under positive pressure. The reaction was then stirred under an inert atmosphere for the desired reaction time. At the end of the reaction, several aliquots were removed, weighed, and titrated with dibutyl amine to determine their NCO content, as discussed in Section 2.2.5. The remaining prepolymer was added to dry MeOH and stirred for 24 h, in order to end cap the unreacted NCO groups. [15] The end-capped prepolymer was recovered via rotary evaporation. Samples prepared under conditions yielding a large amount of MDI monomer were white due to precipitated MeOH end-capped MDI. Typical samples were initially clear, but yellow with time.

Prepolymers prepared from the polyesters or the ternary blend have a much higher melt viscosity and require a mechanical stirrer for their synthesis. In addition, since these materials are solid upon cooling, they cannot be easily transferred from a glass reaction flask to a storage container. Thus a special reaction vessel was constructed to prepare these prepolymers, as shown in Figure 2.8. The bottom half of the reactor is an aluminum vessel in which a 1 pint epoxy-coated paint can be placed. The top half is the lid from a standard, glass 3-necked reaction flask. The two are sealed together using a rubber O-ring and a clamp. This vessel can be evacuated to pressures as low as 500 mTorr. The temperature was controlled using heating tape wrapped around the outside of the vessel.

A typical prepolymer synthesis is as follows. Prior to synthesis, the materials were stored in a vacuum oven at 42 °C. Into a 1-pint epoxy-coated, stainless steel paint can was added, 158.31 g PPG (158 mmol OH), 158.31 g PHMA (105 mmol OH), 126.82 g P(MMAnBMA), 0.66 g Modaflow, and 0.66 g DMDEE. The can was placed into the reaction vessel, and the vessel was closed and clamped. The reaction vessel was equipped with: (1) A thermocouple pushed through the center of a syringe needle, and inserted into the reaction mixture through a rubber septum, (2) a mechanical stirrer, and (3) a N_2/vacuum adapter. Without stirring, the reaction vessel was evacuated to 500 mTorr and degassed by successive cycles of nitrogen fill/vacuum evacuation. This step requires care to avoid splashing. The reaction mixture was dried by heating at 100 °C (monitored by thermocouple) under vacuum for 2.0 h. Usually a material was observed to condense on

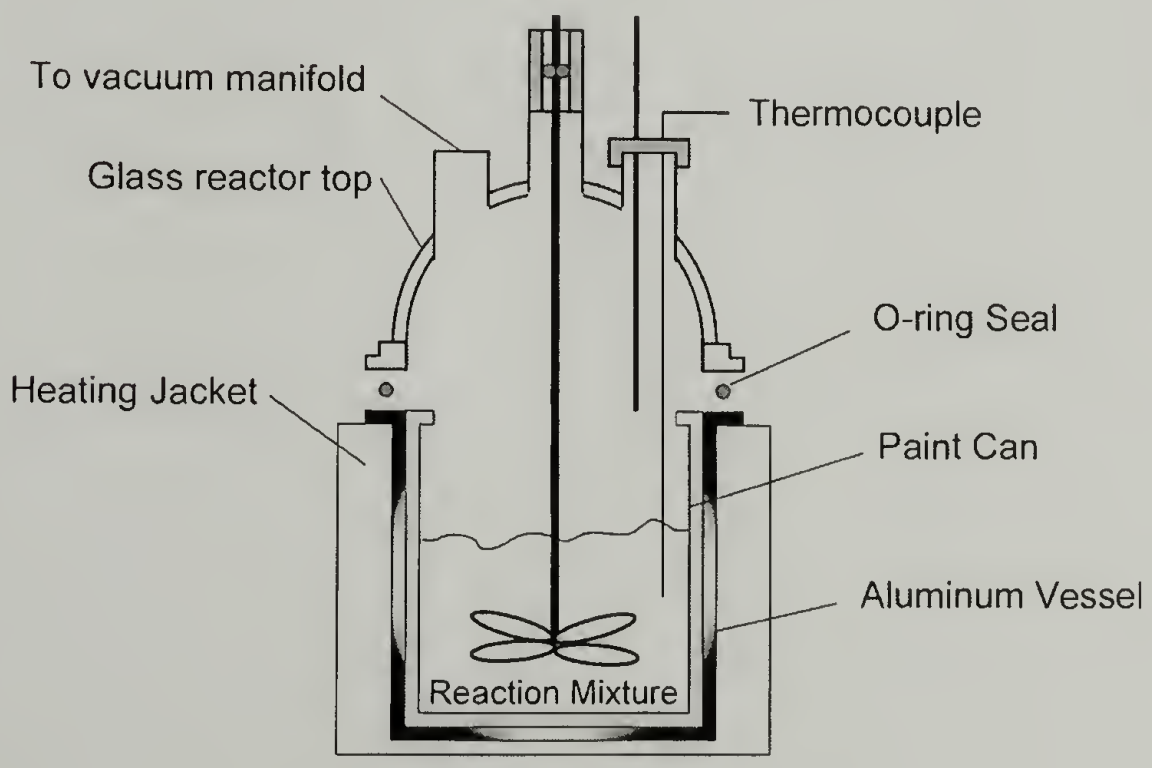

Figure 2.8 Schematic of the reactor used to prepare viscous polyurethane prepolymers.

the top of the glass reactor. Upon cooling, this material was a solid. Infrared spectroscopy showed that the material was a mixture of PHMA and PPG.

After 2.0 h, the reaction mixture was equilibrated at the desired reaction temperature, Meanwhile, 55.41 g (443 mmol NCO) MDI was added to a glass syringe, which was wrapped with heating tape. The MDI was melted in the syringe by heating to 80 °C. The reaction mixture was closed from vacuum, the mechanical stirrer was turned on, and the MDI was added via syringe through the rubber septum. This step requires great care, as MDI is highly toxic. Usually a second person helped by heating the syringe needle with a heat gun. The reaction mixture was then stirred by mechanical stirring for the desired reaction time. At reaction completion, the mechanical stirrer and thermocouple were removed from the reaction mixture, the vessel was pressurized with N_2, and the mixture was allowed to cool under N_2. The can was sealed and stored under N_2. The product was a tough, slightly yellow/orange solid.

2.3 Aliphatic, Semi-crystalline Polyurethanes

The influence of hydrogen bonding on polyurethane order formation was examined using a series of aliphatic polyurethanes, as shown in Figure 2.9. The phase behavior of polyurethanes is often attributed to the hydrogen bonding characteristics of the system. The polymers shown in Figure 2.9 were used to determine the correlation between hydrogen bonding and crystallization behavior. Their well-defined structures are ideal candidates for this study because the contribution from hydrogen bonding will depend upon the periodicity between functional groups, which can be controlled with X = 12, 22, and 32. However, a large contribution from secondary linkages such as

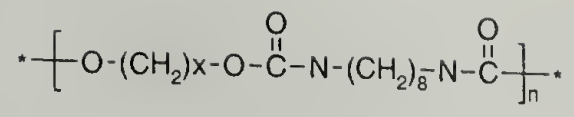

Figure 2.9 Chemical structure of X,8-polyurethanes.

allophanates or alcohol end groups, both of which also form hydrogen bonds, would make correlations within the series meaningless. Therefore the polymers were fully characterized.

The synthesis of these polymers has been reported.[16] The polymers were prepared from the corresponding diol and 1,8-octanediisocyanate. 1,12-Dodecanediol and the diisocyanate are commercially available. 1,22-Docosanediol and 1,32-dotriacontanediol were prepared according to literature procedures.[16] The polymers were prepared in the melt by step polyaddition of equimolar amounts of diol and diisocyanate. The appropriate polymerization temperature is critical and must be high enough to melt the diol, but low enough to prevent the formation of secondary linkages, such as allophanates. 12,8 PU, 22,8 PU, and 32,8 PU were polymerized at 100, 120, and 130 °C, respectively.

A combination of infrared, NMR, and SEC was used to determine the structure. These polymers are generally insoluble in most solvents. Hot, polar solvents such as DMSO, m-cresol, DMF, and o-dichlorobenzene dissolve the X,8 PU's. In addition, a mixture of 1:1 (v/v) $CHCl_3$ and trifluoroethanol dissolved 22,8 PU at room temperature. Due to the limited solubility of these polymers, SEC was carried out on a Polymer Laboratory PL-GPC 220 ultra high temperature chromatograph with a Hewlett-Packard 1100 series isocratic pump and a set of 200 μm MIXED-A columns. The system was equipped with a Polymer Labs, Inc., differential refractive index detector, Viscotek

viscometer, and Wyatt Technology heated miniDAWN light scattering detector. Experiments using this system could be carried out at 135 °C using 1,2,4-trichlorobenzene as the mobile phase.

The results from SEC are shown in Table 2.2. The molecular weights are fairly high, but considering the high molecular weight per repeat unit, the average number of repeat units is 28, 25, and 98 for 12,8 PU, 22,8 PU, and 32,8 PU, respectively. The polydispersity is in the range that is expected for a step polymerization.

Table 2.2 Molecular weights of the X,8-polyurethanes

X,8 PU	MW repeat unit	$Mn \cdot 10^{-3}$	PDI	dn/dc
12,8	398.6	11.4	1.9	-0.031
22,8	538.8	13.8	2.0	-0.071
32,8	679.1	63.8	2.2	-0.069

The spectra obtained by infrared and NMR were consistent with the structures shown. However, in the case of 32,8 PU, infrared spectroscopy suggested that the sample may have contained some allophanate linkages, evident by additional contributions in both the Amide I and N-H stretching region. This is consistent with the higher PDI observed for this sample. Attempts to remove the impurity by crystallization from DMF were unsuccessful.

2.4 Polyurethane Foams

The role of hard segment anisotropy on morphology development was examined in polyurethane foams. The hard segment distribution of hydrolyzed plaques will be

determined in order to understand the statistics governing hard segment formation. This information was transferred to a reactive system, where structural evolution based on two different diisocyanates was studied. The materials and procedure for preparing the plaques is presented here first. This is followed by a discussion of the two different diisocyanates.

2.4.1 Preparation of Plaques

The procedure for preparing polyurethane foams in a plaque geometry under isothermal conditions has been previously reported.[17] The materials necessary are shown in Figure 2.10. The polyether used to prepare foams was Voranol® 3137 (V3137) from Dow Chemical Company and is a glycerin initiated poly(propylene oxide) polyether with ~13% ethylene oxide randomly polymerized into the chain, terminated with secondary hydroxyl groups. It has an equivalent weight of 1075 $g \cdot mol^{-1}$ OH and an average functionality of 2.79. The molecular weight and sequence length distribution have been characterized by MALDI-TOF.[18] The diisocyanate used to make plaques was T-80, an 80/20 (v/v) mixture of 2,4-toluenediisocyante (TDI) and 2,6-TDI (T80, Aldrich, tech, 80%). The catalyst package used in this study was a mixture of Dabco® BL-11 (Air Products), Dabco® 33-LV (Air Products), and Dabco® T-9 (Air Products). Dabco® BL-11 is composed of 70% bis(dimethylaminoethyl) ether in a solution of dipropylene glycol. Dabco® 33-LV is a solution of 1,4-diazobicyclo[2,2,2]octane (33%) in dipropylene glycol. Dabco® T-9 is a stannous octanoate. All materials were used as received. The general naming scheme is "(H_2O/OH)-(T_{rxn})".

V3137

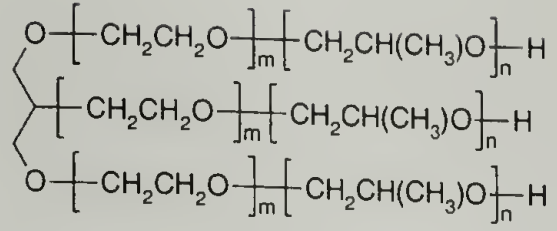

T-80

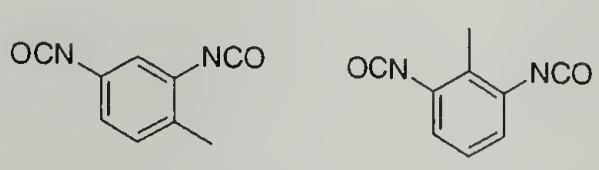

Figure 2.10 Chemical structures of raw materials used to prepared polyurethane plaques and foams.

A typical procedure is as follows. A steel mold was placed inside a melt press and equilibrated at the desired reaction temperature for at least 1.0 h. Prior to reaction, the mold was removed from the melt press and the inside surfaces were sprayed with Fluoroglide, a mold release agent. A stock mixture of BL-11 and 33-LV was prepared in a 1:2 ratio by weight and stored in the refrigerator until use. 10.0007 g of Voranol 3137 and 0.0301 g of stock amine catalysts were mixed with a glass rod in a plastic beaker. In separate syringes, 0.3603 g of deionized H_2O and 4.4112 g of T-80 were weighed, accounting for the volume that remains in the syringe after ejection. Immediately prior to reaction, 0.0140 g T-9 was added to the plastic beaker and mixed. H_2O was added via the syringe and stirred hard with a glass rod for 2 minutes, at which point the mixture became clear. Next, the TDI was added rapidly and stirred hard for 15 s. After 15 s, foaming was observed. The foaming mixture was poured into the hot mold, the lid was replaced, and the mold was returned to the melt press. After 3 min, 15000 psi was applied to the mold and held for 60 min. The mold was cooled with water, and the plaque removed.

2.4.2 Hard Segments Based on TDI's

The two different diisoeyanates are pure 2,6-TDI and T-80 TDI. An example of the types of hard segments expected from these two different diisoeyanates is shown in Figure 2.11. As discussed in Chapter 1, one mechanism for phase separation is the entropie eontribution from these rigid moleeules. The hard segments based on these two different diisoeyanates are expected to exhibit different orientation dependant excluded volume, herein simply "anisotropy." In liquid erystals, the liquid crystalline phase ean be suppressed by the addition of co-units or asymmetric units, whieh increase the melt entropy.[19] The differenee between the two hard segments is in the placement of the methyl groups. In 2,6-TDI based systems, the methyl group is placed symmetrically between the two urea groups. In T-80 based systems, the methyl group is placed asymmctrically, incorporated with different head-to-head or head-to-tail configurations, and eopolymerized with 2,6-units. While the struetures are drawn in a linear fashion, they may, in fact, be bent and frce to rotate. The question is how big the effeet of methyl

2,6-TDI

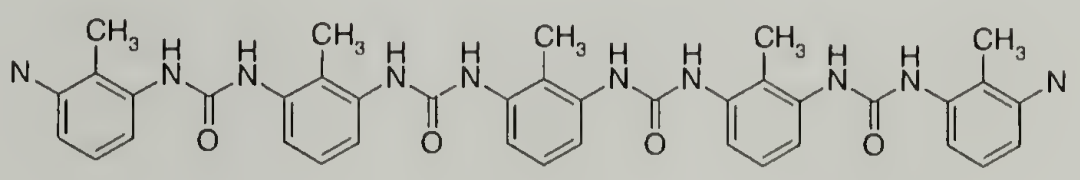

T-80-TDI

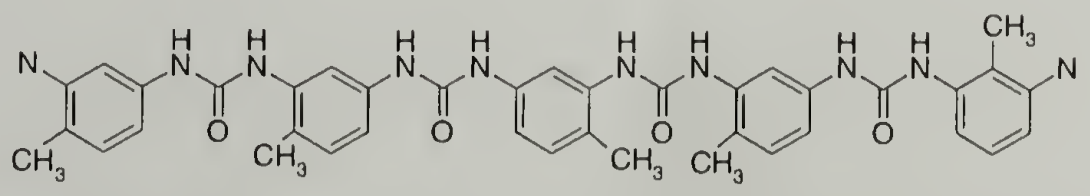

Figure 2.11 Examples of the types of hard segments expected from 2,6-TDI and T-80.

groups is. This effect can be estimated by comparing the melting point of 2,6-diamine toluene and 2,4-diamine toluene. The melting point of the symmetric diamine (2,6-) is 20 ˚C higher than that of the asymmetric diamine (2,4-). The melting points are 120-122 and 97-99 ˚C, respectively.

2.5 Conclusions

This chapter presented the polyurethane systems that were used to study aspects of structure and morphology development. Polyurethane prepolymers, specifically formulated for hot melt adhesives but also relevant to other applications, were presented as a model system for studying the effect of processing variables on the build-up of molecular weight distribution and structure. Semi-crystalline polyurethanes with periodic placement of urethane groups were presented as a model system for studying the effect of hydrogen bonding on order formation. The molecular weight of these polymers was determined to be high enough to neglect the end groups. Finally, polyurethane foams and, specifically, the two different diisocyanates, were presented as a system to understand the combination of reaction, structure formation, and morphology development in reactive systems. In addition, the synthetic methods for preparing the polymers were described.

2.6 References

(1) Fernandes, E. G.; Lombardi, A.; Solaro, R.; Chiellini, E. *J. Appl. Polym. Sci.* **2001**, *80*, 2889.

(2) De Genova, R. D.; Harper, M. D.; Clay, W. A.; Cranley, P. E.; Hunter, M. K. *TAPPI J.* **1996**, *79*, 196.

(3) Duffy, D. J.; Stidham, H. D.; Hsu, S. L.; Sasaki, S.; Takahara, A.; Kajiyama, T. *J. Mater. Sci.* **2002**, *37*, 4801.

(4) Odian, G. *Principles of Polymerization*; Wiley: New York, 1991.

(5) Braun, S.; Kalinowski, H.-O.; Berger, S. *100 and More Basic NMR Experiments*; VCH: New York, 1996.

(6) Silverstein, R. M.; Webster, F. X. *Spectrometric Identification of Organic Compounds*; 6th ed.; Wiley: New York, 1998.

(7) Sievers, R. E.; Rondeau, R. E. *J. Am. Chem. Soc.* **1971**, *93*, 1522.

(8) *Annual Book of ASTM Standards* **2000**, *08.03*.

(9) Jacobson, H.; Stockmayer, W. H. *J. Chem. Phys.* **1950**, *18*, 1600.

(10) Jacobson, H. B., C.O.; Stockmayer, W.H. *J. Chem. Phys.* **1950**, *18*, 1607.

(11) Mehl, J. T.; Murgasova, R.; Dong, X.; Hercules, D. M.; Nefzger, H. *Anal . Chem.* **2000**, *72*, 2490.

(12) Murgasova, R.; Brantley, E. L.; Hercules, D. M.; Nefzger, H. *Macromolecules* **2002**, *35*, 8338.

(13) *Annual Book of ASTM Standards* **2000**, *08.03*, D5155-5110.

(14) *Annual Book of ASTM Standards* **1996**, *15.05*, E203-296.

(15) Christenson, C. P.; Harthcock, M. A.; Meadows, M. D.; Spell, H. L.; Howard, W. L.; Creswick, M. W.; Guerra, R. E.; Turner, R. B. *J. Polym. Sci., B Polym. Phys.* **1986**, *24*, 1401-1439.

(16) McKiernan, R. L.; Gido, S. P.; Penelle, J. *Polymer* **2002**, *43*, 3007.

(17) Yontz, D. J.; Hsu, S. L.; Lidy, W. A.; Gier, D. R.; Mazor, M. H. *J. Polym. Sci., B Polym. Phys.* **1998**, *36*, 3065.

(18) Suen, W.; Percy, J.; Hsu, S. L. *Macromolecules* **submitted**.

(19) Ciferri, A. In *Polymer Liquid Crystals*; Ciferri, A., Ed.; Academic Press, 1982.

CHAPTER 3

MOLECULAR WEIGHT DISTRIBUTIONS

3.1 Chapter Overview

This chapter discusses molecular weight distributions in step polymerization, an old topic in polymer science in which many theories have been developed. Only recently has instrumentation advanced to allow experimental verification of these theories. In this chapter, the molecular weight distribution of polyurethane prepolymers is determined quantitatively using a combination of MALDI-TOF and SEC. Under homogeneous reaction conditions, the prepolymer should obey a most probable molecular weight distribution. For the first time, this assumption is confirmed experimentally for PPG prepolymers. The influence of secondary reactions on perturbing the molecular weight distribution will be examined in Chapter 4. The molecular weight of polyurea hard segments obtained from solution polymerization are compared with those obtained from hydrolyzed plaques. The hard segment length distribution of plaques is abnormally narrow, indicating the importance of miscibility behavior on controlling the local stoichiometry. The molecular weight distribution of polyurea prepared under homogeneous conditions follows the Schultz-Flory distribution, but is narrower and with a lower average molecular weight than predicted.

3.2. Molecular Weight Distributions in Polyurethane Systems

As discussed in Chapter 1, the molecular weight distribution of polyurethane structural elements (macrodiols, polyols, prepolymers, and polyureas) influences both the

physical and mechanical properties of the final material. This chapter is concerned with experimental determination of molecular weight distributions of polyurethane prepolymers and polyurea hard segments. While changes in the average molecular weight have been frequently determined, the molecular weight distribution of prepolymers and polyurea components has rarely been determined experimentally. In this Chapter, a homo-prepolymer based on PPG will be examined. In addition, the polyurea hard segments will be isolated from a foam and compared with those formed under identical stoichiometry but in solution.

3.2.1 Theoretical Description

The molecular weight distribution of an ideal step polymerization, where reaction can occur randomly between the two reactive functional groups, will obey the Schultz-Flory distribution, described in detail below. Deviations from this behavior reflect features of the kinetics or miscibility of the reaction. One of the main objectives of this Chapter is to determine if the Schultz-Flory distribution accurately represents the molecular weight distribution of the structural elements formed in polyurethanes.

In the simplest prepolymer system, a macrodiol is reacted with a diisocyanate in the absence of water. Under stoichiometric control, the size distribution is described by Equation 3.1.[1]

$$N_x = p^{x-1}(1-p) \qquad (3.1)$$

In Equation 3.1, N_x is the mole fraction of oligomers with x monomer units and p is the extent of reaction. A stoichiometric excess of one monomer is usually used to prepare prepolymers. The prepolymers discussed in this chapter are prepared with excess

diisocyanate. The molecular weight may be limited or controlled by changing the stoichiometric imbalance, r (defined as less than 1). At incomplete conversion, the distributions of oligomers terminated by two OHs, two NCOs, or one OH and one NCO is predicted by equations 3.2-3.4, where the diisocyanate is in excess.

$$N_{x_{OH,NCO}} = p^{x-1} r^{x/2} \left[\frac{2 \cdot (1-p) \cdot (1-rp)}{[1+(1/r)-2p] \cdot r} \right] \tag{3.2}$$

$$N_{x_{OH,OH}} = p^{x-1} r^{x/2} \left[\frac{(1-p)^2 \cdot r^{-1/2}}{[1+(1/r)-2p]} \right] \tag{3.3}$$

$$N_{x_{NCO,NCO}} = p^{x-1} r^{x/2} \left[\frac{(1-rp)^2 \cdot r^{-3/2}}{[1+(1/r)-2p]} \right] \tag{3.4}$$

These relationships assume that the reactivity does not depend upon molecular size, reaction is irreversible, and side reactions are negligible.

The hard segment length distribution in foams results from the consecutive reaction of diisocyanate and water. The foam studied in this Chapter is composed of a mixture of TDI isomers, as discussed in Chapter 2. Upon reaction of one NCO group, the reactivity of the other NCO groups changes and this affects the molecular weight distribution. The NCO groups of 2,6-TDI groups have equivalent reactivity before reaction, but the reactivity of the second NCO group decreases after the first one reacts. The reactivity difference ($K = k_1/k_2 = 5.32/0.86$) is 6.2 for the reaction between 2,6-TDI and n-butanol.[2] Relative to these values, the *para* NCO group of 2,4-TDI is more reactive than the *ortho* NCO group even before reaction, and $K= 2.70$ ($k_1 = 11.9$, $k_2 = 4.42$). After reaction, the reactivity of the *ortho* group decreases to $k_2 = 1.0$, and $K=11.9$. These values may be different for reaction with water or amine.

The effect of changes in reactivity has been treated for diol chain-extended hard segments using both probabilistic and deterministic approaches.[3-5] Monte Carlo simulations have also been employed.[6] However in foams, both monomers show a change in reactivity after reaction. The reaction between water and isocyanate is much slower than the reaction between the resulting amine and isocyanate. For reactions with phenyl isocyanate in toluene, the rate constants for reaction with aromatic amine versus water are 20 and 0.4, respectively.[7]

Due to the complicated, and rather unknown, reaction kinetics, the molecular weight distribution cannot be predicted reliably. The general deviations from the Flory distribution can be determined. The influence of a change in reactivity for one of the monomers on X_w is shown in Figure 3.1 for r = 0.81.[5] The effect of K is most dramatic at conversion greater than 0.4. In general, a decrease in the reactivity of one functional group

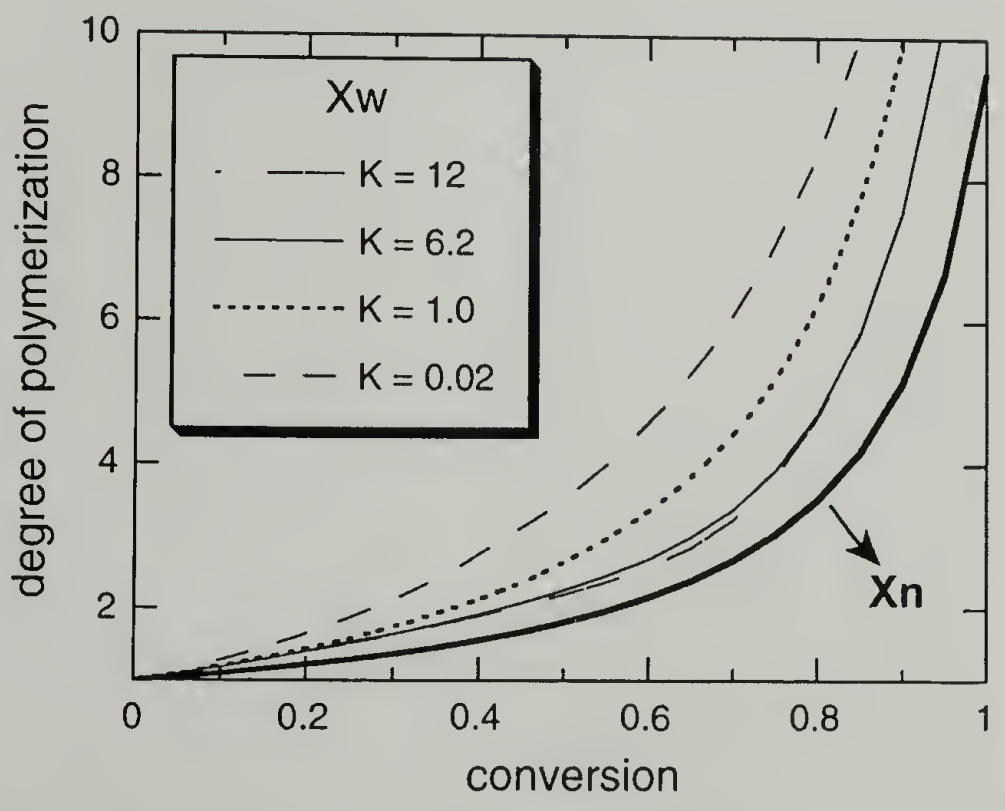

Figure 3.1 Effect of monomer reactivity difference on the average degree of polymerization.

upon reaction of the other group (K>1) results in a decrease in the polydispersity. Conversely, an increase in reactivity (K<1) results in an increase in polydispersity. The effect of increasing K from 6.1 to 12 on M_w is very small, as noted previously.[3] Due to the high reactivity of the amine and the stoichiometric excess of NCO, the most abundant species will be odd x-mers with NCO ends. Due to the decrease in reactivity of the second NCO, the TDI monomer will completely depleted between 75-85% conversion.

3.2.2 Experimental Studies

A detailed study of model oligomers prepared from a mixture of TDI and a stoichiometric excess of 1,4-butanediol found that the materials followed statistical expectations for a system in stoichiometric imbalance; the conclusion is perhaps surprising since the differences in reactivity were not accounted for in the calculation.[8] In another study, the hard segment length distribution of segmented polyester-polyurethane prepolymers was determined by first selectively hydrolyzing the polyester component and then by size exclusion chromatography (SEC) coupled to a UV detector.[9] The synthetic conditions are not reported (temperature, solution or bulk), nor is the procedure used to convert SEC data to mole fractions of oligomers. The authors report that samples containing 12.6 and 16.4 wt % hard segment followed a most probable distribution, while samples containing 14.2 and 23.7 wt % hard segment had much narrower distributions than expected. They attribute this result to the influence of phase separation, despite the lack of trend with wt %.

The polyurea hard segment length distribution of foams prepared from TDI or MDI and different polyols was determined by MALDI-TOF after hydrolysis of the

urethane linkages.[10] The hard segments formed in polyester polyol exhibited a Schultz-Flory distribution; while those formed in polyether polyol did not. The latter was much narrower, with a lower X_n than expected. This was attributed to the lower solubility of hard segments in the polyether matrix. A similar result was observed in foams prepared from TDI and polyether polyol with different concnetrastions of water. Increasing the stoichiometric ratio of water to NCO did not greatly change the distribution.[11]

3.3 Experimental

PPG prepolymers were prepared according to the procedure described in Chapter 2. Cure catalyst was not added. The reaction time varied between 0.2 and 3.0 h. The reaction temperature was 108 °C. The samples used for molecular weight analysis were end-capped with MeOH immediately after the prepolymer reaction was completed.

Polyurea hard segments were isolated from 4-50 plaques as previously described.[11] The plaques were first cryo-milled into a powder. Then 1.0 g was added to 100 mL of a 5 wt % solution of NaOH in 50:50 water and n-butanol. The reaction was stirred at 100 °C for 24 h. MeOH was added to the mixture until a single phase formed. The solution was centrifuged, the liquid decanted, and the precipitate filtered, washed, and dried. This precipitate was a mixture of both the polyurea hard segments and $NaHCO_3$. Infrared spectroscopy of the concentrated mother liquor did not show any characteristic aromatic bands, indicting efficient isolation of the entire polyurea molecular weight distribution.

Polyurea hard segments were prepared under homogeneous conditions by reaction of T-80 TDI and H_2O in DMSO. DMSO was dried over CaH_2 and then vacuum distilled

prior to use. A three neck round bottom flask equipped with a N_2 inlet, air-cooled condenser, and a stir bar was charged with 0.405 g (0.0225 mol) H_2O, 1.006 g (0.0112 mol) 1-methoxy-2-propanol, 0.014 g T9, 0.033 g mixed amine catalyst, and 100 mL of DMSO. Using a syringe, 5.028 g (0.0289 mol) of T-80 TDI was added. The clear solution was stirred overnight at room temperature, after which time residual NCO was not detected via infrared spectroscopy. The hard segments were isolated by removing the DMSO under reduced pressure.

The extent of reaction conversion was determined for PPG prepolymers by titration and by ^{1}H NMR. The extent of NCO reaction (p_{NCO}) was determined according to the titration procedure described in Chapter 2.2.5. The extent of OH conversion (p_{OH}) can then be calculated, assuming no side reactions, according to Equation 3.5.

$$p_{OH} = \frac{p_{NCO}}{r} \tag{3.5}$$

^{1}H NMR was used to directly determine p_{OH} of MeOH end-capped prepolymers. ^{1}H NMR spectra were recorded using a Bruker DPX300 spectrometer. 512 scans were signal averaged. The sample concentration was approximately 20 mg·ml^{-1} in pyridine-d5. This solvent gives clear resolution of PPG methynes adjacent to a carbamate from those adjacent to an alcohol.[12] The hydroxyl-containing end groups could not be resolved from the backbone when acetone-d6 was the solvent. D1 up to 30 sec was not enough time to allow aromatic protons to relax, but the methyne resonances showed no changes when D1 was varied between 2 and 30 sec.

For prepolymers, MALDI-TOF mass spectra were recorded as described in Chapter 2.2.1. The procedure for polyurea is as follows. Solutions of 4 mg·mL^{-1} polyurea in 50/50 (v/v) DMSO and THF and 30 mg·ml^{-1} dithranol in 50/50 (v/v) DMSO and THF

were prepared and mixed together by volume in the ratio of 1:6. 1 μL of this solution was spotted onto a stainless steel target. The solvent was evaporated using a heat gun. Spectra were recorded in reflectron mode. A typical spectrum contains 20 shots.

SEC was carried out as described in Chapter 2.2.4. A SEC calibration curve of $\log(M_w)$ versus elution volume could be constructed for PPG prepolymers by combining the peak molecular weight (M_p) obtained from MALDI with curve fitting of the SEC traces. The SEC traces were fit as a series of Lorentzian functions. The first six of these with highest elution volumes are related to distributions that can be observed by MALDI-TOF. M_p was thus determined experimentally from MALDI-TOF. The last three Lorentzian functions were assigned M_p based upon the structure expected for those distributions. A 3rd order polynomial was used to fit the data in the range of 1800 to 15000 $g \cdot mol^{-1}$. The results are shown in Figure 3.2. The weight fraction distribution was determined based on this calibration curve

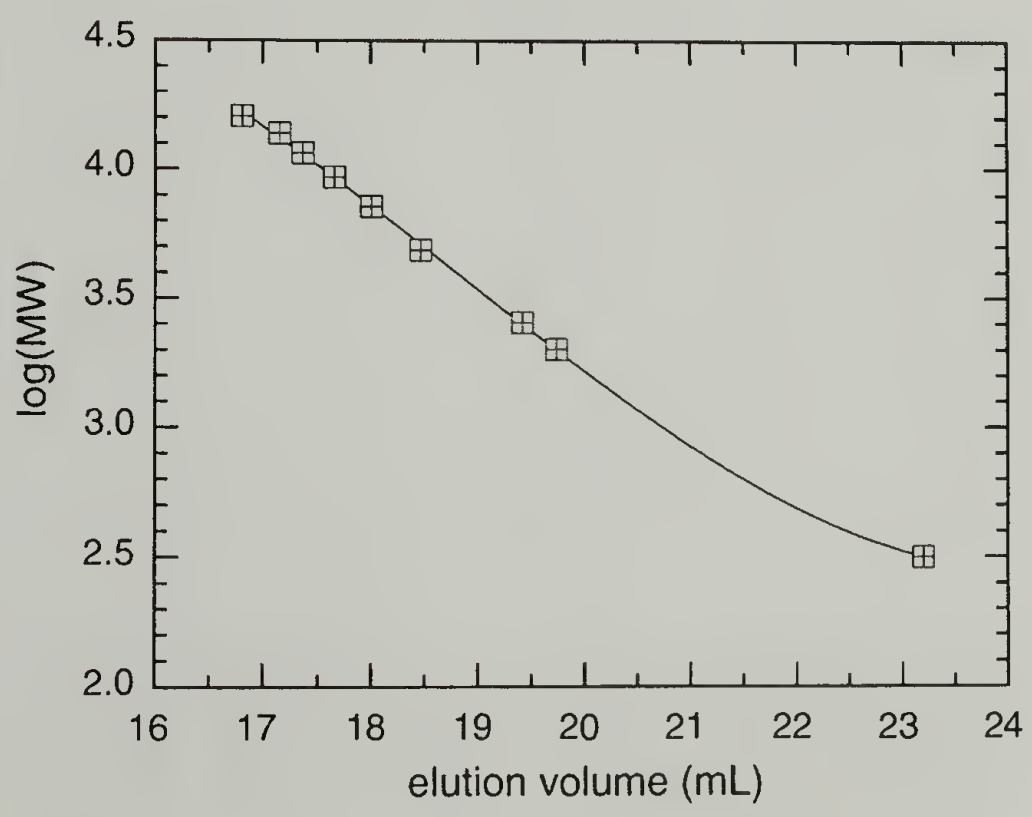

Figure 3.2 SEC calibration curve used for MeOH end-capped PPG prepolymers.

3.4 Polyurethane Prepolymers

As discussed in Chapter 2, the adhesive prepolymer is a ternary blend of a poly(propylene glycol) prepolymer, one of three polyester prepolymers, and a poly(butyl acrylate) acrylate copolymer. Prior to reaction, the PPG, PHMA, and acrylic were characterized by a combination of MALDI-TOF and SEC in order to determine their molecular weight distributions. Upon reaction, the distributions of PPG and PHMA monomers are converted to a dispersion of oligomers, including:

MDI, MDI-PPG-MDI, MDI-PPG-MDI-PPG-MDI, …
MDI-PHMA-MDI, MDI-PHMA-MDI-PHMA-MDI, …
MDI-PPG-MDI-PHMA-MDI

The populations of these should be detectable by MALDI-TOF since each will have a discrete mass distribution. Unfortunately, due to the broad polydispersity of the ternary blend, including the high molecular weight acrylic, spectra could not be obtained, even under a variety of conditions. The differential solubility of the polymers in MeOH could be used to fractionate the blend into two different fractions: a PPG rich fraction and a PHMA/acrylic rich fraction. ^{1}H NMR showed that the fractionation was not clean. This is, in part, due to the heterogeneity in the structure, which will be discussed in Chapter 4.

Due to these issues, a simpler system was examined, namely PPG homo-prepolymers. PPG prepolymers were prepared at 108 °C for reaction times between 0.2 and 3 h. The MDI was added in excess so that the ratio of OH/NCO (r) groups was 0.62. The conversion (ρ_{NCO}) of the prepolymers prepared for reaction times of 0.2, 1, and 3 hours at 108 °C was determined by reaction of the isocyanate groups with a known excess of dibutyl amine. The amount of remaining dibutyl amine was then determined by titration with HCl. Assuming no side reactions, ρ_{OH} can be calculated; the results are

tabulated in Table 3.1. As expected, increasing the reaction time increases the conversion. After 3 h, urethane formation is nearly complete at 97% conversion.

Table 3.1. Reaction conversion for prepolymer formation at 108 °C calculated using various methods

Time (h)	ρ_{NCO} (titration)	ρ_{OH} (titration)	ρ_{OH} (NMR in pyr)	ρ_{NCO} (NMR in acet)
0.2	0.1037	0.1672	0.14	0.09
1.0	0.3984	0.6471	0.60	0.40
3.0	0.6000	0.9677	0.95	0.64

^{1}H NMR spectroscopy can be used directly to determine ρ_{OH} of the prepolymers after first reacting the residual NCO with methanol. The use of pyridine-d5 as solvent, allows resolution of the methyne protons adjacent to the alcohol end group from the backbone methyne groups. After reaction, this resonance shifts downfield from 4.18 to 5.35 ppm. HMQC (inverse ^{1}H, ^{13}C correlation) confirmed that these resonances were correlated to a methyne carbon. The conversion was then calculated by integrating the areas of the two resonances. The results are shown in Table 3.1. The degree of conversion obtained from ^{1}H NMR is consistently slightly lower than that determined from titration. The error in the conversion calculated from ^{1}H NMR is expected to be ~5%. The relative error associated with titration is less than 0.2%. Taking into account the experimental errors, the two methods yielded similar results.

To determine the number and weight molecular weight distributions of the PPG prepolymers, a combination of MALDI TOF mass spectrometry and SEC was used. The MALDI-TOF spectra for MeOH end-capped prepolymers in the mass range between

1500 to 3000 m/z are shown in Figure 3.3. These spectra were recorded in linear mode. Prior to reaction, PPG has M_n = 2000 and PDI = 1.02. Each ion is separated by 58 m/z, the mass of a repeat unit. After prepolymer synthesis, different oligomers formed, with slightly higher molecular weights. Based upon the mass of the expected products (Figure 3.4), the dominant distributions are assigned as Na+ adducts of PPG monomer, dimer, and trimer. At low conversion, the major product is monomer, after 1.0 h it is dimer and after 3 h it is trimer.

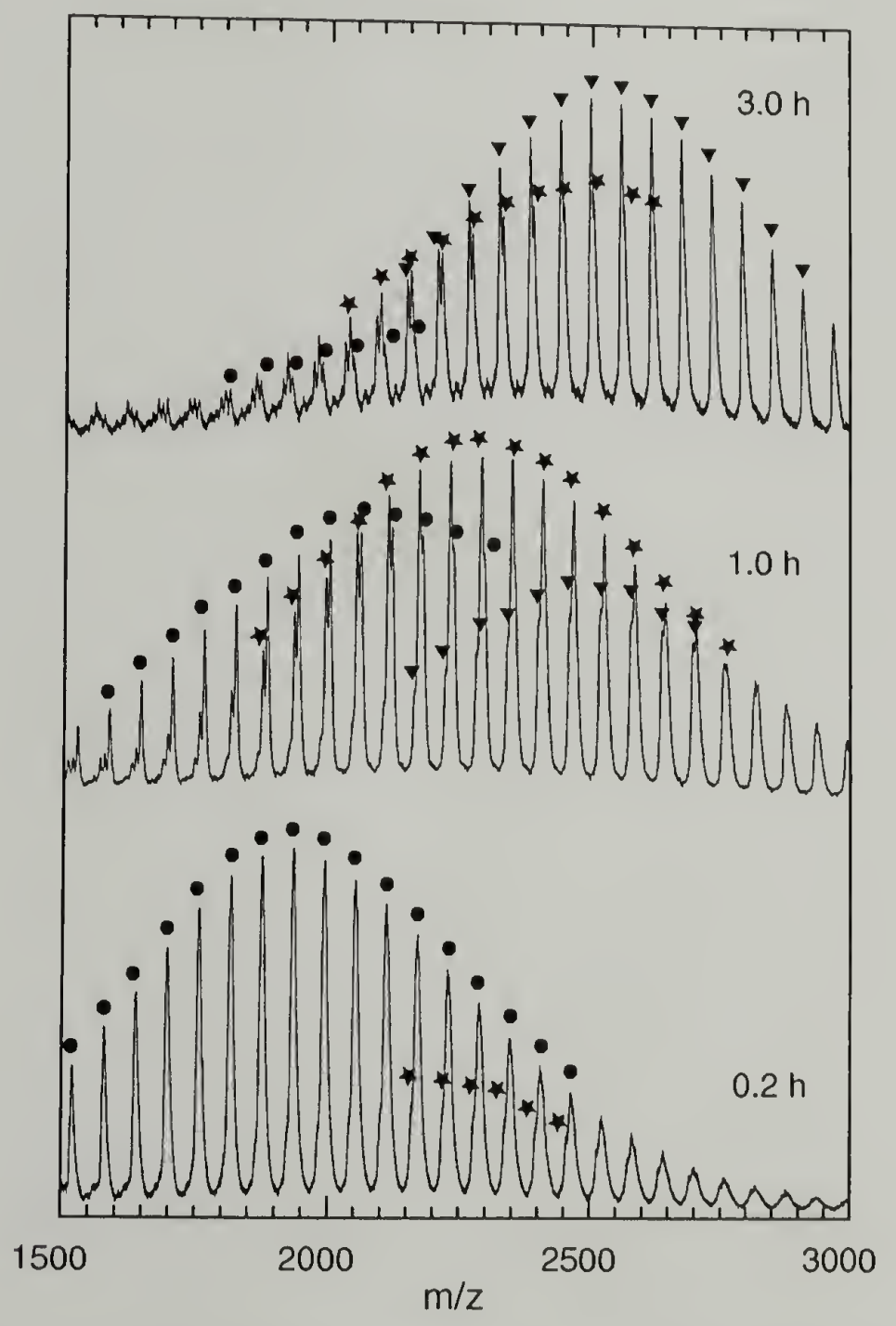

Figure 3.3. MALDI-TOF mass of MeOH end-capped PPG prepolymers; circles, stars, and triangles are from monomers, dimers, and trimers, respectively.

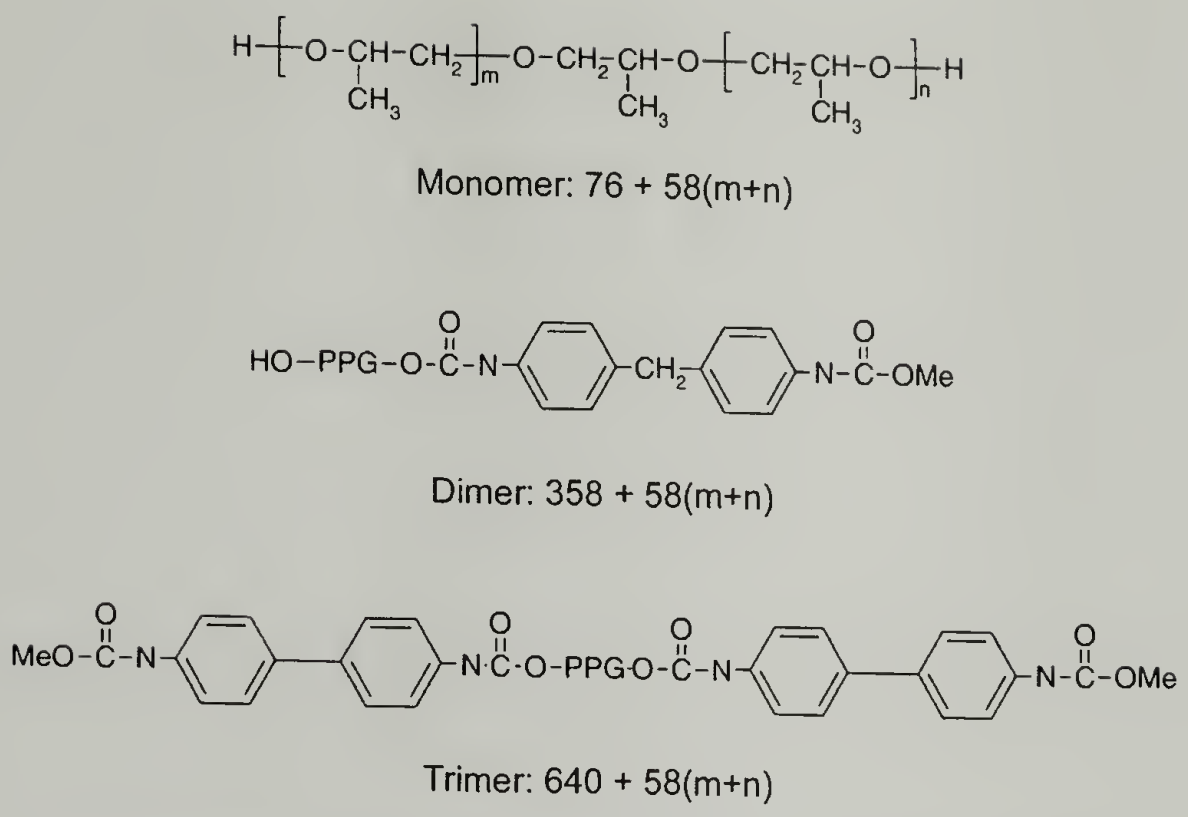

Figure 3.4 Mass distributions of expected products of PPG prepolymer synthesis.

MALDI-TOF in linear mode can analyze a wide range of molecular weights; in this case, spectra were recorded from 200 to 25000 m/z. If the spectra are instead recorded in reflectron mode, isotopic resolution can be obtained, albeit over a narrower molecular weight range. Reflectron mode was used to resolve the distributions from monomer, dimer, and trimer. The low molecular weight PPG chains should react with the same probability as the high molecular weight chains. This can be confirmed by analyzing the shape of the distributions during reaction.

The spectrum obtained for the sample reacted at 1.0 hour contains a mixture of all three species. After subtracting the mass added from the new MDI units, the distributions from monomer, dimer, and trimer may be compared. The results are shown in Figure 3.5 where the intensies of the maxima in the distributions are normalized to unity. The shape

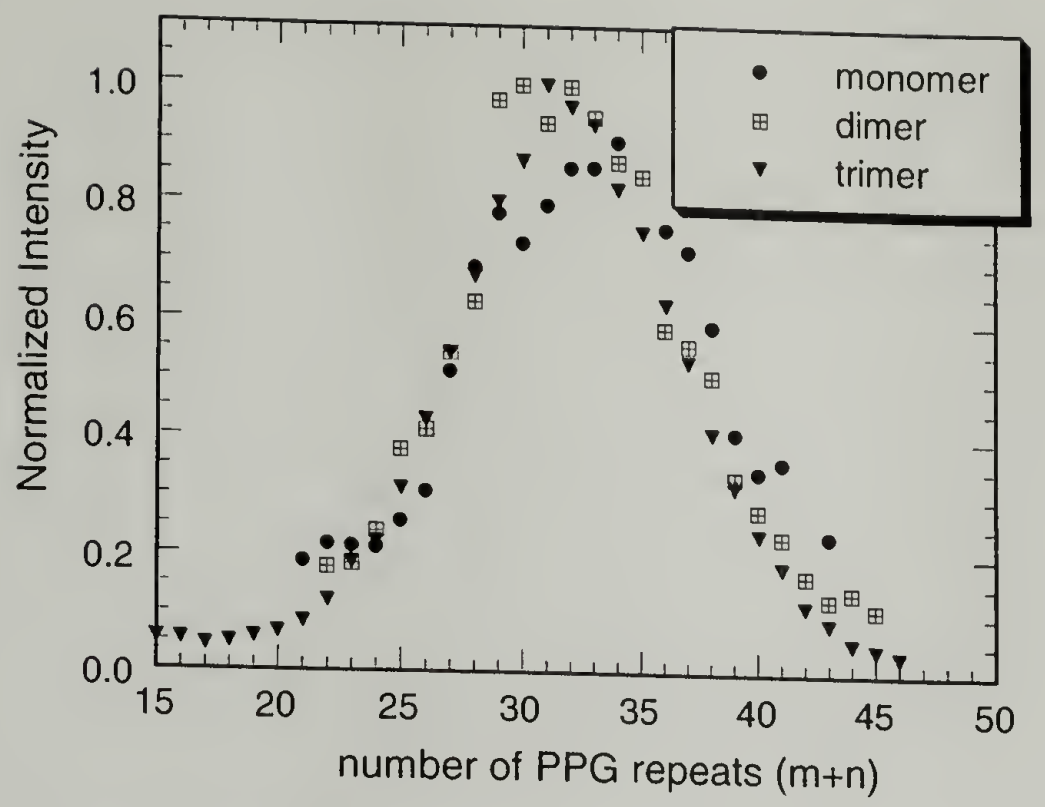

Figure 3.5 Molecular weight distribution of PPG monomer, dimer, and trimer in PPG prepolymer reacted for 1 h.

of the distributions is essentially identical. Each PPG chain indeed reacts randomly with MDI.

Dimer and trimer are not the only species that are formed. The MALDI-TOF spectra obtained in linear mode are shown in Figure 3.6 over the entire mass range. After 3 h ($\rho_{OH} = 0.97$), four sets of distributions formed with M_P of 2548, 4867, 7180, and 9320 $g \cdot mol^{-1}$. These distributions correspond to trimer, pentamer, heptamer, and nonomer. Better resolution of these higher molecular weight distributions could not be obtained, despite numerous attempts under different conditions.

SEC is a more suitable technique for observing the high molecular weight species due to its sensitivity to M_w. The change in oligomer distribution with conversion is clearly observed from SEC results as shown in Figure 3.7. After a reaction time of 0.2 h, two main peaks at elution volumes of 19.76 and 23.20 ml correspond to MDI and PPG

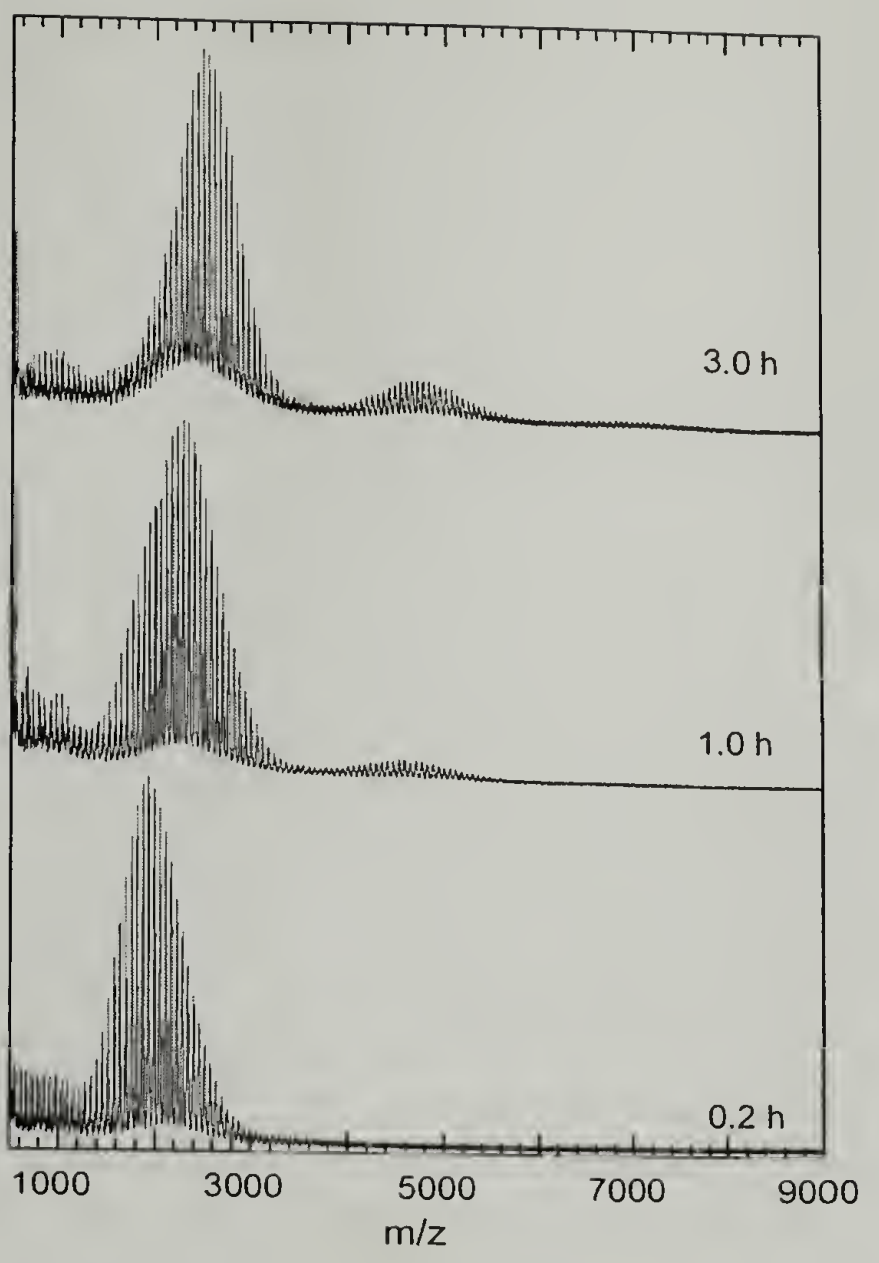

Figure 3.6 MALDI-TOF mass of MeOH end-capped PPG prepolymers prepared at 108 °C for different amounts of time.

that is largely unreacted. A small peak at 22.13 ml is also observed and corresponds to MDI dimer. After 1.0 h, two additional peaks emerge. Owing to the narrow polydispersity of PPG, oligomer species with different numbers of PPG units are resolvable. Increasing the number of MDI units in an oligomer gives a shift in the peak elution volume (i.e. molecular weight). Thus in the trace at 1.0 h, the discrete peaks at 19.52, 18.50, and 18.12 ml correspond to species with 1, 2, and 3 PPG units, respectively. The shift in peak elution volume for the 0.2 h reaction versus the 1.0 h reaction from 19.76 to 19.52 ml

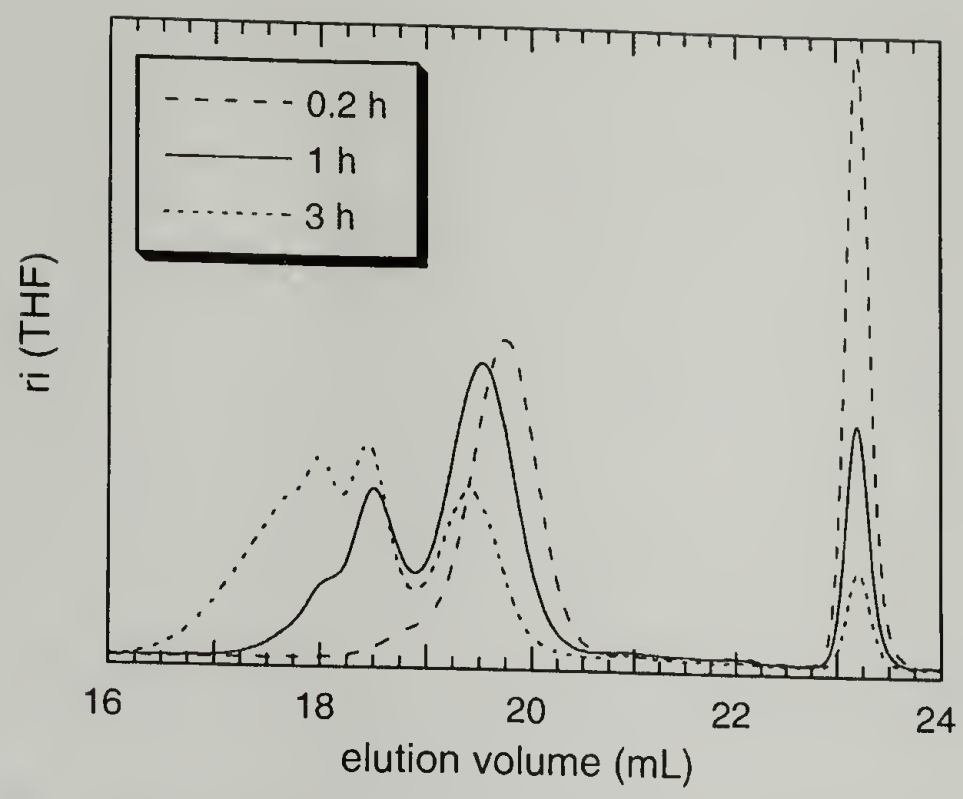

Figure 3.7 SEC traces for MeOH end-capped PPG prepolymers prepared for different reaction times.

corresponds to a change in the amount of monomer, dimer, and trimer in each sample.

Having developed methods for measuring the individual oligomer populations in these prepolymers, the molecular weight distribution can be compared with the ones outlined in the introduction. First the number fraction and weight fraction distributions must be determined from the data. The MALDI TOF results can be separated into several different distributions, depending on the number of PPG units in the oligomer. The number fractions determined by integration of these distributions can be compared with those determined by a probabilistic approach. [1] The amount of free MDI is grossly under-represented by the MALDI data. For example, 38-54% monomeric MDI is expected to exist in the prepolymers. However, integration of the MDI peak at 337 m/z gives between 2-7%. This may be due to large differences in the ionization efficiency of MDI and PPG.

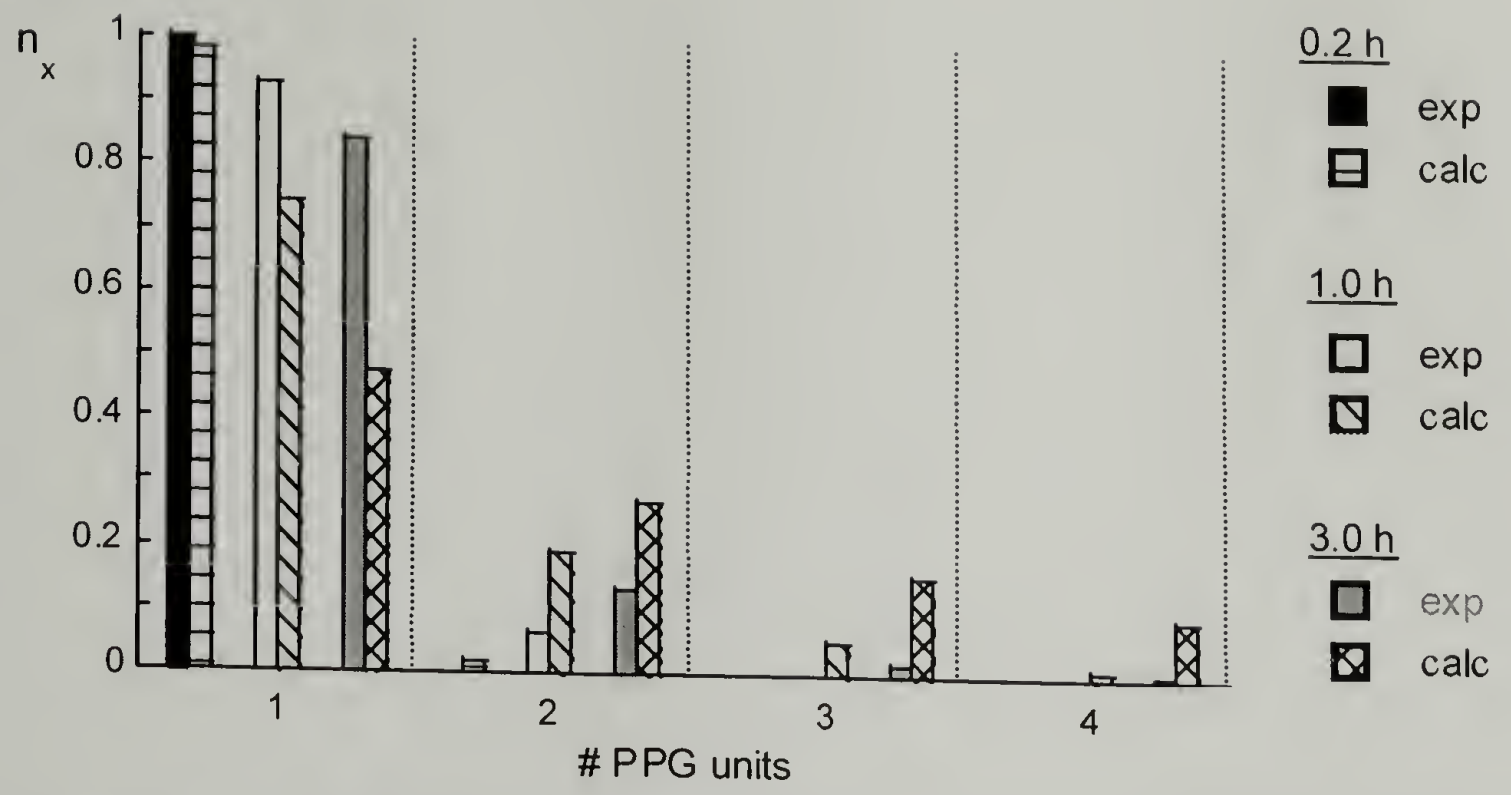

Figure 3.8 Comparison between number fraction distributions determined experimentally from MALDI-TOF results and calculated based upon probabilistic theory using the appropriate conversion (p=0.17, 0.65, and 0.97).

Therefore, the contribution from the free MDI was neglected in the calculations. The results are shown in Figure 3.8. Although the overall trend of increasing molecular weight as a function of conversion is predicted, a quantitative agreement is absent. This is most likely due to the experimental conditions. MALDI-TOF mass spectrometry is often considered as a measure of absolute molecular weight. In the limit that molecular resolution can be achieved, this is true. However, samples with high polydispersity or molecular weights over a large mass range may not be accurately represented. [13,14] It has been shown that small perturbations in end groups can have a large effect on ionization efficiency.[15] In addition, instrumental effects can lead to a mass bias during the MALDI desorption/ionization process. [16]

SEC gives relative molecular weights. In order to use it effectively, the elution times must be calibrated against molecular weight standards. In this case, the PPG

prepolymers themselves were used as standards, with M_p's determined from MALDI-TOF. The weight fraction distributions are shown in Figure 3.9.

The SEC weight fraction data was in surprisingly good agreement with the predictions. As described above, the data was divided into several distributions, depending on the number of PPG units in the oligomer: 0 (MDI monomer and dimer), 1, 2, 3, 4,and ≥5. The amount in each group was determined by integrating the plots in 2200 $g \cdot mol^{-1}$ intervals. This method yielded more consistent results than those involving more sophisticated but laborious deconvolution routines. The results are shown in Figure 3.10.

The agreement is good, the differences in most cases being approximately 10%. PPG monomer contained approximately 5% monofunctional materials, which upon reacting with MDI maintain a molecular weight similar to dimers. This may be the reason the experimentally observed weight fraction of lower oligomers is higher than predicted.

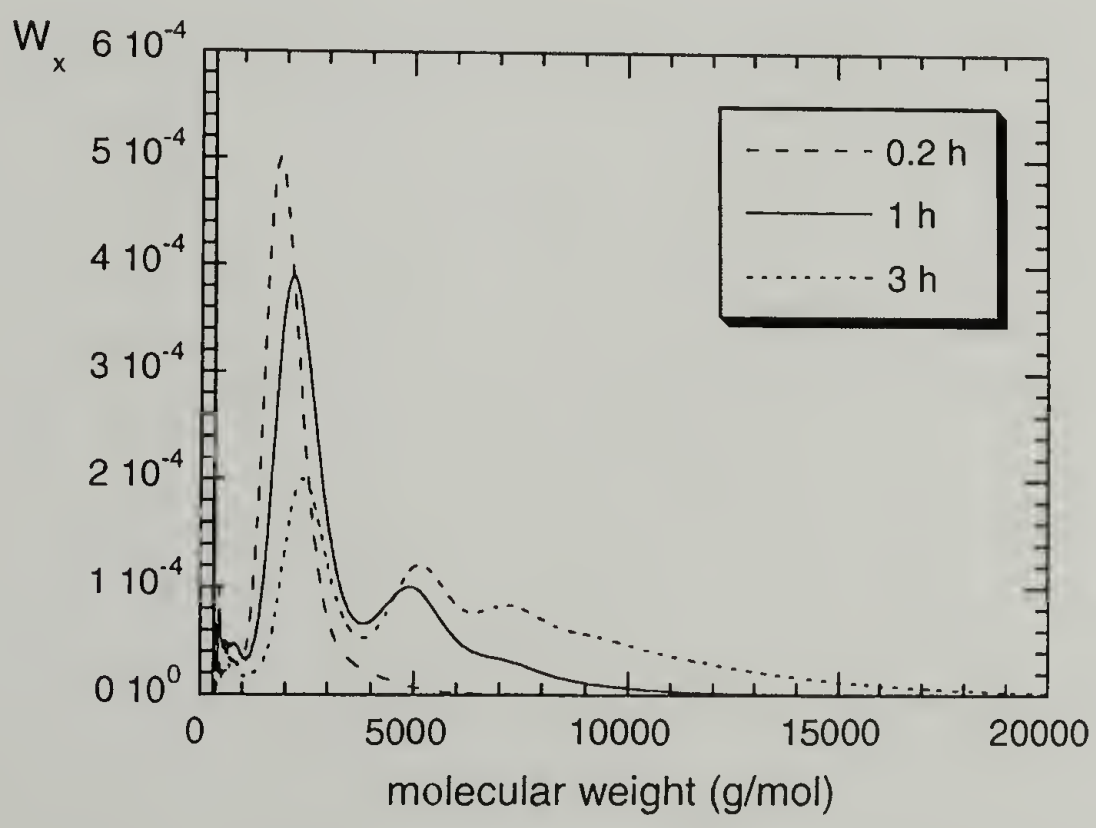

Figure 3.9 Weight fraction distributions of MeOH end-capped PPG prepolymers determined from SEC traces.

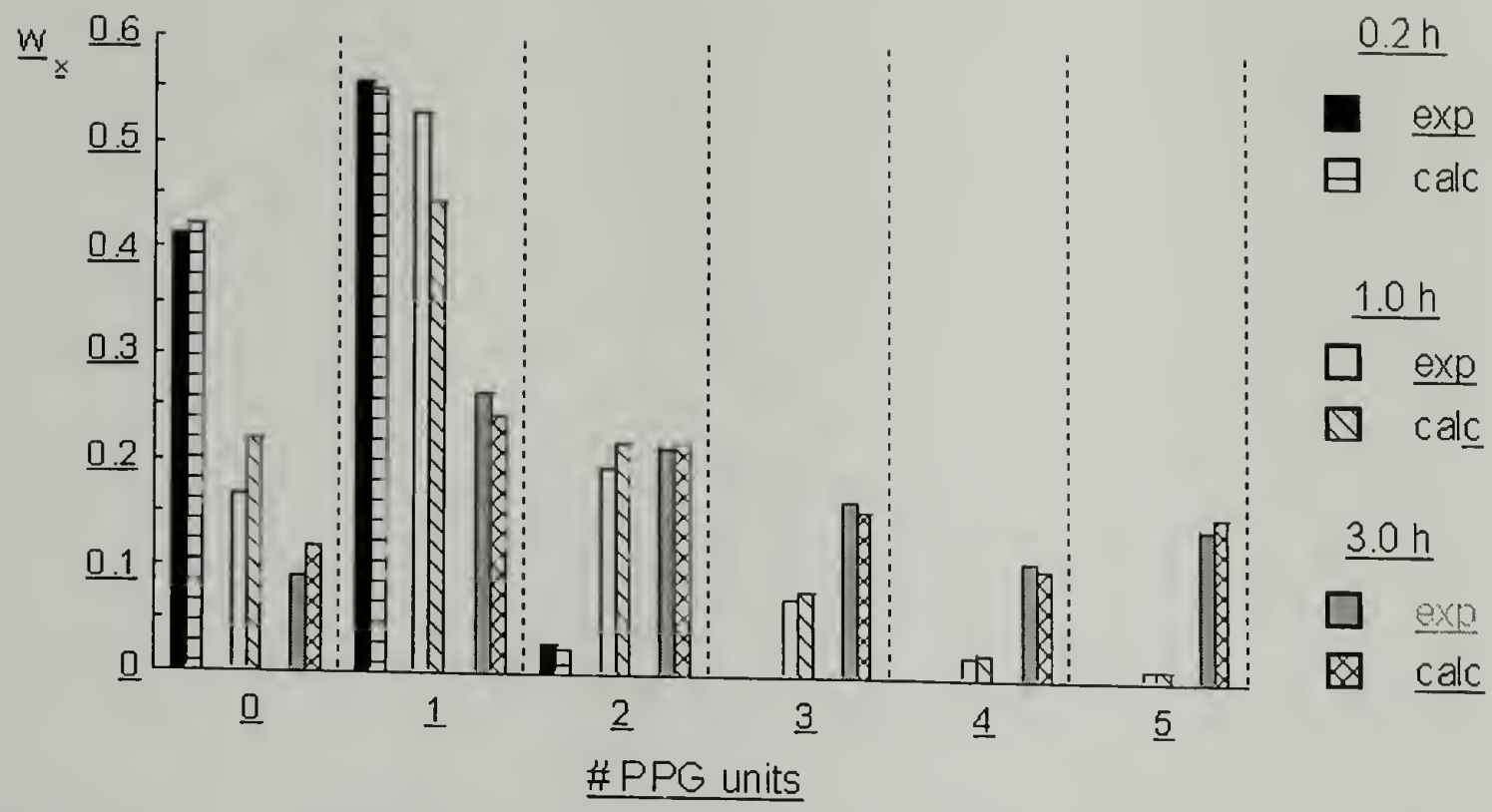

Figure 3.10 Comparison between weight fraction distribution determined experimentally from SEC results and calculated based upon probabilistic theory using the appropriate conversion (p=0.17, 0.65, and 0.97).

Under homogeneous conditions, the molecular weight distribution of PPG prepolymers depends upon conversion and stoichiometric imbalance as predicted by Flory. In addition, MALDI-TOF data showed that the reactivity of PPG chains is independent of chain length. During subsequent curing of the prepolymer, either by water or by chain extension, the monomeric MDI becomes the hard segments. Knowing that under homogenous conditions the amount of MDI monomer is determined statistically, one could now control the amount of free MDI remaining for hard segment formation.

3.5 Polyurea Hard Segments

The initial synthesis of foams occurs in a homogeneous reaction medium. TDI is added to a miscible blend of water, polyol, and catalysts. Analogous to the situation of

the polyurethane prepolymers, initial molecular weight build-up should obey a Schultz-Flory distribution. The only caveat is how important the change in water and TDI reactivity is on modifying the distribution, with the reaction of water and TDI producing opposite effects. As temperature rises, water may phase separate from the polyol. As reaction proceeds, phase separation of hard segments will occur. Further molecular weight build-up in this heterogeneous medium will depend on the local stoichiometry.

TDI-based polyurea can be synthesized to complete conversion under homogeneous conditions in DMSO solution. In order to compare these model hard segments with the hard segments obtained from plaques, the stoichiometry imbalance between water and TDI was the same as that used for 4-50 plaques and 3-methoxy-2-propanol replaced the polyol. The hard segments were isolated from 4-50 plaques using a hydrolysis procedure that selectively cleaves urethane linkages, leaving the polyurea linkages intact.

MALDI-TOF mass spectra of the two different hard segments were recorded in reflectron mode. Compared to PPG prepolymers, ionization is much easier. In general, high quality spectra could be obtained in 10 to 20 shots. The results are shown in Figure 3.11. In addition to the Na(+) adducts, adducts from H (+) and K(+) were also observed. Addition of an ionizing salt, like NaTFA, seemed to selectively ionize lower molecular weight species, since fewer high molecular weight species were observed. The amount of H(+) and K(+) adducts varied from sample to sample; although no correlation was observed between the amount observed and sample preparation. In the spectra shown in Figure 3.11, the model polyurea contains more of these other adducts.

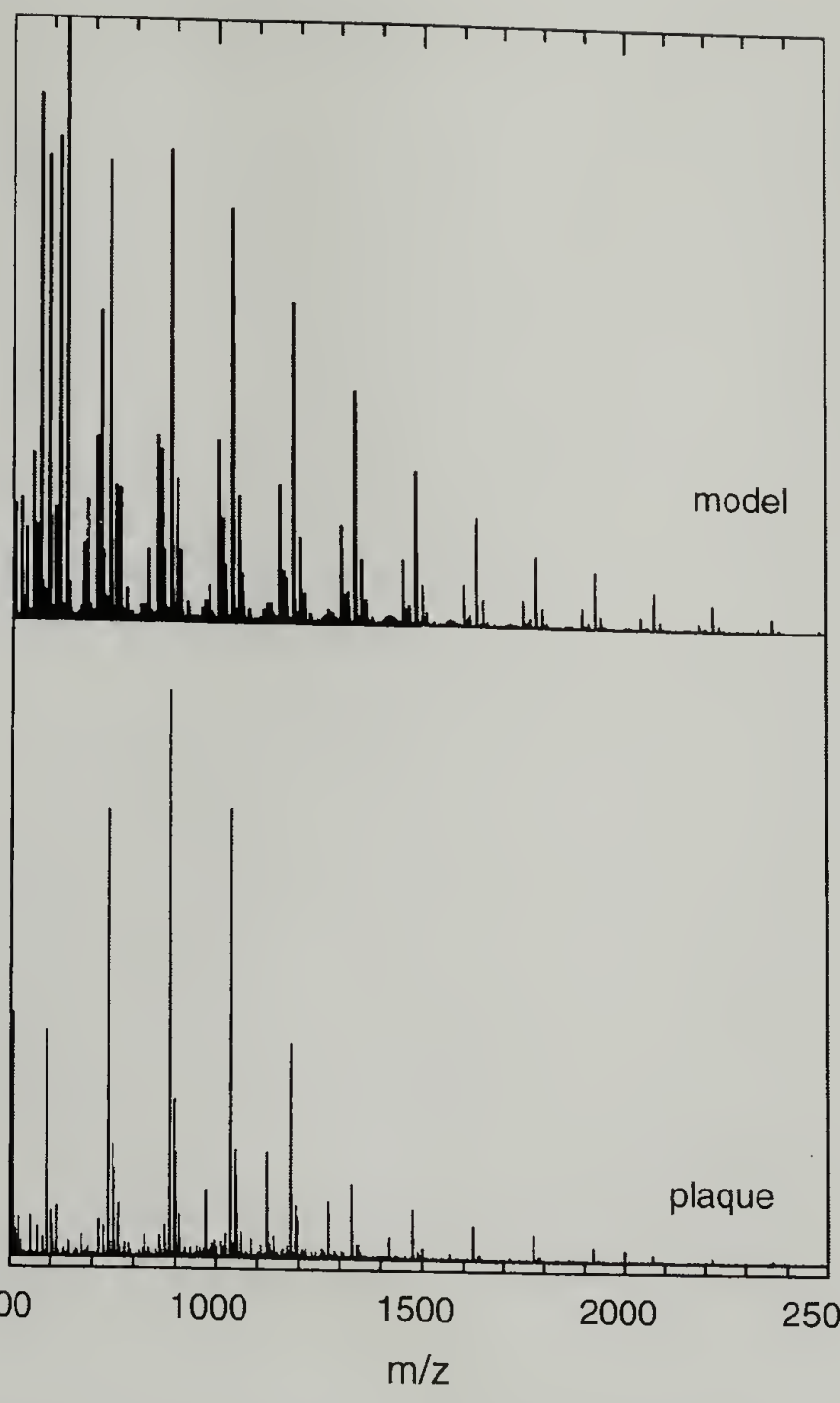

Figure 3.11 MALDI-TOF mass spectra of TDI-polyurea prepared under homogeneous (model) and homogeneous (plaque) conditions.

Comparison of the two spectra shows that the model polyurea exhibits a much broader distribution than the plaques. The hard segment distribution obtained from the plaque is surprisingly narrow. As mentioned in Section 3.2.2, similar results were observed by two different authors. The data suggests that the final hard segment distribution is determined by the miscibility behavior. One author concluded that the narrow distribution occurred due to phase separation of the polyurea and its terminal

NCO.[10] The other author concluded that the narrow distribution occurred due to phase separation of the water.[11] Based on the data shown here, the latter conclusion is more reasonable. Phase separation of water would give a local stoichiometric imbalance lower than expected (water/NCO decreases), while phase separation of the polyurea, and its terminal NCOs would give a local increase in the stoichiometric imbalance. Only a decrease in the stoichiometric imbalance would skew the distribution to lower molecular weight.

The number fraction distribution can be determined based on the peak assignments as described previously.[11] All the adducts were accounted for in this calculation. The results are shown in Figure 3.12. According to the previous definition, one repeat has a degree of polymerization of three. The number fraction distribution reflects the differences discussed above. The shape of the model hard segment distribution obeys a Schultz-Flory distribution, while those from the plaques do not. In order to obtain a reasonable fit to the Schultz-Flory distribution, two modifications were made. The degree of polymerization was redefined as being equivalent to the number of repeat units. Presumably this accounts for the fact that the amine reacts much faster than water. In addition, while the actual stoichiometric imbalance was $r = 0.78$, this value, when used in Equation 3.4, did not give a good fit of the data. If a value of $r = 0.66$ was used instead, a fairly good fit was obtained. The data exhibits a slightly narrower distribution than predicted. The fact that a lower value of r gave a better fit indicates that the probability of a growing hard segment to react is lower than expected, due to the decrease in NCO reactivity after one reaction.

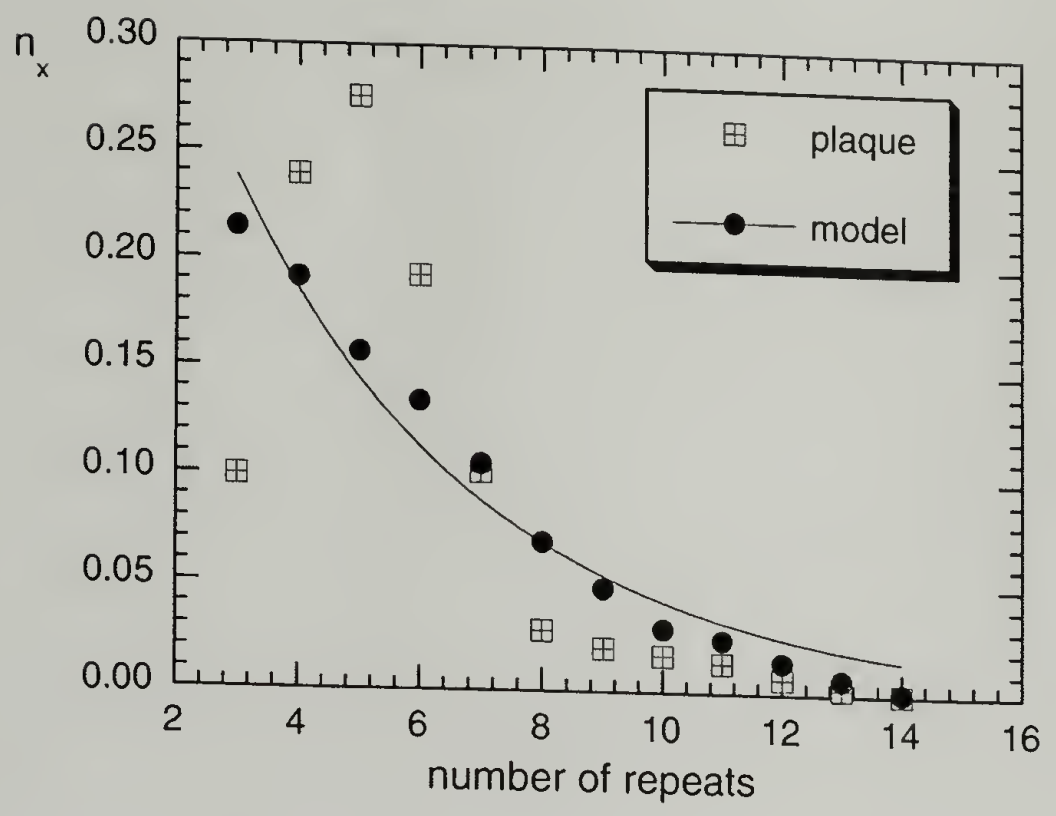

Figure 3.12 Number fraction distribution of TDI-polyurea prepared under homogeneous (model) and heterogeneous (plaque) conditions with r = 0.78. The line shows a fit for a Schultz-Flory distribution with r = 0.61.

The hard segment length distribution observed under homogeneous conditions obeys a Schultz-Flory distribution, but one that is narrower and lower in molecular weight than predicted. In plaques, where heterogeneous conditions occur, the distribution is extremely narrow. Based on the preference for low molecular species, this is most likely due to phase separation of the water from the reacting blend.

3.6 References

(1) Flory, P. J. *J. Am. Chem. Soc.* **1936**, *58*, 1877.

(2) Brock, F. H. *J. Org. Chem.* **1959**, *24*, 1802.

(3) Peebles, L. H., Jr. *Macromolecules* **1974**, *7*, 872.

(4) Macosko, C. W.; Miller, D. R. *Macromolecules* **1976**, *9*, 199.

(5) Gandhi, K. S.; Babu, S. V. *AIChE J* **1979**, *25*, 266.

(6) Johnson, A. F.; O'Driscoll, K. F. *Eur. Polym. J.* **1984**, *20*, 979.

(7) Szycher, M. *Szycher's Handbook of Polyurethanes*; CRC Press: Boca Raton, 1999.

(8) Lesar, M.; Zigon, M.; Malavasic, T. *J. Appl. Polym. Sci.* **1993**, *47*, 805.

(9) Barreiro, M. F.; Dias, R. C. S.; Costa, M. R. N. *Macromolecules* **1994**, *27*, 7650.

(10) Mertes, J.; Stutz, H.; Schrepp, W.; Kreyenschmidt, M. *J. Cell. Plast.* **1998**, *34*, 526.

(11) Yontz, D. J.; Hsu, S. L. *Macromolecules* **2000**, *33*, 8415.

(12) Rondeau; Sievers *J. Am. Chem. Soc.* **1971**, *93*, 1522.

(13) Schriemer, D. C.; Li, L. *Anal. Chem.* **1997**, *69*, 4169.

(14) Schriemer, D. C.; Whittal, R. M.; Li, L. *Macromolecules* **1997**, *30*, 1955.

(15) Puglisi, C.; Samperi, F.; Alicata, R.; Montaudo, G. *Macromolecules* **2002**, *35*, 3000.

(16) Mehl, J. T.; Murgasova, R.; Dong, X.; Hercules, D. M.; Nefzger, H. *Anal . Chem.* **2000**, *72*, 2490.

CHAPTER 4

FORMATION OF SECONDARY LINKAGES

4.1 Chapter Overview

As discussed in Chapter 1, isocyanates undergo a multitude of different chemical reactions, making secondary reactions in polyurethanes ubiquitous. While these reactions are well known, they are difficult to measure. The reactive functional groups exist in relatively dilute concentration with respect to the surrounding polymeric medium. In addition, the materials are often chemically crosslinked, precluding their dissolution and analysis through typical methods. This Chapter continues the quantification of prepolymer structure. The influence of processing conditions on the formation of secondary linkages is determined.

4.2 Polyurethane chemistry

The reactions that NCO's undergo is shown in Chapter 1 Figure 1.1. Several qualitative studies have been carried out to determine the influence of processing variables on the chemical structure of polymeric systems. For example, infrared spectroscopy has been used to analyze the relative amounts of allophanate and biuret, leading to the general conclusion that existence of these structures is unlikely, typically occurs only upon storage, and biurets are more probable.[1-3] Similar conclusions were reached using ^{13}C NMR.[4]

One quantitative study was carried out on PPG-TDI prepolymers.[5] The authors developed an amine degradation technique which selectively degrades allophanates.

Samples with stoichiometric imbalance (r = OH/NCO) between 0.3 and 1.0 and reaction temperatures between 80 and 120 °C were analyzed as a function of conversion. In general, allophanates were only found at conversions greater than 25%; however, with a large excess of isocyanate, allophanates were observed almost immediately. The linkages were observed at all temperature at complete conversion with values ranging from 1.5 to 6.0 mole %. The reaction temperature had very little effect; whereas conversion, effectively the concentration of isocyanate, was the most important factor. These results are somewhat unexpected based upon previous qualitative findings. The other anomalous linkages, isocyanurate and uretidinedione, have not been determined quantitatively.

Finally, another study quantitatively determined that the gel fraction of PPG prepolymers reached a maximum between stoichiometric imbalances of 0.5 and 0.66 and decreased with increasing temperature from 90 to 140 °C.[6] This last result was thought to be due to the thermal instability of allophanates and biurets. In fact, the reaction time was not kept constant in these studies, in order to reach a steady state gel point. Samples prepared at 90 °C were held for 21 days, while samples prepared at 120 and 140 °C were held for only 5 and 4 days, respectively. In addition, the authors believe that some of the discrepancy between the determined gel fraction and that predicted based on their branching theory was due to the existence of other anomalous linkages, which consume isocyanates but do not add branches (e.g. cyclics, uretedindione).

Given the lack of data, or contradictory data, about polyurethane structural elements, a review of isocyanate chemistry in small molecules is necessary. Unfortunately, depending on each author's purpose, a variety of solvent polarities (from

toluene to dimethyacetamide), catalysts, and temperatures have been used, which makes comparisons very difficult. Nonetheless, several main points can be reached.

The reaction mechanism of alcoholysis is not agreed. The mechanism is generally considered to follow a second order dependence, independent of catalyst, as first suggested by Baker.[7-12]

$$-\frac{d[NCO]}{dt} = k[NCO][OH] \qquad (4.1)$$

Considerable complications have been observed, however.[13-16] The rate constant was found to depend upon the initial stoichiometric alcohol concentration and to change within a single run. This has led to the conclusion that the reaction proceeds largely by alcohol polymers.[17,18] This also explains why the reaction occurs fastest in non-coordinating solvents. The difference in reactivity of the various alcohol species is most evident in non-polar solvents.[16,19] The reactivity of the alcohol species is tetramer ≈ trimer > dimer > monomer. A complete understanding of this phenomenon is still being developed.[20]

One conclusion from previous work is that hydrogen bonding is very important in the reaction kinetics. Other complications, for example catalysis by urethanes and water has been observed. During polyurethane synthesis, changes in the medium polarity and the number of hydrogen bonding pairs is expected to influence structure development. The other conclusion is that model studies should be carried out under conditions where the alcohol aggregation will not change, for example in polar solvents or with large excess of isocyanate. Unfortunately, several of the studies done to determine rate constants were carried out with equimolar concentration of OH and NCO, often in toluene.

The formation of urethane is catalyzed by a variety of catalysts including, tin carboxylates, tertiary amines, alkoxides, and many others. [21] Stannous (II) compounds exhibit the highest catalytic activity. There is a drastic increase in its activity with temperature.[22-25] Urethanes are thermally stable up to temperatures of 150 °C, though this depends upon the catalysts present, reaction medium, etc. The urethane NH is acidic and urethanes can react further with isocyanates.

Obviously, the complications in understanding the urethane mechanism hinder a full understanding of allophanate formation. Allophanates are believed to form through an enolate-ion-type intermediate.[26] At high temperatures (>150 °C), the equilibrium constants for reactions giving allophanates are smaller than the ones for reactions giving urethanes. At lower temperatures, the catalyst is the deciding factor. Without catalyst and with catalytic tin (II) or tertiary amines, the rate of urethane formation is faster than the rate of allophanate formation.[21] With catalytic quaternary ammonium salts, multi-functional amines, and carboxylates, the rate of allophanate formation can be favored. [21,27] The allophanate NH is acidic, and this compound may react with another isocyanate molecule, cyclize, and lose an alcohol to form isocyanurate. The intermediate is not observed, presumably because this second step is very fast.

Isocyanurate is thermally stable up to 200 °C, higher than the other linkages. At high temperatures, the isocyanurate is formed as the thermodynamically controlled end product of reactions between isocyanate and alcohol. For the same reason, the catalysts that favor allophanates also give isocyanurates. This material is also reported to form from the trimerization of three isocyanates.[9]

Finally, the last reaction is the dimerization of two isocyanates to give uretidinediones. These molecules form easily and are usually found in aromatic isocyanates after storage. Phosphines can be used to catalyze the reaction. Uretidinediones are referred to as blocked isocyanate, since they can react with hydroxyl groups at temperatures above 80 °C. Thus these compounds are often intentionally used in order to "activate" urethane formation at a higher temperature than isocyanates allow.[28]

4.3 Prepolymers

4.3.1 Effect of Conversion

^{1}H NMR is a likely method to quantify the amount of side products. Urethane, allophanate, urea, and biuret NH's all have unique resonances.[29] Their positions depend largely on the nature of the degree of hydrogen bonding, which is influenced by solvent choice, water content, and concentration. For quantitative analysis of NH resonances, exchangeable solvents such as $CDCl_3$ or D_2O can obviously not be used. Pyridine, which was used above for determining the conversion, was a less attractive candidate because its residual solvent resonances overlap those of the aromatic protons. In addition, the long relaxation time of the aromatic protons in this solvent would require very long scan times.

PPG homo-prepolymers prepared at 108 °C for t_{rxn} = 0.2 to 3.0 h were considered first. These materials have been end-capped with MeOH. Their reaction conversion and molecular weight distributions were described in Chapter 2. To determine the percentage of N (i.e. NCO and urethane groups) that participates in side reactions, the ^{1}H NMR

spectra were collected in acetone-d_6. The data obtained for methanol end-capped prepolymers is shown in Figure 4.1. The main region used for analysis is that from 4.5 to 11.0 ppm, which focuses on the MDI unit.

The ratio of OH/NCO remains fixed in each reaction, and since each side reaction maintains the phenyl ring intact, the total number of phenyl ring protons will remain constant. This region, shown in Figure 4.2, is thus used as an internal standard to carry out quantitative analysis. However, though the total area remains intact, it is not insensitive to changes in the structure. Samples with low conversion have a higher concentration of unreacted NCO, which after end-capping with MeOH is methyl carbamate. With increasing conversion, MDI units substituted with methyl carbamate groups are converted to PPG carbamate groups, as shown in Figure 4.3. Resonances arising from protons *meta* to a carbamate are found at 7.12 and 7.15 ppm and are not particularly sensitive to changes in the carbamate substituent. Resonances from those

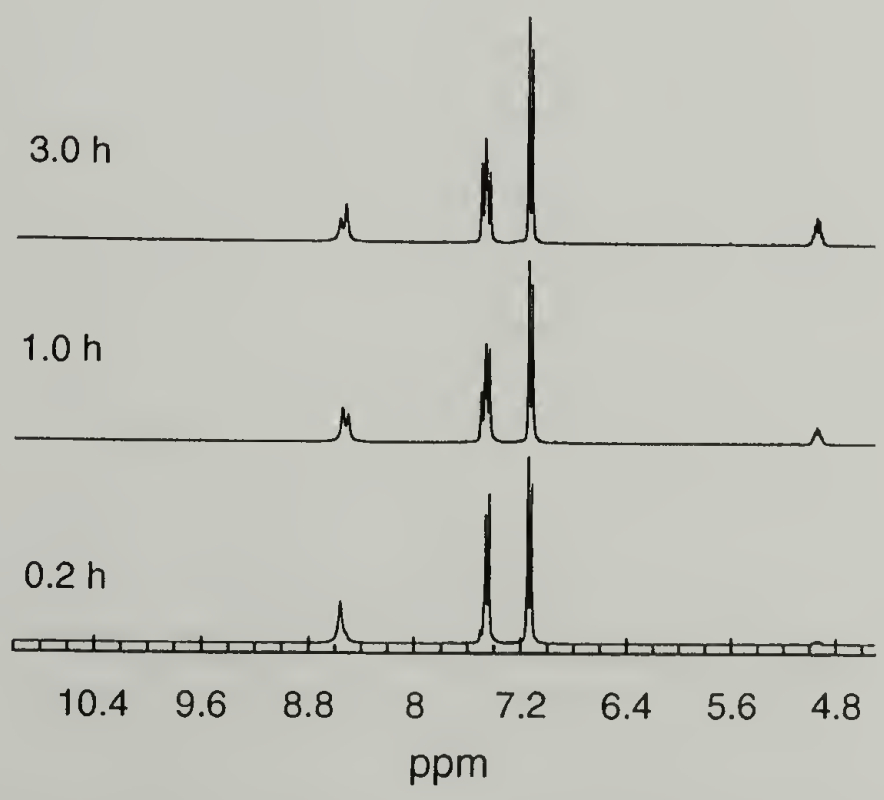

Figure 4.1 ^{1}H NMR spectra of PPG prepolymers prepared at 108 °C.

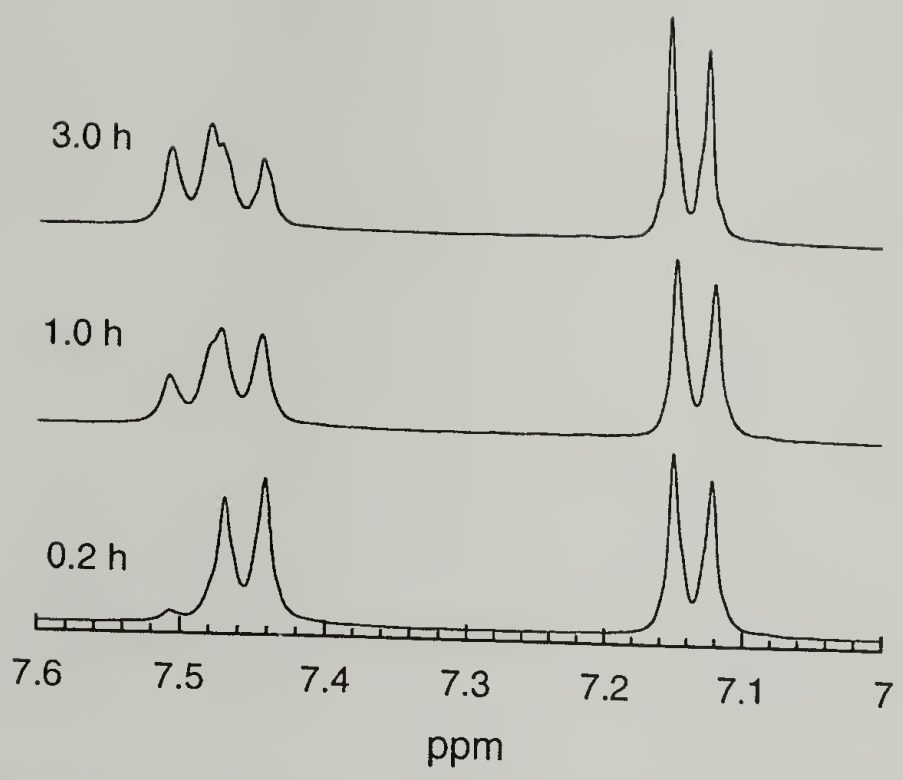

Figure 4.2 ^{1}H NMR spectra of PPG prepolymers prepared at 108 °C in the region of aromatic proton resonances.

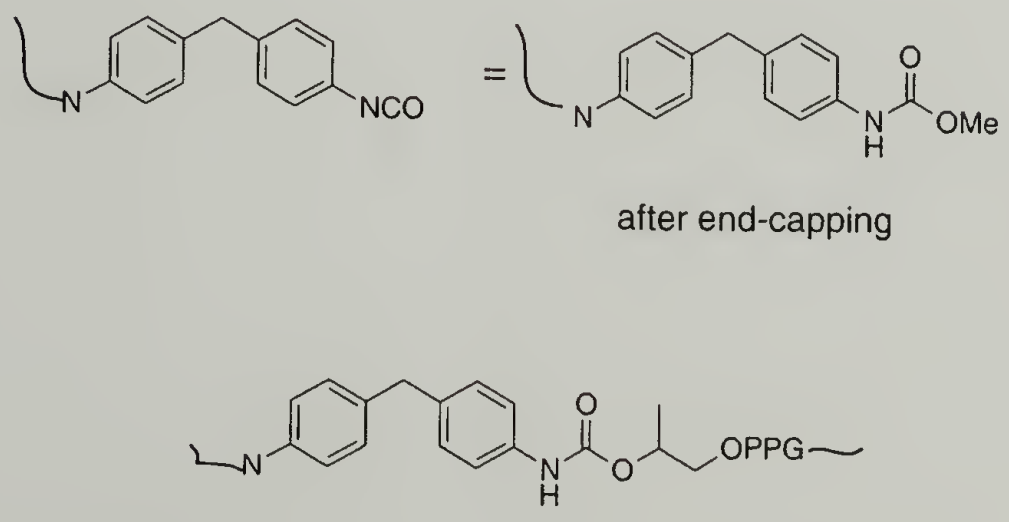

Figure 4.3 Structure of the MDI unit before and after reaction.

protons *ortho* to the carbamate are sensitive to whether the carbamate is attached to a methyne (formed during the reaction between NCO and PPG) or a methyl (an unreacted NCO, after end-capping with methanol). As complete conversion is approached, the resonances at 7.44 and 7.47 ppm shift downfield to 7.48 and 7.51 ppm.

Figure 4.4 shows a complex resonance at 4.95 ppm, which can be assigned to the PPG chain end methyne proton after reaction. Its intensity increases with conversion, as more of these units are formed. As discussed in Chapter 2.2.1, the methyne alpha to hydroxyl ends can not be resolved from the other backbone methynes and methylenes in acetone-d_6. Thus the conversion cannot be calculated using this pair, except with reference to the aromatic region.

The region arising from carbamate NH is shown in Figure 4.5.[29] The narrow lines observed in acetone-d_6 allow resolution of the two different carbamate species, those arising from reacted NCO and those arising from unreacted NCO that have been end-capped with methanol. The higher field resonance can be attributed to the PPG carbamate based on the changes in the spectra observed with increasing conversion. There has been controversy regarding the validity of using NH resonances for quantitative analysis,[30] so the intensity observed in this region was confirmed by using it to calculate the conversion. Within experimental error, the degree of conversion agrees with titration.

The integrals of the various resonances are shown in Table 4.1. In the absence of side reactions, every urethane proton is associated with four phenyl ring protons.

$$\%\text{urethaneNH} = \frac{4 \cdot (\text{integral})_{\text{urethane}}}{(\text{integral})_{\text{aromatics}}} \cdot 100 \qquad (4.2)$$

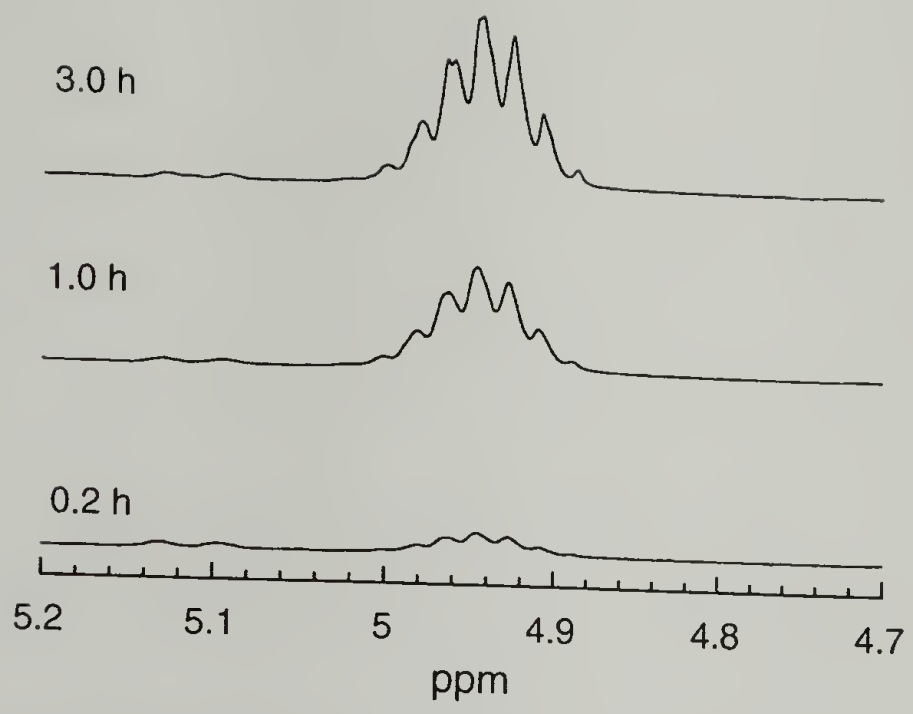

Figure 4.4 ^{1}H NMR spectra of PPG prepolymers prepared at 108 °C in the region of reacted PPG methyne ends.

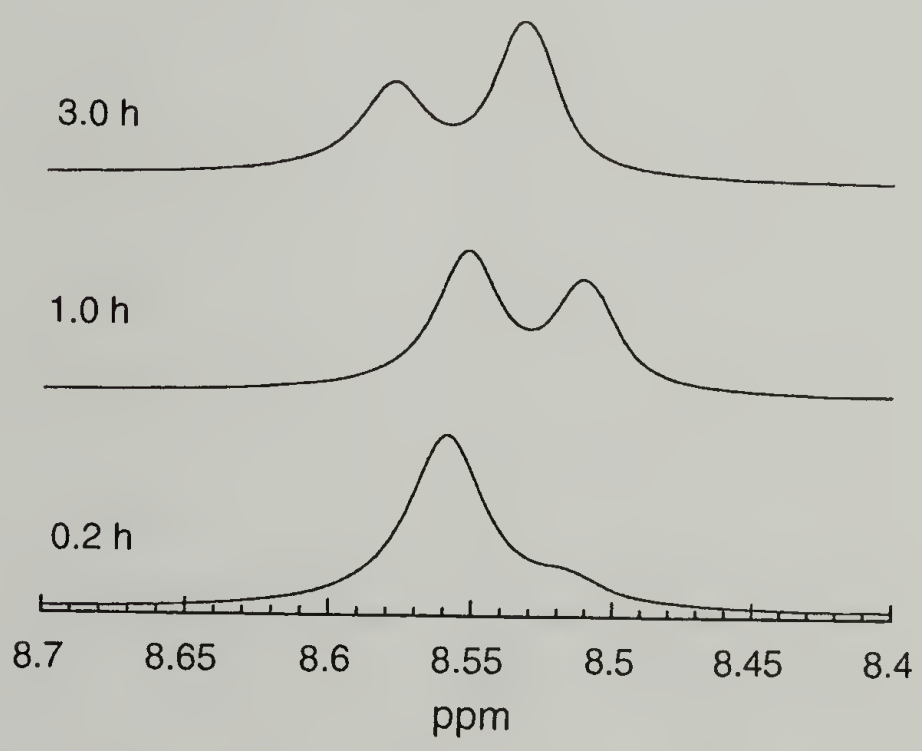

Figure 4.5 ^{1}H NMR spectra of PPG prepolymers prepared at 108 °C in the region of urethane protons.

Additional isocyanate or urethane consuming reactions will alter this ratio. As can be seen from Table 4.1, the fraction of MDI nitrogen characterized by urethane is between 89-90%. The remaining 10% must be involved in other types of linkages. Several of these linkages contain nitrogen-bound protons, such as allophanate, urea, and biuret. On the other hand, uretidinedione and isocyanurates do not contain NH. Thus, while these linkages will contribute intensity to the aromatic region, they will not display any other characteristic resonances in ^{1}H NMR.

Table 4.1 Results from the analysis of ^{1}H NMR spectra for prepolymers prepared at 108 °C.

Time (h)	Integrals from ^{1}H NMR in acetone-d_6		
	Aromatic	Urethane x 4	Allophanate x 8
0.2	1.00	0.888	0.000
1.0	1.00	0.901	0.003
3.0	1.00	0.888	0.009

The resonances that can be assigned to allophanate NH are shown in Figure 4.6.[29] At this reaction temperature, the number of these linkages is small. With increasing time, the intensity at 10.82 and 10.85 ppm increases. The origin of the two different resonances could not be determined. The total integrated area of this region is used to quantify this side reaction. The amount of allophanate is determined by first accounting for the 8 aromatic protons associated with this linkage, as shown in Equation 4.3. Then the total percentage of N that formed allophanates will be twice this number, since two nitrogen nuclei are involved in that linkage.

$$\%\text{allophanateNH} = \frac{8 \cdot (\text{integral})_{\text{allophanate}}}{(\text{integral})_{\text{aromatics}}} \cdot 100 \qquad (4.3)$$

At 108 °C for a reaction time of 3.0 h (98% conversion), only 1.8 mole% of N has formed allophanate. This is consistent with the amount of allophanate determined by the titration method for PPG prepolymers prepared in the melt, as discussed in the introduction.

The MDI used in this study contained 2% uretidinedione (mole% N). The sum of this species plus the urethane, allophanate, and urea populations should equal 1.0. In fact, the amount observed is always closer to 0.93. This would suggest that other linkages are formed during synthesis. Uretidinediones could be formed by the dimerization of MDI during reaction. Isocyanurates could be formed by the trimerization of MDI or by the reaction of an allophanate with another MDI.

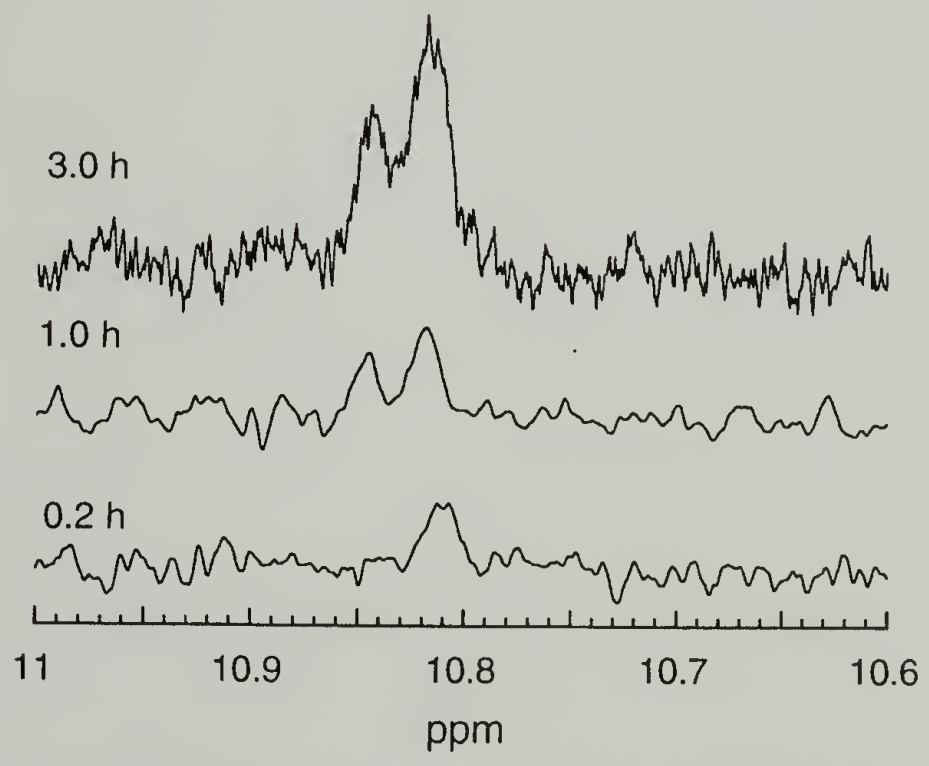

Figure 4.6 ^{1}H NMR spectra of PPG prepolymers prepared at 108 °C in the region of allophanate protons.

The rate of dimerization was determined for pure MDI by heating the sample at 108 ° for 8 h. The change in NCO content was determined by titration. After 8 h, only 2 mol% N had formed uretidinedione. This species was confirmed by end-capping the material with MeOH. The end-capped dimer and monomer have different solubility in a 50/50 (v/v) mixture of MeOH and $CHCl_3$. The dimer is insoluble in this solvent mixture. Infrared spectroscopy shows that the Amide I band is at 1777 cm^{-1} for this species. The dimer is only soluble in DMSO. Thus the ^1H NMR of this species cannot be directly compared with the ones above. However, ^1H NMR spectroscopy recorded in DMSO-d_6 reveals that the aromatic region is indeed sensitive to different structures. As observed for the prepolymers with conversion, the protons *meta* to the carbamate are not sensitive to structure. The dimer exhibits two resonances on the high field side. However, the region corresponding to the ortho protons is quite complicated as shown in Figure 4.7. The dimer has 4 additional resonances here, compared to the monomer. These do not overlap with the ones from the prepolymer. Three of these are on the low field side, and the other is downfield.

This region may be useful for quantification of the other secondary linkages. Isolation of a sample rich in MDI-MeOH allophanate showed that the allophanate also has several unique resonances, as shown in Figure 4.8. Incidentally, this material exhibits a single NH resonance at 10.81 ppm. The aromatic region appears to be highly sensitive to structure. This region is also convenient because the number of aromatic protons is much greater than the number of urethane protons. Unfortunately, close inspection of the prepolymer ^1H NMR spectra in the aromatic region did not aid in the assignment of the missing 7%.

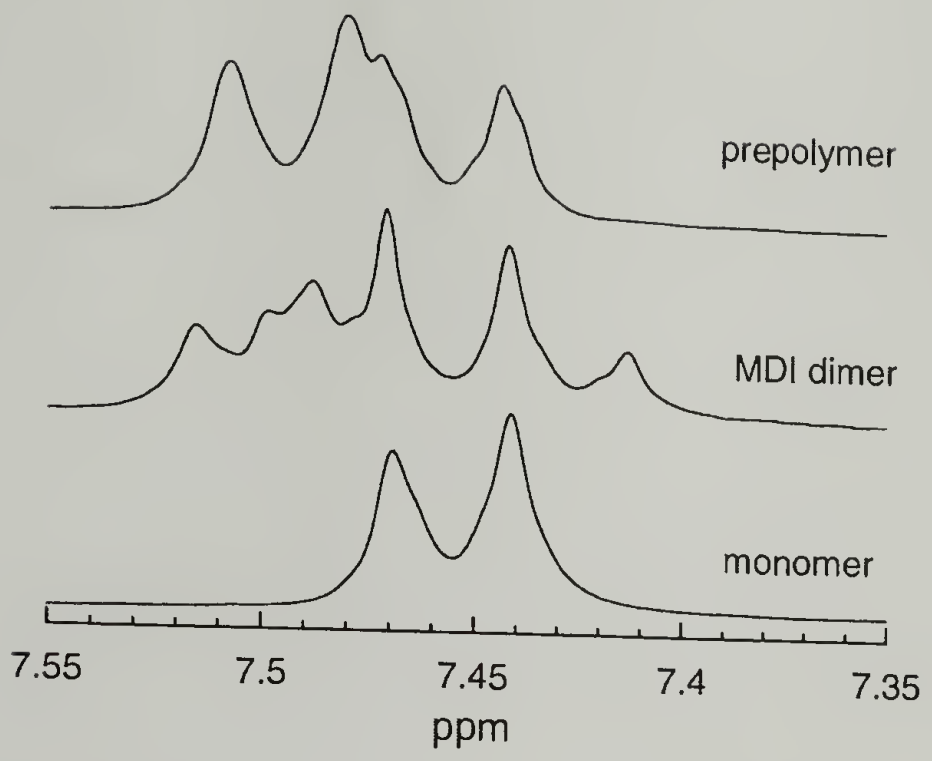

Figure 4.7 ^{1}H NMR spectra of MeOH end-capped MDI monomer, dimer, and prepolymer.

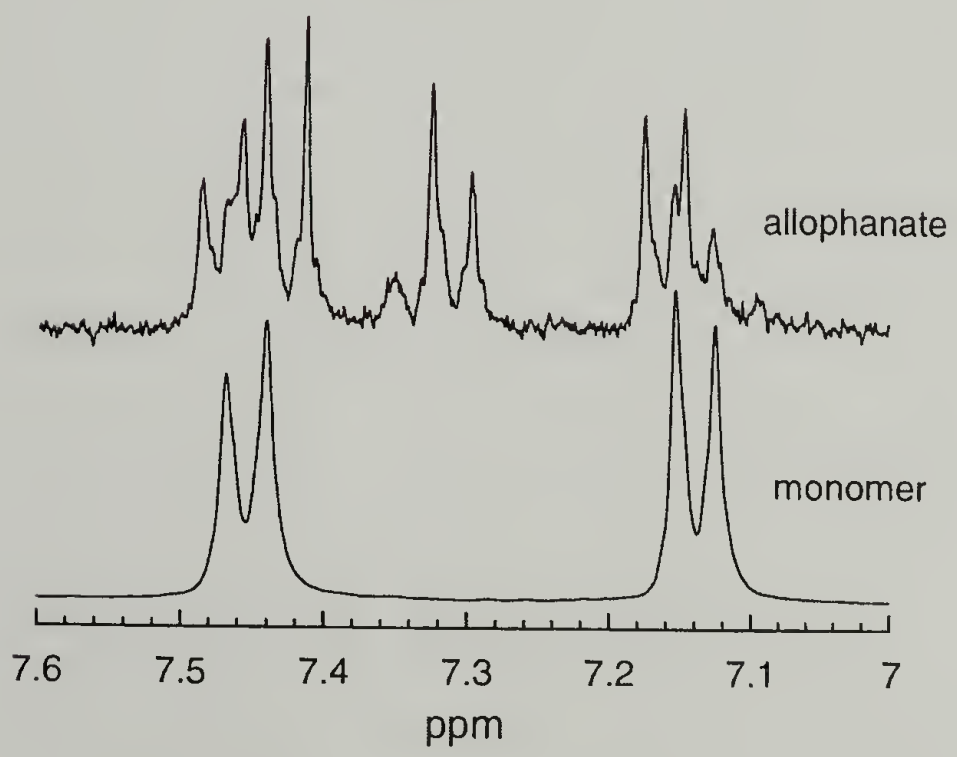

Figure 4.8 ^{1}H NMR spectra of a sample rich in allophanate prepared from MeOH and MDI.

The titration data for the prepolymers does not support any side reactions that only consume NCO, such as MDI dimerization or trimerization. These reactions would clearly decrease the amount of NCO measured and increase the apparent p_{OH} determined by titration. The data in Chapter 3 Table 3.1 shows that p_{OH} by titration is only 2-4% greater than p_{OH} by NMR. Thus the other possibility is a reaction that consumes urethane, such as isocyanurate. Because there are three nitrogens per isocyanurate, a small amount of this species would have a fairly large effect. ^{13}C NMR could not confirm the presence of isocyanurate. Considering the low concentration of allophanate formed and the fact that model studies have shown that in the absence of catalyst the population of isocyanurate is much less than the population of allophanate, it seems unlikely the 7% arises from isocyanurate.

The last possibility is that the 7% is due to the technique itself, possibly from exchange with the nitrogen quadrupole.[30] However, integration of the aromatic H and NH resonances for MeOH end-capped MDI gives quantitative 4:1 agreement. At present, it is not possible to account for the "missing" 7%.

4.3.2 Effect of Reaction Temperature

The influence of reaction temperature on structure formation was determined using a combination of ^{1}H NMR and SEC. Three reaction temperatures (108, 122, and 145 °C) were chosen since they correspond to the range generally used in most applications. Reactions were carried out for 1 to 3 h. (Table 4.2). One hour is insufficiently long to allow complete reaction, except for the sample at 145 °C. A reaction time of three hours gives complete or nearly complete conversion.

Titration detects the number of NCO groups. Calculation of ρ_{OH} is indirect and assumes no side reactions. The values obtained for 122 and 145 °C are greater than 1.0, which yields clear evidence that other NCO-consuming side reactions must have taken place. An additional 5.2 mole % and 7.9 mole % of NCO's were consumed by side reactions.

Table 4.2 Results for PPG prepolymers prepared under different reaction conditions

temp (°C)	time (h)	ρ_{NCO} (titration)	ρ_{OH} (titration)	ρ_{OH} (NMR in pyr)	allophanate (% N)
108	1.0	0.3984	0.6471	0.60	0.6
108	3.0	0.6000	0.9677	0.95	1.8
122	1.0	0.50	0.81	0.79	1.4
122	3.0	0.662	1.052	>0.95	3.5
145	1.0	0.5935	0.9707	0.93	5.6
145	3.0	0.6602	1.0788	>0.95	10.2

Using ^{1}H NMR spectroscopy, the percentage of N forming allophanate linkages can be determined (Table 4.2). Clearly, both reaction time and temperature have a dramatic effect on the allophanate population. For the sample prepared at 108 °C, the amount of allophanate is nearly negligible with only 1.8 mole % of N forming allophanates. Even after three hours at 122 °C, the amount of allophanate formed remained low. The amount observed was 1.4 and 3.5 mole % for reaction times of 1 and 3 h, respectively. At 145 °C, however, this reaction is no longer negligible. Comparing two prepolymers at similar conversion (122 °C, 3h versus 145 C, 1 h), the one prepared for a shorter reaction time at 145 °C contains a higher allophanate content. After 3 h, the amount reached 10 mole % N. In this case, the viscosity was noticeably higher.

Additionally, other side reaetions must have occurred. The error in the titration and the ^{1}H NMR is about 0.2 and 5.0%, respectively. Given that each allophanate linkage consumes one equivalent of urethane (already aceounted for in the titration) and one equivalent of isocyanate, the number of additional reaetions can be deduced from the titration and NMR data. For the sample prepared at 145 °C for 3 h, 7.88 mole % additional NCO is eonsumed. 5.1 mole % of this used to make allophanates. Thus approximately 3 mole % of the NCO groups are eonsumed by another reaction.

SEC results ean be combined with the data from NMR to determine how side reaetions perturb the moleeular weight distribution. Sinee the effeets of conversion have already been diseussed in the preeeding section, this part will focus on the threc samples that have reached similar eonversions, i.e. those prepared at 96, 122, and 145 °C for 3 h. The results are shown in Figure 4.9. Several eonelusions can bc reaehed. The prepolymers prepared at higher reaetion temperatures, and thus having larger allophanate eontent, exhibit higher moleeular weight. Second, M_P of the main oligomcr distribution near 2500 g·mol^{-1} shifts to slightly higher molecular weight (from 2300 to 2400), suggesting that the ineorporation of allophanate linkages into trimer molecules oeeurred. Finally, the diserete distributions that were evident at 108 °C are eonverted to broader distributions as allophanates are formed between ehains of various moleeular weights.

Beeause of the breadth of these distributions, the change in weight fraetion was caleulated for different ranges: 0 PPG, 1 PPG, 2 PPG, and ≥3 PPG. As the temperature was inereased the amount of 1 and 2 PPG-eontaining oligomers progressively deereased. On the other hand, the amount of free MDI deereased and seems to become constant. High moleeular weight speeies progressively increased. The conelusion based upon these

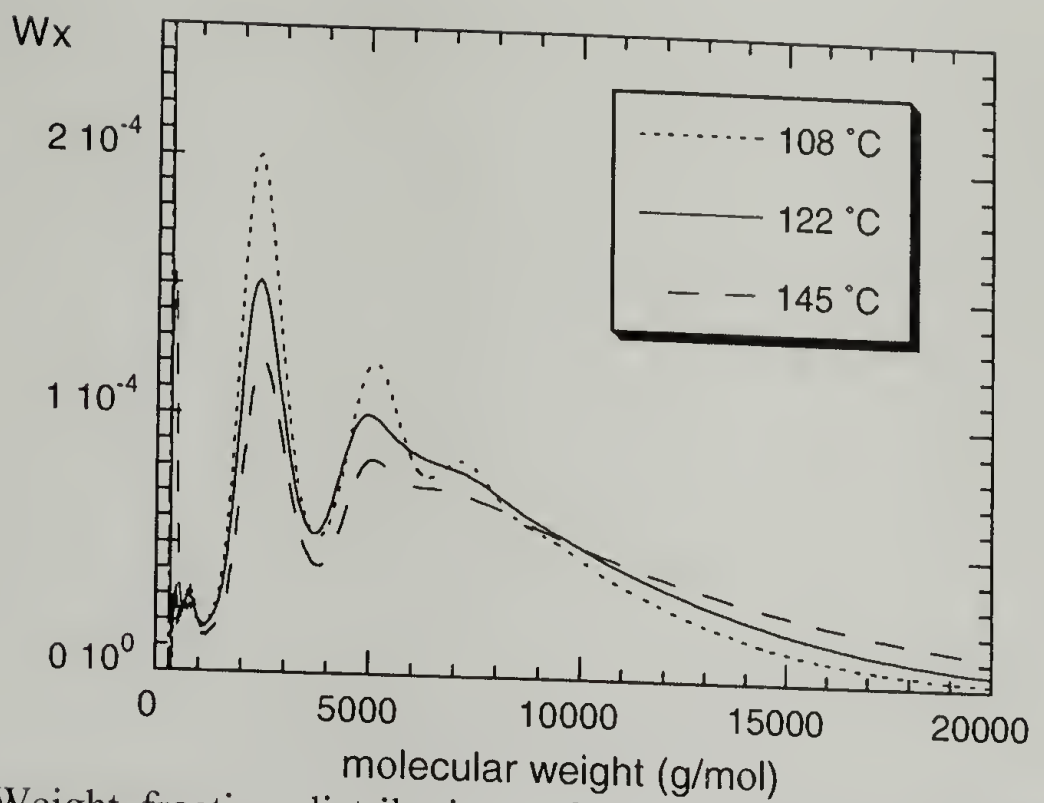

Figure 4.9 Weight fraction distributions of PPG prepolymers prepared at different temperatures.

observations is that free MDI is not preferentially consumed to form allophanates. Under these reaction conditions, it appears that it is equally favorable for both low and high molecular weight species to participate in the reaction.

4.3.3 Different Macrodiols

Ultimately, the adhesive is composed of a blend of polyether and polyester prepolymers. Other prepolymer systems may be composed of a single polyester or a blend of polyesters. Several differences exist between PPG and the various polyesters PHMA, PHMS, and PCL. The polyesters are end-functionalized with primary alcohols while PPG is end-functionalized with secondary alcohols. This should result in different rates of reaction with isocyanate. A second difference is that the polyesters, in particular PHMA and PCL, contain many impurities including carboxylic acid end groups. These

polymers are often prepared in the presence of tin catalysts. The PPG, on the other hand, often contains trace base. The final difference is in the polarity of their backbones.

The amount of allophanate was determined using ^{1}H NMR, as described above. The results based on an average of at least 3 different samples are shown in Table 4.3. In addition, the results from the prepolymer based on the ternary blend (PPG, PHMA, and acrylic) are shown.

Table 4.3. The amount of allophanate formed in different homo-prepolymers and blended prepolymers

Prepolymer	Allophanate (%N)
PPG (Batch 1)	8.0
PPG (Batch 2)	3.5
PHMA	0.5
PCL	0.5
Ternary Blend	9.0

Prepolymers prepared from PPG from two different sources yielded different amounts of allophanate. This may be attributed to different amounts of residual basic catalyst, though this has not been confirmed. Prepolymers prepared from both PHMA and PCL contain little to no allophanate. Because the PCL contains virtually no carboxylic acid end groups, the difference between PPG and polyester samples cannot be attributed to trace acid. It is interesting that the ternary blend contains almost the same amount of allophanate as the PPG prepolymer. The polarity of the acrylic and the polyester should be similar. Considering the ternary blend contains only 30 wt% PPG, the differences observed between the polyester homo-prepolymers and the other samples is most likely not due to the dielectric constant of the reaction medium. The reason for this result is

unclear. Very little is known about the acrylic structure and what types of impurities it contains.

The data shown in Table 4.3 strongly suggest that trace impurities in the raw materials can have important catalytic or inhibitory effects on the rate of allophanate formation. The data on small molecule literature is quite useful for determining which catalysts favor each reaction.[21] For example, the reaction of phenyl isocyanate with butanol and butyl N-phenylcarbamate in acetonitrile (0.4 M) using various catalysts ($3 \cdot 10^{-4}$ M) showed that the rate of urethane relative to allophanate formation was 10^5 and 0.31 for dibutyltin dilaurate and 1,8-diazabicyclo[5.4.0]undec-7-ene (DBU), respectively. The problem is determining the trace impurities in these samples.

4.4 Discussion of Polyurethane Prepolymer Structures

The structure determinations for polyurethane raw materials and prepolymers in the current Chapter and Chapters 2 and 3 shows that polyurethane prepolymers do not necessarily exhibit the idealized structures often assumed. Polyester raw materials were shown to exhibit significant amounts of cyclic structure. Cyclic polymers have low molecular weight and, as there is no participation in reaction, can remain "mobile" after curing. At moderate temperatures and at low conversion, the reaction between diol and diisocyanate exhibits a molecular weight distribution governed by step polymerization theory. At higher temperatures and higher conversion, other reactions besides linear polymerization occur, such as allophanate and isocyanurate formation. In addition to adding branched linkages, these reactions increase and broaden the molecular weight distribution.

With regards to allophanate formation, the most telling data is from the different prepolymer systems. The results point to the importance of trace impurities in the raw materials. In fact, trace impurities may explain some of the "discrepancies" observed in the literature. Three different studies, including the one in this Chapter, on allophanate formation or degradation give different results. In this study, increasing reaction temperature (80 to 140 °C), conversion, and time were found to increase the allophanate content. Yokoyama found that increasing conversion increased the allophanate content, but temperature (80 to 140 °C) had little effect.[5] Dusek found that increasing temperature (90 to 140 °C) and time (~days) decreased the amount of allophanate observed.[6] Examination of the specific conditions used in each case may explain some of the results. Dusek used dibutyltin dilaurate to catalyze polymerization, which may account for the dramtically different results observed. The difference between the data in this Chapter and Yokoyama's is not easy to explain. The PPG employed for the latter study had a lower molecular weight (Mn=1066); the source is not stated. Perhaps due to differences in the M_n or the methods used to obtain this product (Nagasaki, Japan 1977), more or less trace base may have been present in Yokoyama's samples.

The additional structures observed in the prepolymer systems may influence the phase behavior. In trying to characterize the end-capped ternary prepolymer blends, some results suggesting the importance of structure were observed. Prior to reaction, the raw materials had slightly different solubility, as shown in Table 4.4. The preferential solubility of PPG in MeOH was used to fractionate the adhesive prepolymer into two fractions, one containing PPG prepolymer and the other containing polyester prepolymer and acrylic. MALDI-TOF and ^{1}H NMR were used to characterize these fractions.

Table 4.4 Solubility of polyurethane raw materials at 22 °C

	CCl_4	DMF	DMSO	THF	Acetone	MeOH	Benzene	Dioxane	$CHCl_3$	CH_3CN
PHMA	N	N	N	Y	N	N	Y	Y	Y	N
PPG	Y	Y	Y	Y	Y	Y	Y	Y	Y	Y
Acrylic	Y	Y	N	Y	Y	N	Y	Y	Y	Y

1 part material in 5 parts solvent
Y=soluble, N=insoluble

This method, in fact, worked reasonably well. PPG-rich and PHMA-rich fractions could be obtained. However, the fractionation was not completely efficient. MALDI-TOF showed that all the cyclic polyester was in the PPG-rich phase; in other words, this non-functional polyester had different solubility than the functionalized version. ^{1}H NMR showed that the PPG-rich phase contained fewer allophanates than the PHMA-rich phase, 4 and 12 mol% N, respectively. The fact that PPG resonances were also observed in the PHMA-rich phase and that PPG homo-prepolymers contained the same amount of allophanate as blends lead to the conclusion that allophanate-containing PPG prepolymers are less soluble than the linear version. That the solubility of the polymers is so dramatically influenced by the end groups and/or linkages along the backbone demonstrates the importance of identifying these structures.

4.5 Conclusions

^{1}H NMR spectroscopy was combined with titration data to determine the influence of reaction temperature, conversion, and time on the types of structures observed in polyurethane prepolymers. For PPG homo-prepolymers, the amount of

allophanate increased with increasing reaction temperature. At 145 °C, 10 mole% of N is involved in allophanate linkages. For polyester prepolymers, allophanate formation is negligible. On the other hand, ternary prepolymer blends exhibit behavior similar to PPG prepolymers. The results from the different systems cannot be rationalized according to differences in end group reactivity or medium polarity.

4.6 References

(1) Listemann, M. L.; Savoca, A. C.; Wressell, A. L. *J. Cell. Plast.* **1992**, *28*, 360.

(2) Illger, H.-W.; Dorner, K.-H.; Hettel, H. In *Polyurethanes World Congress*; Technomic Publishing Co., Inc.: Aachen, Federal Republic of Germany, 1987; p 305.

(3) Sandridge, R. L.; Morecroft, A. S.; Hardy, E. E.; Saunders, J. H. *J. Chem. Eng. Data* **1960**, *5*, 495.

(4) Kaji, A.; Arimatsu, Y.; Murano, M. *J. Polym. Sci., A Polym. Chem.* **1992**, *30*, 2877.

(5) Yokoyama, T.; Furukawa, M. In *International Progress in Polyurethanes*; Ashida, K., Frisch, K. C., Eds.; Technomic: Westport, CT, 1977; Vol. 2, p 125.

(6) Dusek, K.; Spirkova, M.; Havlicek, I. *Macromolecules* **1990**, *23*, 1774.

(7) Baker, J. W.; Gaunt, J. *J. Chem. Soc.* **1949**, 9.

(8) Kogon, I. C. *J. Org. Chem.* **1959**, *24*, 83.

(9) Saunders, J. H.; Frisch, K. C. *Polyurethanes Chemistry and Technology. Part I. Chemistry*; John Wiley & Sons: New York, 1962; Vol. XVI.

(10) Wong, S.-W.; Frisch, K. C. *J. Polym. Sci., A Polym. Chem.* **1986**, *24*, 2867.

(11) Ajithkumar, S.; Kansara, S. S.; Patel, N. K. *Eur. Polym. J.* **1998**, *34*, 1273.

(12) Sivakamasundari, S.; Ganesan, R. *J. Org. Chem.* **1984**, *49*, 720.

(13) Baker, J. W.; Holdsworth, J. B. *J. Chem. Soc.* **1947**, 713.

(14) Robertson, W. G. P.; Stutchbury, J. E. *J. Chem. Soc.* **1964**, *19*, 4000.

(15) Ephraim, S.; Woodward, A. E.; Merobian, R. B. *J. Am. Chem. Soc.* **1958**, *80*, 1326.

(16) Oberth, A. E.; Bruenner, R. S. *J. Phys. Chem.* **1968**, *72*, 845.

(17) Satchell, D. P. N. S., R.S. *Chem. Soc. Rev.* **1971**, 231.

(18) Caraculacu, A. A.; Coseri, S. *Prog. Polym. Sci.* **2001**, *26*, 799.

(19) Donohoe, G.; Satchell, D. P. N.; Satchell, R. S. *J. Chem. Soc.-Perkin Trans. 2* **1990**, 1671.

(20) Raspoet, G.; Nguyen, M. T.; McGarraghy, M.; Hegarty, A. F. *J. Org. Chem.* **1998**, *63*, 6878.

(21) Schwetlick, K.; Noack, R. *J. Chem. Soc.-Perkin Trans. 2* **1995**, *2*, 395.

(22) Sojecki, R. *Acta Polym.* **1989**, *40*, 619.

(23) Sojecki, R. *Acta Polym.* **1991**, *42*, 411.

(24) Sojecki, R. *Acta Polym.* **1992**, *43*, 96.

(25) Sojecki, R. *Eur. Polym. J.* **1994**, *30*, 725.

(26) Stovbun, E. V.; Kuzaev, A. I.; Baturin, S. M. *Polym. Sci., Ser. A.* **1996**, *38*, 691.

(27) Pisareva, I. V.; Bakalo, L. A.; Gritsenko, V. P. *Kinet. Kat.* **1988**, *29*, 547.

(28) Querat, E.; Tighzert, L.; Pascault, J. P.; Dusek, K. *Angew. Makromol. Chem.* **1996**, *242*, 1.

(29) Sumi, M. C., Y.; Nakai, Y.; Nakabayshi, M.; Kanzawa, T. *Makromol. Chem.* **1964**, *78*, 146.

(30) Kricheldorf, H. R.; Hull, W. E. *Makromol. Chem.* **1981**, *182*, 1177.

CHAPTER 5

ORDER FORMATION IN CRYSTALLIZABLE POLYURETHANES

5.1 Chapter Overview

In the previous chapters, the chemical structure of reactive polyurethane blends was examined. Changes in the molecular weight and chemical linkages were generally predicted to have opposing effects on the miscibility. Based on solubility data, it was suggested that other variables, such as secondary linkages and branching, may also be important. In addition to miscibility behavior, crystallization, or order formation, is also critical to the material properties. The crystallization behavior of the crystallizable macrodiols of reactive blends may be modified upon incorporation of urethane functionality. And while the phase separation of hard domains may be driven by the entropic contribution from the rigid polyurea segments, the nature of the hydrogen bonds may influence the kinetics of this transition and also the final order achieved.

In this chapter, crystallization behavior of model polyurethanes is examined. The influence of hydrogen bonding on crystallization kinetics and morphology is described. In this chapter, infrared spectroscopic techniques are developed to study changes in the ensemble of hydrogen bonds. This technique will be used in Chapter 6 to follow reaction and phase evolution during ordering.

5.2 Crystallization of Strongly Interacting Chains

The problem considered in this chapter is the crystallization of polymers under constraint. Typical polymer crystallization can be considered as crystallization under one

degree of constraint, since the molecular repeat unit loses a degree of freedom by being confined to a chain. In strongly interacting systems, the repeats lose another degree of freedom due to the strong interactions in the melt. A strongly interacting polymer is any of the polyamides, polyurethanes, polyureas, polyesters, or other polymers containing strong secondary interactions between chains. A relationship must exist between the crystallization behavior and the magnitude, number, and sequence length between functional groups. Depending on this spacing and the specificity of the interactions, the functional groups could be incorporated into the crystal, and may in fact drive the crystallization, or the groups may be segregated as defects at the crystal surface. That the type of crystal structure, fold surface, and morphology formed depends on the periodicity between functionalities has already been observed for aliphatic poly(amides)[1-3] and polyesters.[4,5] Similarly for aliphatic polyesters, the lamellar thickness of the crystallites formed has also been attributed to the interchain dipole-dipole interactions. [6] In proteins, short-range attractive interactions are observed to facilitate aggregation rather than nucleation.[7,8]

The system studied here is a crystallizable polyurethane, X,8 PU, as described in Chapter 2.3. The structure is shown again in Figure 5.1, The periodicity of the urethane units can be modified with X = 12, 22, 32. Ordering in this system has an enthalpic component (hydrogen bonding of the urethane functionalities) and an entropic component

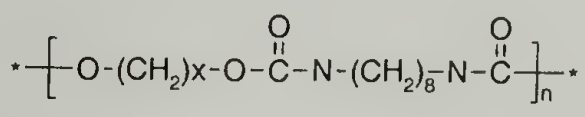

Figure 5.1 Chemical structure of X,8-polyurethanes.

(ordering of the aliphatic segments). The contribution from each of these components can be modified through varying the periodicity.

To understand the expected influence of constraining a polymer in two dimensions, it is logical to look at how crystallization is influenced by constraining a molecule in one dimension. Thus the crystallization behavior of small molecules and polymers will first be compared.

5.3 Crystallization Theory

The crystallization of inorganic salts and organic molecules has been studied since the late 17th century.[9] A crystal is defined as a regular three dimensional arrangement of molecules into a rigid lattice. The mechanism of crystallization can be generally broken down to three main requirements: achievement of supersaturation or supercooling, formation of crystal nuclei, and subsequent crystal growth. A nucleus is defined as a small aggregate that acts as a center of crystallization. Nucleation can be broken into several categories. Primary nucleation can be either homogeneous or heterogeneous, if induced by foreign particles. A distinction can also be made from secondary nucleation, which is induced by crystals. Exactly how a nucleus is formed is not known. To form a nucleus, molecules must aggregate and become oriented into a lattice. Homogeneous nucleation is usually envisoned as occurring through fluctuations in the supersaturated, or supercooled, state, causing temporary aggregation of the molecules. When groups of freely moving molecules become aggregated into a condensed state, there is a decrease in free energy, associated with the free energy of fusion (Δg_f). However, the formation of a condensed particle requires an expenditure of

energy to create a surface (γ). The interfacial tension is positive, and, assuming a spherical nucleus, goes as the square of the nucleus radius. The bulk free energy change is negative and goes as the radius cubed.

$$\Delta G = 4\pi r^2 \gamma - \frac{4}{3}\pi r^3 \Delta g_f \tag{5.1}$$

Ostwald was the first to develop the concept of a critical size nucleus – one whose size balances the bulk and surface terms.[10] Below this critical size, the nucleus is unstable and dissolves, or melts. The size of the critical nucleus can be determined by setting $d\Delta G/dr = 0$. Equations 5.2 and 5.3 give the free energy of fusion and critical size in terms of supercooling.

$$\Delta g_f = \frac{\Delta h_f \Delta T}{T^o} \tag{5.2}$$

$$r_c = -\frac{2\gamma T^o}{\Delta h_f \Delta T} \tag{5.3}$$

T^o is the solid-liquid equilibrium temperature and ΔT is the supercooling.

The energy required for surmounting this energy barrier comes from the statistical distribution of energy in the supercooled, or supersaturated, state. The rate of nucleation can thus be expressed in Arrhenius form as shown in Equation 5.4.

$$N = A \cdot \exp\left(-\frac{\Delta G}{RT}\right) = A \cdot \exp\left(\frac{16\pi\gamma^3}{3kT^o \Delta h_f^2 T_r \Delta T_r^{\,2}}\right) \tag{5.4}$$

$T_r = T/T^o$ and $\Delta T_r = \Delta T/T^o$. The amount of supercooling clearly has a very large effect on both the critical size nucleus and the rate of nucleation.

The above treatment is considered classical nucleation theory based on the capillarity approximation. There has been much new effort focused on atomistic

descriptions of nucleation.[11-15] The main point is that while nucleation is widely discussed, the concept is still not well understood, even for small molecules.

Crystal growth is defined as the development of stable nuclei into larger size. Crystal growth is a phenomenon that is easy to measure experimentally, via light microscopy or dilatometry, but is difficult to explain mechanistically. There are several theories to explain the mechanism of growth, and they will only be mentioned briefly. The first, based on the idea that the shape formed during growth is the one that minimizes the surface free energy, are referred to as surface free energy theories. Diffusion theories began with the assumption that crystallization is the reverse of dissolution (or melting) and that it is governed by the difference in concentration at the solid surface versus the bulk (or the difference in heat transfer between the crystal face and the bulk liquid). In fact, the rate of crystallization is not the same as that for dissolution. This led to the notion that an additional "reaction" must take place once the molecule has diffused to the growing crystal face. Depending on the degree of supercooling, or supersaturation, the growth rate is considered to be either diffusion controlled or reaction rate controlled. A final set of theories was developed by Gibbs and Volmer and is referred to as absorption layer theories. When molecules move to the crystal face, they are not immediately added to the lattice. Instead they become loosely adsorbed and form an adsorption layer. Once there they will add into the lattice where the attractive forces are the greatest. For example, "corners' and "edges" are the most favorable positions. A further modification of this theory, developed by Kossell, imagines that crystals with rough surfaces will grow the fastest.

Having established some of the important overall concepts in crystallization, the influence of constraining the molecules in one dimension, i.e. a polymer chain, will be addressed. First the initial states will be compared, then the overall morphology, and finally the differences in kinetics will be examined.

Because the main difference between polymers and small molecules is that the repeat units remain covalently linked upon melting, the entropy gain upon melting is much smaller for polymers than for small molecules. Polymer chains exist in random coil conformations in order to maximize the amount of disorder. The flexibility of the chain is described by the potential energy required to rotate about the backbone bonds. More flexible chains exhibit a larger distribution of conformations at any given time compared to more rigid chains.

The equilibrium state for a polymer crystal would be a crystal composed of extended chains. However, this is not what is observed. When polymers crystallize, they do so by forming chain-folded lamellae. The exact nature of the fold surface depends upon whether the polymer was crystallized from the melt or from solution. In contrast to small molecules, polymer crystals have a finite size in one direction, called the lamellar thickness. In addition, polymers are usually semi-crystalline. In other words, there is usually amorphous material either at the lamellar surface or between stacks of lamellae. These facts highlight the importance of kinetics in determining the morphology of polymer crystals.

Similar to the case of small molecule crystallization, nucleation and growth theories are used to explain the kinetics of polymer crystallization. Many different theories exist, and the exact description of the mechanism and rate determining steps is

not agreed.[16-19] The nucleation theory discussed above is also invoked to describe polymer nucleation. Through this treatment, the important fact that the lamellar thickness is dependant on supercooling, as dictated by the energy barrier to forming a stable nucleus, can be deduced. The fold surface free energy is typically higher than the lateral surface free energy. [16]

The rate determining step in Hoffman-Miller's kinetic theory at low supercooling is the adsorption of an aligned and segmentalized chain stem to the substrate (primary surface nucleation). This approach is not unlike the adsorption layer theories mentioned above. There has been some effort to relate the lateral surface free energy to the characteristic ratio, C_∞.[20] The important consequence of this relationship is that it predicts that the nucleation rate of stiff chains is faster than that for flexible chains since the loss of entropy upon approaching the substrate is not as great. This theory is controversial.[21]

At large supercooling, growth becomes the rate-limiting step. In particular, the mobility of the chains ceases at T_g and prohibits polymer crystal growth. Thus a plot of spherulitic growth rates as a function of supercooling is bell-shaped due to the competing effects of nucleation and growth. A general description of growth curves is given by Equation 5.5.

$$G = G_o \exp\left(-\frac{\Delta G_c}{kT}\right)\exp\left(-\frac{\Delta U^*}{kT}\right) \qquad (5.5)$$

G is the growth rate at temperature T, G_o is a pre-exponential factor, ΔG_c is the free energy of formation of a critical nucleus, and ΔU^* is the activation energy of the elementary jump process. The first term describes nucleation while the second term described growth. The sensitivity of the mobility term to temperature and molecular weight is another distinction from small molecule crystallization. In order for a crystal to

form, the polymer chains must be reeled in from the surrounding entangled melt. Molecular mobility and ΔU^* has traditionally been described by the WLF equation.

Depending on the relative rates of secondary nucleation and surface spreading (growth), three different regimes have been found to exist. Regime I is the classical case for small molecules where surface spreading is much faster than nucleation. Regime II is the case where the rates are similar. Regime III describes the case where the rate of nucleation is faster than the rate of surface spreading. This last case is thought to be unique to polymers. Evidence for these regimes is found from the kinetics and also indirectly from the crystal morphology. Needles, spherulites, and axialites are found in Regime I, II, and III, respectively. [22]

The main modifications that constraining the molecules in one dimension has on the crystallization behavior is as follows:

1) Crystals have finite thickness. The polymer chain accommodates the kinetic obstacle of completely disentangling itself by forming chain-folded lamellae. The lamellar thickness is governed by supercooling.

2) Polymer crystals are almost always semi-crystalline. The lamellar surface is a higher energy surface than the lateral surface and probably contains various defects, end-groups and folding homogeneities. When crystallized from the melt, lamellae also have amorphous material layered between stacks, much like wafer cookies.

3) Nucleation may be easier for polymers since the entropic loss upon crystallization is not as great as for small molecules.

4) Due to the limited mobility of polymer chains at high supercooling, a crystallization regime can be found where the rate of nucleation is faster than the rate of growth.

How is the crystallization behavior of a segment modified by constraining it in two dimensions? In fact, this question has not been considered in this manner. A combination of vibrational spectroscopy, WAXS and differential scanning calorimetry were used in the present work to address this question. The influence of hydrogen bonding interactions on crystallization were studied by first considering a single polyurethane system, 22,8 PU. The initial molten phase, crystalline morphology, and crystallization kinetics were considered. Then the influence of changing the length of the methylene spacer was considered.

5.4 Experimental

Infrared spectroscopic measurements were carried out on a Perkin Elmer 2000 system with a wide band MCT detector. Samples were prepared by dissolving the polymer in hot *o*-dichlorobenzene and casting a film onto KBr plates. The plates were dried under vacuum at 90 °C for several hours. No evidence of residual solvent was observed spectroscopically.

Measurements of the molten samples were performed with 2 cm^{-1} spectral resolution and 16 scans were signal averaged. The temperature was controlled using a bespoke heating cell attached to an Omega proportional controller that could be accommodated into the N_2 purged sample chamber. The temperature was calibrated to the melting point of benzoic acid. Sample temperature was simultaneously monitored

using two other thermocouples to assure thermal equilibrium had been attained in the heating cell. Samples were equilibrated at a given temperature for at least 30 minutes.

During crystallization experiments, rapid measurements were necessary, so the resolution was set to 4 cm^{-1} and only one scan was needed to obtain high quality data for analysis. A Mettler hot stage was used to control the temperature and cooling rate to within an accuracy of ± 0.6 °C. The sample was sandwiched between two KBr plates and placed in the hot stage. This hot stage was then mounted in the N_2 purged sample chamber and adjusted until sufficient throughput could be obtained. Spectra were recorded approximately every 5 seconds. The melted sample was held at 160 °C (20 °C over the melting point) for at least 30 minutes. The length of time held in the molten phase was used to prevent any possibility that memory remains.[23] During this holding time, the infrared spectrum was monitored, and no spectral changes were seen after the first minute. Observation of higher holding temperatures (up to 185 °C) showed that 160 °C was sufficient to remove any spectroscopic evidence of crystallinity. The molten phase was then crystallized at a given cooling rate ranging from 2.5 to 15 $°C \cdot min^{-1}$.

Band deconvolution of the Amide I region was carried out following the procedure established previously.[24] To observe crystallization of the methylene chains, the contribution from disordered sequences was subtracted. The intensity at 1405 and 1335 cm^{-1} arises from particular methylene defect sequences in the molten or amorphous phases.[25] The spectrum of the disordered structure was determined in the region from 1270-1420 cm^{-1} by the spectrum obtained immediately prior to crystallization. Different percentages of this spectrum were subtracted from the succeeding spectra so that the baseline at 1405 cm^{-1} and 1335 cm^{-1} was zero. The remaining contribution is from the

"straight" methylene sequences. The intensity increases as the low wavenumber side is approached due to the contribution from the Amide III mode near 1250 cm^{-1}.

The rate of primary crystallization for various cooling rates was determined from the increase in intensity of the ordered hydrogen bonds (1684 cm^{-1}) with time using numerical differentiation as shown in Equation 5.6.

$$\left.\frac{dI_{1684}}{dt}\right|_j = \frac{\left(I_j - I_{j-1}\right)}{\left(t_j - t_{j-1}\right)} \tag{5.6}$$

Raman spectroscopic measurements were either performed on a Fourier transfer Raman (FT Raman) or dispersive Raman spectrometer. A Bruker FRA 106 spectrometer equipped with a Nd:YAG laser (1.064 μm) was used to record the FT Raman spectra. A total of 256 scans were performed, and spectral resolution was 4 cm^{-1}. The laser power was 150 mW, and the excitation/collection geometry was 180 °. Dispersive Raman spectra were obtained using the incident intensity of a vertically polarized Spectra Physics Model 165-08 argon ion laser tuned to the 5145 Å excitation line and collected at 90 °. A Newport Model RSA-2 polarizer selected scattered light of the appropriate linear polarization state, and this light was subsequently converted to circular polarization by a scrambler, ensuring that the gratings of the detection system would not induce polarization artifacts in the spectra. Photons of the desired wavelength were subsequently passed to a photomultiplier tube by an ISA Ramanor U-1000 double monochromator. Photon counts were acquired using Spectra-Link software. The region of interest was scanned at 1 s/point at 0.5 cm^{-1} increments. Spectral resolution was 4 cm^{-1}, and the laser power after the filter was 100 mW. Isotropic Raman scattering intensities were calculated from the parallel and perpendicular components of the experimentally measured Raman

scattered light: $I_{iso} = I_{\parallel}(\nu) - 4/3\ I_{\perp}(\nu)$. The 314 cm^{-1} band of carbon tetrachloride was used to verify the accuracy of the scattering geometry and light collection and gave the expected value of 0.75 within 2%.

Wide-angle X-ray scattering (WAXS) experiments were performed at room temperature using a Ni-filtered Cu Kα radiation of wavelength 1.542 Å from a Siemens D500 diffractometer mounted with a θ-2 θ goniometer. Instrumental line broadening was determined using calcite ($CaCO_3$) standard and calculating the full width at half maximum (FWHM).

Differential scanning calorimetry (DSC) was performed on a Perkin Elmer DSC-7. The temperature scale was calibrated using indium and eicosane, and the enthalpy was calibrated using indium.

5.5 22,8 PU

5.5.1 Characterization of the Melt

One of the major differences between strongly interacting polymers and polyethylene is that the intermolecular interactions in the former may persist in the melt. Complete characterization of the disordered molten phase includes defining the number of interactions, the strength of the interactions, and the distribution of chain conformations at a given temperature.

Historically, the existence of hydrogen bonds has been most readily illustrated from changes in the N-H stretching region, shown in Figure 5.2 for both molten and crystalline 22,8 PU. This region contains several contributions depending on the state of hydrogen bonding of the N-H. Species that are not hydrogen bonded, but free, N-H are

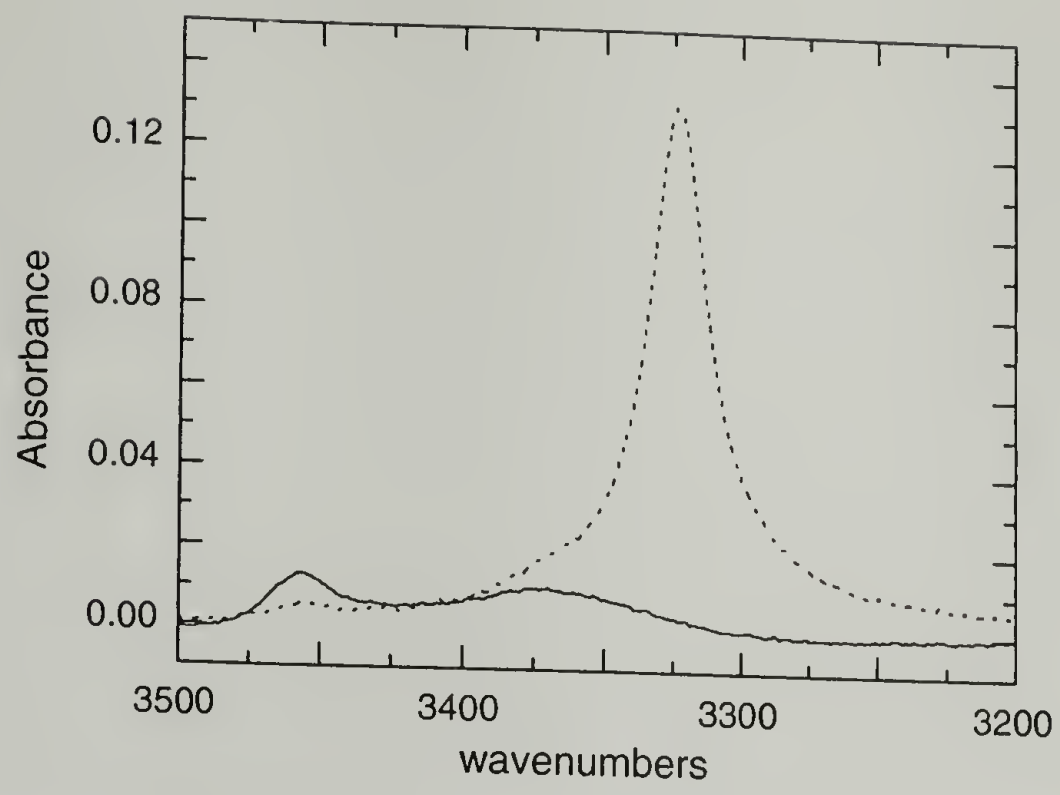

Figure 5.2 Infrared spectra of 22,8 PU in the N-H stretching region showing the melt at 160 ˚C (solid line) and the crystal (dashed line).

observed at 3456 cm^{-1}. In the crystal, the N-H forms a hydrogen bond with a specific geometry, which in this case is observed at 3322 cm^{-1}, "ordered." The hydrogen bonds in the melt exhibit a broad N-H band near 3370 cm^{-1}. This broad band reflects that the N-H hydrogen bonds are not characterized by a single geometry, but rather a distribution of geometries. In the melt, the hydrogen bonds are continuously breaking and reforming, and the shape of the N-H band represents this ensemble.

The inherent resonance contribution to the relative intensities of the these bands make using this region for quantitative analysis difficult.[26] However, the frequency difference, $\Delta\nu$, between free and hydrogen bonded species provides a simple measure of the strength of the hydrogen bond. The enthalpic contribution can be determined using Equation 5.7. [27]

$$-\Delta H_{sp.int.}^{NH/O=C} = \frac{59.3 \cdot \Delta v}{\Delta v + 674} \qquad (5.7)$$

Using this approach, 22,8 PU has an interchain interaction in the range from -7.03 to -6.40 $kJ \cdot mol^{-1}$, depending on the temperature.

This technique, while quite easy to use, provides only an indirect measure of the hydrogen bond strength. The thermodynamic parameters in the melt can be obtained more directly using the Amide I region, shown in Figure 5.3. Like the N-H stretching region, the Amide I bands reflect the strength and geometry of the hydrogen bonds. In contrast, this region is more appropriate for quantitative analysis due to the relative insensitivity of the absorption coefficient to hydrogen bond strength; thus the number of hydrogen bonded species can be determined.

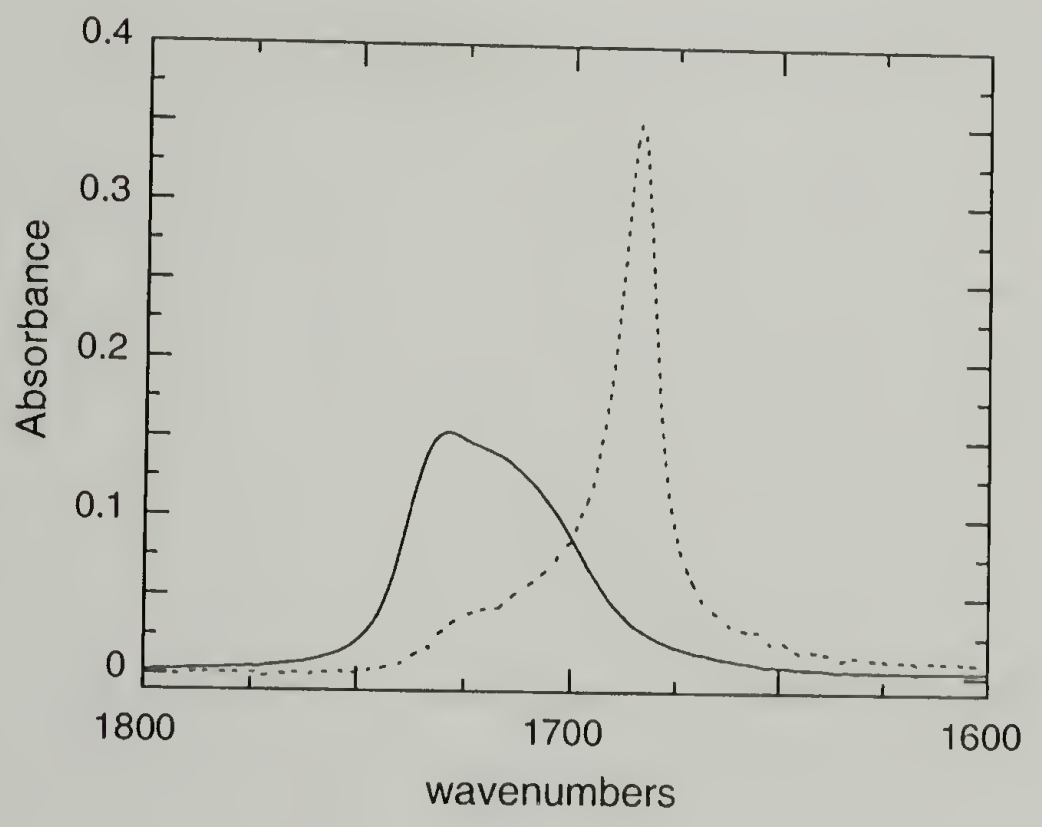

Figure 5.3 Infrared spectra of 22,8 PU in the Amide I region showing the melt at 160 °C (solid line) and the crystal (dashed line).

The bands owing their intensity to free C=O (1732 cm^{-1}), disordered hydrogen bonded C=O (1718-1709 cm^{-1}), and ordered hydrogen bonds (1685 cm^{-1}) are overlapping, so a curve fitting routine must be used to resolve the amount of each species, as shown, for example, in Figure 5.4. Results for molten samples are shown in Table 5.1. The absorption coefficients for the free species is slightly lower than that for the associated species but was corrected by adjusting the hydrogen bonded intensities by a factor, k=1.81, such that the total area remained invariant with temperature. This then allows calculation of the fraction of each species present. [24]

The thermodynamic properties of the molten phase can be determined using the amount of free species ([free]) determined from the spectra. By assuming that hydrogen bonds associate as dimers, the equilibrium constant can be determined from the fraction of free urethanes by Equation 5.8.

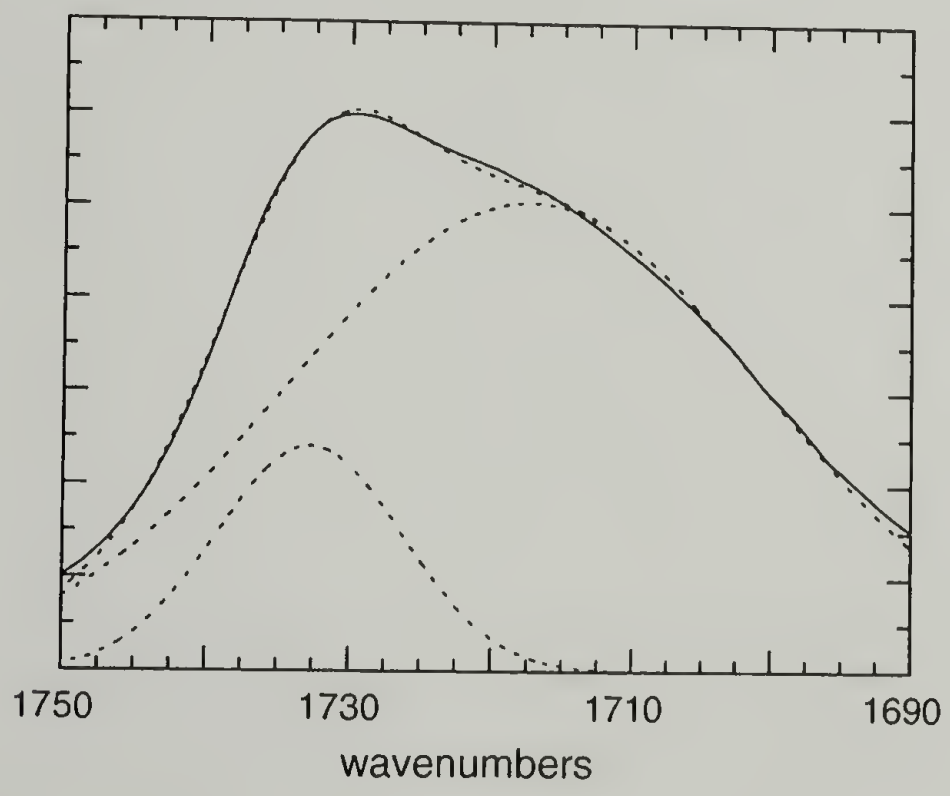

Figure 5.4 Infrared spectrum in the Amide I region (solid line) and the corresponding curve fit into free and disordered hydrogen bonded components (dashed lines).

$$K = \frac{1 - [\text{free}]}{2 \cdot [\text{free}]^2} \tag{5.8}$$

As shown in Figure 5.5, the enthalpy and entropy of hydrogen bond formation ean be determined from a van't Hoff plot. This method assumes that the hydrogen bond strength does not depend upon temperature. The enthalpy of hydrogen bond formation (ΔH_{HB}) was found to be –7.20 kJ·mol^{-1}. The entropy was found to be -2.09 J·mol^{-1}·K^{-1}.

Both methods have yielded similar interaetion values. The enthalpie differenee, ΔH_{HB}, is approximately -7.11 kJ·mol^{-1} per urethane or -14.22 kJ·mol^{-1} per repeat. Speetroseopie data shows that approximately 75% of the urethane groups are hydrogen bonded in the melt at 155 °C. Given the motions available to the polymers, this value is an average of many possible states. Hydrogen bonds have been shown to hinder ehain relaxation.[28] Thus the mobility of ehains in strongly interaeting melts is mueh lower than in polyethylene.

Table 5.1 Results from eurve fitting of amide I region

	Disordered H-Bonds			Free Carbonyls					
Temp (°C)	position (em^{-1})	width (em^{-1})	Area	position (em^{-1})	width (em^{-1})	Area	Total	Total a	[free]
143	1716	39.8	20.75	1732	15.2	3.72	24.47	15.06	0.247
154	1717	39.8	20.53	1732	15.2	3.78	24.31	14.99	0.252
164	1717	39.8	20.49	1732	15.3	3.84	24.33	15.04	0.256
171	1718	39.8	20.45	1732	15.3	3.89	24.34	15.07	0.258
182	1718	39.8	20.22	1732	15.5	4.00	24.22	15.05	0.266
186	1719	39.8	20.11	1733	15.6	4.04	24.14	15.02	0.269

a) Total area eorreeted by a faetor (k) as described in the text.

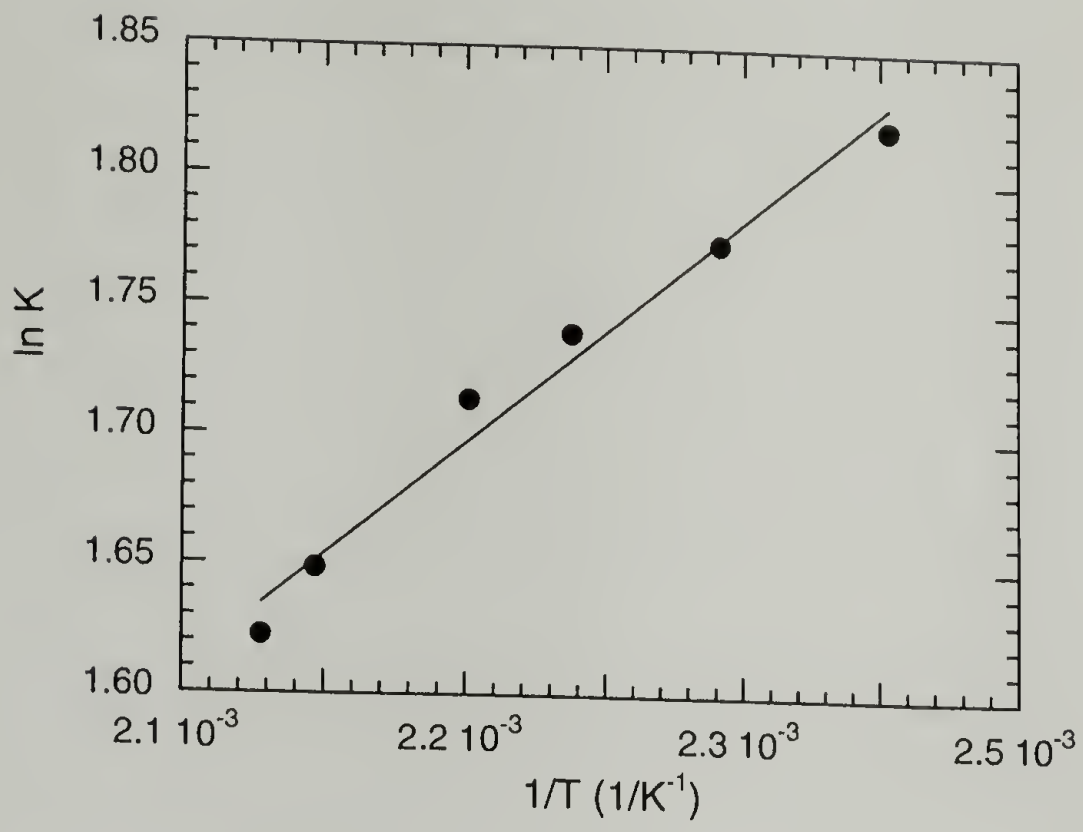

Figure 5.5 Van't Hoff plot determined based on data from Amide I curve fitting.

Determination of the methylene chain conformation is much more difficult. Raman spectroscopy can be used to calculate the difference in energy between gauche and trans conformations (E_g). For example, the shape of the C-C stretch in the isotropic Raman spectrum is sensitive to changes in conformation.[29] For a system like the n-paraffins, where the force field is known[30], the disordered Raman spectra can be calculated for an ensemble of conformers, where the conformers are chosen depending on the rotational isomeric state model using a conditional probability matrix.[31] Raman spectra are calculated as a function of increasing E_g from 400 to 1000 cal/mol. Using this method, the ratio of I_{877}/I_{892} was found to be directly proportional to E_g. [29]

The isotropic Raman spectra for $C_{22}H_{46}$ and 22,8 PU in the melt at 40 and 150 °C, respectively are shown in Figure 5.6. Tetracosane was recorded using an FT-Raman spectrometer (256 scans) with 1.064 um excitation, while 22,8 PU was recorded using a

dispersive Raman spectrometer (1 scan) with 514.5 nm excitation, thus the reason for differences in signal to noise ratio. Using Snyder's method, the ratio of I_{877}/I_{892} for $C_{22}H_{46}$ gives E_g = 500 cal/mol, which is in the range expected for paraffins. There is more error in determining the ratio for 22,8 PU due to the signal to noise and sample fluorescence. E_g is approximately 700 cal/mol, much higher than for $C_{22}H_{46}$ despite the fact that the temperature is higher. However, the shape of this band is much different.

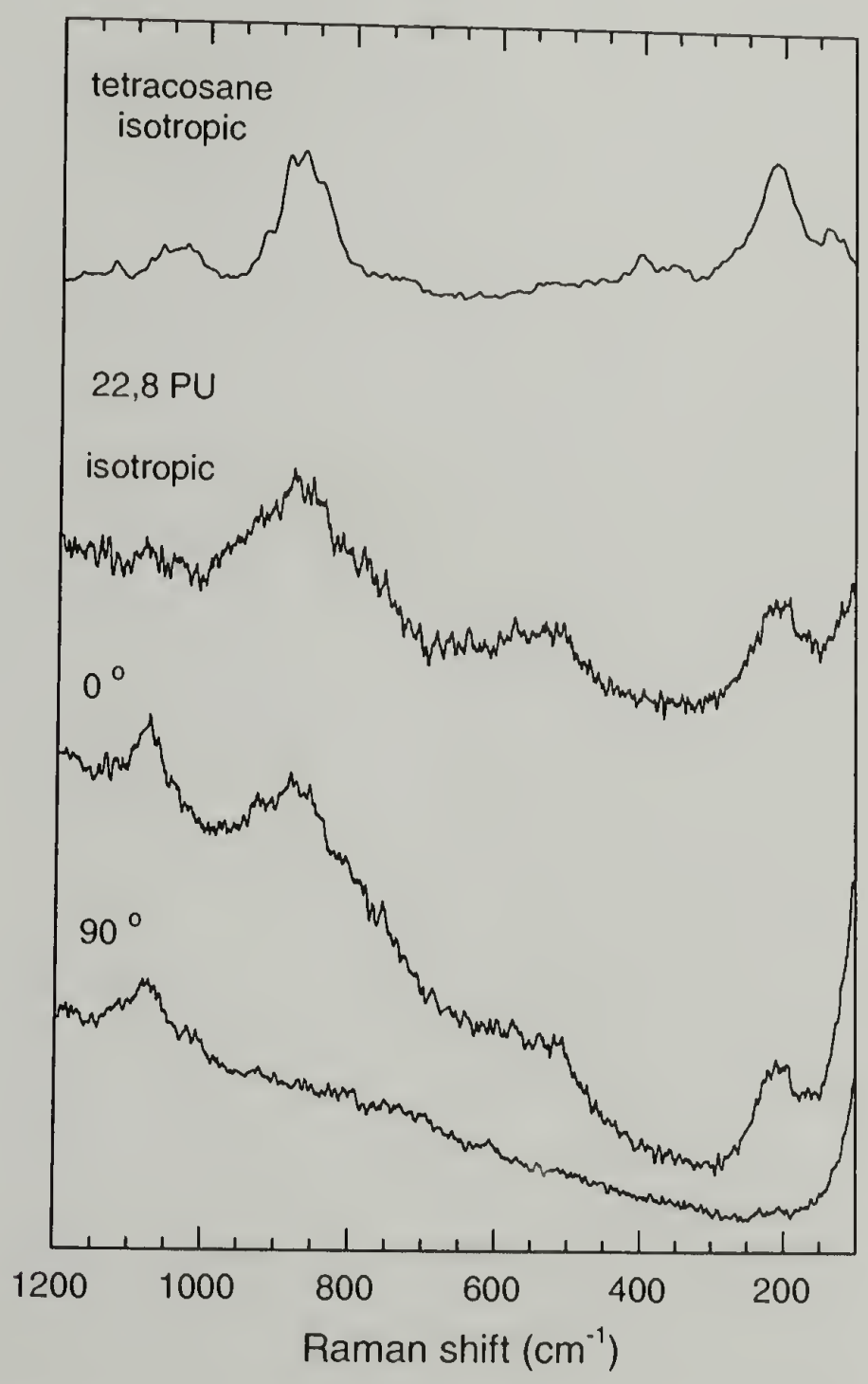

Figure 5.6 Raman spectra of $C_{22}H_{46}$ and 22,8 PU recorded in the melt at 40 and 150 °C, respectively.

Because the origin of the bands is not entirely known, nor is the force field for 22,8 PU, this method is a qualitative approximation at best. Nonetheless, it suggests that the hydrogen bonds serve to increase the rigidity of the methylene segments in the melt.

5.5.2 Morphology and Properties of Melt Crystals

22,8 PU was crystallized from the melt under isothermal and thermal conditions. For simplicity in comparison, the data obtained from samples crystallized from the melt with a cooling rate of 5 ° $C \cdot min^{-1}$ are compared. An image obtained from polarized optical microscopy is shown in Figure 5.7. Typically, polymers crystallized from the melt exhibit spherulitic morphologies. Under cross polarizers, spherulites typically exhibit a characteristic Maltese cross pattern due to the radial symmetry of the spherulites. As seen in Figure 5.7, a Maltese cross pattern was not observed for 22,8 PU; although cracks from where spherulitic impingement occurred are evident as are concentric rings within these cracked boundaries. Both AFM and TEM show that the morphology is spherulitic. The absence of a Maltese cross pattern suggests that the spherulites are of limited size and perfection.[32]

When the same sample is crystallized in the presence of 1 wt% benzoic acid, a Maltese cross pattern is observed, as shown in Figure 5.7. Presumably, the carboxylic acid groups can disrupt the hydrogen bonding interactions between urethane groups. The average dimensions of the spherulites formed with benzoic acid is 30 μm, and in its absence is 10 μm This suggests that disruption of the hydrogen bonding decreases the crystallization rate.

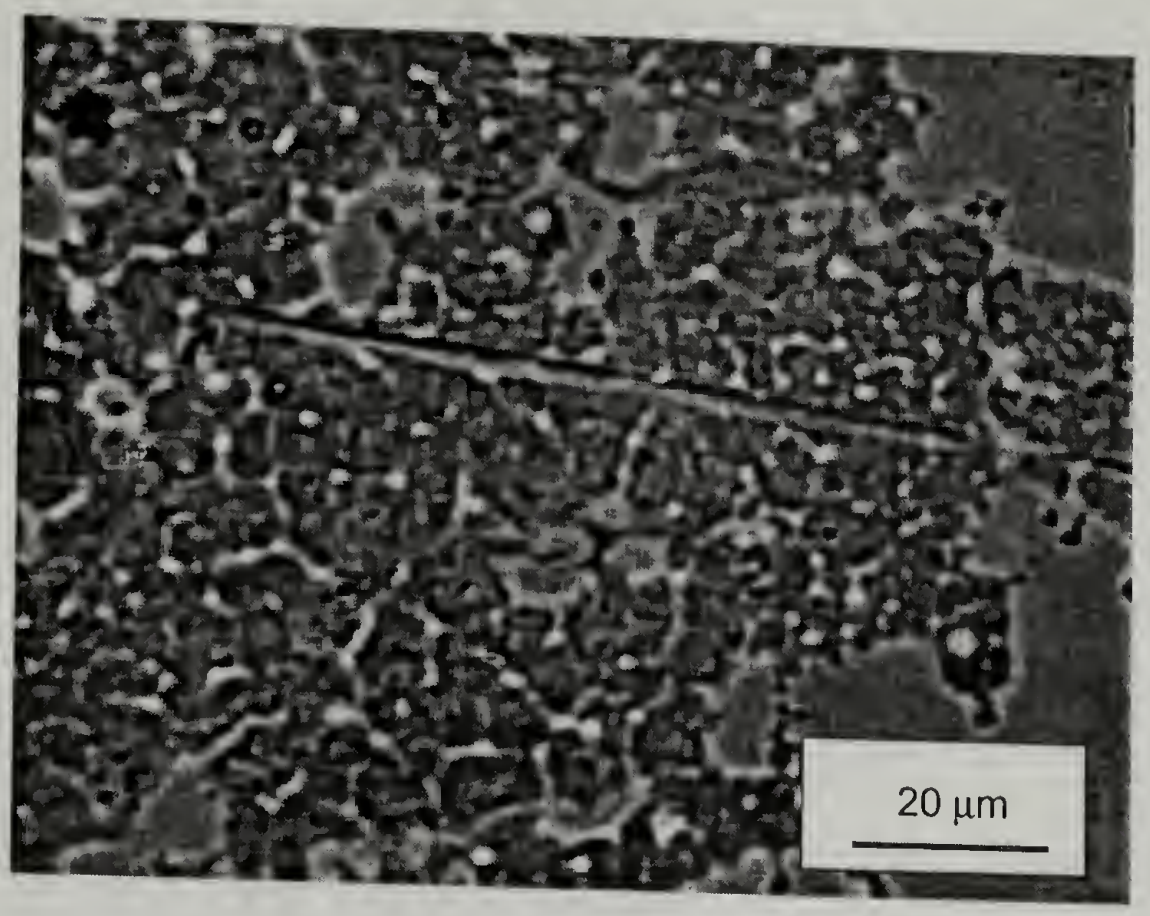

Figure 5.7 Polarized optical microscopy image of 22,8 PU crystallized from the melt.

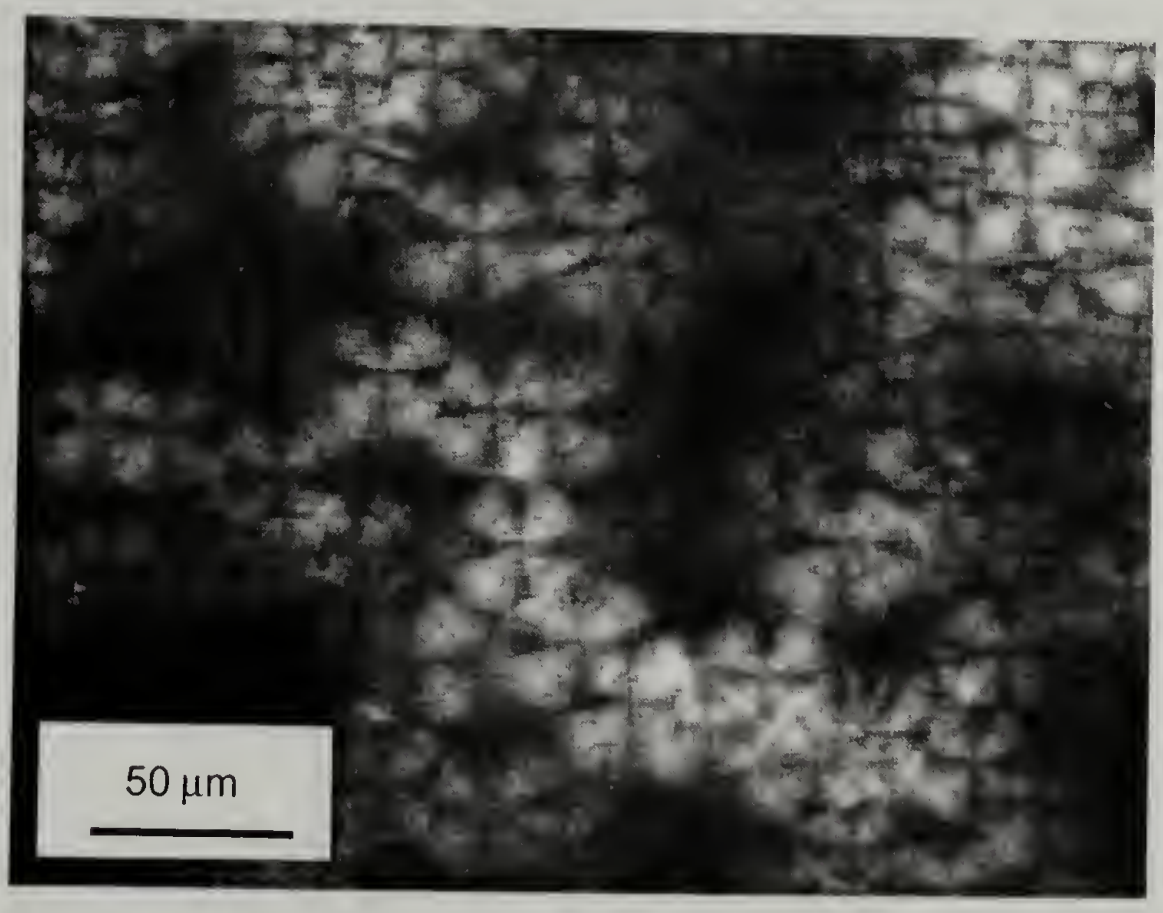

Figure 5.8 Polarized optical microscopy image of 22,8 PU crystallized from the melt in the presence of 1 wt% benzoic acid.

The crystal structures of these X,Y PU's have been studied using a combination of TEM and WAXS for samples crystallized from solution and melt.[33] When crystallized from DMF, 22,8 PU crystallizes in a triclinic unit cell with a lathlike morphology, similar to the behavior exhibited by the corresponding even-even m,n-polyamides.[34] Crystallization from solution requires a highly polar solvent, again something that will disrupt the interactions.

When crystallized from the melt, the sample forms a mixture of two different structures, the triclinic and a pseudo-hexagonal. The fraction of each formed depends on the crystallization conditions. Figure 5.9 shows the WAXS pattern of 22,8 PU obtained from a diffractometer. The diffraction peaks at 4.6 and 3.7 Å are from d_{100} and d_{010}, respectively, of the triclinic phase. The weaker diffraction peak at a d-spacing of 4.1 Å is

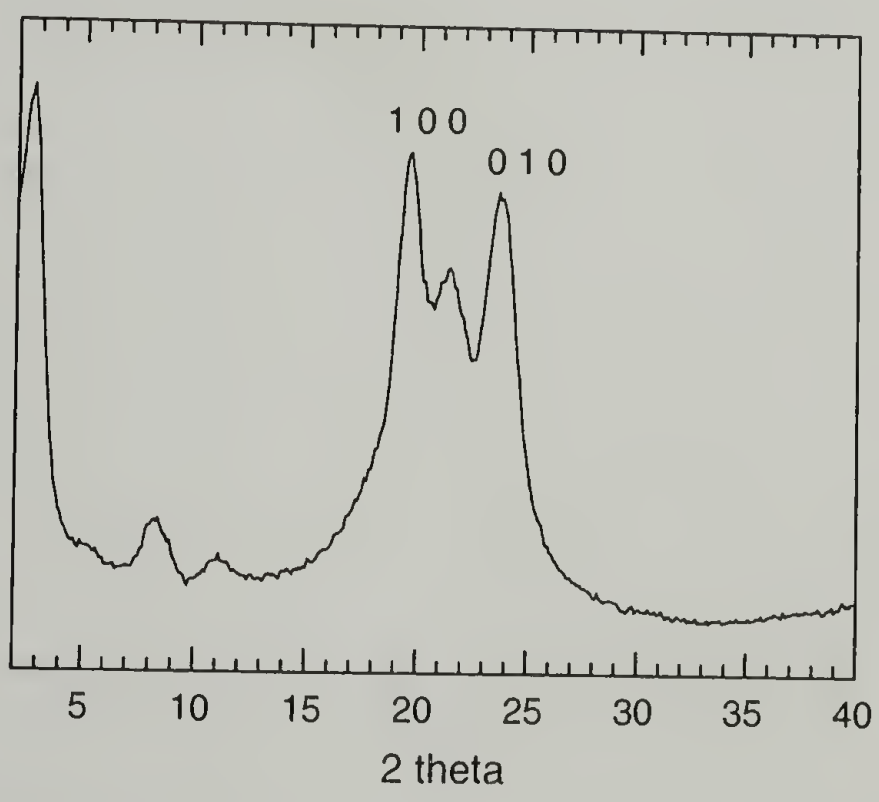

Figure 5.9 WAXS pattern for 22,8 PU crystallized from the melt.

from the pseudohexagonal phase. The diffraction peaks with higher d-spacing are higher orders of the fundamental repeat

The crystalline size and perfection can be determined from the WAXS pattern using Scherrer's equation shown in Equation 5.9.

$$L_{hkl} = \frac{K\lambda}{\left(\beta_s^2 - \beta_i^2\right)^{1/2} \cos\theta} \tag{5.9}$$

B_s and β_i are the full width at half maximum of the diffraction peak of interest and of a calcium carbonate standard (which accounts for instrument response). The results are shown in Table 5.2. L_{100} gives the crystal size in the direction held together only by van der Waals interaction. L_{010} gives the crystal size in the hydrogen bonding direction. As shown in Table 5.2, the results give crystal sizes that are unreasonably small, 90 and 60 Å for L_{100} and L_{010} respectively. Typical dimensions for polyethylene crystals are between 250 and 600 Å. The reason for these low values is that line width is also a function of the crystal perfection. The crystal perfection must be very low in this melt-crystallized sample.

Table 5.2 Results from WAXS analysis of 22,8 PU melts crystals using Scherrer's equation

2θ (°)	FWHM (°)		L_{hkl} (Å)
19.5	1.0	d_{100}	90
23.7	1.5	d_{010}	60

Using a combination of DSC and vibrational spectroscopy, the thermodynamics of the crystal can be determined. The results are shown in Table 5.3 and compared with

polyethylene. The strength of the hydrogen bonds in the crystal are determined using the N-H stretch and Equation 5.7. T_m for 22,8 PU and HDPE is similar. The enthalpy of fusion (ΔH_f) is best compared in J/g because of the high molecular weight of the 22,8 PU repcat unit. ΔH_f is much higher for HDPE, indicating better packed crystals. The entropic gain upon melting is 4 times higher for HDPE than for 22,8 PU. This was cxpectcd because the interactions that persist in the melt decrease the entropy gain upon melting; although ΔS_{HB} was actually found to be quite low. In fact, the small ΔS_f could also be due to the disordered crystal structure (i.e. not much entropy loss on crystallizing).

Comparison of the enthalpy of fusion and hydrogen bonding shows that the packing in the crystal can not be accounted for by hydrogen bonding interactions alone. The van der Waals interactions contribute half of the energy. This emphasizes the point that while van der Waals interactions are much weaker than hydrogen bonds, and while their effect decreases faster with distance, their greater number makes them important.

Table 5.3 Thermodynamic parameters of 22,8 PU crystals compared with polyethylene

	T_m (°C)	ΔH_f ($J \cdot g^{-1}$)	ΔS_f ($J \cdot g^{-1}K^{-1}$)	ΔH_f ($kJ \cdot mol^{-1}$)	$-\Delta H_{HB}$ ($kJ \cdot mol^{-1}$)
22,8 PU	140	90	0.164	45.6	22.9
HDPE	142	293	0.706		

5.5.3 Crystallization Kinetics

The results of the last two sections suggest that constraining a polymer chain in one dimension decreases thc ovcrall crystal perfection achicvablc. The crystals are small

and disordered with a high fraction of amorphous material. In this section, the kinetics to transform the interacting melt to the crystal are discussed.

The ordering phenomenon in the methylene units (intramolecular ordering or "straightening") was studied separately from the urethane hydrogen bonding (intermolecular ordering). 22,8 PU was crystallized at several different cooling rates ranging from 2.5 to 15 °C·min^{-1}, and the infrared spectra were simultaneously collected. Although isothermal crystallization is conventionally used to study polymer crystallization, thermal conditions are the ones that exhibited differences in the relative kinetics between the two functionalities.

Changes in the urethane units due to ordered hydrogen bond formation were studied using the Amide I band already discussed. The methylene wagging vibrations were used to study ordering of the methylene segments. These modes have been used to characterize the crystallinity of other aliphatic polyurethanes.[35] The region from 1280-1380 cm^{-1} is shown in Figure 5.10.

In the melt, only the broad component at 1335 cm^{-1} associated with disordered chains was observed. Upon crystallization, several new bands appeared as part of the methylene wagging progression series for the octyl and docosyl segments. The methylene units in a particular segment can be modeled as a series of coupled oscillators. Usually the nearest neighbors are considered. As a result, the vibration of each methylene unit becomes non-degenerate. In this case, instead of observing one wagging vibration, a progression of several vibrations is observed. For a chain of parallel dipoles, the frequency is related to the segmental length as shown in Equation 5.10.

$$\omega^2 = \omega_o^2 + 4\omega'^2 \sin^2 \frac{dk}{2} \qquad (5.10)$$

ω' is related to the intramolecular coupling force constant, d is the distance between two oscillators, and **k** is the wave vector. The observed frequencies are sensitive to both the numbers of units in a segment and the conformation. Changes in these bands are characteristic of conformational changes of an entire segment. The bands at 1308 and 1361 cm^{-1} can be attributed to the octyl segments while the band at 1296 cm^{-1} owes its intensity to the docosyl segment. [36]

The changes that occured in the Amide I region upon crystallization of 22,8 PU with a cooling rate of -5 °C·min^{-1} are shown in Figure 5.11. At the onset of crystallization, a sharp increase was seen in the ordered hydrogen bonded (1684 cm^{-1}) component. This was accompanied by a simultaneous decrease in the number of free

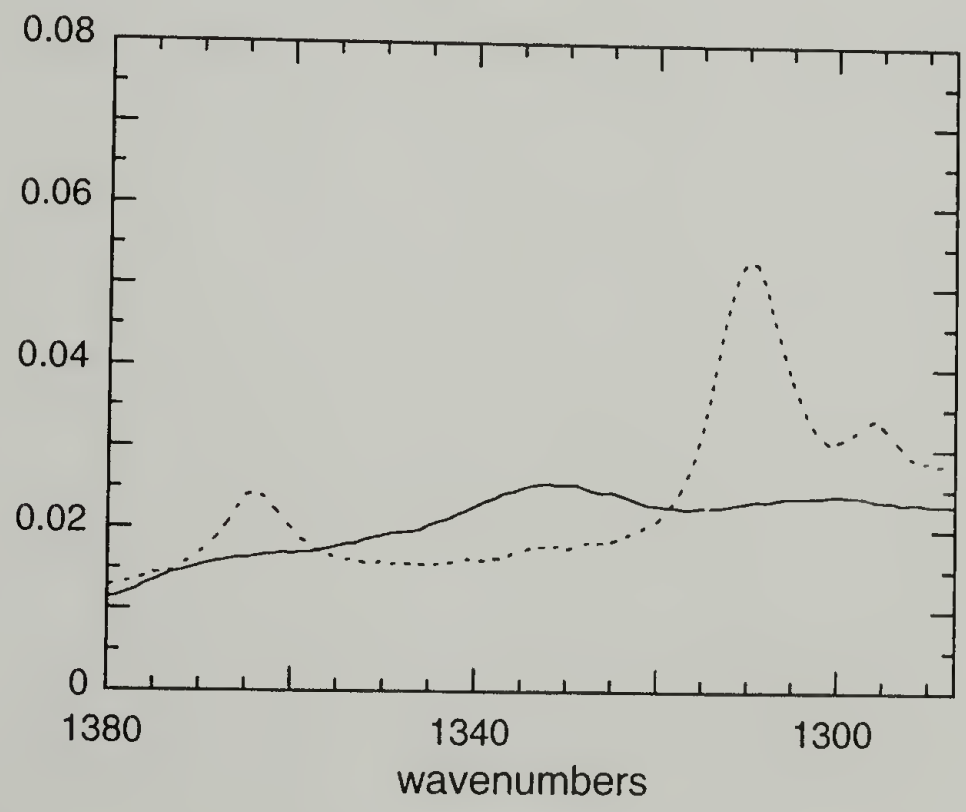

Figure 5.10 Infrared spectra of 22,8 PU in the methylene wagging region showing the melt at 160 °C (solid line) and the crystal (dashed line).

urethanes and disordered hydrogen bonds. After this initial stage, defined as primary crystallization, the crystallization rate diminished significantly as shown. Order formation then continued to consume both free and disordered hydrogen bonds. Disordered hydrogen bonds can exist either within the amorphous phase or within the crystal. The free urethanes, on the other hand, can only exist in the amorphous phase or at the lamellar surface. In fact, it has been suggested that the ratio of ordered hydrogen bonds to free urethanes should be related to the crystal thickness.[26] The second crystallization stage could occur by two different processes: conversion of amorphous material to crystal or the removal of defects within the crystal. From the relative intensities measured, the total amount of hydrogen bonded component reached 90%. If the sharp 1684 cm^{-1} band is

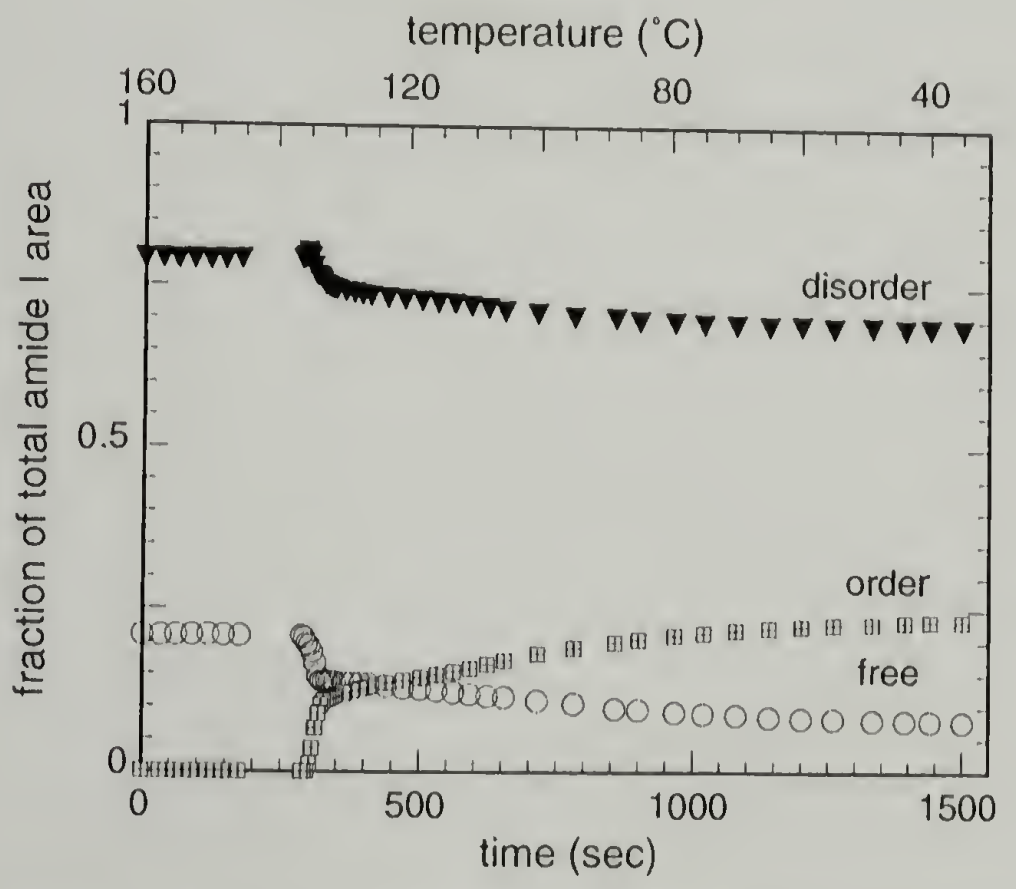

Figure 5.11 Results from crystallization of 22,8 PU at a cooling rate 5 °C·min^{-1} showing changes in the urethane units based on curve fitting of the Amide I region.

taken to represent the volume fraction of fully crystalline structure, the degree of crystallinity is 25% at 1500 seconds. This value is comparable to the degree of crystallinity generally associated with neat aliphatic nylons.[23]

Analysis suggests that an additional component might exist at 1692 cm^{-1}. However, the contribution of this component contributes at most 5% to the overall intensity in this region. As two crystalline phases were detected in x-ray diffraction experiments, each of these Amide I bands may correspond to a different crystal structure. The pseudo-hexagonal phase was most apparent in rapidly quenched samples. Thus the dominant vibration at 1684 cm^{-1} may be attributed to the pseudo-hexagonal phase, and the vibration at 1692 cm^{-1} from the triclinic phase. However, this situation is not that simple since even solution crystallized samples that are dominated by triclinic phase exhibit a strong band at 1684 cm^{-1}.

The order formation of the methylene segments is shown in Figure 5.12. After removing the amorphous contribution of the disordered band at 1335 cm^{-1}, the sharp prominent 1308 cm^{-1} CH_2 wagging band in this region was used to monitor order formation. As was seen for the urethane components, the spectroscopic feature of the aliphatic segments also exhibit different rates of change associated with different stages of crystallization. During the second stage, defined to be secondary crystallization, the position of the CH_2 wagging progression band typically shifted 4 cm^{-1} higher from 1306 to 1310 cm^{-1}. This result was typical for crystallization at several cooling rates (2.5-15 $°C \cdot min^{-1}$) and was not correlated to temperature. Rather, this shift must be related to segmental conformation changes that occur during secondary crystallization. A measure of the conformational order associated with the polymethylene chains can be deduced

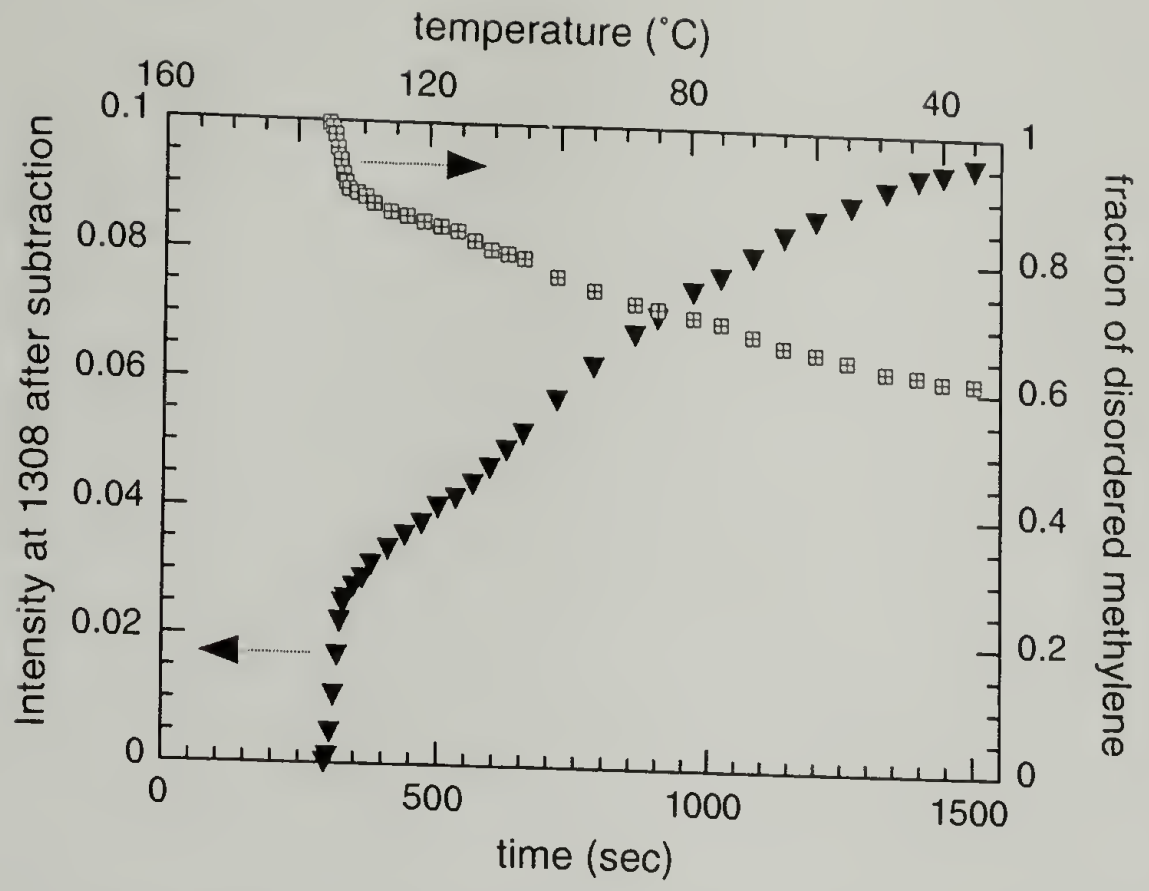

Figure 5.12 Results from crystallization of 22,8 PU at a cooling rate 5 °C·min^{-1} showing changes in the methylene segments based on the wagging region.

from the intensity of the wagging defect band. Analysis indicates that 40% of the polymethylene sequences exhibit conformational order.

The difference in the order associated with interchain interactions (25%) versus the conformational order (40%) may be a unique feature of interacting chains. However, even in polyethylene, when the interchain interactions are disrupted during the phase transition from orthorhombic to the hexagonal state, the chain stem maintains its straightness.[37]

This difference arises because the kinetics for the two structural transformations was different. The kinetics of conformational order in comparison to interchain order formation is shown in the Figure 5.13. To relate the differences between the hydrogen bonds and the aliphatic conformation, the intensities observed at 1684 and 1308 cm^{-1}

were normalized to the final state. Crystallization is marked by three stages. In the initial stage, both hydrogen bonds and chain conformation form order quickly and at similar rate. Relatively speaking, the hydrogen bonds form a higher degree of order than the methylene segments in this initial stage, but as shown in Figures 5.11 and 5.12, the degree of crystallinity at this point is ~12% based on both hydrogen bonding and aliphatic conformation. This first stage of crystallization is followed by a slower, but linear increase in the urethane and aliphatic order. In this second stage, conformational order forms slightly faster and to a higher degree compared to the order achieved by the hydrogen bonds. The third stage is characterized by the point where the kinetics of interchain and conformational order formation deviate from each other, for example, at the 750 seconds interval when the cooling rate is 5 °C·min^{-1}. At this time, the rate of order

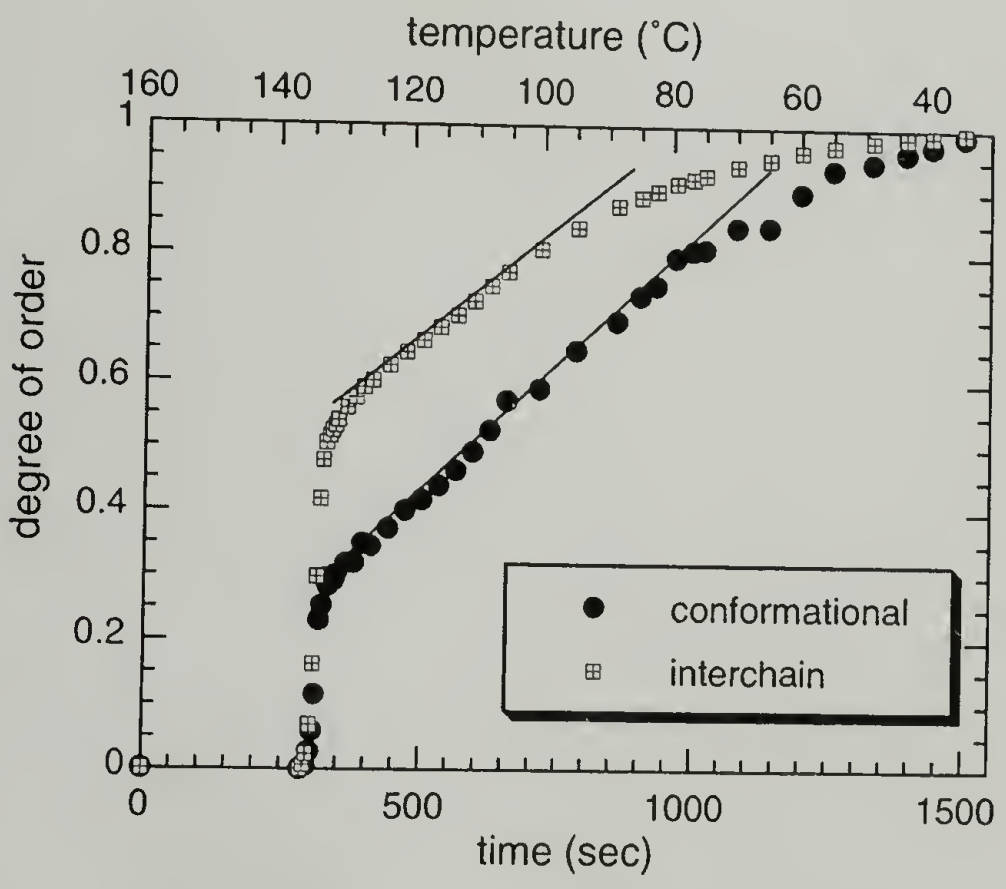

Figure 5.13 Kinetics of ordered hydrogen bond formation (intensity at 1685 cm^{-1}) versus aliphatic conformational order (intensity at 1308 cm^{-1}) during melt crystallization at a cooling rate of 5 °C·min^{-1}. Intensities are normalized to the final state.

formation begins to diminish for the urethanes. The aliphatic segments, on the other hand, dominate the crystallization process here for another 250 seconds. This behavior was observed for all crystallization rates ranging from 2.5 to 15 $°C \cdot min^{-1}$. However, the transition point to this third stage is independent of temperature.

These different crystallization regimes can be monitored in more detail by observing changes in the disordered interchain interactions. Figure 5.14 shows the Amide I disordered band shapes along the crystallization curve after the free and ordered components have been subtracted. This asymmetric band shape reflects the population of hydrogen bond strengths and changes in the population as the crystallization occurs. At the start of crystallization (t = 0), the system is at equilibrium in the melt. The broad band shape is asymmetric with a full width at half maximum (FWHM) of 34 cm^{-1} and considerable intensity at 1716 cm^{-1}. Prior to crystallization (for example at t = 284 s), both a change in the position and FWHM occurred. This behavior was also observable from the raw data. In the dozens of crystallization experiments performed, a continuous increase in the FWHM of the Amide 1 band was always observed. No features of crystalline structure are evident at this time.

The changing shape of this band represents a continuous transformation of disordered states into more favorable ones. The order formation or crystallization of these model polyurethanes clearly is not a discontinuous process. The induction period encompasses an entire distribution of interactions of different strength. The entire ensemble evolves into a more ordered state over a time scale slower than expected.

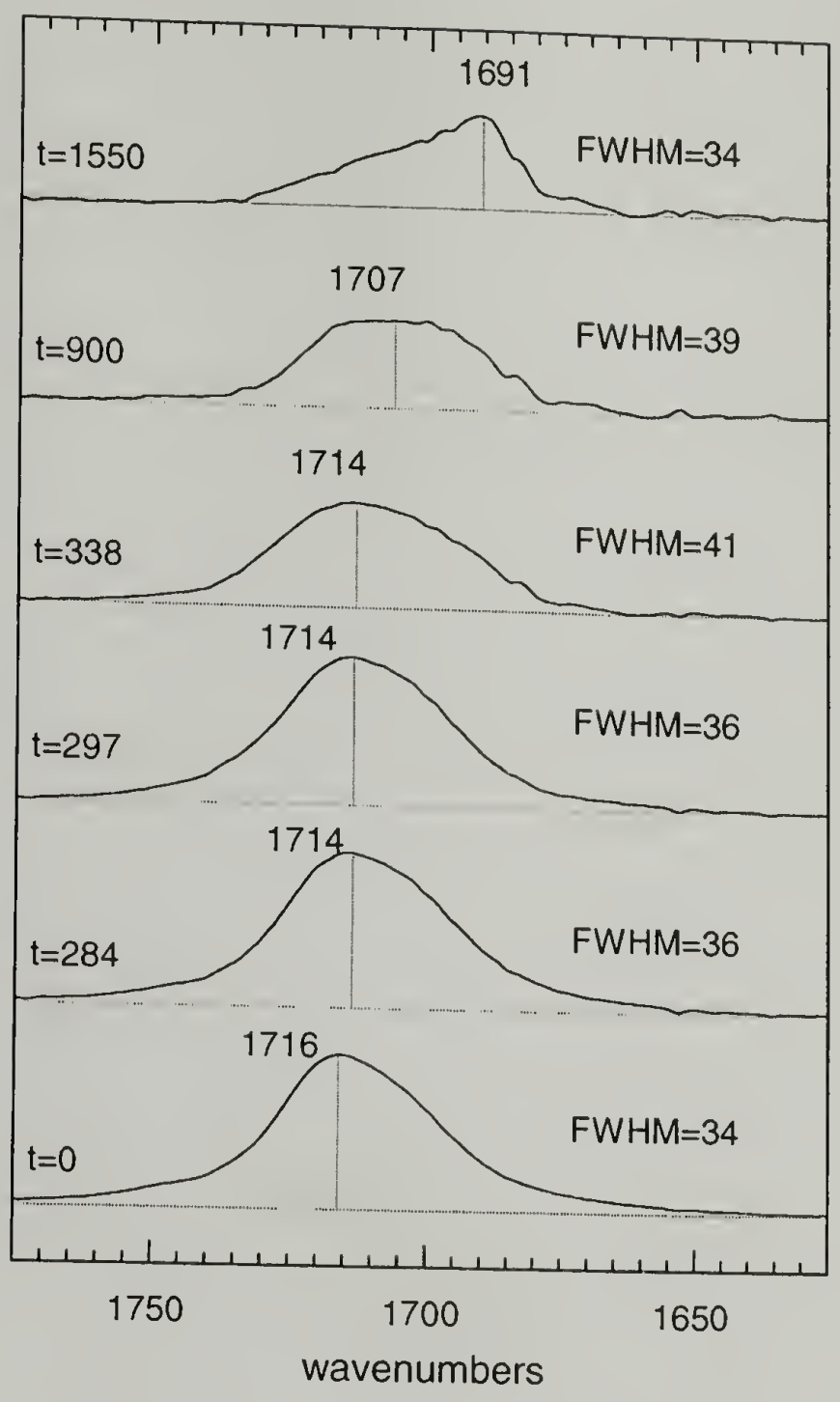

Figure 5.14 Changes in the Amide I disordered band contour during crystallization at a cooling rate of 5°C·min^{-1}. The spectral contributions from the free and ordered hydrogen bonds have been subtracted. The onset of primary crystallization is at t=297 s and the transition to secondary crystallization is at t=338 s.

The secondary crystallization is also characterized by the presence of a broad distribution of hydrogen bonds. This ensemble is reflected in the intensity and particularly the shape of the composite band in the region of 1692 cm^{-1} between the well-defined free component and the ordered one. At the start of secondary crystallization (t = 338 s), the maximum position remained fixed, although an increase in FWHM was

observed. The most dominant population shifted to lower wavenumber, which is associated with refinement in geometry. The changing shape of the disordered composite band reflects either crystallization of the amorphous phase or crystalline perfection. Growth in these domains was evidently inhibited. After crystallization is complete, the disordered band is highly asymmetric with a maximum intensity at 1691 cm^{-1}. The amorphous regions are not liquid-like.

The crystallization rates for the initial crystal formation as a function of different cooling rates were also studied. As expected, higher cooling rates gave higher rates of crystallization but requiring higher supercooling. These observations are expected for the polymer crystallization process.[38] These crystal growth rates can now be used to obtain the energy for the process using the simple relation based on modification of the Arrhenius equation to account for cooling rate, as shown in Equation 5.11.[39-41]

$$\ln\left(\frac{\Phi}{T_c^2}\right) = -\frac{\Delta E_p}{RT_c} + \text{const} \qquad (5.11)$$

Φ is the cooling rate and T_c is the peak crystallization temperature. The energy change for primary crystallization (ΔE_p) can be found by plotting ln (Φ/T_c^2) versus $1/T_c$. This gives ΔE_p = -22.01 $kJ \cdot mol^{-1}$.

The energy contribution from hydrogen bonding can be assessed using the values for ΔH_{HB} determined for the melt and the crystal and the amount of each species present. After accounting for the amount of ordered hydrogen bonds that are obtained by depletion of free urethanes (56% with $H_{free} - H_{ordered\ HB}$ = -22.93 $kJ \cdot mol^{-1}$ repeat) and by depletion of disordered hydrogen bonds (44% $H_{disordered\ HB} - H_{ordered\ HB}$ = -8.71 $kJ \cdot mol^{-1}$ repeat), the total contribution from hydrogen bonding is –16.67 $kJ \cdot mol^{-1}$ repeat. On the

basis of comparison with ΔE_p, initial crystal formation is apparently driven almost entirely by the interchain interactions between urethane units. The methylene chain seems to contribute little to the enthalpy of the initial crystal.

From the data, it can be concluded that a characteristic of strongly interacting systems is that the free energy change associated with nucleus size is perturbed to favor smaller nuclei. Hydrogen bonds stabilize an interaction with little entropic penalty. The hydrogen bonds that persist in the melt represent a state where pairwise "nuclei" are already stable.

An energy diagram of the thermal crystallization of 22,8 PU can be postulated, as shown in Figure 5.15. The free energy of the melt depends on the equilibrium constant between free and hydrogen bonded species. As the temperature is increased, the number

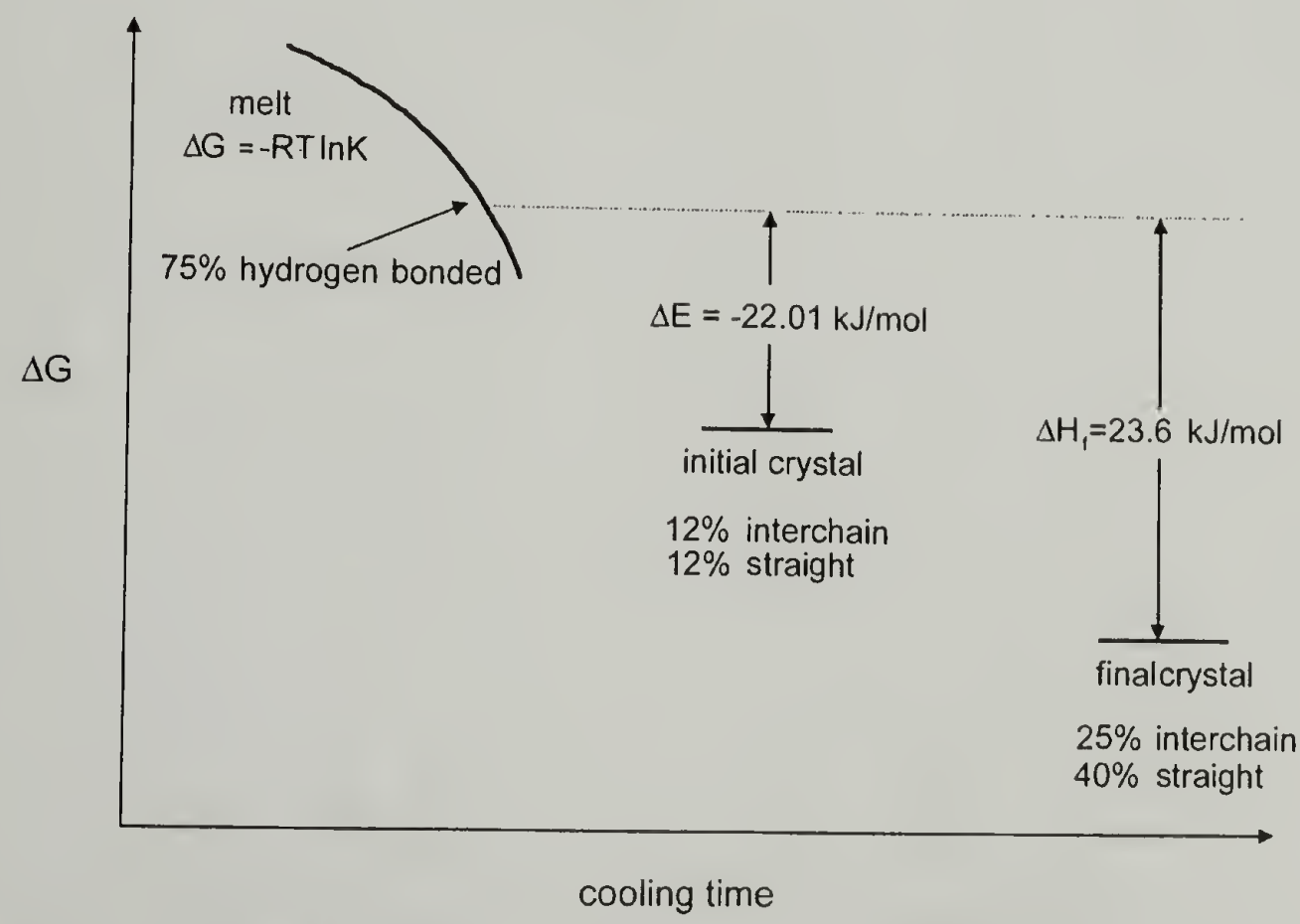

Figure 5.15 The energy diagram for thermal melt crystallization of 22,8 PU cooled from 160 °C at -5 °C·min^{-1}.

of free urethanes increasse. A completely free state can never be observed, however, before the polymer decomposes. Thus, starting with 75% of the urethanes interacting initially, primary crystal formation shows an enthalpic gain comparable to the hydrogen bond strength and a structure where 12% of the urethanes and methylene segments exhibit order. The secondary crystallization stage shows the degree of order increases in the hydrogen bonds to 25%, but the methylene segments order to a greater extent of 40%. The enthalpy of fusion (ΔH_f) obtained from DSC (-45.60 $kJ \cdot mol^{-1}$) shows that the overall enthalpic gain during secondary crystallization is –23.60 $kJ \cdot mol^{-1}$. These values suggest that for this system of polymers, hydrogen bonding is the dominant term. Even in the melt, 22,8 PU is seen as a physically crosslinked network. This system evolves into order and is driven by the ordering of hydrogen bonds into a semi-crystalline state.

5.6 Influence of Periodicity Between Functional Groups

Data from the previous sections suggests that hydrogen bonds facilitate nucleation, but inhibit growth. The formation of ordered hydrogen bonds drives the ordering of the methylene segments. The kinetics of conformational ordering is different from the kinetics of the interchain ordering. The resultant crystals are small and imperfect. In this section, the "density" of interactions along the chain are considered by comparing the behavior of 12,8 PU, 22,8 PU, and 32,8 PU. At some periodicity, the van der Waals interactions are expected to overcome the contribution from the hydrogen bonding interactions, and the polymer may exhibit polyethylene-like behavior.

Differences in the melt are considered first. The NH stretching band is shown in Figure 5.16 for molten samples at 183 °C. This band was the most intense for 12,8 PU.

32,8 PU had a small impurity as evidenced by two additional shoulders at 3350 and 1690 cm^{-1}. As before, Δv between free and hydrogen bonded species was used to determine the strength of the hydrogen bonds. Due to its breadth, the frequency of the hydrogen bonded band was difficult to define. The results are shown in Table 5.4. ΔH_{HB} is similar for the three polymers, with 12,8 PU having the largest ΔH_{HB}= -7.68 $kJ \cdot mol^{-1}$.

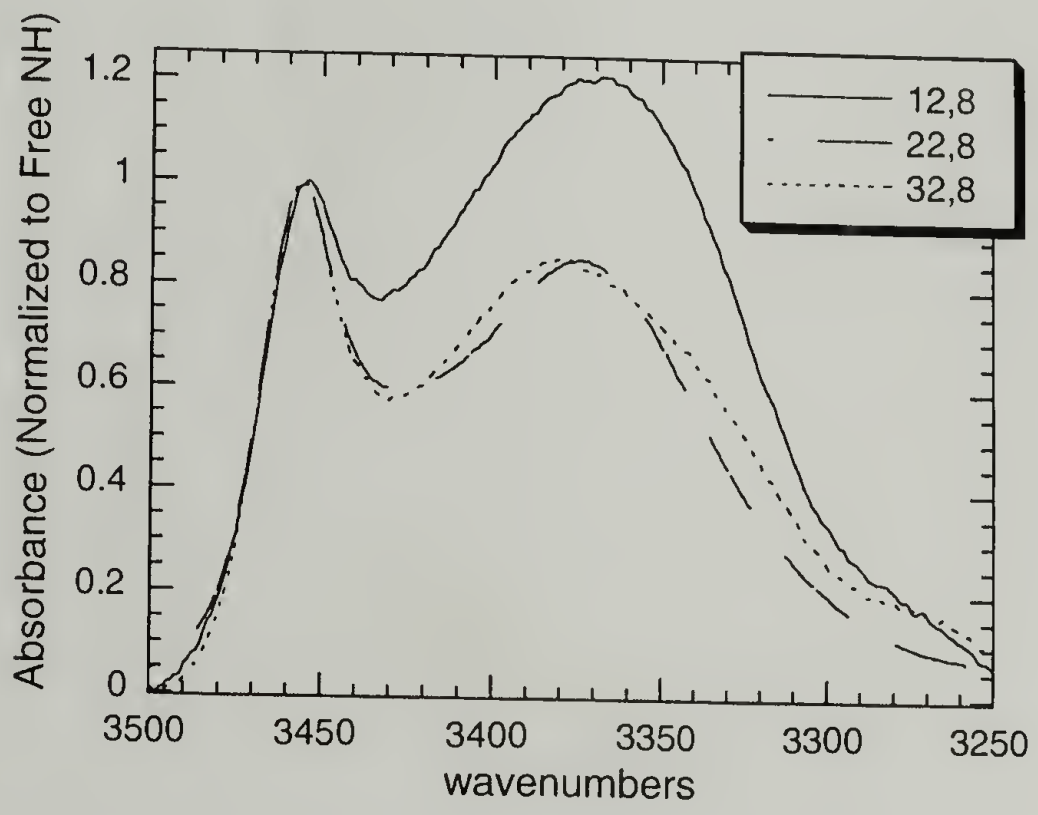

Figure 5.16 Infrared spectra of X,8 PU obtained at 183 °C showing the N-H stretch.

Table 5.4 Data determined from infrared spectra of X,8 PU melts

PU	ΔH_{HB} (Δv) kJ/mol	$A_{free\ NH}$	$A_{HB\ NH}$	ΔH_{HB} (vh) kJ/mol	ΔS_{HB} (vh) kJ/mol
12,8	-7.68	1.04	3.92	-16.2	-4.35
22,8	-7.02	1.05	2.51	- 7.1	-2.07
32,8	-6.98			-6.1	-11.8

The Δv method, when used for 22,8 PU, was verified by correlating the results with that obtained from a van't Hoff plot. Some have disputed using Δv for quantification, citing that the intensification of the hydrogen bonded band compared to the free is a more direct measure.[42] This method uses an empirical relationship between calorimetric data to determine the hydrogen bond strength, and the integrated intensity of the NH stretch. As reported above, the small impurity in 32,8 PU precluded using this NH intensity method. The results are shown in Table 5.4. These results are much different from those obtained using Δv. 12,8 PU has ΔH_{HB} almost 1.5 times as strong as 22,8 PU.

The Amide I mode is shown in Figure 5.17. As observed for the NH stretch, 12,8 PU was quite different from the other two samples. In order to obtain a van't Hoff plot, the Amide I must be deconvoluted into free and hydrogen bonded components and the difference in absorption coefficient corrected determined. It was presumed that for this series of samples, differing only in the length of the methylene spacer, that all parameters (band position, width, absorption coefficients) should be the same. This was generally found to be true; although the exact position of the free C=O in 12,8 PU was difficult to determin, so it was assumed to be the same. However, the correction factor for the change in absorption coefficient was different for the three samples. The factor was 0, 1.8 and 4.9 for 12,8 PU, 22,8 PU, and 32,8 PU. This suggests that the effective change in medium polarity changes the free carbonyl dipole moment, similar to dissolving a polar molecule in solvents of different polarity.

The calculated results from the van't Hoff plot are shown in Table 5.4. The differences between 12,8 PU and 22,8 PU agree with the results obtained from the

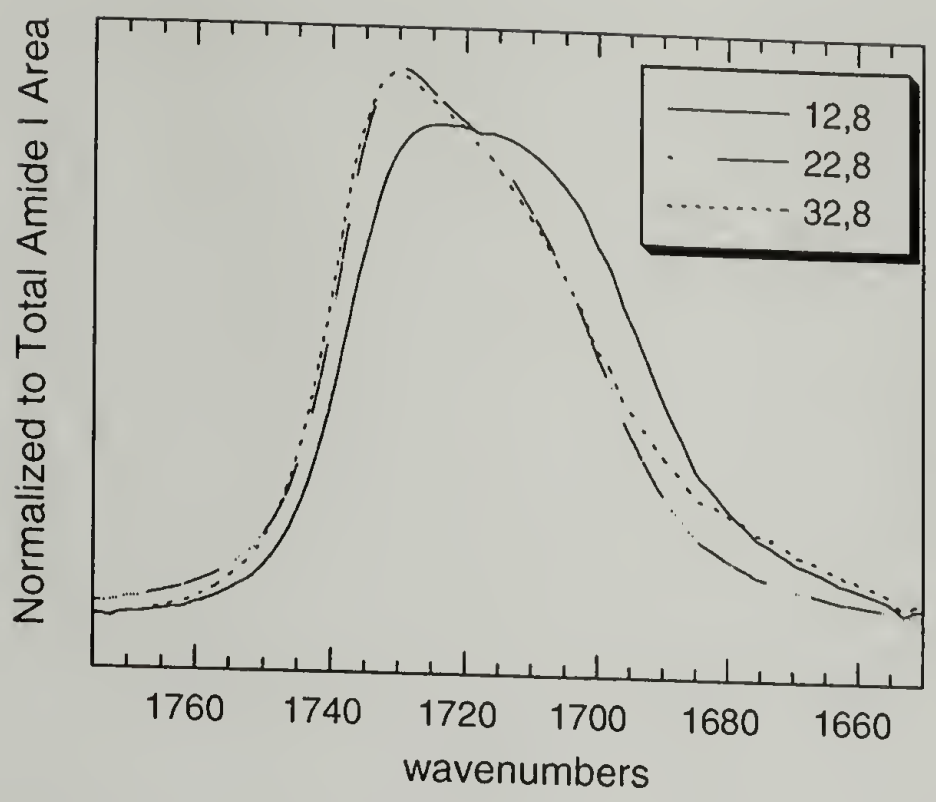

Figure 5.17 Infrared spectrum of X,8 PU in the region of the Amide I mode.

intensification of the NH stretch. ΔH_{HB} is –16.2 and –7.1 kJ·mol^{-1} for 12,8 and 22,8 PU, respectively. 32,8 PU has slightly weaker hydrogen bonds, as also suggested from the data obtained from N-H stretching. ΔS_{HB} does not follow a clear trend. The entropic penalty for forming a hydrogen bond is quite large for 32,8 PU (-11.6 J·mol^{-1}K^{-1}). ΔS_{HB} for 12,8 PU was the next largest at -4.35 J·mol^{-1}K^{-1}, although considering the error in this value it is similar to the one for 22,8 PU.

Thus, even with the weaknesses inherent in each method, the results are similar. The hydrogen bonding in the melt is much stronger, about two times as much, in 12,8 PU than in 22,8 and 32, PU. The entropic penalty for hydrogen bonding the melt is much greater for 32,8 PU.

The crystallization kinetics was studied under thermal conditions as described for 22,8 PU. Interchain and conformational ordering was determined based on the Amide I and methylene wagging modes as shown in Figures 5.18 and 5.19 for a cooling rate of 5

$^{\circ}C \cdot min^{-1}$. The Amide I intensity was normalized to the total number of methylenes, and the wagging mode was normalized to the total number of methylenes in X (since this mode arises from the octyl segment). Under identical cooling rates, crystallization of 12,8 and 22,8 PU occurred at nearly the same time and temperature. 32,8 PU crystallized somewhat later. As shown in Figure 6.18, the degree of interchain order achieved increased for 12,8 PU < 22,8 PU < 32,8 PU, inversely proportional to the interaction strength in the melt. This agrees with the concept that strong interactions tend to inhibit the growth of well-organized crystals.

On the other hand, the interaction strength must not be the dominant feature in determining the onset of order formation, since 12,8 and 22,8 PU crystallize at the same time. The large entropic penalty for forming a hydrogen bond in 32,8 PU results in fewer

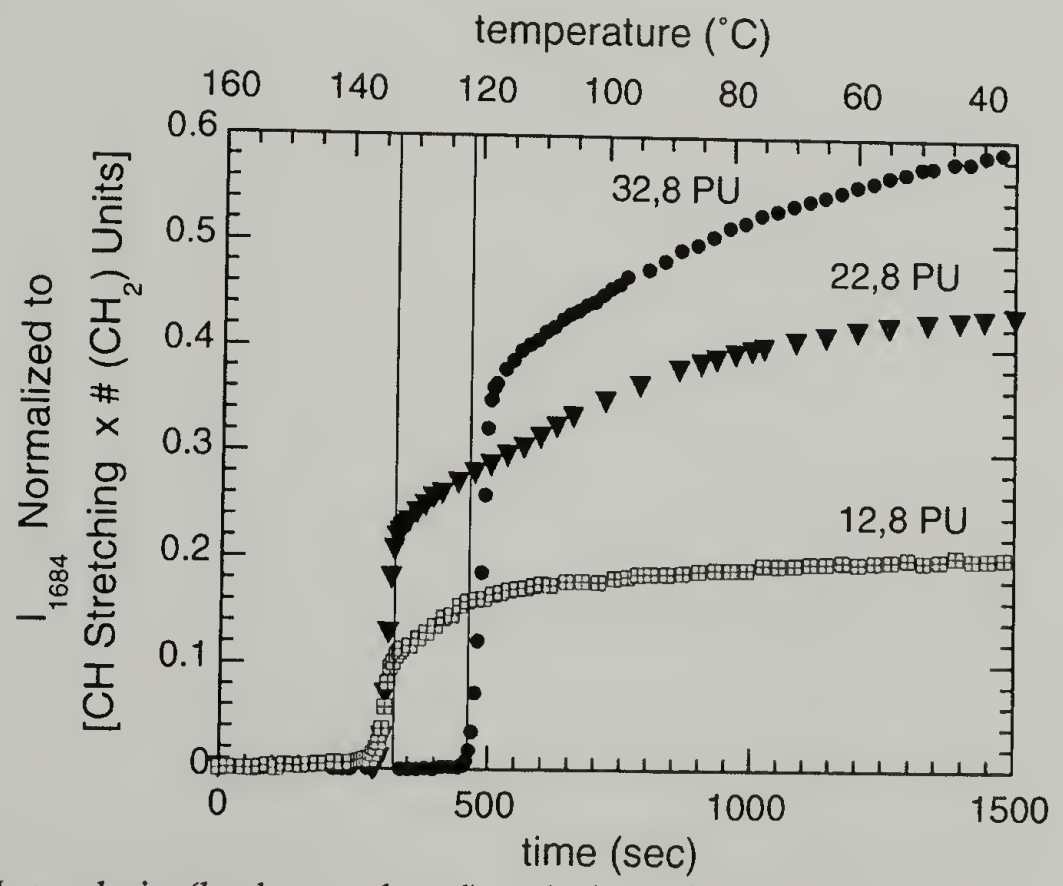

Figure 5.18 Interchain (hydrogen bond) ordering of X,8 PU's based on the intensity of the Amide I mode at 1684 cm^{-1}.

hydrogen bonds existing in the melt (around 50% at 160 °C) than in the other two systems. One of the conclusions arrived at in Section 5.5.3 was that the introduction of strongly interacting groups decreases the necessary size of stable critical nuclei. The data here suggests that this is due to an entropic effect rather than an enthalpic one.

Figures 5.18 and 5.19 reveal another intriguing result, particularly evident in Figure 5.19. The crystallization curves can be broken into two different regimes. The first one occurs between 160 and 120 °C. In this region, primary crystallization of 12,8 and 22,8 PU occurs. The overall order achieved in the methylene segments is nearly identical in the two systems at the end of primary crystallization. Between 130 and 120 °C, ordering of 12,8 and 22,8 PU occur at a slower rate (secondary crystallization), but again the ordering is at the same rate. In the second region, below about 120 °C, 32,8 PU begins

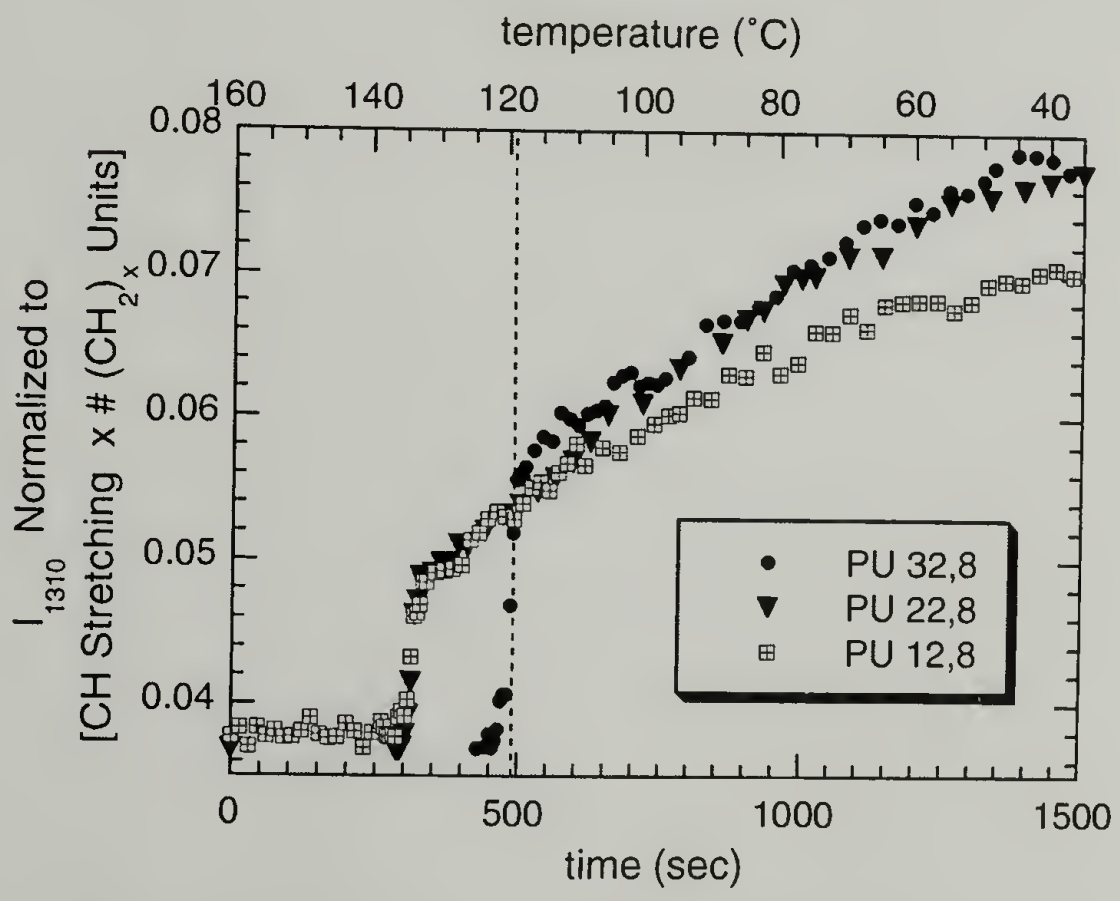

Figure 5.19 Conformational (methylene) ordering of X,8 PU's based on the intensity of the methylene wagging mode at 1310 cm^{-1} .

to crystallize. At this point, the behavior of 22,8 PU crosses over. While its kinetics was identical to 12,8 PU, in this second region, its kinetics are the same as 32,8 PU.

One explanation for this data is as follows. 22,8 PU system is capable of crystallizing into 2 phases, denoted phase X and phase Y. Initially 12,8 and 22,8 PU crystallize into phase X. At a later point, 32,8 crystallizes into a different structure, having phase Y. 12,8 continues to crystallize as phase X, but 22,8 PU begins forming or converting to phase Y. The infrared data suggests that phase X has weaker or less well-ordered hydrogen bonds. The Amide I region for 12,8 PU has a large contribution from 1691 cm^{-1}, in addition to the major component at 1684 cm^{-1}.

Without detailed X-ray data, conclusive statements cannot be made. Short aliphatic nylons preferentially form the triclinic α-phase, while longer aliphatic nylons form the pseudo-hexagonal γ-phase[1]-- suggesting that 22,8 PU forms a triclinic crystal structure from the melt and converts to a hexagonal phase on cooling. This conclusion is at odds with Keller's crystallization theory based on the idea of Ostwald's rule of stages: the phase that is most stable down to the smallest size will form first. The initial phase, which has a high longitudinal mobility, may become metastable upon reaching certain dimensions and convert to the ultimately more stable state.[17] The pseudo-hexagonal form of polyurethanes is expected to meet this criterion. Parrafins of similar length (22 to 24) also exhibit crossover behavior of forming a stable triclinic and stable hexagonal phase.[43]

5.7 Conclusions

In conclusion of this chapter, constraining a polymer chain with strong interactions has an effect on all aspects of the crystallization behavior. Where the entropic

penalty for maintaining a pairwise interaction is low, nucleation is enhanced. The growth of the crystalline phase is inhibited as the interaction strength increases. Crystals formed from the melt tend to be small with a high degree of imperfection. The amorphous phase, on the other hand, exhibits a conformational distribution unlike that observed in the melt.

5.8 References

(1) Aharoni, S. M. *n-Nylons, their synthesis, structure, and properties*; J. Wiley and Sons: Chichester; New York, 1997.

(2) Jones, N. A.; Atkins, E. D. T.; Hill, M. J.; Cooper, S. J.; Franco, L. *Macromolecules* **1997**, *30*, 3569.

(3) Waddon, A. J. *J. Polym. Sci. B Polym. Phys.* **1997**, 1175.

(4) Kanamoto, T.; Tanaka, K. *J. Polym. Sci. Polym. Phys. Ed.* **1971**, *9*, 2013.

(5) Ihn, K. J.; Yoo, E. S.; Im, S. S. *Macromolecules* **1995**, *28*, 2460.

(6) Wunderlich, B. *Macromolecular Physics*; Academic Press: New York, 1976; Vol. 2.

(7) Poon, W. C. K. *Phys. Rev. E* **1997**, *55*, 3762.

(8) ten Wolde, P. R.; Frenkel, D. *Science* **1997**, *277*, 1975.

(9) Van Hook, A. *Crystallization: theory and practice*; Reinhold Pub. Corp.: New York, 1961.

(10) Mullin, J. W. *Crystallization*; 4th ed.; Butterworth-Heinemann: Oxford; Boston, 2001.

(11) Vilsanen, Y.; Strey, R.; Reiss, H. *J. Chem. Phys.* **1993**, *99*, 4680.

(12) Oxtoby, D. W.; Kashchiev, D. *J. Chem. Phys.* **1994**, *100*, 7665.

(13) Ford, I. J. *J. Chem. Phys.* **1996**, *105*, 8324.

(14) Talanquer, V.; Oxtoby, D. W. *J. Chem. Phys.* **1995**, *103*.

(15) Talanquer, V.; Oxtoby, D. W. *J. Chem. Phys.* **1993**, *99*, 4670.

(16) Hoffman, J. D.; Miller, R. L. *Polymer* **1997**, *38*, 3151.

(17) Keller, A.; Cheng, S. Z. D. *Polymer* **1998**, *39*, 4461.

(18) Sadler, D. M.; Gilmer, G. H. *Phys. Rev. B* **1988**, *38*, 5684.

(19) Strobl, G. *Acta Polym.* **1997**, *48*, 562.

(20) Hoffman, J. D.; Miller, R. L.; Marand, H.; Roitman, D. B. *Macromolecules* **1992**, *25*, 2221.

(21) Tonelli, A. E. *Macromolecules* **1992**, *25*, 7199.

(22) Phillips, P. J. *Rep. Prog. Phys.* **1990**, *53*, 549.

(23) Kohan, M. I. *Nylon Plastics Handbook*; Carl Hanser Verlag: New York, 1995.

(24) Coleman, M. M.; Lee, K. H.; Skrovanek, D. J.; Painter, P. C. *Macromolecules* **1986**, *19*, 2149.

(25) Snyder, R. G. *J. Chem. Phys.* **1967**, *47*, 1316.

(26) Skrovanek, D. J.; Howe, S. E.; Painter, P. C.; Coleman, M. M. *Macromolecules* **1985**, *18*, 1676.

(27) Stolov, A. A.; Borisover, M. D.; Solomonov, B. N. *J. Phys. Org. Chem.* **1996**, *9*, 241.

(28) Jasse, B.; Tassin, J. F.; Monnerie, L. *Prog. Colloid Polym. Sci.* **1993**, *92*, 8.

(29) Snyder, R. G. *J. Chem. Soc. Faraday Trans.* **1992**, *88*, 1823.

(30) Snyder, R. G.; Schachtschneider, J. H. *Spectrochim. Acta* **1965**, *21A*, 169.

(31) Flory, P. J. *Statistical Mechanics of Chain Molecules*; Interscience Publishers: New York, 1969.

(32) Schonherr, H.; Wiyatno, W.; Frank, C. W.; G., F. G.; Gast, A. P.; Pople, J. A.; Waymouth, R. M. *Macromolecules* **2002**, *35*, 2654.

(33) McKiernan, R. L.; Heintz, A. M.; Hsu, S. L.; Atkins, E. D. T.; Penelle, J.; Gido, S. P. *Macromolecules* **2002**, *35*, 6970.

(34) Jones, N. A.; Atkins, E. D. T.; Hill, M. J.; Cooper, S. J.; Franco, L. *Macromolecules* **1996**, *29*, 6011.

(35) Maklakov, L. I.; Furer, V. L.; Alekseev, V. V.; Furer, A. L. *Zh. Prikl. Spektrosk.* **1979**, *31*, 691.

(36) Snyder, R. G.; Schachtschneider, J. H. *Spectrochim. Acta* **1963**, *19A*, 85.

(37) Barnes, J. D.; Fanconi, B. M. *J. Chem. Phys.* **1972**, *56*, 5190.

(38) Liu, S. Y.; Yu, Y. N.; Cui, Y.; Zhang, H. F.; Mo, Z. S. *Journal of Applied Polymer Science* **1998**, *70*, 2371-2380.

(39) Di Lorenzo, M. L.; Silvestre, C. *Prog. Polym. Sci.* **1999**, *24*, 917-950.

(40) Li, Y. J.; Zhu, X. Y.; Yan, D. Y. *Polym. Eng. Sci.* **2000**, *40*, 1989.

(41) Kissinger, H. E. *J. Res. Nat. Bur. Stand.* **1956**, *57*, 2712.

(42) Iogansen, A. V. *Spectrochim. Acta* **1999**, *55A*, 1585.

(43) Sirota, E. B. *Langmuir* **1998**, *14*, 3133.

CHAPTER 6

SPECTROSCOPIC ANALYSIS OF STRUCTURAL EVOLUTION IN POLYURETHANE FOAMS

6.1 Chapter Overview

In the previous chapters, the molecular weight and structural distribution was determined for different polyurethanes. Data analysis showed that under homogeneous conditions, the molecular weights exhibited a Schultz-Flory distribution; although polymers prepared from TDI had narrower distributions than ones prepared from MDI. The formation of allophanate linkages occurs predominantly at high conversion and high temperatures, and its formation causes a broadening and a shift in the molecular weight distribution. During polyurethane synthesis, groups that can participate in hydrogen bonding are formed. These groups were observed to inhibit growth of ordered domains.

The subject of this Chapter is polyurethane foam. As discussed in Chapter 1, obtaining the desirable mechanical properties depends upon forming appropriate phase-separated morphologies. It is the formation of a critical hard segment length or critical concentration of urea and urethane functional groups that initiates phase separation. The final morphology achieved also depends upon the kinetics of morphology development. This chapter presents a study of the reaction and phase evolution of polyurethanes by infrared spectroscopy. The growth of polyurea structural elements was determined at low conversion, prior to phase separation for hard segments of different anisotropy. Changes in this variable along with changes in reaction temperature serve to elucidate the relationship between structure and the onset, rate, and degree of phase separation.

6.2 Experimental

6.2.1 Foaming Kinetics

The procedure to prepare foams is similar to the one described in Chapter 2 for plaques. The formulations used are shown in Table 6.1. After the addition of TDI, and stirring for 15 s, a spatula was used to drip the foaming mixture onto the infrared crystal, as described below, at 27-30 s. The infrared spectra were collected. The specific mixing time and add time are critical to obtaining reproducible results.

Table 6.1 Polyurethane formulations used in this study

Sample	wt% TDI	H_2O/TDI	H_2O/OH
oo-4-22	0.30	0.81	4.42
T80-6-22	0.37	0.82	6.33
T80-4-22	0.30	0.80	4.36
T80-4-40	0.30	0.79	4.30
T80-4-56	0.30	0.77	4.17
T80-4-87	0.30	0.79	4.40
T80-4-113	0.30	0.79	4.35

Infrared spectroscopic measurements were carried out on a Perkin-Elmer 2000 system with a narrow-band MCT detector. Measurements were performed with 4 cm^{-1} spectral resolution. A low number of scans (4) were signal averaged in order to record spectra approximately every 8 s. A 9-pass liquid attenuated-total-reflectance (ATR) cell with a ZnSe crystal was used to measure the foaming kinetics. Sufficient throughput was obtained by applying material to the top of the crystal and leaving the reservoir empty.

This also made cleaning the apparatus much easier. A heating jacket was used to control the temperature of the crystal. The crystal then acts as a heat sink, and the reaction temperature at the foam/crystal interface can be controlled. The apparatus was mounted in the N_2 purged sample chamber. Scanning was initiated. Then a droplet of the mixed formulation is allowed to drip from a wedge-shaped spatula to the crystal. This "dripping" process is important to obtaining reproducible results. Droplets that are simply placed in contact with the crystal exhibit different kinetics. After reaction completion, the crystal was cleaned by soaking in DMSO. DMSO swells and delaminates the foam.

6.2.2 Analysis of Infrared Spectra

Analysis of the spectra was carried out as described previously.[1] The baseline remains unchanged during foaming. The set of spectra for each foaming experiment were first normalized to account for changes in the contact with the crystal. The integrated CH stretch from 3025-2800 cm^{-1} was used to normalize the spectra. The CH stretch was arbitrarily set equal to 8 for all formulations. Except for T80-6-22, all formulations contained the same weight fraction of polyether (the main contributor to CH stretch intensity), and thus the samples were normalized to each other. Because T80-6-22 contained a lower weight fraction of polyether, the intensity of its aromatic, NCO and urea vibrations were higher compared to the 4-22 systems.

The NCO conversion was determined from the integrated asymmetric NCO stretch from 2320-2050 cm^{-1}. The conversion is defined as shown in Equation 6.1.

$$p_{NCO_t} = \left(\frac{[NCO]_o - [NCO]_t}{[NCO]_o} \right) \tag{6.1}$$

$[NCO]_o$ is the integrated intensity of the NCO stretch at zero reaction time. $[NCO]_o$ was determined as described previously, by extrapolating the initial data points to zero time.[1-3] This calculation assumes apparent second order reaction kinetics, which is not unreasonable at early stages in the reaction.[4] Further confidence in this method was provided by the samples T80-4-T_{rxn}, where T_{rxn}=22-113 °C. The y-intercept in these identical formulations was 35.6 ± 1.4.

Band deconvolution of the amide I region was carried out using the Spectrum 2000 software package. No baseline correction was used. All bands were fit as a mixture of Gaussian and Lorentzian, and the position, bandwidth (bw), shape, and intensity were allowed to change during iteration. The spectra for oo-4-22 were fit from 1740-1635 cm^{-1} as 3 bands near 1732 (bw 22-26), 1712 (bw 22-26), and 1640 cm^{-1} (bw 11-15). The limits were chosen to avoid changes in the baseline due to shoulders from the aromatic C=C stretch and Amide II bands. The spectra for T80-based samples were fit from 1740-1590 cm^{-1} as 6 bands near 1732 (bw 22-26), 1712 (bw 22-26), 1670-1655 (bw 40-55), 1640 (bw 11-15), 1617 (bw 11-15), and 1596 cm^{-1} (bw 22-26). 2,4-TDI exhibits a C=C stretch at 1617 cm^{-1} (whereas 2,6-TDI does not) and thus the fitting limits cannot be truncated in the same way.

In general, this method works well. However some difficulties have arisen from trying to fit the monodentate ureas as a single band. At temperatures higher than 87 °C, the component near 1690 cm^{-1} was substantial, and using only one band centered at 1675 forced an unnaturally broad, intense free urea to give the best fit. At 87 °C, the contribution at 1655 cm^{-1} was large, which in this case, forced an unnaturally broad bidentate urea to fit best.

In addition, at high conversion, the urethane and free urea bands were significantly overlapping, and thus this fit became rather arbitrary. There may be additional components in this region as well (e.g. hydrogen bonded urethane, isocyanurate). The formation of secondary linkages such as bidentates also complicates curve fitting at high conversion.

6.3 Results

6.3.1 Spectroscopic Details

As discussed in Chapter 2, hard segments prepared from 2,6-TDI are expected to exhibit a higher degree of anisotropy than those prepared from T-80. This difference in anisotropy should manifest as differences in phase behavior. The phase behavior was monitored in this study by changes in the infrared spectrum. Infrared spectroscopy has been previously used to monitor phase behavior of polyurethanes.[5-7] Nonetheless, this method is indirect compared to direct techniques such as SAXS. Therefore, two formulations based on T-80 were studied, each with different volume fractions of TDI. This served as a control, since the effects of volume fraction on phase behavior are known. The three systems were prepared from hydroxyl end-capped polyether (V3137), water, diisocyanate, and a catalyst package as discussed in the experimental section. The difference between oo-4-22 and T80-4-22 is the diisocyanate used, where oo-4-22 was prepared from pure 2,6-TDI (*o*,*o*-TDI) and T80-4-22 was prepared from T-80. The concentration of TDI is 0.30 and 0.37 % (w/w) for T80-4-22 and T80-6-22, respectively.

The infrared spectra during the initial stages of foaming are shown as a function of time for T80-6-22 in Figures 6.1 to 6.4. Several changes generally occurred for all

systems. Reaction with water depletes isocyanate and produces urea groups. Reaction with alcohol (from the polyether) depletes isocyanate and produces urethane groups. Thus spectroscopic features characteristic of OH and NCO decreased with conversion, while those features characteristic of urea and urethane increased with conversion. The region of OH, NH, and CH stretching is shown in Figure 6.1. The overall intensity of the integrated C-H stretch should stay constant through the experiment, so the spectra were normalized to this region to account for density changes that occurred as reaction progressed.

A decrease in the asymmetric NCO stretch between 2050 and 2400 cm^{-1} was observed as shown in Figure 6.2. This region was used to quantify the overall reaction conversion. A fairly dramatic frequency shift was observed from 2259 to 2272 cm^{-1} during reaction. Closer inspection of this band reveals that there are actually two components here. The reason for these two components is unclear. A frequency shift was observed previously during rubber surface modification with TDI.[8] The possibility of an OH/NCO or NH/NCO hydrogen bond is ruled out because the two components were observed even in systems without hydrogen donors. A band observed in some aromatic isocyanates at 2320 cm^{-1} has been attributed to Fermi resonance,[9,10] but this is higher in frequency than the components here. The two different bands could arise from the different NCO species present (e.g. 2,6-TDI, 2,4-TDI, once reacted 2,4-TDI). Hoyer found that depending on the structure, the asymmetric NCO stretch occurs between 2249 to 2273 cm^{-1}.[11] Finally, low frequency infrared spectroscopy suggests that NCO groups can form a strong intramolecular bond.[12] The origin of the different bands is most likely a combination of the latter two explanations.

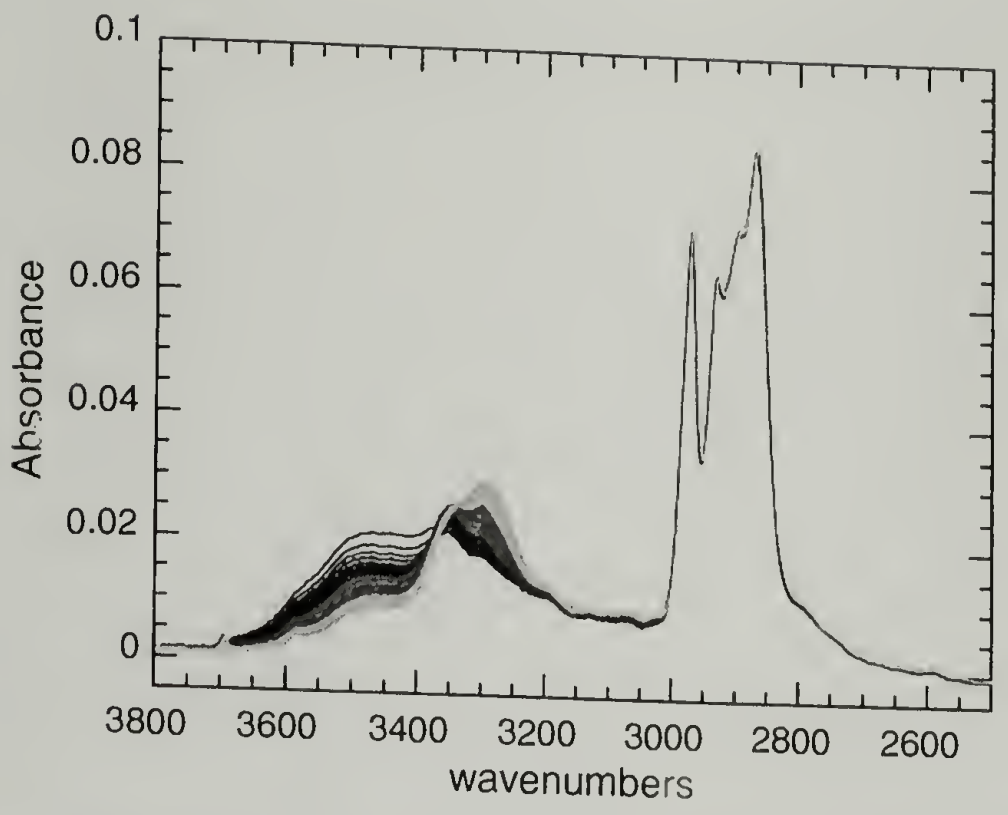

Figure 6.1 Infrared spectra obtained during reaction of T80-6-22 in the region of OH, NH, CH stretching. Time increases as spectra go from black to light gray.

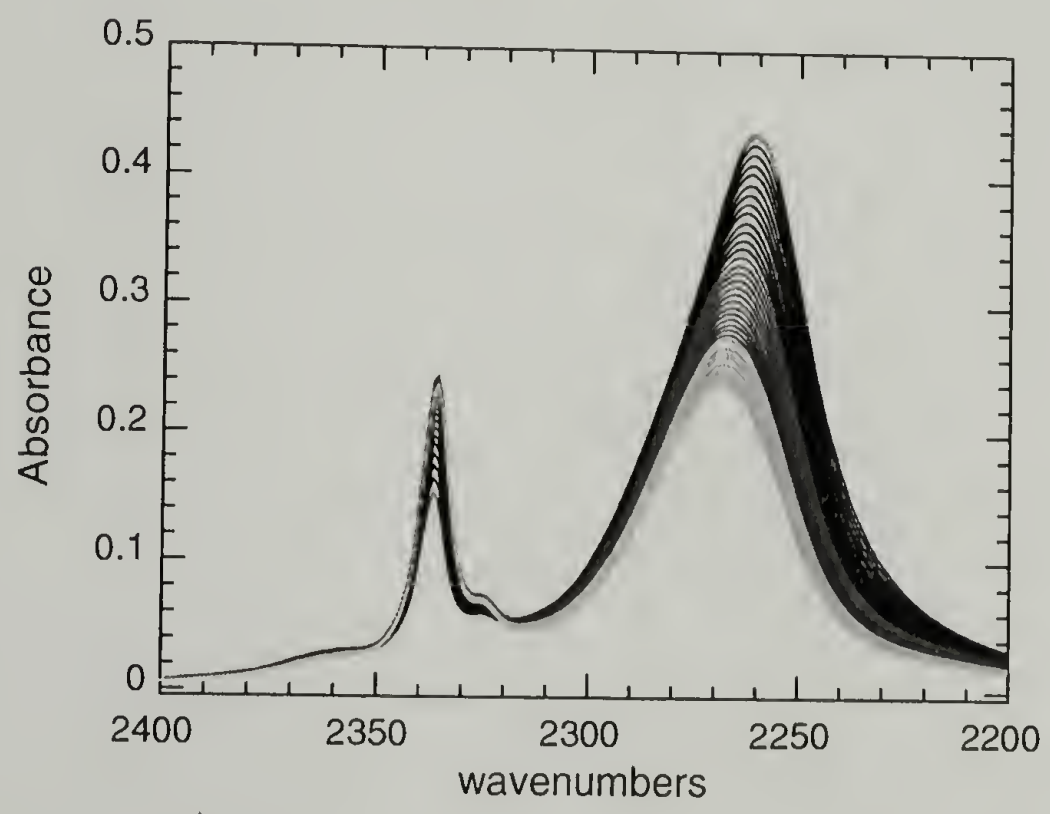

Figure 6.2 Infrared spectra obtained during reaction of T80-6-22 in the asymmetric NCO stretch. Time increases as spectra go from black to light gray.

Several vibrations are associated with the urea and urethane groups. Many of these modes occur between 1000 to 1600 cm^{-1} as shown in Figure 6.3. These modes are highly mixed, depending on the structure.[13-16] The Amide II mode occurs between 1500 to 1600 cm^{-1}. The Amide III mode occurs between 1200 to 1300 cm^{-1}. The Amide III mode seems to be sensitive to both the functional group (urea or urethane) and the morphology (type of hydrogen bond). However, detailed assignment is not clear. Other vibrations arising from the aromatic ring and the polyol backbone also appear here. In addition, a band at 1410 cm^{-1} arises from isocyanurate.[3]

The Amide I mode, already discussed in Chapter 5 for polyurethanes is shown in Figure 6.4. The Amide I mode again proves to be the most straightforward for quantitative analysis. Vibrations for urea and urethane groups occur at different frequencies, allowing distinction between the two chemical reactions. The Amide I vibration is also very sensitive to hydrogen bonding, whether free, bonded but not "ordered" ("monodentate"), and bonded and ordered. This is convenient because changes in the morphology during phase separation are associated with changes in the hydrogen bonding as polyurea segments orient and pack. The band at 1735 cm^{-1} is attributed to free urethane groups, while vibrations at 1715, 1655-1790, and 1640 cm^{-1} are attributed to free, monodentate, and ordered ureas. The vibration at 1640 cm^{-1}, in particular, arises from bidentate urea and is often used as a characteristic feature of organized hard domains. The Amide I region for the other two systems are shown in Figures 6.5 and 6.6.

Vast differences were observed between the oo- and T80- systems. The T80-4-22 and T80-6-22 systems are considered first. At early stages of the reaction, an initial increase at 1715 cm^{-1} is observed, corresponding to the formation of free urea. The number

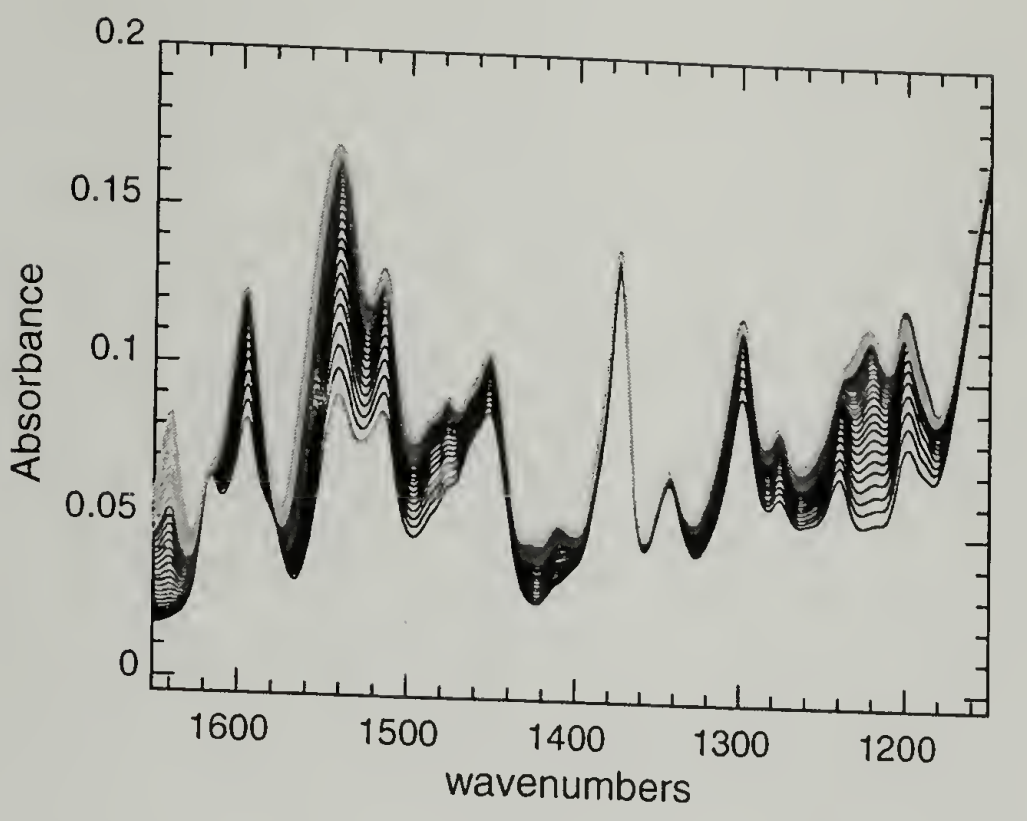

Figure 6.3 Infrared spectra obtained during reaction of T80-6-22. Time increases as spectra go from black to light gray.

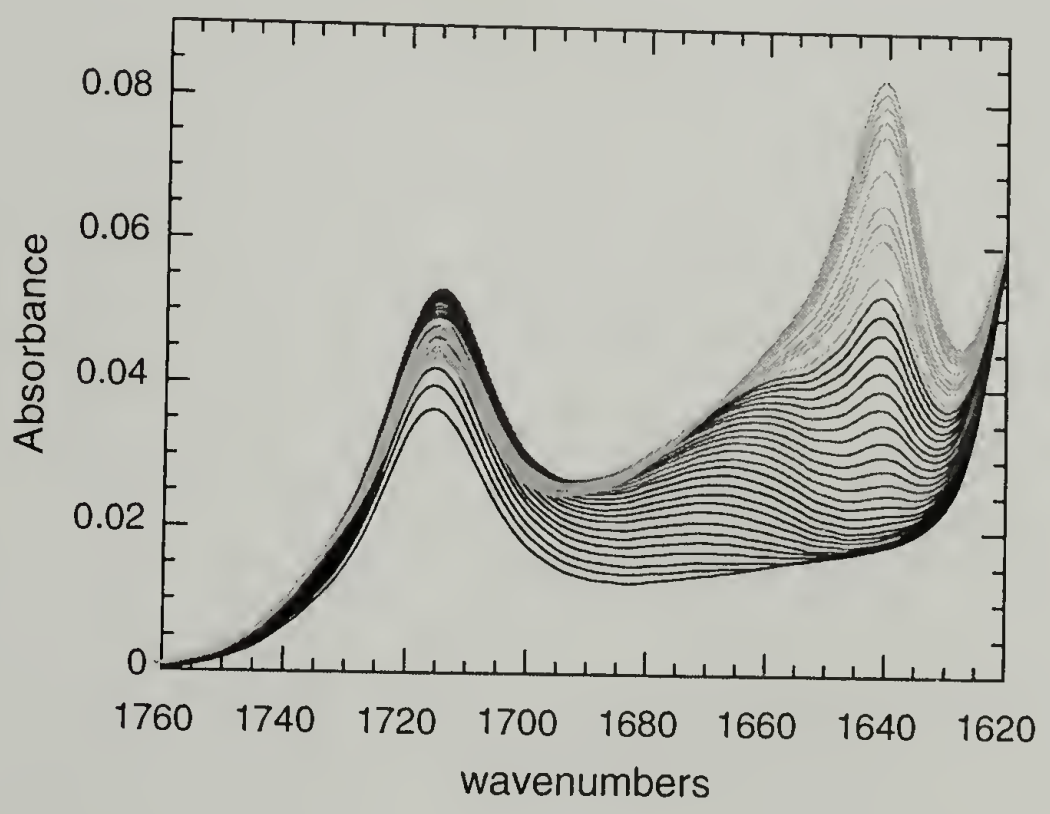

Figure 6.4 Infrared spectra obtained during reaction of T80-6-22 in the Amide I region. Time increases as spectra go from black to light gray.

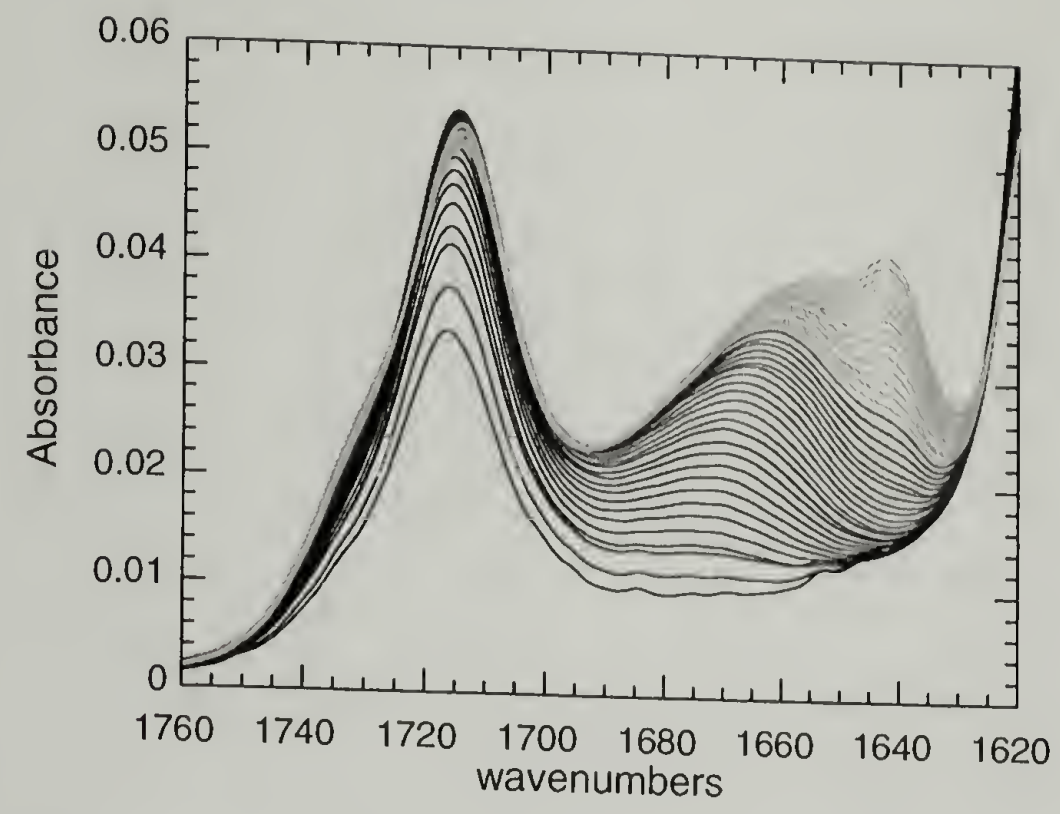

Figure 6.5 Infrared spectra obtained during reaction of T80-4-22 in the Amide I region. Time increases as spectra go from black to light gray.

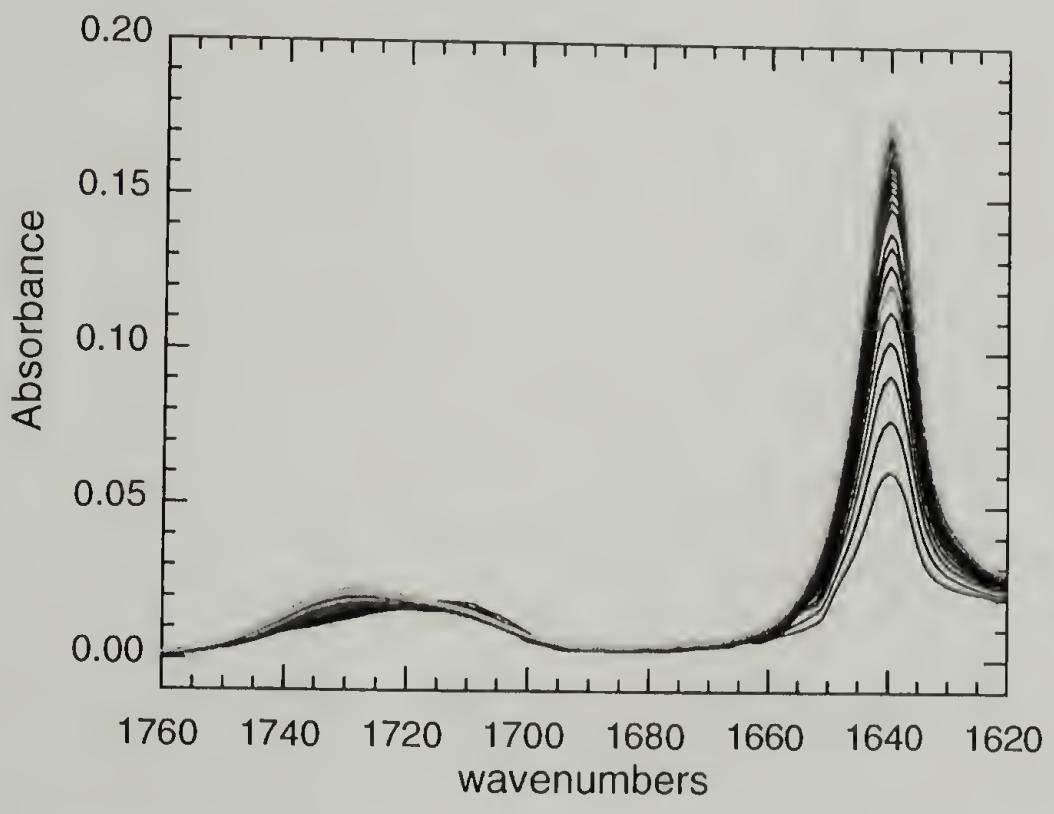

Figure 6.6 Infrared spectra obtained during reaction of oo-4-22 in the Amide I region. Time increases as spectra go from black to light gray.

of free urea groups increases. Meanwhile, a broad band appears and increases in intensity near 1670 cm^{-1}, corresponding to hydrogen-bonded urea. The rate of formation of free urea begins to decrease, and the number of hydrogen-bonded ureas continues to increase. This band shifts to lower frequency (~ 10 cm^{-1} shift) with increasing conversion, which may be associated with the formation of stronger or "better" hydrogen bonds, as shown in the previous Chapter. Finally, at later conversion a band at 1640 cm^{-1} emerges, owing to the formation of bidentate urea and, presumably, phase separation. A plot of the intensity at 1716, 1665, and 1640 cm^{-1} is shown in Figure 6.7 for T80-6-22. As conversion increases, the formation of hydrogen-bonded urea occurs through both depletion of NCO (reaction) and depletion of free urea. This behavior was observed for all the systems, but became less apparent when the contribution from the overlapping urethane vibration is significant.

The foaming reaction for *oo*-4-22 exhibited several notable differences from the T80-systems. The formation of bidentate urea is so rapid in this system that a state prior to its formation could not be captured. The rise and successive depletion of free urea is observed. However, monodentate hydrogen bonded urea is not formed. The morphology is exclusively described by the sharp bidentate urea band at 1640 cm^{-1} and a small contribution from free urea at 1715 cm^{-1}. The slow formation of urethane, which was difficult to observe in the other system, is also apparent at 1732 cm^{-1}.

6.3.2 Onset of Phase Separation

The importance of hard segment length and symmetry on influencing the phase behavior was determined by comparing the conversion at the onset of phase separation

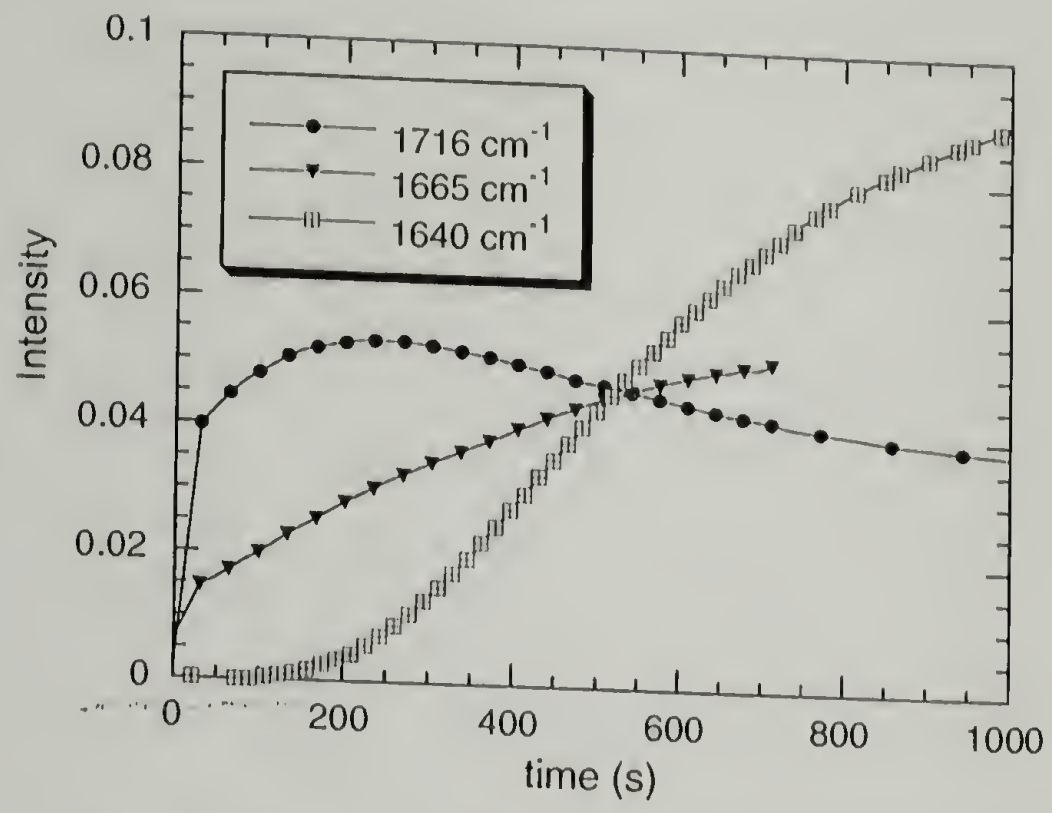

Figure 6.7 Change in intensity for different Amide I species during foaming of T80-6-22.

for the different systems. The growth of bidentate urea, measured by monitoring the intensity at 1640 cm^{-1}, is shown for oo-4-22, T80-6-22 and T80-4-22 in Figure 6.8. The rapid rise in bidentate urea is associated with the phase separation of the polyurea. Despite the fact that the stoichiometry of the oo-4-22 and T80-4-22 systems is identical, the *oo*-4-22 TDI phase separates at much lower conversion.

The onset of phase separation based on spectroscopic features is related to changes in the local aggregation, which is not necessarily correlated with the onset that would be made using techniques such as scattering. Thus, spectroscopic definition of "onset" is somewhat subjective. Here it will be taken as the point where an increase in intensity at 1640 cm^{-1} is first observed. This removes the influence of domain growth rate.

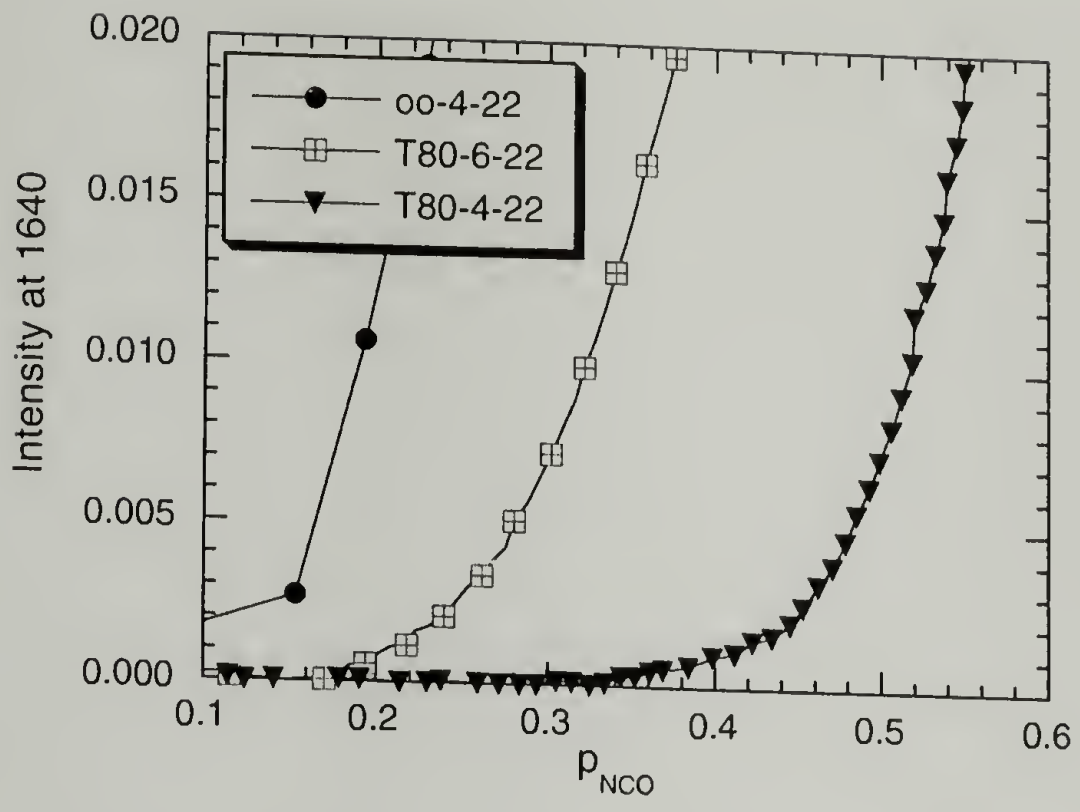

Figure 6.8 Onset and growth of bidentate urea as a function of conversion, determined from the intensity of the Amide I band at 1640 cm^{-1}.

The onset occurs near 10% and 28% conversion for the oo-4-22 and T80-4-22 system, respectively. When the concentration of TDI is increased from 30 to 37%, T80-6-22, the onset of phase separation occurs much sooner at 19% conversion.

There are several possible explanations for the difference in behavior between oo-4-22 and T80-4-22. The first could be due to differences in chain length distribution. X_n only depends upon stoichiometry, but X_w depends upon other factors as well. As discussed in Chapter 3, the reactivity of the second NCO group of 2,6-TDI and 2,4-TDI decreases after the first NCO group reacts. The decrease is more dramatic for 2,4-TDI, which decreases from 12 to 1, while 2,6-TDI only decreases from 6 to 1. This effect could potentially manifest as a higher X_w for oo-4-22. However, as shown in Chapter 3, Figure 3.1, the difference between the TDI isomers has a negligible effect on X_w. Thus,

the onset of phase separation does not occur at lower conversion in oo-4-22 due to differences in chain length distribution.

The other explanations for the behavior are related to differences in the excluded volume or the interaction strength of the two types of hard segments. Excluded volume effects are considered by comparing the data with Flory's calculations for non-interacting rods. Flory calculated the minimum X_n required to induce phase separation in a polydisperse mixture of undiluted, non-interacting rods.[17] He found that when $X_n = 2...$ a polydisperse mixture will phase separate into anisotropic and isotropic domains. The Xn at onset can be determined for the data shown here, assuming the conversion due to urethane formation is negligible, as shown in Table 6.2. Accounting for the fact that $p_{H_2O} = p_{NCO}/r$, X_n at onset is 1.12, 1.26, and 1.46 for oo-4-22, T80-6-22, and T80-4-22, respectively. These values are clearly much lower than the ones Flory obtained for perfectly rigid rods (which these are not). This suggests that the interactions must make an important contribution to phase separation in this system.

Table 6.2 Structural features at the onset of phase separation for different foam formulations

Sample	p_{NCO}	P_{H2O}	X_n
oo-4-22	0.10	0.12	1.12
T80-6-22	0.19	0.23	1.26
T80-4-22	0.28	0.35	1.46
T80-4-40	0.28	0.35	1.45
T80-4-56	0.27	0.35	1.44
T80-4-87	0.23	0.29	1.34
T80-4-113	0.26	0.33	1.41

In order to understand better the contribution from interaction parameter on the onset of phase separation, the foam reaction of T80-4-22 was also measured at temperatures ranging from 40-113 °C (T80-4-T). In systems where hydrogen bonding is important, the interaction parameters should depend on temperature.[18] The growth of bidentate urea for different reaction temperatures is shown in Figures 6.9. The conversion reflects ooth conversion to urea and conversion to urethane. The average hard segment length is related only to the urea concentration. The ratio of the urea to urethane kinetics was not constant with temperature due to the catalyst package used here. Urethane formation is much more strongly dependent on temperature, as shown in Figure 6.10. However, only for the samples prepared at 87 and 113 °C (T80-4-87 and T80-4-113) did any appreciable amounts of urethane formed prior to 50% conversion.

As shown in Figure 6.9, the temperature had little to no effect on the onset of phase separation. In particular, when $I_{1640} < 0.001$ the curves are nearly identical. It is only the time evolution of the bidentate urea that was influenced by temperature. The rate of growth was fastest for the sample prepared at 87 °C, making extrapolation to the onset point less reliable. Considering that a more appreciable amount of urethane formed for the samples prepared at 87 and 113 °C, p_{H20} represents an upper limit. This suggests that a lower concentration of urea or average hard segment length causes phase separation as temperature is increased. The effect, however, is only minor.

These results suggest that for a single system, hydrogen bonding does not dominate the phase separation process. However, as suggested by comparison Flory's calculations, this does not mean that the interactions are not important. It has been observed in previous elastomeric systems that the temperature has only a small influence

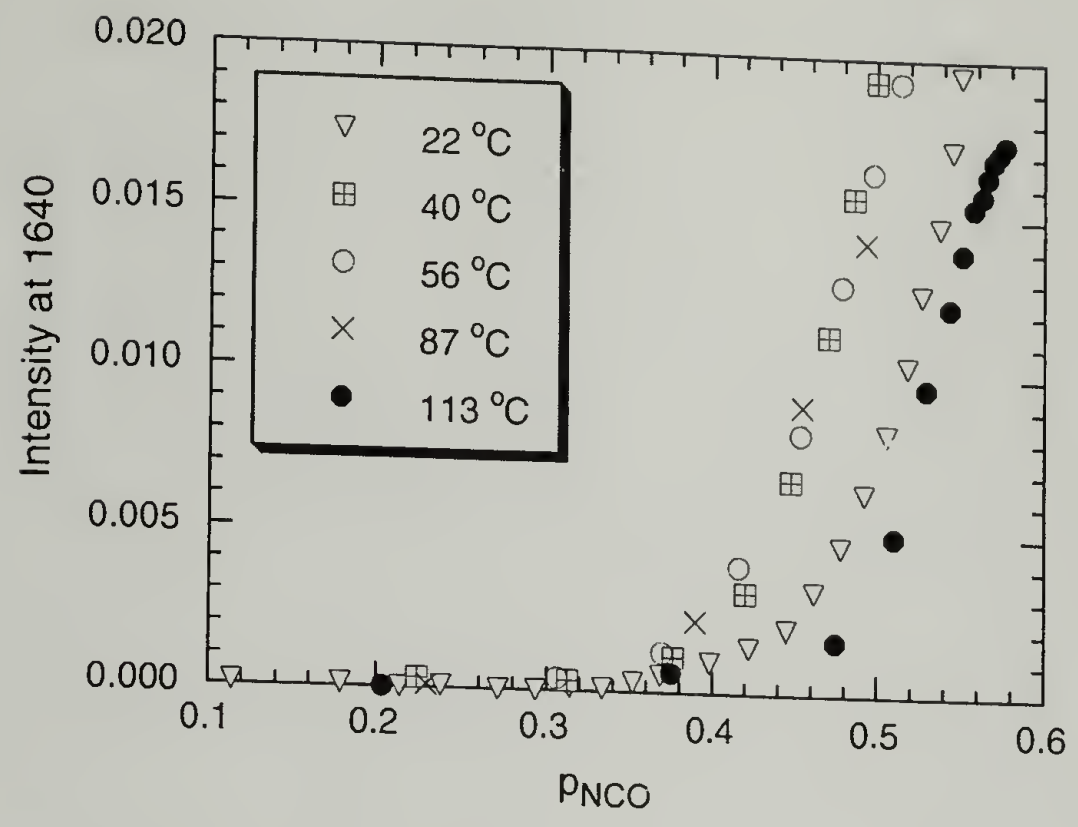

Figure 6.9 Onset and growth of bidentate urea as a function of conversion for T80-4- formulations prepared at different reaction temperatures.

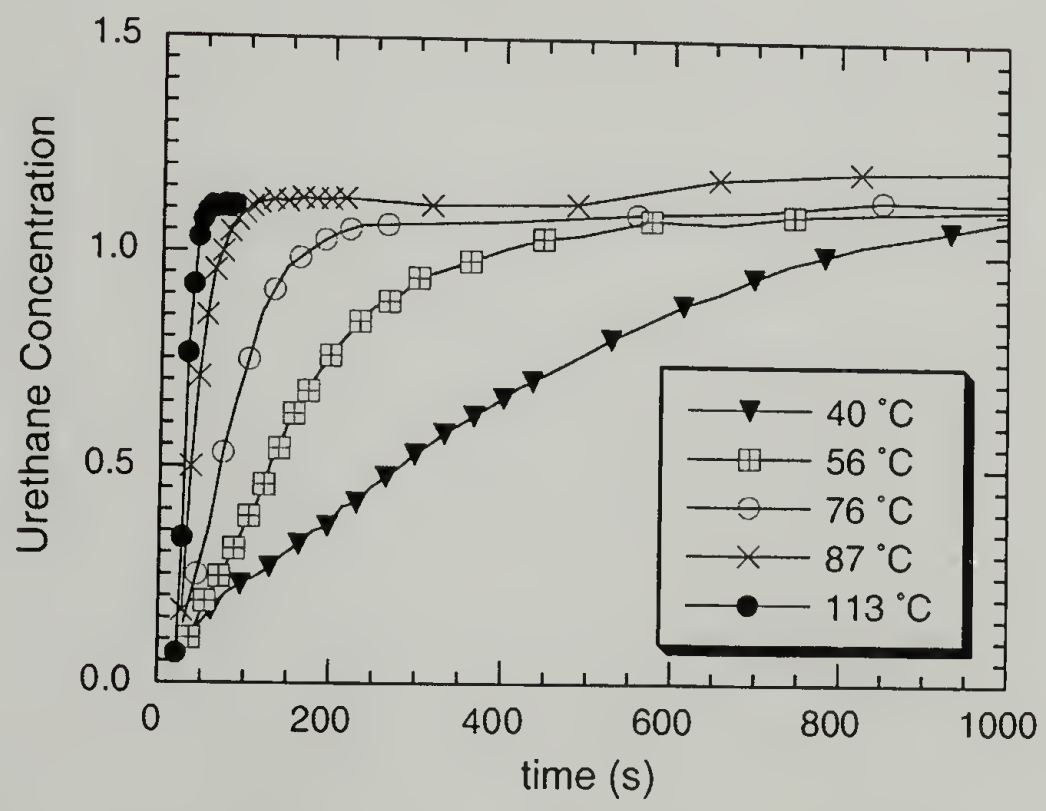

Figure 6.10 Kinetics of urethane formation in T80-4- formulation prepared at different reaction temperatures.

on phase behavior.[19] The most likely reason for the difference between oo-4-22 and T80-4-22 is that the structural irregularity of the latter hard scgmcnts prevents optimal interaction overlap or the translational mobility to achieve this interaction.

6.3.3 Morphology Development

The morphology development is refleeted by changes in the hydrogen bonding. In order to understand the data shown in Figure 6.7 for T80-6-22 more completely, the spectra were deeonvoluted into the separate contributions from urethane and free and hydrogen bonded urea, and band areas rather than band intensities were followed. The absorption eoefficients for the different bands arc not thc same, and thus band deconvolution does not give quantitative results. However, this method allows distinetion of overlapping bands, sueh as the monodcntate and bidentate hydrogen bonds. The results are shown in Figures 6.11 to 6.13 for samples oo-4-22, T80-6-22, and T80-4-22, respectively.

The differenee between oo- and T80- samples is striking. As already mentioned, the morphology of oo-4-22 is described exclusively by free and bidentate urea. The initial growth of bidentate urea is accompanied by a depletion of frce urea. After 200 s, the growth of bidentate urea begins to plateau and, accordingly, the free urea begins to increase again. As shown in Figure 6.11, as well as evident in Figure 6.6, the amount of urcthanc at this point makes aecurate dcconvolution of the free band somewhat unfeasible. Thus, it is not clear whether this sccond growth of free urea is real.

The behavior of T80-6-22 and T80-4-22 is similar. The stoichiomctry of T80-6-22 gives fcwer urethane linkages, making this sample casier to study via band deeonvolution.

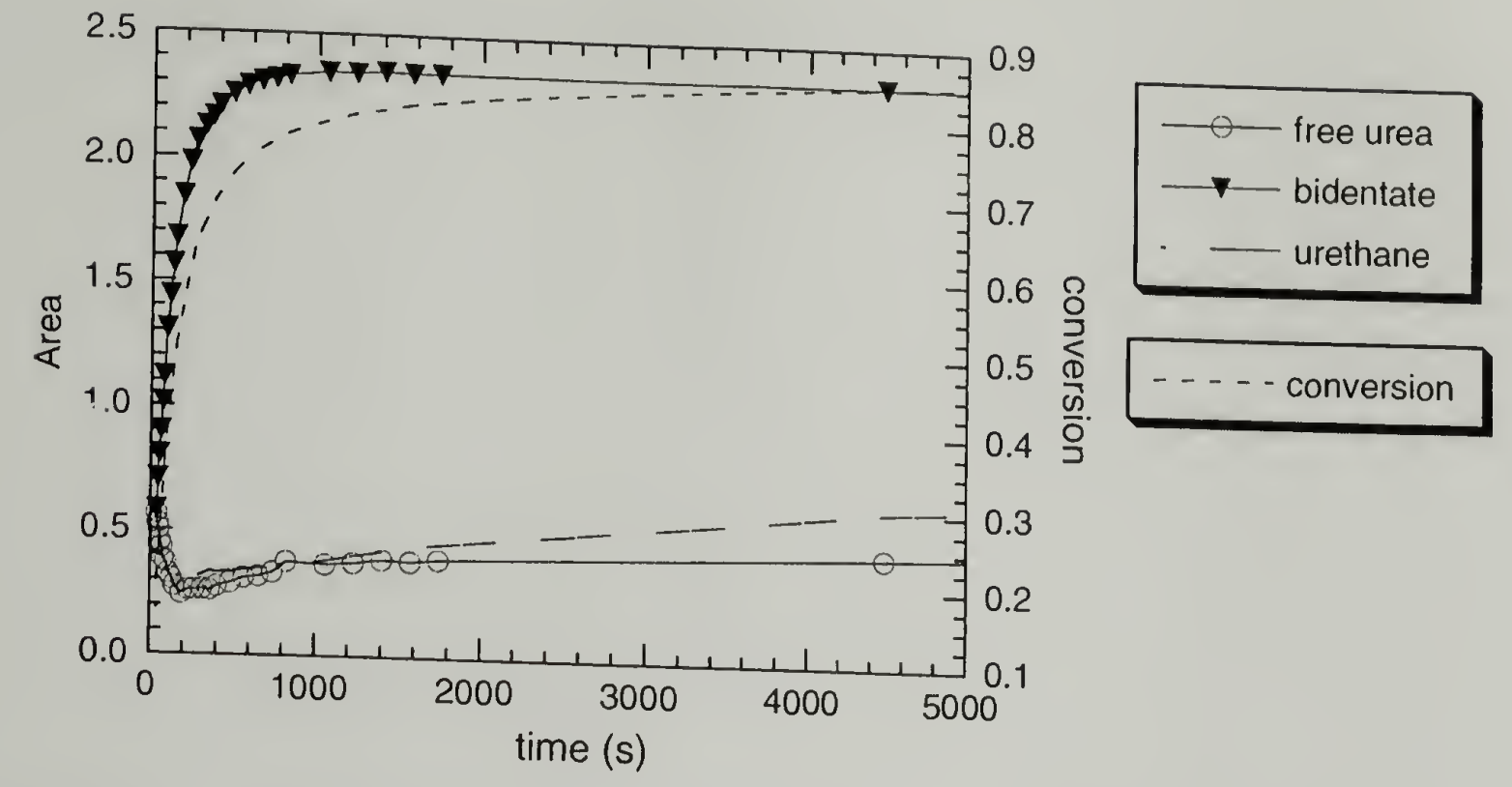

Figure 6.11 Changes in the population of different species during morphology development in oo-4-22.

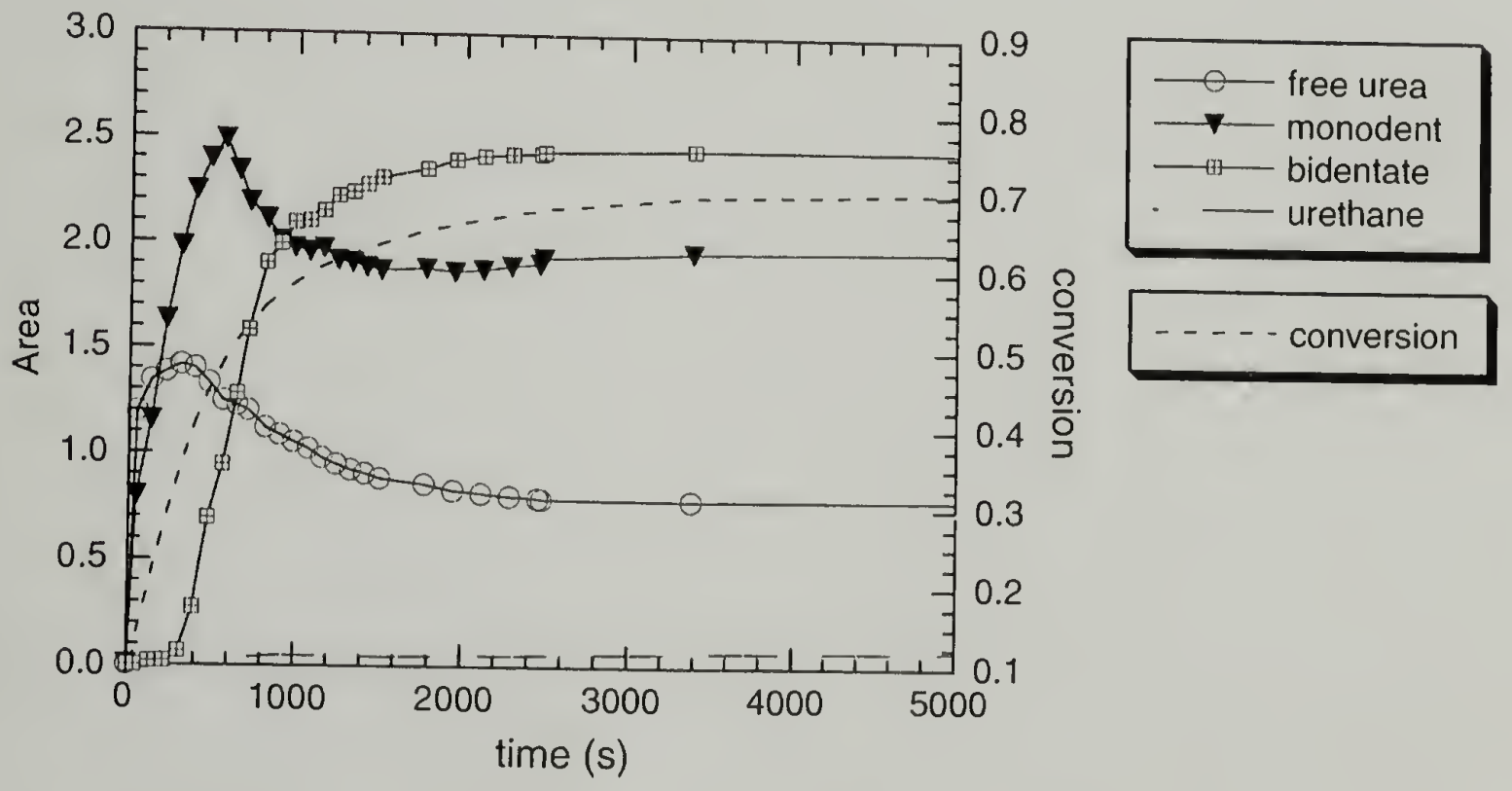

Figure 6.12 Changes in the population of different species during morphology development in T80-6-22.

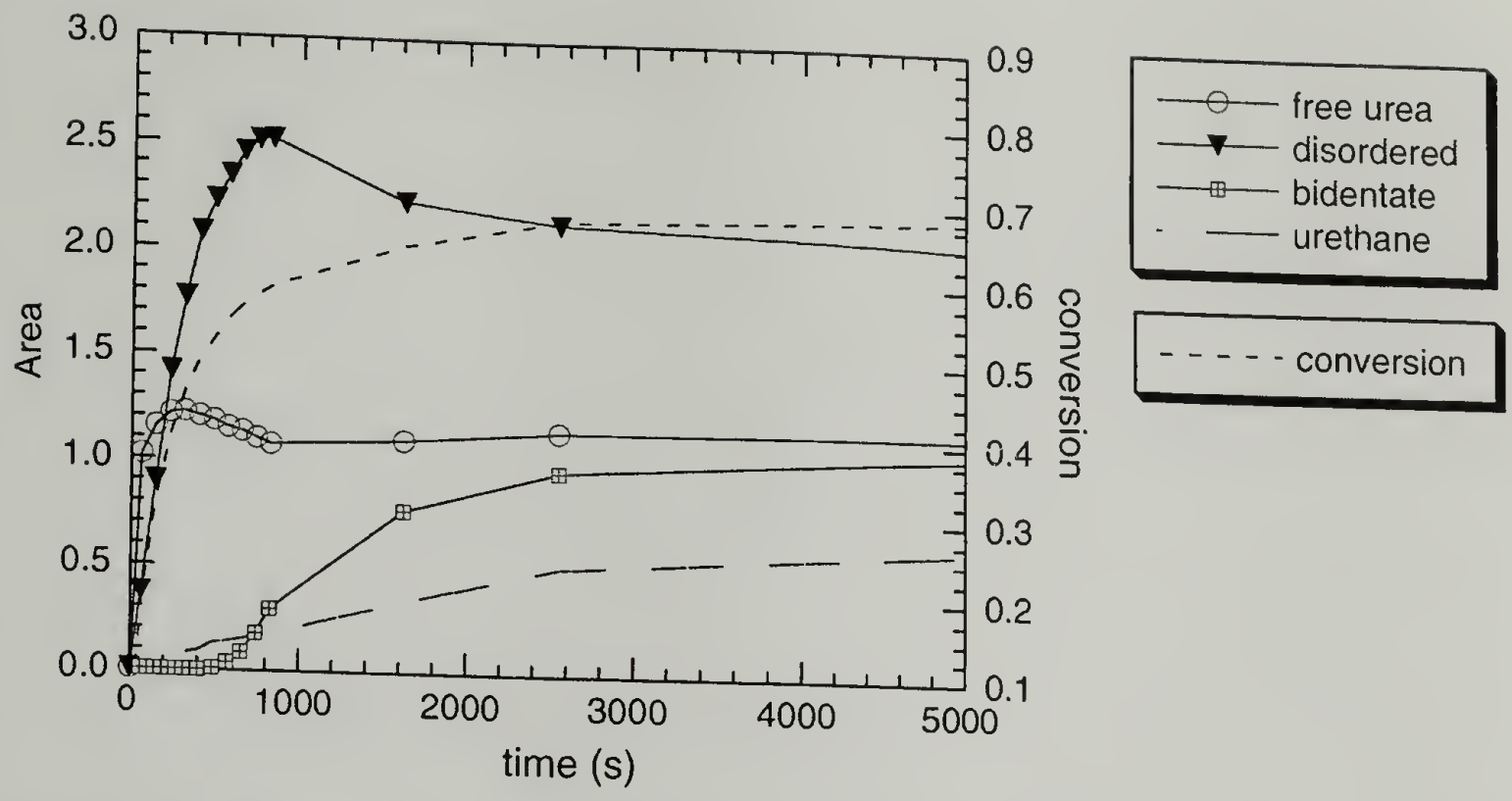

Figure 6.13 Changes in the population of different species during morphology development in T80-4-22.

Both samples are composed of free and bidentate urea, as well as a broad monodentate hydrogen bonded urea. This latter band is composed of an ensemble of different hydrogen bonded conformations of various geometry and strength.

Like oo-4-22, the growth of bidentate urea in the T80-6-22 sample, shown in Figure 6.12, is accompanied by a depletion of free urea. It is also evident that as the bidentate growth reaches a plateau, the amount of free urea reaches a minimum. The monodentate hydrogen bonds also show an initial increase followed by a decrease. However, in contrast to the free ureas, the depletion of monodentate hydrogen bonds does not occur until after a sufficient population of bidentate urea has formed. This will be discussed in greater detail below.

As shown in Figure 6.13, the formation of bidentate urea is much slower for T-80-4-22 than for T80-6-22. The time scale to reach a plateau value is approximately 2500 and 5000 s for T80-6-22 and T80-4-22, respectively. It should be noted that T80-6-22 contains a higher concentration of urea groups, so the absolute area cannot be compared.

By neglecting the differences in absorption coefficient for free and hydrogen-bonded species, the fraction of free and bidentate urea can be determined from the area of the three bands, as shown in Table 6.3. The free urea is often referred to as "soluble" urea and, presumably, is only found in the hard segment-poor domains (i.e. isotropic domains). If this amount is taken as being related to the degree of phase separation, the relative amount of urea that remains in the isotropic phase is 11, 15, and 30% for oo-4-22, T80-6-22, and T80-4-22, respectively. The bidentate urea corresponds to a very specific geometry and is only found in the hard segment rich domains. If this amount is taken as being related to the degree of phase separation, the relative amount of urea that is found in hard segment-rich domain is 89, 47, and 30% for oo-4-22, T80-6-22, and T80-4-22, respectively. Both values show a qualitatively similar trend. However, the magnitude of these differences depends upon where the monodentate hydrogen bonds are found. Are monodentate hydrogen bonds found in the isotropic phase or in the anisotropic phase?

Table 6.3 Degree of phase separation for different samples

Sample	Free (%)	Bidentate (%)
oo-4-22	11	89
T80-6-22	15	47
T80-4-22	30	30

The observation of monodentate hydrogen bonds is not unusual on its own. In any hydrogen-bonded system, an equilibrium will exist between free and hydrogen bonded species, for example as observed for X,8 PU melts. While the isotropic reacting system is not at thermodynamic equilibrium due to the rapid depletion/formation of functional groups, the system is nonetheless expected to contain some population of hydrogen-bonded species. In other words, monodentate ureas can exist in the absence of a phase-separated morphology. Under equilibrium conditions, the number of free and hydrogen-bonded ureas should depend on temperature and concentration.

The hydrogen bonding characteristics of the reacting isotropic (i.e. prior to phase separation) system was studied as a function of reaction temperature. At higher temperatures urethane and secondary reactions, such as the formation of isocyanurate and biuret, become more important, and their bands overlap the urea bands in this region. Despite these limitations in the analysis, band deconvolution can still be carried out. A plot of free urea versus total urea (i.e. increasing conversion) is shown in Figure 6.14 prior to phase separation. Two important observations can be made. The first is that the reaction temperature has virtually no effect on the fraction of free species observed. Under equilibrium conditions, increasing the temperature should increase the fraction of free species observed. The second is the trend that the fraction of free species increases as the total number of urea (area of monodentate + free). The x-axis of this plot is directly proportional to the concentration of urea groups, since the number of urea groups is increasing as the volume stays constant. Thus, under these reactive conditions, the number of free species increases as the concentration increases. This is the opposite of what is expected under equilibrium conditions.

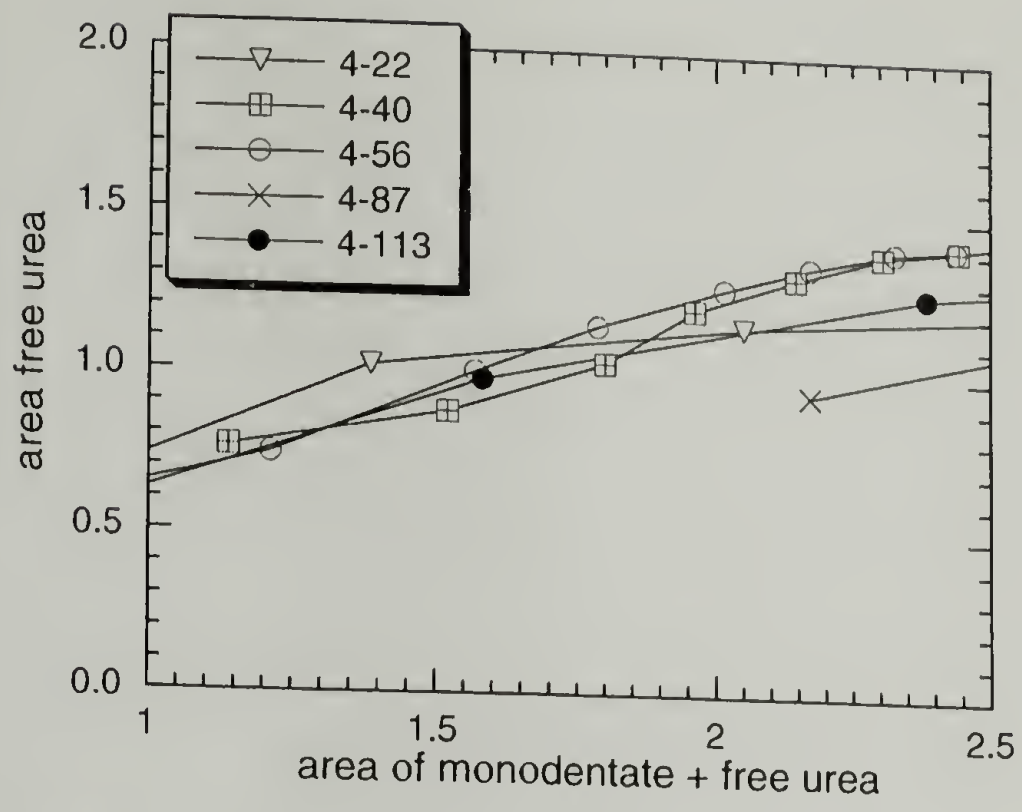

Figure 6.14 Change in fraction of free species during the reaction of T80-4- formulations prepared at different temperatures.

Both results suggest that the reaction to form urea groups is faster than the time it takes to reach the equilibrium hydrogen-bonded state for a given temperature and concentration. In other words, the system is below its equilibrium concentration of monodentate hydrogen bonds. This may explain why the number of monodentate species continues to increase even after phase separation occurs. The isotropic phase may be trying to approach its steady state. In addition, fewer processes lead to a decrease in monodentate species compared with free species, as shown in Figure 6.15. The continued rise in the number of monodentate species even after the onset of phase separation suggests that the free and monodentate species are depleted from the isotropic phase to form hard domains containing both bidentate and monodentate urea. In other words, the hard domains in the T80- systems are not well-organized, but perhaps owing to the structural irregularity of the hard segments are somewhat disordered.

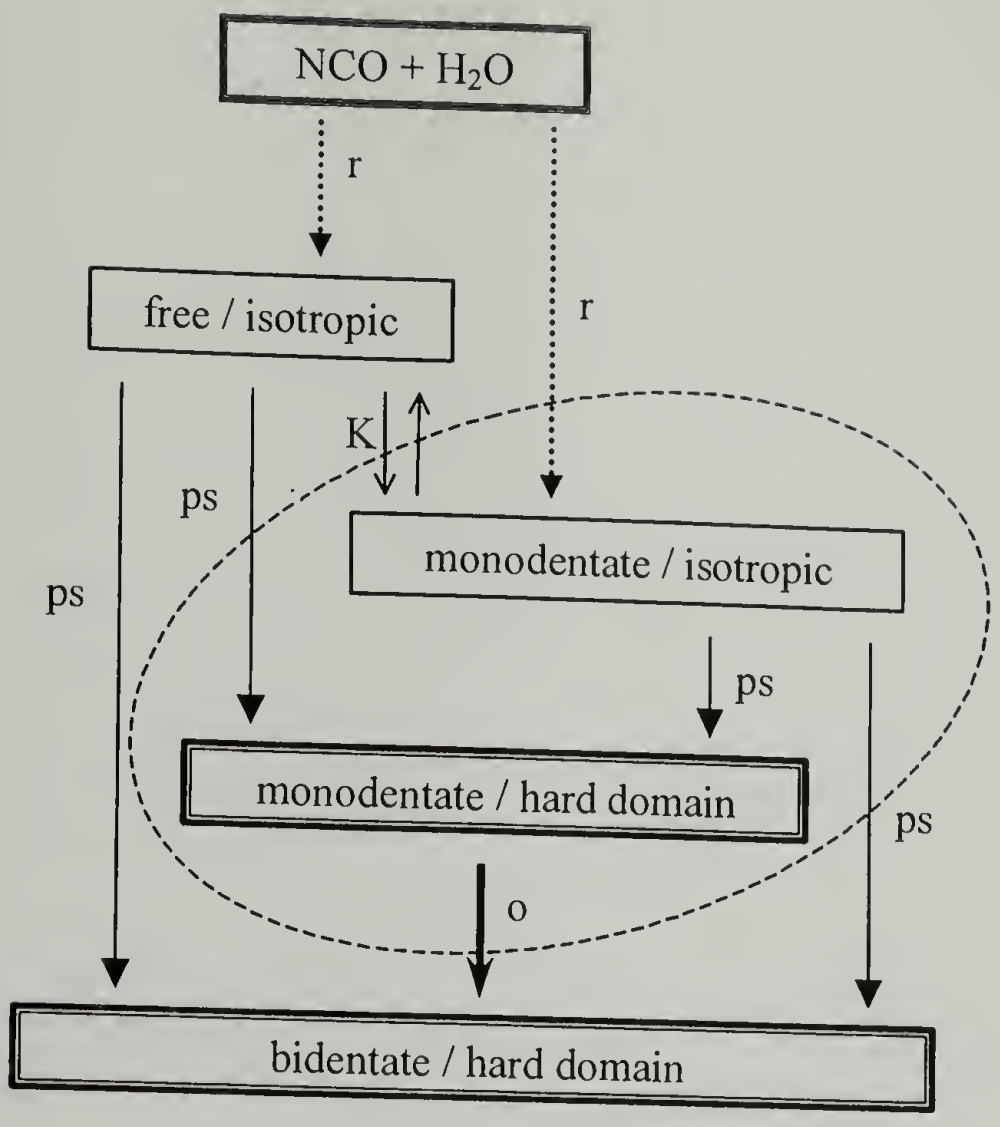

Figure 6.15 Schematic showing the various types of urea that can form during reaction (r), equilibration of the isotropic phase (K), phase separation (ps), and organization of disordered hard domains (o).

Finally, as the rate of reaction begins to decrease and the isotropic phase reaches its equilibrium concentration of hydrogen-bonded species, the concentration of monodentate species begins to decrease. According to Figure 6.15, a decrease may occur due to phase separation of the monodentate isotropic species or due to organization of monodentate species within the hard domains. Annealing studies of elastomers suggest that the time scale necessary to observe ordering of disordered hard domains is much

slower than the time scales observed here.[19] Thus, depletion of monodentate species most likely arises from the continued phase separation of isotropic domains.

6.4 Discussion

The data obtained can be used to develop a model of how the reacting system evolves into a phase-separated morphology. For oo-4-22, the initial isotropic system containing 2,6-TDI, water, and polyether reacts and ureas begin to form. After 12% of the water has been converted to urea, the system begins to phase separate. This occurs through association of longer polyurea segments into ordered bidentate urea. The reaction between water and NCO continues to occur during phase separation. Each new urea is immediately converted into a bidentate urea. This suggests that even the lowest molecular weight oligomers are effectively partitioned to the hard segment rich domain as soon as they are formed.

For the T80- systems, a higher concentration of urea groups in the isotropic phase causes association of the ureas into monodentate hydrogen bonds. As the concentration of free and hydrogen-bonded urea increases, the average strength of the hydrogen bonds increases. The formation of bidentate urea occurs at a much later stage. At initial stages, spatial ordering occurs through an apparent depletion of free polyurea segments. At later stages, monodentate hydrogen bonded ureas are also depleted. This observation is related to the rates of the various competing processes: reaction, equilibration, and phase separation. In contrast to oo-systems, further reaction between the water and isocyanate in T80-systems leads to an increase in hydrogen-bonded structures, due to a lower degree of phase separation and hence a higher concentration of urea within the isotropic domains. The "slowness" of the morphology development indicated by changes in the

monodentate hydrogen bonds suggests a morphology that is not fully evolved. The spatial ordering may not be complete or in the preferred state. Despite the fact that the concentration of TDI is the same for oo-4-22 and T80-4-22, the entire T80-system seems more condensed. The behavior observed here is interesting considering that the morphology of polyurethanes is often described as consisting of either isolated domains or interconnected domains.[20] Interconnectivity may be achieved by preventing the formation of well-organized hard domains.

6.5 Conclusions

Infrared spectroscopy was used to study polyurethane structural evolution, including reaction, hard segment growth, onset of phase separation, order formation, and morphology development. Changes in the different types of urea groups, free or hydrogen bonded, were used to understand organization of the entire ensemble. Hard segments based on 2,6-TDI and an 80/20 mixture of 2,4-/2,6-TDI were assumed to give hard segments with different anisotropies. This factor proved to be crucial in influencing the morphology development. Phase separation occurred at earlier conversion, i.e. with shorter and fewer hard segments, and faster in the more anisotropic system. Based on changes in the monodentate urea groups, phase evolution may be incomplete, or trapped, in the less anisotropic system. The degree of spatial order achieved in this system is much lower.

6.6 References

(1) Elwell, M. J.; Ryan, A. J.; Grunbauer, H. J. M.; Van Licshout, H. C. *Polymer* **1996**, *37*, 1353.

(2) Artavia, L. D.; Macosko, C. W. *J. Cell. Plast.* **1990**, *26*, 490.

(3) Priester, R. D.; McClusky, J. V.; O'Neill, R. E.; Turner, R. B.; Harthcock, M. A.; Davis, B. L. *J. Cell. Plast.* **1990**, *26*, 346.

(4) Satchell, D. P. N. S., R.S. *Chem. Soc. Rev.* **1971**, 231.

(5) Lee, H. S.; Hsu, S. L. *Macromolecules* **1989**, *22*, 1100.

(6) Lee, H. S.; Wang, Y. K.; Hsu, S. L. *Macromolecules* **1987**, *20*, 2089.

(7) Meuse, C. W.; Tao, H.-J.; Hsu, S. L.; MacKnight, W. J. *Polym. Prepr. (Am. Chem. Soc., Div. Polym. Chem.)* **1993**, *34*, 266-267.

(8) Kondyurin, A.; Klyachkin, Y. *J. Appl. Polym. Sci.* **1994**, *54*, 1385.

(9) Ham, N. S.; Willis, J. B. *Spectrochim. Acta* **1960**, *16A*, 279.

(10) Klapstein, D.; Nau, W. N. *Spectrochim. Acta* **1993**, *50A*, 307.

(11) Hoyer, H. *Chem. Ber.* **1956**, *89*, 2677.

(12) Chantry, G. W.; Nicol, E. A.; Harrison, D. J.; Bouchy, A.; Roussy, G. *Spectrochim. Acta* **1974**, *30A*, 1717.

(13) Miyazawa, T.; Shimanouchi, T.; Mizushima, S. I. *J. Chem. Phys.* **1956**, *24*, 408.

(14) Miyazawa, T.; Shimanouchi, T.; Mizushima, S. I. *J. Chem. Phys.* **1958,** *29*, 611.

(15) Ishihara, H.; Kimura, I.; Saito, S.; Ono, H. J. *Macromol. Sci. Phys.* **1974**, *B10*, 591-618.

(16) Zavodov, I. A.; Maklakov, L. I.; Atovmyan, E. G. *Spectrochim. Acta* **1999**, *A55*, 923.

(17) Flory, P. J. *Macromolecules* **1978**, *11*, 1138.

(18) Painter, P. C.; Graf, J. F.; Coleman, M. M. *Macromolecules* **1991**, *24*, 5630.

(19) Leung, L. M.; Koberstein, J. T. *Macromolecules* **1986**, *19*, 706.

(20) Aneja, A.; Wilkes, G. L. *Polymer* **2002**, *43*, 5551.

CHAPTER 7

CONCLUSIONS

The molecular weight distributions, end groups, and linkages of polyurethane structural elements were quantitatively determined. These elements included macrodiols (Chapter 2), prepolymers (Chapters 3 and 4), and polyureas (Chapter 3). PPG was found to consist of a mixture of 95% diol and 5% monol, where the alcohol groups are secondary hydroxyls. The monol has a lower M_n than the diol. The polyesters contained an additional nonfunctional, cyclic component. The amount of this species in PHMA and PHMS, determined by MALDI-TOF, was 26 and 32%, respectively.

The macrodiols were used to prepare MDI-capped prepolymers. In the absence of side reactions, the molecular weight distribution of prepolymers obeyed a Schultz-Flory distribution, which depends upon conversion and stoichiometric imbalance. On the other hand, typical polyurethane side reactions, such as allophanate and isocyanurate formation, increase the average molecular weight and broaden the distribution. Allophanate formation is most prevalent in PPG prepolymers prepared at temperatures greater than 124 °C. For samples prepared at 145 °C for 3h, as much as 10 mole % N participated in allophanate linkages. Prepolymers prepared from polyesters exhibited negligible amounts of allophanate. However, the allophanate content of a prepolymer prepared from the ternary blend containing PPG, PHMA, and acrylic was similar to PPG prepolymers. The propensity of PPG and blended polymers to form allophanate is unclear.

The molecular weight distribution of polyurea hard segments prepared from TDI and water is dependant on whether the sample was prepared under homogeneous conditions. Under homogeneous conditions, the molecular weight distribution exhibited a Schultz-Flory shape. But due the change in reactivity of NCO groups during reaction, the distribution was narrower and shifted to lower molecular weight. Hard segments isolated from foams have strange molecular weight distributions, consisting of only a few species. The results suggest that the local stoichiometric imbalance is different than the initial feed. Based on the high population of low molecular species, this is most likely due to phase separation of the water from the reacting blend.

The structural parameters were found to influence the solubility parameters (Chapter 4), crystallization behavior (Chapter 5), and phase behavior (Chapter 6) of polyurethanes. Fractionation of the ternary prepolymer blend into two fractions, MeOH soluble and insoluble, showed that the cyclic polyesters were more soluble than the corresponding functionalized polyesters, while the allophanated PPG prepolymers were less soluble than the corresponding linear prepolymers.

Hydrogen bond strength of the groups was shown to influence all aspects of the crystallization behavior, including the initial state, nucleation and growth rates, and the final morphology. The initial state is "pinned" by the hydrogen bonds that persist in the melt. Where the entropic penalty for maintaining this pairwise interaction is low, nucleation is enhanced. On the other hand, growth of the crystalline phase is inhibited by strong interactions, resulting in crystalline morphologies with a high degree of imperfection. Microscopy and scattering data suggest that the crystals formed from the melt were small, consistent with the picture of fast nucleation and slow growth.

Hydrogen bond strength proves to be less erueial in the onset of phase separation in polyurethane foams. The most erueial parameter was shown to be hard segment anisotropy. Foams prepared from pure 2,6-TDI exhibited very different morphology development than foams with the same stoiehiometry but based on a mixture of 2,4- and 2,6-TDI. Phase separation oeeurred mueh sooner, when the hard segments were mueh shorter and in lower eoneentration, for 2,6-TDI based foams. The reaetion temperature was found to have little influenee on the onset, supporting the idea that hydrogen bonding is not the driving foree. On the other hand, the influenee of hydrogen bonding on the kineties of morphology development eannot be ruled out. The rate and degree of phase separation was faster and more eomplete for the system based on 2,6-TDI. For T80-TDI, a high eoneentration of spatially disordered monodentate urea groups was observed. The origin of these speeies is unelear. Depending upon whether or not they reside in the hard segment rieh domains, their behavior may suggest that phase separation and order formation are two separate proeesses. The slower rate of phase separation may be attributed to the faet that they are less anisotropie, more irregular, or more strongly interaeting than pure 2,6-TDI hard segments.

BIBLIOGRAPHY

Annual Book of ASTM Standards **1996**, *15.05*, E203-296.

Annual Book of ASTM Standards **2000**, *08.03*, D5155-5110.

Annual Book of ASTM Standards **2000**, *08.03*.

Abouzahr, S.; Wilkes, G. L. *J. Appl. Polym. Sci.* **1984**, *29*, 2695.

Aharoni, S. M. *n-Nylons, their synthesis, structure, and properties*; J. Wiley and Sons: Chichester; New York, 1997.

Ahn, T. O.; Lee, M.; Jeong, H. M.; Cho, K. *J. Polym. Sci., B Polym. Phys.* **1998**, *36*, 201.

Ajithkumar, S.; Kansara, S. S.; Patel, N. K. *Eur. Polym. J.* **1998**, *34*, 1273.

Aneja, A.; Wilkes, G. L. *Polymer* **2002**, *43*, 5551.

Armistead, J. P.; Wilkes, G. L. *J. Appl. Polym. Sci.* **1988**, *35*, 601.

Artavia, L. D.; Macosko, C. W. *J. Cell. Plast.* **1990**, *26*, 490.

Bailey, F. E. J.; Critchfield, F. E. *J. Cell. Plast.* **1981**, *17*, 333.

Bakalo, I. A.; Pisareva, I. V. *Zh. Org. Khim.* **1986**, *22*, 1701.
Baker, J. W.; Holdsworth, J. B. *J. Chem. Soc.* **1947**, 713.

Baker, J. W.; Gaunt, J. *J. Chem. Soc.* **1949**, 9.

Barnes, J. D.; Fanconi, B. M. *J. Chem. Phys.* **1972**, *56*, 5190.

Barreiro, M. F.; Dias, R. C. S.; Costa, M. R. N. *Macromolecules* **1994**, *27*, 7650.

Bayer, O.; Siefken, W.; Rinke, H.; Orthner, L.; Schlid, H., "A process for the production of polyurethanes and polyureas." German Patent 728,981, 1937.

Bayer, O. *Angew. Chem.* **1947**, *A59*, 275.

Beck, R. A.; Truss, R. W. *J. Appl. Polym. Sci.* **1999**, *71*, 959.

Boczkowska, A.; Gruin, I. *Eur. Polym. J.* **1999**, *35*, 1569.

Bonart, R. *J. Macromol. Sci.-Phys.* **1968**, *B2*, 115.

Bonart, R.; Morbitzer, L.; Hentze, G. *J. Macromol. Sci.-Phys* **1969**, *B3*, 337.

Braun, S.; Kalinowski, H.-O.; Berger, S. *100 and More Basic NMR Experiments*; VCH: New York, 1996.

Broek, F. H. *J. Org. Chem.* **1959**, *24*, 1802.

Buist, J. M. *Developments in Polyurethanes*; Applied Science Publishers: London, 1978.
Caraculacu, A. A.; Coseri, S. *Prog. Polym. Sci.* **2001**, *26*, 799.

Castro, J. M.; Lopez-Serrano, F.; Camargo, R. E.; Macosko, C. W.; Tirrell, M. *J. Appl. Polym. Sci.* **1981**, *26*, 2067.

Chai, Z.; Sun, R.; Li, S.; Karasz, F. E. *Macromolecules* **1995**, *28*, 2297.

Chambers, J.; Moore, T.; Huber, L.; Frank, D. *Adhesives Age* **1998**, *8*, 24.

Chantry, G. W.; Nicol, E. A.; Harrison, D. J.; CBouchy, A.; Roussy, G. *Spectrochim. Acta* **1974**, *30A*, 1717

.

Chapman, T. M. *J. Polym. Sci., A Polym. Chem.* **1989**, *27*, 1993.

Christenson, C. P.; Harthcock, M. A.; Meadows, M. D.; Spell, H. L.; Howard, W. L.; Creswick, M. W.; Guerra, R. E.; Turner, R. B. *J. Polym. Sci., B Polym. Phys.* **1986**, *24*, 1401.

Ciferri, A. In
Polymer Liquid Crystals; Ciferri, A., Ed.; Academic Press, 1982.

Clayden, N. J.; Nijs, C.; Eeckhaut, G. *Macromolecules* **1998**, *31*, 7280.

Clough, S. B.; Schneider, N. S.; King, A. O. *J. Macromol. Sci.-Phys.* **1968**, *B2*, 641.

Coleman, M. M.; Lee, K. H.; Skrovanek, D. J.; Painter, P. C. *Macromolecules* **1986**, *19*, 2149.

Coleman, M. M.; Graf, J. F.; Painter, P. C. *Specific Interactions and the Miscibility of Polymer Blends*; Technomic Publishing Co.: Lancaster, 1991.

Coleman, M. M.; Sobkowiak, M.; Pehlert, G. J.; Painter, P. C.; Iqbal, T. *Macromolecular Chemistry and Physics* **1997**, *198*, 117.

Cooper, S. L.; Tobolsky, A. V. *J. Appl. Polym. Sci.* **1966**, *10*, 1837.

Cui, Y. J.; Chen, D. H.; Wang, X. L.; Tang, X. Z. *Int. J. Adh. Adh.* **2002**, *22*, 317.

De Genova, R. D.; Harper, M. D.; Clay, W. A.; Cranley, P. E.; Hunter, M. K. *TAPPI J.* **1996**, *79*, 196.

De Genova, R.; Grier, L.; Murray, D. P.; Clay, W. *TAPPI J.* **1998**, *81*, 196.
Di Lorenzo, M. L.; Silvestre, C. *Prog. Polym. Sci,* **1999**, *24*, 917.

Donohoe, G.; Satchell, D. P. N.; Satchell, R. S. *J. Chem. Soc.-Perkin Trans. 2* **1990**, 1671.

Dounis, D. V.; Wilkes, G. L. *J. Appl. Polym. Sci.* **1997**, *65*, 525.

Duffy, D. J.; Stidham, H. D.; Hsu, S. L.; Sasaki, S.; Takahara, A.; Kajiyama, T. *J. Mater. Sci.* **2002**, *37*, 4801.

Dusek, K.; Spirkova, M.; Havlicek, I. *Macromolecules* **1990**, *23*, 1774.

Eceiza, A.; de la Caba, K.; Gascon, V.; Corcuera, M. A.; Mondragon, I. *Eur. Polym. J.* **2001**, *37*, 1685.

Ellis, T. S. *Macromolecules* **1995**, *28*, 1882.

Elwell, M. J.; Mortimer, S.; Ryan, A. J. *Macromolecules* **1994**, *27*, 5428.

Elwell, M. J.; Ryan, A. J.; Grunbauer, H. J. M.; Van Lieshout, H. C. *Macromolecules* **1996**, *29*, 2960.

Elwell, M. J.; Ryan, A. J.; Grunbauer, H. J. M.; Van Lieshout, H. C. *Polymer* **1996**, *37*, 1353.

Entelis, S. G.; Nesterov, O. V. *Russ. Chem. Rev.* **1966**, *35*, 917.

Ephraim, S.; Woodward, A. E.; Merobian, R. B. *J. Am. Chem. Soc.* **1958**, *80*, 1326.

Fernandes, E. G.; Lombardi, A.; Solaro, R.; Chiellini, E. *J. Appl. Polym. Sci.* **2001**, *80*, 2889.

Flory, P. J. *J. Am. Chem. Soc.* **1936**, *58*, 1877.

Flory, P. J. *Proc. R. Soc., London A* **1956**, *234*, 73.

Flory, P. J. *Statistical Mechanics of Chain Molecules*; Interscience Publishers: New York, 1969.

Flory, P. J. *Macromolecules* **1978**, *11*, 1138.

Flory, P. J. *Macromolecules* **1978**, *11*, 1119.

Flory, P. J.; Frost, R. S. *Macromolecules* **1978**, *11*, 1126.

Ford, I. J. *J. Chem. Phys.* **1996**, *105*, 8324.

Forschner, T. C.; Gwyn, D. E.; Xiao, H. X.; Suthar, B.; Sun, L.; Frish, K. C. *Adhesives Age* **1999**, 20.

Gandhi, K. S.; Babu, S. V. *AIChE J* **1979**, *25*, 266.

Gandhi, K. S.; Babu, S. V. *Macromolecules* **1980**, *13*, 791.

Gelfer, M.; Horst, R. H.; Winter, H. H.; Heintz, A. M.; Hsu, S. L. *Polymer* **2003**, *44*, 2363.

Gheluwe, P. V.; Leroux, J. *Journal of Applied Polymer Science* **1983**, *28*, 2053.

Glotzer, S. C.; Gyure, M. F.; Sciortino, F.; Antonio, C.; Stanley, H. E. *Phys. Rev. E* **1994**, *49*, 247.

Gorce, J. N.; Hellgeth, J. W.; Ward, T. C. *Polym. Eng. Sci.* **1993**, *33*, 1170.

Gupta, T.; Adhikari, B. *J. Polym. Sci., A Polym. Chem.* **2001**, *39*, 2978.

Ham, N. S.; Willis, J. B. *Spectrochim. Acta* **1960**, *16A*, 279.

Harrell, L. L., Jr. *Macromolecules* **1969**, *2*, 607.

Hayakawa, T.; Adachi, K. *Macromolecules* **2000**, *2000*, 6834.

Heintz, A. M.; McKiernan, R. L.; Gido, S. P.; Penelle, J.; Hsu, S. L.; Sasaki, S.; Takahara, A.; Kajiyama, T. *Macromolecules* **2002**, *35*, 3117.

Heintz, A. M.; De Silva, A.; Hsu, S. L. *Polym. Prepr.* **2003**, *45*.

Heintz, A. M.; Duffy, D. J.; Hsu, S. L.; Suen, W.; Chu, W.; Paul, C. W. *Macromolecules* **2003**, *36*, 2695.

Herrington, R.; Hock, K., Eds. *Flexible Polyurethane Foams*; 2 ed.; The Dow Chemical Company: Midland, 1997.

Hoffman, J. D.; Miller, R. L.; Marand, H.; Roitman, D. B. *Macromolecules* **1992**, *25*, 2221.

Hoffman, J. D.; Miller, R. L. *Polymer* **1997**, *38*, 3151.

Hoyer, H. *Chem. Ber.* **1956**, *89*, 2677.

Ihn, K. J.; Yoo, E. S.; Im, S. S. *Macromolecules* **1995**, *28*, 2460.

Illger, H.-W.; Dorner, K.-H.; Hettel, H. In *Polyurethanes World Congress*; Technomic Publishing Co., Inc.: Aachen, Federal Republic of Germany, 1987; p 305.

Iogansen, A. V. *Spectrochim. Acta* **1999**, *55A*, 1585.

Ishihara, A. *J. Chem. Phys.* **1951**, *19*, 1142.

Ishihara, H.; Kimura, I.; Saito, S.; Ono, H. *Journal of Macromolecular Science-Physics* **1974**, *B10*, 591.

Jacobson, H.; Stockmayer, W. H. *J. Chem. Phys.* **1950**, *18*, 1600.

Jacobson, H. B., C.O.; Stockmayer, W.H. *J. Chem. Phys.* **1950**, *18*, 1607.

Jasse, B.; Tassin, J. F.; Monnerie, L. *Prog. Colloid Polym. Sci.* **1993**, *92*, 8.

John, R.; Thachil, E. T.; Ravindran, P.; Neelakantan, N. R.; Subramanian, N. *Polym. Plast. Technol. Eng.* **1991**, *30*, 227.

Johnson, A. F.; O'Driscoll, K. F. *Eur. Polym. J.* **1984**, *20*, 979.

Jones, N. A.; Atkins, E. D. T.; Hill, M. J.; Cooper, S. J.; Franco, L. *Macromolecules* **1996**, *29*, 6011.

Jones, N. A.; Atkins, E. D. T.; Hill, M. J.; Cooper, S. J.; Franco, L. *Macromolecules* **1997**, *30*, 3569.

Kaji, A.; Arimatsu, Y.; Murano, M. *J. Polym. Sci., A Polym. Chem.* **1992**, *30*, 2877.

Kanamoto, T.; Tanaka, K. *J. Polym. Sci. Polym. Phys. Ed.* **1971**, *9*, 2013.

Kaushiva, B. D.; Wilkes, G. L. *Polymer* **2000**, *41*, 6981.

Kaushiva, B. D.; Wilkes, G. L. *J. Appl. Polym. Sci.* **2000**, *77*, 202.

Keller, A.; Cheng, S. Z. D. *Polymer* **1998**, *39*, 4461.

Kim, J.; Ryba, E. *J. Adh. Sci. Tech.* **2001**, *15*, 1747.

Kissinger, H. E. *J. Res. Nat. Bur. Stand.* **1956**, *57*, 2712.

Klapstein, D.; Nau, W. N. *Spectrochim. Acta* **1993**, *50A*, 307.

Koberstein, J. T.; Russell, T. P. *Macromolecules* **1986**, *19*, 714.

Kogon, I. C. *J. Org. Chem.* **1959**, *24*, 83.

Kohan, M. I. *Nylon Plastics Handbook*; Carl Hanser Verlag: New York, 1995.

Kondyurin, A.; Klyachkin, Y. *J. Appl. Polym. Sci.* **1994**, *54*, 1385.

Kornfield, J. A.; Spiess, H. W.; Nefzger, H.; Eisenbach, C. D. *Macromolecules* **1991**, *24*, 4787.

Kricheldorf, H. R.; Hull, W. E. *Makromol. Chem.* **1981**, *182*, 1177.

Krol, P. *Polimery* **1997**, *42*, 458.

Lee, H. S.; Wang, Y. K.; Hsu, S. L. *Macromolecules* **1987**, *20*, 2089.

Lee, H. S.; Hsu, S. L. *Macromolecules* **1989**, *22*, 1100.

Lee, M. H.; Fleisher, C. A.; Morales, A. R.; Koberstein, J. T.; Koningsveld, R. *Polymer* **2001**, *42*, 9163.

Lesar, M.; Zigon, M.; Malavasic, T. *J. Appl. Polym. Sci.* **1993**, *47*, 805.

Leung, L. M.; Koberstein, J. T. *Macromolecules* **1986**, *19*, 706.

Li, C.; Cooper, S. L. *Polymer* **1990**, *31*, 3.

Li, Y.; Stein, M.; Jungnickel, B. J. *Colloid Polym. Sci.* **1991**, *269*, 772.

Li, Y. J.; Zhu, X. Y.; Yan, D. Y. *Polym. Eng. Sci.* **2000**, *40*, 1989.

Li, W.; Ryan, A. J.; Meier, I. K. *Macromolecules* **2002**, *35*, 6306.

Lin, S. B.; Hwang, K. S.; Tsay, S. Y.; Cooper, S. L. *Colloid Polym. Sci.* **1985**, *263*, 128.

Listemann, M. L.; Savoca, A. C.; Wressell, A. L. *J. Cell. Plast.* **1992**, *28*, 360.

Liu, S. Y.; Yu, Y. N.; Cui, Y.; Zhang, H. F.; Mo, Z. S. *J. Appl. Polym. Sci.* **1998**, *70*, 2371.

Longhenry, J. L.; Love, B. J.; Murthy, N. S. *J. Mater. Sci.* **1997**, *32*, 2283.

Macosko, C. W.; Miller, D. R. *Macromolecules* **1976**, *9*, 199.

Maklakov, L. I.; Furer, V. L.; Alekseev, V. V.; Furer, A. L. *Zh. Prikl. Spektrosk.* **1979**, *31*, 691.

McClusky, J. V.; Priester, R. D., Jr.; O'Neill, R. E.; Willkomm, W. R.; Heaney, M. D.; Capel, M. A. *J. Cell. Plast.* **1994**, *30*, 338.

McKiernan, R. L.; Gido, S. P.; Penelle, J. *Polymer* **2002**, *43*, 3007.

McKiernan, R. L.; Heintz, A. M.; Hsu, S. L.; Atkins, E. D. T.; Penelle, J.; Gido, S. P. *Macromolecules* **2002**, *35*, 6970.

Mehl, J. T.; Murgasova, R.; Dong, X.; Hercules, D. M.; Nefzger, H. *Anal . Chem.* **2000**, *72*, 2490.

Merten, R.; Lauerer, D.; Dahm, M. *J. Cell. Plast.* **1968**, *4*, 262.

Mertes, J.; Stutz, H.; Schrepp, W.; Kreyenschmidt, M. *J. Cell. Plast.* **1998**, *34*, 526.

Meuse, C. W.; Tao, H.-J.; Hsu, S. L.; MacKnight, W. J. *Polym. Prepr. (Am. Chem. Soc., Div. Polym. Chem.)* **1993**, *34*, 266.

Miller, J. A.; Lin, S. B.; Hwang, K. K. S.; Wu, K. S.; Gibson, P. E.; Cooper, S. L. *Macromolecules* **1985**, *18*, 32.

Miyazawa, T.; Shimanouchi, T.; Mizushima, S. I. *J. Chem. Phys.* **1956**, *24*, 408.

Miyazawa, T.; Shimanouchi, T.; Mizushima, S. I. *J. Chem. Phys.* **1958**, *29*, 611.

Moreland, J. C.; Wilkes, G. L. *J. Appl. Polym. Sci.* **1991**, *43*, 801.

Mullin, J. W. *Crystallization*; 4th ed.; Butterworth-Heinemann: Oxford; Boston, 2001.

Murgasova, R.; Brantley, E. L.; Hercules, D. M.; Nefzger, H. *Macromolecules* **2002**, *35*, 8338.

Nakao, K. *J. Adhesion* **1972**, *4*, 95.

Neff, R.; Macosko, C. W. In *Proc. Polyurethanes, Society of the Plastics Industry*: Chicago, IL, 1995; p 344.

Neff, R.; Adedeji, A.; Macosko, C. W.; Ryan, A. J. *J. Polym. Sci., B Polym. Phys.* **1998**, *36*, 573.

Nierzwicki, W.; Walczynski, B. *J. Appl. Polym. Sci.* **1990**, *41*, 907.

Ning, J.; De-Ning, W.; Sheng-Kang, Y. *Polymer* **1996**, *37*, 3045.

Nishi, T.; Wang, T. T.; Kwei, T. K. *Macromolecules* **1975**, *8*, 227.

Nitzsche, S. A.; Hsu, S. L.; Hammond, P. T.; Rubner, M. F. *Macromolecules* **1992**, *25*, 2391.

Oberth, A. E.; Bruenner, R. S. *J. Phys. Chem.* **1968**, *72*, 845.

Odian, G. *Principles of Polymerization*; Wiley: New York, 1991.

O'Shaughnessy, B.; Vavylonis, D. *Eur. Phys. J. B* **1998**, *6*, 363.

Oxtoby, D. W.; Kashchiev, D. *J. Chem. Phys.* **1994**, *100*, 7665.

Paik Sung, C. S.; Schneider, N. S. *Macromolecules* **1975**, *8*, 68.

Paik Sung, C. S.; Smith, T. W.; Hu, C. B.; Sung, N. H. *Macromolecules* **1978**, *12*, 538.

Paik Sung, C. S.; Smith, T. W.; Hu, C. B.; Sung, N.-H. *Macromolecules* **1979**, *12*, 538.

Paik Sung, C. S.; Hu, C. B.; Wu, C. S. *Macromolecules* **1980**, *13*, 111.

Paik Sung, C. S.; Smith, T. W.; Sung, N. H. *Macromolecules* **1980**, *13*, 117.

Painter, P. C.; Graf, J. F.; Coleman, M. M. *Macromolecules* **1991**, *24*, 5630.

Peebles, L. H., Jr. *Macromolecules* **1974**, *7*, 872.

Peebles, L. H., Jr. *Macromolecules* **1976**, *9*, 58.

Petrovic, Z. S.; Javni, I.; Banhegy, G. *J. Polym. Sci., B Polym. Phys.* **1998**, *36*.

Phillips, P. J. *Rep. Prog. Phys.* **1990**, *53*, 549.

Pisareva, I. V.; Bakalo, L. A.; Gritsenko, V. P. *Kinet. Kat.* **1988**, *29*, 547.

Poon, W. C. K. *Phys. Rev. E* **1997**, *55*, 3762.

Priester, R. D.; McClusky, J. V.; O'Neill, R. E.; Turner, R. B.; Harthcock, M. A.; Davis, B. L. *J. Cell. Plast.* **1990**, *26*, 346.

Puglisi, C.; Samperi, F.; Alicata, R.; Montaudo, G. *Macromolecules* **2002**, *35*, 3000.

Querat, E.; Tighzert, L.; Pascault, J. P.; Dusek, K. *Angew. Makromol. Chem.* **1996**, *242*, 1.

Raspoet, G.; Nguyen, M. T.; McGarraghy, M.; Hegarty, A. F. *J. Org. Chem.* **1998**, *63*, 6878.

Rego, J. M.; Campo, J. J.; Katime, I. *Thermochim. Acta* **1989**, *142*, 127.

Robertson, W. G. P.; Stutchbury, J. E. *J. Chem. Soc.* **1964**, *19*, 4000.

Roe, R. J.; Rigby, D. *Adv. Polym. Sci.* **1987**, *82*, 103.

Rondeau; Sievers *J. Am. Chem. Soc.* **1971**, *93*, 1522.

Rossmy, G.; Lidy, W.; Schator, H.; Wiemann, M.; Kollmeier, H. J. *J. Cell. Plast.* **1979**, *15*, 276.

Ryan, A. J. *Polymer* **1990**, *31*, 707.

Ryan, A. J.; Wilkomm, W. R.; Bergstrom, T. B.; Macosko, C. W.; Koberstein, J. T.; Yu, C. C.; Russell, T. P. *Macromolecules* **1991**, *24*, 2883.

Sadler, D. M.; Gilmer, G. H. *Phys. Rev. B* **1988**, *38*, 5684.

Sandridge, R. L.; Morecroft, A. S.; Hardy, E. E.; Saunders, J. H. *J. Chem. Eng. Data* **1960**, *5*, 495.

Satchell, D. P. N.; Satchell, R. S. *Chem. Soc. Rev.* **1971**, *4*, 213.

Saunders, J. H.; Frisch, K. C. *Polyurethanes: Chemistry and Technology*; Interscience Publishers: New York, 1962; Vol. 1.

Schneider, N. S.; Desper, C. R.; Illinger, J. L.; King, A. O.; Barr, D. *J. Macromol. Sci.-Phys.* **1975**, *B11*, 527.

Schneider, N. S.; Paik Sung, C. S.; Matton, R. W.; Illinger, J. L. *Macromolecules* **1975**, *8*, 62.

Schonherr, H.; Wiyatno, W.; Frank, C. W.; G., F. G.; Gast, A. P.; Pople, J. A.; Waymouth, R. M. *Macromolecules* **2002**, *35*, 2654.

Schriemer, D. C.; Li, L. *Anal. Chem.* **1997**, *69*, 4169.

Schriemer, D. C.; Whittal, R. M.; Li, L. *Macromolecules* **1997**, *30*, 1955.

Schwetlick, K.; Noack, R.; Stebner, F. *J. Chem. Soc.-Perkin Trans. 2* **1994**, 599.

Schwetlick, K.; Noack, R. *J. Chem. Soc.-Perkin Trans. 2* **1995**, *2*, 395.

Seymour, R. W.; Allegrezza, A. E.; Cooper, S. L. *Macromolecules* **1973**, *6*, 896.

Seymour, R. W.; Cooper, S. L. *J. Polym. Sci. Polym. Symp.* **1974**, *46*, 69.

Shih, H. H.; Hamed, G. R. *J. Appl. Polym. Sci.* **1997**, *63*, 323.

Shih, H. H.; Hamed, G. R. *J. Appl. Polym. Sci.* **1997**, *63*, 333.

Sievers, R. E.; Rondeau, R. E. *J. Am. Chem. Soc.* **1971**, *93*, 1522.

Silverstein, R. M.; Webster, F. X. *Spectrometric Identification of Organic Compounds*; 6th ed.; Wiley: New York, 1998.

Sirota, E. B. *Langmuir* **1998**, *14*, 3133.

Sivakamasundari, S.; Ganesan, R. *J. Org. Chem.* **1984**, *49*, 720.

Skrovanek, D. J.; Howe, S. E.; Painter, P. C.; Coleman, M. M. *Macromolecules* **1985**, *18*, 1676.

Snyder, R. G.; Schachtschneider, J. H. *Spectrochim. Acta* **1963**, *19A*, 85.

Snyder, R. G.; Schachtschneider, J. H. *Spectrochim. Acta* **1965**, *21A*, 169.

Snyder, R. G. *J. Chem. Phys.* **1967**, *47*, 1316.

Snyder, R. G. *J. Chem. Soc. Faraday Trans.* **1992**, *88*, 1823.

Sojecki, R. *Polish J. Chem.* **1978**, *54*, 1549.

Sojecki, R. *Polish J. Chem.* **1980**, *54*, 1549.

Sojecki, R. *Acta Polym.* **1989**, *40*, 619.

Sojecki, R. *Acta Polym.* **1991**, *42*, 411.

Sojecki, R. *Acta Polym.* **1992**, *43*, 96.

Sojecki, R. *Eur. Polym. J.* **1994**, *30*, 725.

Spirkova, M.; Dusek, K. *Polym. Bull.* **1989**, *22*, 191.

Spirkova, M.; Budinskisimendic, J.; Ilavsky, M.; Spacek, P.; Dusek, K. *Polym. Bull.* **1993**, *31*, 83.

Stolov, A. A.; Borisover, M. D.; Solomonov, B. N. *J. Phys. Org. Chem.* **1996**, *9*, 241.

Stovbun, E. V.; Kuzaev, A. I.; Baturin, S. M. *Polym. Sci., Ser. A.* **1996**, *38*, 691.

Strobl, G. *Acta Polym.* **1997**, *48*, 562.

Strobl, G. *The Physics of Polymers*; 2nd ed.; Springer-Verlag: Berlin, 1997.

Suen, W.; Percy, J.; Hsu, S. L. *Macromolecules* **submitted**.

Sumi, M. C., Y.; Nakai, Y.; Nakabayshi, M.; Kanzawa, T. *Makromol. Chem.* **1964**, *78*, 146.

Szycher, M. *Szycher's Handbook of Polyurethanes*; CRC Press: Boca Raton, 1999.

Tabor, R. L.; Hinze, K. J.; Priester, R. D.; Turner, R. B. In *SPI 34th Ann. Tech/Mark Conf.*, 1992; Vol. October 21-24, p 514.

Takemoto, M.; Kajiyama, M.; Mizumachi, H.; Takemura, A.; Ono, H. *J. Appl. Polym. Sci.* **2002**, *83*, 726.

Talanquer, V.; Oxtoby, D. W. *J. Chem. Phys.* **1993**, *99*, 4670.

Talanquer, V.; Oxtoby, D. W. *J. Chem. Phys.* **1995**, *103*.

Tao, H.-J.; Fan, C. F.; MacKnight, W. J.; Hsu, S. L. *Macromolecules* **1994**, *27*, 1720.

Tao, H.-J.; Meuse, C. W.; Yang, X.; MacKnight, W. J.; Hsu, S. L. *Macromolecules* **1994**, *27*, 7146.

ten Wolde, P. R.; Frenkel, D. *Science* **1997**, *277*, 1975.

Thomas, O.; Priester, R. D., Jr.; Hinze, K. J.; Latham, D., D. *J. Polym. Sci., B Polym. Phys.* **1994**, *32*, 2155.

Tonelli, A. E. *Macromolecules* **1992**, *25*, 7199.

Tsubomura, H. *J. Chem. Phys.* **1956**, *24*, 927.

Turreda, L. D.; Sekiguchi, Y.; Takemoto, M.; Kajiyama, M.; Hatano, Y.; Mizumachi, H. *J. Appl. Polym. Sci* **1998**, *70*, 409.

Van Bogart, J. W. C.; Gibson, P. E.; Cooper, S. L. *J. Polym. Sci. Polym. Phys. Ed.* **1983**, *21*, 65.

Van Gheluwe, P.; Leroux, J. *Journal of Applied Polymer Science* **1983**, *28*, 2053.

Van Hook, A. *Crystallization: Theory and Practice*; Reinhold Pub. Corp.: New York, 1961.

Vick, C. B.; Okkonen, E. A. *For. Prod. J.* **1998**, *48*, 71.

Vilsanen, Y.; Strey, R.; Reiss, H. *J. Chem. Phys.* **1993**, *99*, 4680.

Waddon, A. J. *J. Polym. Sci., B Polym. Phys.* **1997**, 1175.

Wang, C. B.; Cooper, S. L. *Macromolecules* **1983**, *16*, 775.

Wang, G.; Fang, B.; Zhang, Z. *Polymer* **1994**, *35*, 3178.

Winey, K. I.; Berba, M. L.; Galvin, M. E. *Macromolecules* **1996**, *29*, 2868.

Wong, S.-W.; Frisch, K. C. *J. Polym. Sci., A Polym. Chem.* **1986**, *24*, 2867.

Wunderlich, B. *Macromolecular Physics*; Academic Press: New York, 1976; Vol. 2.

Yokoyama, T.; Furukawa, M. In *International Progress in Polyurethanes*; Ashida, K., Frisch, K. C., Eds.; Technomic: Westport, CT, 1977; Vol. 2, p 125.

Yontz, D. J.; Hsu, S. L.; Lidy, W. A.; Gier, D. R.; Mazor, M. H. *J. Polym. Sci., B Polym. Phys.* **1998**, *36*, 3065.

.

Yontz, D. J.; Hsu, S. L. *Macromolecules* **2000**, *33*, 8415.

Yu, T. L.; Lin, T. L.; Tsai, Y. M.; Liu, W. J. *J. Polym. Sci., B Polym. Phys.* **1999**, *37*, 2673.

Zavodov, I. A.; Maklakov, L. I.; Atovmyan, E. G. *Spectrochim. Acta* **1999**, *A55*, 923.